

**Developing nanoparticulate oligonucleotides
as a target-specific antimicrobial
for modulation of complex gut microbiota**

Nichola Wong

Submitted for the Degree of Doctor of Philosophy

University of East Anglia
School of Biology
Quadram Institute Bioscience

May 2018

© This copy of the thesis has been supplied on condition that anyone who consults it is understood to recognise that its copyright rests with the author and that use of any information derived there from must be in accordance with current UK Copyright Law. In addition, any quotation or extract must include full attribution

Abstract

Developing nanoparticulate oligonucleotides as a target-specific antimicrobial for modulation of complex gut microbiota

The complex human gut microbiota harbours trillions of bacteria that are critical to health. Imbalances in the microbiota have been associated with conditions such as inflammatory bowel disease and metabolic disorder. Broad spectrum antibiotics that are used as therapy for bacterial infections cause major disruption to the diversity and structure of the gut microbiota, leading to dysbiosis.

For the advancement of microbiome-targeting, exploration of technologies that modulate the gut microbiota in a specific manner that minimise disruption to the gut microbiota is essential. In this thesis we examined a nucleic acid based-antimicrobial called Transcription Factor Decoys (TFDs), which are coupled with a proprietary nanoparticle for delivery to modulate the microbiota in a targeted manner. A TFD designed to target *Enterobacteriaceae* and delivered using nanoparticles was shown to enter the *E. coli* cells and inhibit bacterial growth. This system was also shown to work in a target-specific manner in an *in vitro* batch fermentation model of the human colon, and analysis by both culturing and 16S rRNA gene based metataxonomic analysis showed no major disruption to the rest of the gut microbiota. Metabonomic changes were evaluated to explore possible pathways involved for the TFD used to target *Enterobacteriaceae*. This TFD-specific antimicrobial activity against *Enterobacteriaceae* was also successfully translated to an *in vivo* mouse model with minimal changes to the gut microbiota.

The design of TFD targeting a phylogenetically diverse group with a similar metabolic function – sulphate reducing bacteria (SRB) – was also explored. Human SRB were isolated and a qPCR quantification method was designed. The work in this thesis serves as a proof-of-principle that TFD technology can specifically-target bacteria of interest and has the capability to selectively modulate the gut microbiota. This technology can potentially be developed to target other members of the gut microbiota to improve health status.

Contents

Abstract.....	ii
List of figures.....	x
List of tables.....	xviii
Acknowledgements.....	xix
Chapter 1 - General Introduction.....	1
1.1 The Human gut microbiota.....	2
1.1.1 Overview of the human gut microbiota.....	2
1.1.2 The role of human gut microbiota in health.....	3
Physiological functions of the gut microbiota.....	3
Core microbiota.....	4
1.1.2 The role of human gut microbiota in disease.....	6
1.1.3 Current tools for the study of gut microbiota.....	10
1.2 Modulation of the gut microbiota.....	11
1.2.1 Existing agents available for the rebalancing/modulating of the gut microbiota.....	11
Non-specific therapeutics.....	11
Faecal Microbiota Transplantation (FMT).....	12
Prebiotics, probiotics and polyphenols.....	13
1.2.2 Target-specific therapeutic agents.....	14
Utilisation of bacterial and bacteriophage systems.....	14
Oligonucleotide-based targeting.....	14
1.3 Antimicrobial system used in this thesis.....	16
1.3.1 Transcription Factor Decoys (TFDs).....	16
1.3.2 TFD designed against Enterobacteriaceae.....	18
1.3.3 Delivery molecule.....	19
1.3.5 Functional interaction between the delivery particle and Transcription Factor Decoy.....	21
1.3.6 Established knowledge on TFD antimicrobials on toxicity and in vivo animal studies.....	22

1.4 Potential bacterial targets for microbiota engineering for TFD antimicrobials.....	23
1.4.1 Enterobacteriaceae	23
1.4.2 Sulphate reducing bacteria	25
1.5 Aims and objectives of the research.....	26
Chapter 2 - General Materials and Methods.....	27
2.1 Culturing bacteria.....	28
2.1.1 Culture media.....	28
2.1.2 Bacterial strains and growth conditions	28
2.2 Biological characterisation of LNPs.....	29
2.2.1 Making TFD and NPs	29
TFD preparation	30
Nanoparticle preparation	30
2.2.2 Minimum inhibitory concentrations (MIC) and minimum bactericidal concentrations (MBC)	31
2.3 Physical characterisation of LNPs	31
2.3.1 Dynamic light scattering for NP size measurement.....	31
2.3.2 Flow cytometry and fluorescence-activated cell sorting (FACS)	32
2.3.3 Time course stability study using exonuclease treatment against TFD.....	32
2.3.4 Pendant Drop to measure surface tension of NPs.....	32
2.4 Confocal microscopy	33
2.4.1 Sample preparation	33
2.4.2 Confocal microscopy analysis	34
2.4.3 Data analysis	34
2.5 Batch culture fermentation	35
2.5.1 Preparation of media solutions and selective agar	35
2.5.2 Inoculation of media solutions with faecal bacteria.....	35
2.5.3 Quantification of bacteria and analysis	36
Viable bacterial cell counting.....	36

2.5.4 NMR sample processing.....	37
For batch experiment.....	37
For mouse experiment.....	37
2.6 Phylogenetic analysis of bacterial communities using 16S rRNA gene sequencing	38
2.6.1 Propidium monoazide treatment to differentiate live and dead bacteria	38
2.6.2 DNA extraction for bacterial community (16S rRNA gene) profiling	38
2.6.3 Gel electrophoresis of nucleic acids	39
2.6.4 Measurement of DNA concentration	39
Nanodrop	39
Qubit	39
2.6.5 Illumina Miseq sequencing settings.....	40
2.6.6 Bioinformatic analysis of 16S rRNA gene sequencing.....	40
2.7 Polymerase Chain Reaction (PCR).....	41
2.7.1 PCR preparation and conditions	41
For 16S rRNA gene amplification	41
For amplification from SRB	43
2.7.2. Identification of bacterial isolates	43
2.8 SRB related experiments.....	44
2.8.1. Isolation and identification of human SRB.....	44
2.8.2. SRB identification.....	44
Colony identification using 16S rRNA gene.....	44
Aligning dsrB gene sequences of SRB human isolates.....	44
Gram staining.....	45
2.8.3. qPCR Primer Design	45
2.8.4. Quantitative PCR (qPCR)	47
2.8.5. Genomic DNA extraction of SRB	49
2.9 Mouse model experiment.....	49
2.9.1. Animal Model and experimental design	49

2.9.2 Sample processing and storage conditions.....	50
2.10 Statistical analysis	53
Chapter 3 - Characterisation of nanoparticulate TFDs	54
3.1. Introduction	55
Structures of TFD	56
3.2 Materials and Methods.....	57
3.3 Results.....	58
3.3.1 Dynamic light scattering for NP size measurement.....	58
3.3.2. Minimum inhibitory concentration and minimum bactericidal concentrations of LNPs	59
Minimum inhibitory concentration	59
Minimum bactericidal concentration	61
3.3.3. Flow cytometry and fluorescence-activated cell sorting (FACS) of LNP formulations	61
3.3.4. Measurement of surface tension of 12-bis-THA by pendant drop analysis	67
3.3.5. Time-course stability study using exonuclease treatment against TFD	69
3.4 Discussion.....	70
Determination of NP size for targeted delivery in the human body	70
TFD-specific activity was observed against both GNSig and Crp-FNR TFD against <i>E. coli</i>	71
HPMC improved LNP_I by reducing aggregation.....	72
Aggregation of NPs was reversible in FACS	72
Acridine Orange can differentiate TFD and LNP fluorescence profile with NaTC treatment	73
Pendant drop is not suitable for the CMC measurement of 12-bis-THA.....	73
The preferred HP TFD structure was stable against exonuclease degradation.....	74
Chapter 4 - TFD specific targeting against <i>Enterobacteriaceae</i>	77
4.1. Introduction	78
Confocal scanning microscopy experiment	79
Dosing determination experiment.....	79
Batch culture fermentation	80
4.2. Materials and Methods.....	80

4.2.1. LNP dosing determination experiment.....	80
4.3 Results.....	81
4.3.1 TFD delivery in <i>E. coli</i> using confocal microscopy.....	81
4.3.2. Analysis of viable microbial community in human faecal bacteria cultures in dosing determination experiments.....	83
Bacteriostatic activity was achieved at 1x LNP dose in triplicate experiments.....	83
Variation in minimum bactericidal dose in triplicate dosing determination experiment	85
Dosing determination at a larger volume.....	87
4.3.3 Assessing effects of LNPs in human faecal bacterial cultures mimicking colon condition in vitro.....	88
Batch culture fermentation experiment 1.....	88
Batch culture fermentation experiment 2.....	91
Batch culture fermentation experiment 3.....	95
Batch culture fermentation experiment 4.....	97
4.3.4. Metataxonomic analyses of microbial community in human faecal bacteria cultures.....	104
Principal Coordinates Analysis.....	110
4.3.5. Metabonomic analysis in the human gut microbiome in the presence of TFD.....	112
4.4 Discussion.....	120
Successful TFD delivery by LNPs within <i>E. coli</i>	120
Importance of LNP dosage optimisation for target specific activity.....	121
Non target-specific activity occurs only at very high LNP dose	122
Coliforms: LNP dose ratio for successful bactericidal activity	123
Impact of non-coliforms Enterobacteriaceae on the magnitude of antimicrobial activity	124
Bacterial composition and diversity.....	125
Principal coordinates analysis.....	126
Metabonomic analysis	127
Anaerobic vs aerobic respiration	127
Insight into how the changes in metabolite might indicate the state of the gut microbiota.....	128

Comparing LNPs with currently available antibiotics against Enterobacteria.....	129
Chapter 5 - TFD specific targeting against <i>Enterobacteriaceae</i> in mouse model.....	131
5.1. Introduction	132
5.2 Methods.....	132
5.3 Results.....	133
5.3.1 Analysis of viable microbial community in mouse faeces	133
Experiment 1.....	133
Experiment 2.....	135
5.3.2 Metataxonomic analysis of microbial community in mouse faeces.....	137
Principal Coordinates Analysis.....	141
5.3.3 Metabonomic analysis of mouse faeces.....	142
5.3.4 Experimental observations of mouse health.....	145
Experiment 1.....	145
Experiment 2.....	145
5.3.5 Histological analysis of mouse intestinal tissues	146
5.4 Discussion.....	148
Effects of other antibiotics on the commensal microbiota in mouse models in 16S rRNA gene community analysis	149
Evaluation of mice’s health status	150
Effect of LNP on the histological morphology of colon	151
Lessons learnt and future work	152
Chapter 6 - TFD specific targeting against SRB.....	153
6.1. Introduction	154
6.2. Materials and Methods.....	155
6.3 Results.....	155
6.3.1 SRB Isolation of SRB from human faeces.....	155
6.3.2 Primer designs and qPCR method development	157
Designing dsrB qPCR primers.....	157

Design of dsrB primer	159
qPCR standard curve	160
Differentiation of distinct dsrB genes between human isolates	162
6.3.3 Designing TFD for SRB	164
6.3.4 Minimum inhibitory concentrations of SRB against TFDs	166
6.3.5 Confocal microscopy to visualise the delivery of TFD in <i>D. piger</i>	168
6.4 Discussion.....	169
Isolation of novel SRB strains.....	169
dsrB primers designed for qPCR may be useful for SRB quantification.....	170
Identification of transcription factor targets	170
SRB may be a more difficult target for TFD delivery.....	171
Chapter 7 - General discussion.....	173
7.1. The use of TFD in LNP as target-specific antimicrobials	174
7.1.1 Can TFD specifically target organisms of interest?	174
7.1.2 Does TFD targeting interrupt the commensal gut microbiota community in vitro?	175
7.1.3 Can TFD antimicrobial activity be demonstrated in vivo?	175
7.1.4 Can LNP be used to target sulphate reducing bacteria?.....	176
7.2 Future Research	177
7.2.1 Extensive LNP dosing range studies.....	177
7.2.2 Alternative delivery system for TFD.....	177
7.2.3 Improving understanding of TFD mechanisms	178
7.2.4 Determining which bacteria LNP can transfect in the gut microbiota	178
7.2.5 Incorporating qPCR for Enterobacteriaceae quantification	178
7.2.6 Studying LNPs effect in a disease model.....	179
7.2.7 Improving understanding of host response upon LNP treatment.....	179
7.2.8 Choice of TFD targets.....	180
7.3 Conclusion.....	180
References	182

List of figures

Figure 1.1 Bacterial characteristics in different regions of the human GI tract. Diagram showing the conditions, bacterial abundance and types of bacteria colonising in each part, taken from Aron-Wisnewsky *et al.* (2012).

Figure 1.2 Metabolism of bile acid and SCFA and their mechanism in the a) physiological and b) pathophysiological state. Alteration in SCFA production results in increased intestinal permeability which leads to worsened metabolic endotoxemia, followed by low-grade inflammation. Figure taken from Nieuwdorp *et al.* (2014).

Figure 1.3 The mechanism of Transcription factor decoy (TFD) acting on transcription factors of interest. TFD competitively inhibits the transcription factor binding sites to block gene expression, resulting in the destruction of bacteria cells (McArthur 2009b).

Figure 1.4 FNR is involved in the switch between aerobic and anaerobic respiration in facultative anaerobic bacteria. Under anaerobic conditions, 4Fe-4S FNR is active and drives the *fnr* modulon. FNR TFD is designed to inhibit the growth of *Enterobacteriaceae* by blocking the transcription of these genes. Figure was adapted from Förster *et al.* (2014).

Figure 1.5 Chemical structure of bolaamphiphilic lipids, 12,12'-(dodecane-1,12-diyl)bis(9-amino-1,2,3,4tetrahydroacridinium), referred to as 12-bis-THA, used for the assembly of nanoparticles (McArthur 2009b), figure was adapted from Mamusa *et al.* (2016).

Figure 1.6 Loaded nanoparticles are comprised of transcription factor decoy oligonucleotides that define the antimicrobial spectrum, which are encapsulated by delivery nanoparticles to target bacteria.

Figure 1.7 Increase in facultative anaerobes (*Enterobacteriaceae*) is associated with dysbiosis and disease development including inflammatory bowel disease (IBD), colorectal cancer (CRC) and Type 2 diabetes (T2D). Figure was adapted from Rigottier-Gois (2013).

Figure 3.1 The mechanism of transcription factor decoy (TFD) acting on transcription factors (TF) of interest. Transcription factors control gene expression by binding to specific sequences in the bacterial genome. TFD mimics the binding site and competitively inhibits the transcription factor to change gene expression, resulting in the killing of bacterial cells.

Figure 3.2 Chemical structure of bolaamphiphilic lipid, bola-amphiphile a) 12,12'-(dodecane-1,12-diyl)bis(9-amino-1,2,3,4tetrahydroacridinium) iodide ([12-bis-THA]₂I₂); b) 12,12'-(dodecane-1,12-diyl)bis(9-amino-1,2,3,4tetrahydroacridinium) chloride ([12-bis-THA]₂Cl₂) (Mamusa *et al.* 2016),

used for the assembly of nanoparticle (NP). It consists of two identical polar head groups with delocalised cationic charges and associated with a quaternary ammonium joined by a dodecane chain.

Figure 3.3 TFD structures including dumbbell, hairpin and duplex with modifications to resist nuclease degradation. Asterisk, phosphorothioate nucleotides.

Figure 3.4 Representative correlation curve of 12-bis-THA with 0.1% hydroxypropyl methylcellulose (HPMC) complexing with transcription factor decoy (TFD), forming loaded nanoparticles (LNPs).

Figure 3.5. Minimum inhibitory concentration of empty nanoparticles (ENPs), loaded nanoparticles (LNPs) and scrambled loaded nanoparticles (SLNPs) to exert antimicrobial activity. A fixed volume of *E. coli* DH5 α cells were added to each of the wells of a microtitre plate and were incubated at 37°C with shaking overnight, after which the visible growth/no growth in each well was recorded. a) A representative MIC experiment of ENPs and LNPs loaded with Gram negative sigma factor (GN Sig) TFD in formulation with and without excipient HPMC. Means of 3 biological repeats were calculated \pm standard deviation (SD); b) Minimum inhibitory concentrations of 12-bis-THA of SLNP and LNP using formulation with 0.1% HPMC (loaded with Crp-FNR TFD) against *E. coli* DH5 α . The results are means of 3 technical repeats with 3 biological repeats in each were calculated \pm SD. Single and double asterisks denote $P \leq 0.05$ and $P \leq 0.01$ respectively.

Figure 3.6. Minimum bactericidal concentrations of NPs. Colony counts of *E. coli* significantly decrease ($P \leq 0.001$) from different NP treatment compared to untreated *E. coli* control. ENP and LNP treatments were bactericidal at 0.9275 $\mu\text{g/ml}$ using NP formulation with 0.1% HPMC. ENP, empty nanoparticles; SLNP, scrambled nanoparticles; LNP, loaded nanoparticles. Means of at least 2 repeats calculated \pm SD. Triple asterisks denote $P \leq 0.001$.

Figure 3.7 HPMC decrease LNP aggregation in flow cytometry and fluorescent activated cell sorting (FACS). a) controls showing ENPs contain low levels of autofluorescence b) comparison of LNPs and LNPs + 0.1% HPMC fluorescence profile loaded with alexa488-flourescent TFD; c) left: Profile of LNPs + 0.1% HPMC (loaded with alexa488-flourescent TFD) after 24 h; the populations gated within the aggregated and non-aggregated gates were sorted by FACS in HPMC-lined collection tube) and reanalysed using flow cytometry; middle: sorted cells originated from the non-aggregated gate; and right: sorted cells originated from the aggregated gate. Gates show location of particles before sorting.

Figure 3.8 Aggregates profile of LNPs with Alexa-488-fluorescent TFD in 0.1% HPMC, a) sorted in BSA-lined tube b) sorted in FBS-lined tube. Gates show location of particles before sorting, showing changes in the fluorescent profile of the aggregates.

Figure 3.9 Characterisation of ENP and LNP using flow cytometry. SYBR green and Acridine Orange were used to stain DNA and NP to comparatively assess suitability for fluorescently stained TFDs. Acridine Orange and SYBR green fluorescence profile of a) TFD; b) ENP; c) LNP; d) LNP broken by sodium taurocholate.

Figure 3.10 Surface tension of a) ENP_I and b) ENP_Cl samples using Pendant drop with minimum 2 repeats at different dilutions over time, each line is an average of duplicate data. Blue: 0.4 mM; Red: 0.18 mM; Green: 0.018 mM; Purple: 0.0018 mM.

Figure 3.11 Agarose gel image of time course susceptibility study of TFDs Duplex (with phosphorothioate oligodeoxynucleotides terminal modifications), Dumbbell (DB) and Hairpin (HP) in the presence of fetal bovine serum (FBS) (which degrades TFDs). It is shown that DB survived up to 360 min in the presence of FBS, followed by HP which has a more visible band from 60 min onwards compared to duplex.

Figure 4.1 Confocal scanning image of (a) *E. coli* control and (b) *E. coli* cells with loaded nanoparticles in L media. The incorporation of Transcription Factor Decoy (TFD) from the LNP was shown in (biii) but not when TFD is absent in (a). Red: *E. coli* cell wall; Green: TFD. i) green channel; ii) red channel; iii) red and green channel overlay.

Figure 4.2 Confocal scanning images of a) *E. coli* with LNP + 0.1% HPMC in chemostat media incubated for 1.5 h; i) green channel; ii) red channel; iii) red and green channel overlay; b) broad view of *E. coli* + LNP + 0.1% HPMC incubated in chemostat media for 4 h; c) broad view of *E. coli* + LNP + 0.1% HPMC incubated in water control for 1.5 h; d) broad view of *E. coli* + LNP + 0.1% HPMC incubated in water control for 4 h. Red: *E. coli* cell wall; Green: TFD.

Figure 4.3 Bacterial viable counts of anaerobes (left) and coliforms (right) in dosing determination experiments at 1x NP dose in a) experiment 1; b) experiment 2; c) experiment 3. Same donor was used in all 3 experiments.

Figure 4.4 Bacterial viable counts from anaerobes (left) and coliforms (right) for dosing determination experiment a) experiment 1 - 1x dose is already enough for significant antimicrobial activity specific to *E. coli*, however 90x dose showed some sign of broad spectrum effect on the rest of the gut microbiota; b) experiment 2 - 3x dose is needed for significant antimicrobial activity specific to *E. coli*; c) experiment 3 - 12.5x dose is needed for significant bactericidal ($\geq \log_{10} 3$ decrease in CFU/ml) antimicrobial activity specific to *E. coli*.

Figure 4.5 Bacterial viable counts of anaerobes (left) and coliforms (right) in a scaled up study of a) dosing determination experiment 2; b) dosing determination experiment 3, in 150 ml vessels (with no pH control).

Figure 4.6 Bacterial viable counts for anaerobes, *Bacteroides*, *Clostridium*, *Lactobacillus*, coliforms and *Enterobacteriaceae* for control, SLNP and LNP treatments at 2% doses in batch culture fermentation experiment 1. PD, predose-treatment; treatments were added at 0 h prior to sampling.

Figure 4.7 *Enterobacteriaceae* colonies on MacConkey no. 3 plates for batch culture fermentation experiment 1. Pink colonies were mostly present at predose for all treatments and in control and SLNP treatments at 0 h, 4 h and 8 h, whereas bright pink colonies were mostly present with LNP at 0 h, 4 h and 8 h.

Figure 4.8 Bacterial viable counts for anaerobes, *Bacteroides*, *Clostridium*, *Lactobacillus*, coliforms and *Enterobacteriaceae* for Control, SLNP and LNP treatments at 2% doses in batch culture fermentation experiment 2. PD, predose-treatment; treatments were added at 0 h prior to sampling.

Figure 4.9 *Enterobacteriaceae* colonies on MacConkey no. 3 plates for batch culture fermentation experiment 2. Pink colonies were mostly present at predose for all treatments and in control and SLNP treatments at 0 h, 4 h, 8 h and with LNP at 8 h, whereas straw-coloured colonies were mostly present with LNP treatment at 0 h and 4 h.

Figure 4.10 Bacterial viable counts for anaerobes, *Bacteroides*, *Clostridium*, *Lactobacillus*, coliforms and *Enterobacteriaceae* for control, SLNP and LNP treatments at 2% doses in batch culture fermentation experiment 3. PD, predose-treatment; treatments were added at 0 h prior to sampling.

Figure 4.11 Bacterial viable counts for anaerobes, *Bacteroides*, *Clostridium*, *Lactobacillus*, coliforms and *Enterobacteriaceae* for control, SLNP and LNP treatments at 2% doses in batch culture fermentation experiment 4. PD, predose-treatment; treatments were added at 0 h prior to sampling.

Figure 4.12 Bacterial viable counts for anaerobes, *Bacteroides*, *Clostridium*, *Lactobacillus*, coliforms and *Enterobacteriaceae* for control, SLNP and LNP treatments at 10% doses in batch culture fermentation experiment 4. PD, predose-treatment; treatments were added at 0 h prior to sampling.

Figure 4.13 Linear relationship between starting coliforms quantity and LNP dose for a) dosing determination experiment; and b) batch model fermentation; c) prediction of minimum dose

required for sufficient antimicrobial activity in the batch model with different gut microbiota samples.

Figure 4.14 Averaged viable bacterial colony counts for *in vitro* batch culture fermentation experiments 1, 2 and 4. Bacterial viable counts for anaerobes, *Bacteroides*, *Clostridium*, *Lactobacillus*, coliforms and *Enterobacteriaceae* with control, SLNP and LNP treatments were calculated from bactericidal dose of 2%, 2% and 10% respectively.

Figure 4.15 Bacterial community analysis of 16S rRNA gene sequencing at family level for *in vitro* batch culture fermentation experiment 1; a) live and dead bacterial community in untreated samples; and b) live bacterial community in PMA treated samples.

Figure 4.16 Live bacterial community analysis of 16S rRNA gene sequencing at family level for *in vitro* batch culture fermentation experiment 2 (PMA-treated) at 2% NP dose.

Figure 4.17 Live bacterial community analysis of 16S rRNA gene sequencing at family level for *in vitro* batch culture fermentation experiment 4 (PMA-treated) at a) 2% dose and b) 10% dose.

Figure 4.18 Principal coordinates analysis (PCoA) plots of Illumina sequence data for *in vitro* batch culture fermentation model experiment 1. 3D PCoA plot was generated from weighted UniFrac analysis, where x- and y- and z-axis represents the first, second and third coordinates respectively.

Figure 4.19 Principal coordinates analysis (PCoA) plots of Illumina sequence data for *in vitro* batch culture fermentation model experiment 2; 3D PCoA plot was generated from weighted UniFrac analysis, where x- and y- and z-axis represents the first, second and third coordinates respectively.

Figure 4.20 Principal coordinates analysis (PCoA) plots of Illumina sequence data for *in vitro* batch culture fermentation model experiment 4. 3D PCoA plot was generated from weighted UniFrac analysis, where x- and y- and z-axis represents the first, second and third coordinates respectively. a) at 2% dose; b) at 10% dose.

Figure 4.21 Metabolites concentrations involved in anaerobic metabolism. Ethanol and lactate, and short chain fatty acids propionate, formate and acetaldehyde. A minimum of two repeats were analysed and the mean \pm SD were plotted.

Figure 4.22 Metabolite concentrations of cystine, glucose and glutamate. A minimum of two repeats were analysed and the mean \pm SD were plotted.

Figure 4.23 Metabolite concentrations of phenylalanine, leucine and isoleucine, valine and tyrosine. A minimum of two repeats were analysed and the mean \pm SD were plotted.

Figure 4.24 Metabolite concentrations of histidine and methionine. A minimum of two repeats were analysed and the mean \pm SD were plotted.

Figure 4.25 Metabolite concentrations of asparagine and aspartate. A minimum of two repeats were analysed and the mean \pm SD were plotted.

Figure 4.26 Metabolite concentrations of succinate, 3-phenyllactate and 4-hydroxyphenylacetate. A minimum of two repeats were analysed and the mean \pm SD were plotted.

Figure 4.27 Metabolites concentration of fumarate and pyruvate. A minimum of two repeats were analysed and the mean \pm SD were plotted.

Figure 4.28 Metabolites concentrations of betaine and uracil. A minimum of two repeats were analysed and the mean \pm SD were plotted. Pink, control; purple, SLNP; orange, LNP.

Figure 5.1 Bacterial viable counts for anaerobes, *Bacteroides*, *Clostridium*, *Lactobacillus* and coliforms for mouse experiment 1. Means were calculated from a minimum of 3 samples of faecal pellet (n=3) as some did not produce a faecal pellet at certain time points. Double asterisks denotes $P \leq 0.01$.

Figure 5.2 Bacterial viable counts for anaerobes, *Bacteroides*, *Clostridium*, *Lactobacillus* and coliforms for mouse experiment 2. Means of colony forming units of 5 mice (n=5) were calculated \pm SD. Double and triple asterisks denote $P \leq 0.01$ and $P \leq 0.001$ respectively.

Figure 5.3 Relative abundance of *Enterobacteriaceae* taken from taxa plot from 16S rRNA gene community analysis. Data extracted from taxa plot of community analysis. Left, exp 1; right, experiment 2.

Figure 5.4 Bacterial community analysis of 16S rRNA gene sequencing at family level for mouse experiment with PMA-treatment with average bacterial populations. a) experiment 1; b) experiment 2. (O) indicates an unidentified family in the described order.

Figure 5.5 Principal coordinates analysis (PCoA) plots from 16S rRNA gene community analysis for *in vivo* mouse model. a) experiment 1; b) experiment 2. 3D PCoA plot was generated from weighted UniFrac analysis, where x- and y- axis represents the first and second coordinates respectively.

Figure 5.6 A representative of metabonomic profile from mouse experiment 1, showing the large variation within and among mouse faecal samples.

Figure 5.7 Histological photomicrograph of mouse colon stained with haematoxylin and eosin at 4x and 20x magnification from a) saline control mouse; b) LNP-treated healthy mouse; and c) LNP-treated mouse with signs of illness that was euthanised prior to the end of experiment.

Figure 6.1 Gram staining of human gut SRB isolates. Representative images of isolates as presumptive left) *D. piger* (Gram negative) bacteria; middle) *V. Parvula* (Gram positive) and right) *V. tobetsuensis* (Gram positive).

Figure 6.2 The *dsrB* gene sequence alignment for the design of qPCR primer sets for Human desulfovibrio (using the top 6 gene sequences) and *dsrB* Human (using all gene sequences). Colouring of letters indicates degree of nucleotide conservation between sequences (black, 100%, dark grey, 80%; light grey, 60%). Location for alignment used for the design of primers were marked (green, forward primer; red, reverse primer) for both primer sets.

Figure 6.3 The *dsrB* gene sequence for the design of PCR primers from *D. piger* UC15 of human gut origin. Colouring of letters indicate the location of *dsrB* primer sequences. Grey, *dsrB*_F1; yellow, *dsrB*_F2; blue, *dsrB*_R1. Letters in bold indicate the relative location (but not the sequence of) Human_desulfov and *dsrB*_Human qPCR primers.

Figure 6.4 Gel electrophoresis of PCR products using gDNA of SRB. Successful amplification was achieved with *D. piger* UC15 and presumptive *D. piger* isolates 6 and 19. PCR products from *dsrB*_F1 and *dsrB*_R1 primer sets were preferred and used as DNA template for qPCR standard curves. Primer sets a) *dsrB*_F1 with *dsrB*_R1; and b) *dsrB*_F1 with *dsrB*_R1 were used, showing expected band sizes of 911 bp and 719 bp respectively. HyperLadder 1 (Bioline) was used to reference DNA band size.

Figure 6.5 qPCR standard curves for *D. piger* UC15, presumptive *D. piger* isolate 6 and isolate 19 using Human_desulfov qPCR primers sets. Strong linear correlation was obtained for absolute quantification of SRB. Means of 3 technical replicates were measured with 3 biological replicates in each experiment \pm SD.

Figure 6.6 PCR amplification using left, Human_desulfov primer set; and right, *dsrB*_Human primer set. Isolates identified as *D. piger* were successfully amplified at 336 bp while isolates identified as *V. tobetsuensis* and *V. parvula* were not. *D. piger* UC15 and *D. simplex* were used as a positive control. HyperLadder 1 (Bioline) was used to reference DNA band size.

Figure 6.7 Alignment of a) nucleotide sequences of Gram negative human gut isolates amplified by *dsrB*_F1 and *dsrB*_R1 primers. Colouring of letters indicates the degree of nucleotide conservation between sequences (black: 100%, dark grey, 80%; light grey, 60%), the marked

region indicates the location of Human_desulfov and dsrB_Human primers. Green, forward primers; red, reverse primers.

Figure 6.8 Alignment of translated amino acid sequence of group 1 and group 2 from PCR products amplified by dsrB_F1 and dsrB_R1 primers, showing that isolate 6 (representing isolate group 2) and isolate 19 (representing isolate group 1) have the same amino acid sequence in the dsrB PCR amplicon. Colouring of letters indicates the degree of nucleotide conservation between sequences (black: 100%, dark grey, 80%; light grey, 60%).

Figure 6.9 Predicted consensus binding site motif for a) NrfR TFD based on upstream regions of *nrfHA* orthologs in *Desulfovibrio* and *Bilophila* genomes (WebLogo taken from Rajeev *et al.* (2015)); b) RNAP54.1 TFD based on i) RpoN (σ^{54}) for alternative *Desulfovibrio* sigma factor 54 (WebLogo taken from Price *et al.* (2011)); ii) DNA fork junction, bold nucleotides indicate critical consensus nucleotides of the sigma 54-dependent promoter *nifH* with strong binding to σ^{54} isolated protein (Guo and Gralla 1998). The height of the nucleotide shown in the sequence logo of each motif is proportional to the information content in bits (Crooks *et al.* 2004).

Figure 6.10 Minimum inhibitory concentration of *D. piger* UC15, presumptive *D. piger* isolate 6 and *D. vulgaris*. No TFD-specific antimicrobial activity was observed from LNP compared to ENP and SLNP for all 3 TFD tested. MIC values are means of three technical replicates with three biological replicates in each experiment \pm SD. ENP: empty nanoparticles; SLNP: scrambled loaded nanoparticles; LNP: loaded nanoparticles.

Figure 6.11 Representative confocal scanning microscopy images of Gram negative presumptive *D. piger* isolates. 60 min of LNP incubation of a) isolate 6; and b) isolate 17; c) 120 min of LNP incubation of isolate 19. TFD delivery was observed after prolonged LNP incubation after 120 min. Red: SRB cell wall; Green: TFD. i) green channel; ii) red channel; iii) red and green channel overlay.

List of tables

Table 2.1 List of organisms and growth conditions used.

Table 2.2 Difference between *E. coli* and SRB confocal sample preparation.

Table 2.3 Experimental details for bacterial viable count in batch model fermentation.

Table 2.4 Composition of PCR reactions and PCR cycling conditions.

Table 2.5 PCR conditions for different SRB primers.

Table 2.6 a) qPCR reaction mix and b) reaction conditions.

Table 2.7 Details for each mouse experiments including treatment group, dosing regimen and faecal pellet collection.

Table 2.8 Sample processing for mouse experiment.

Table 2.9 Reagents used for paraffin tissue processing.

Table 3.1. Particle size measured by DLS Malvern Zetasizer Nano ZS. Average of 4 batches of NP made from 12-bis-THA were used for the analysis. Particle size is obtained from size peak intensity as polydispersity index > 0.2. ENP, empty nanoparticles; LNP, loaded nanoparticles; HPMC, hydroxypropyl methylcellulose; GN Sig HP TFD, Gram negative sigma factor hairpin TFD.

Table 4.1 experimental details for dosing determination experiment.

Table 4.2 Summary 16S rRNA gene colony PCR sequencing identity of MacConkey no. 3 colonies from Batch culture fermentation model.

Table 6.1 Summary table of SRB isolated from human faecal samples. S_{ab} score is the percentage of shared similarity between sequences compared.

Table 6.2 a) TFD sequences designed to target SRB. Functional and scrambled sequences (including linker and modifications) were included to investigate the sequence-specific antimicrobial activity. Structures of b) internal C3 Spacer (iSpC3); and c) internal dSpacer (iSpPC). TFD sequences were ordered from Integrated DNA Technologies.

Acknowledgements

I would firstly like to thank the Biotechnology and Biological Sciences Research Council (BBSRC), Quadram Institute and Procarta Biosystems Limited for funding my iCASE studentship.

Secondly, I would like to thank my supervisors Professor Arjan Narbad, Professor Michael McArthur and Dr Melinda Mayer for their guidance and support throughout my PhD, without your help and expertise I will not be here today.

I would also like to thank my team members, both past and present at the Quadram Institute Bioscience and Procarta Biosystems Limited, for all the thought-provoking discussions and helping me through my scientific career.

I would also like to thank Professor Alastair Watson for the opportunity of a collaboration. Thank you Dr Devina Divekar for the handing of animals, Dr Gwenaelle Legall for the NMR analysis in this thesis, and everyone who has lent me a helping hand for the mouse experiments. Not to forget my fellow coffee break gang, not only are they my colleagues, but my dear friends and family for the last 4 years.

I would like to thank my family for their care and support all these years, and allowing me to pursue my interests without limit. Special thanks to mama for her SOS original point treatments and my dad for preparing delicious food and always having me on his mind.

I would like to thank Tim and Denny for doing some strenuous 'proofbreeding', and for seeing me and my PhD grow and seeing it off in the end.

And finally, thanks the one who always make sure I am fed, warm, happy and keep me as close to sanity as I can get during these crazy months. I am eternally grateful to be your Gwi Gwi.

General Introduction

Chapter 1

Chapter 1: General Introduction

1.1 The Human gut microbiota

1.1.1 Overview of the human gut microbiota

The human gastrointestinal (GI) tract, which extends from the oral cavity to the anus, is colonised by a wide variety of microorganisms that coexist with the human body. This large reservoir of microorganisms, including bacteria, archaea, eukarya and viruses (Walker *et al.* 2014) is collectively known as the gut microbiota. They form an organised and complex community that colonise in specific regions of the GI tract depending on the most favourable conditions (Aron-Wisniewsky *et al.* 2012). Out of all the organs in the human body, the colonic microbiota contains the greatest diversity of bacteria (Figure 1.1) that are crucial to human health.

The microbiome - the collective microbial genomes in the microbiota and the gut microbiota itself - encodes unique genes that could impact on the host's physiology, including the acquirement of vitamins, beneficial metabolites (Qin *et al.* 2010), and the metabolism of indigestible dietary compounds by a range of hydrolytic enzymes (Flint *et al.* 2012). An integrated gene catalogue with almost 10 million genes has been identified, which highlights the wide diversity in functions of the gut microbiome (Li *et al.* 2014). The gut microbiota has therefore been widely regarded as a hidden metabolic 'organ', as the gut commensal bacteria play an influential role in nutrient absorption, metabolism (Qin *et al.* 2010), regulation of fat storage (Samuel *et al.* 2008), immune function (Guinane and Cotter 2013) and protection against intestinal epithelium injury (Rakoff-Nahoum *et al.* 2004).

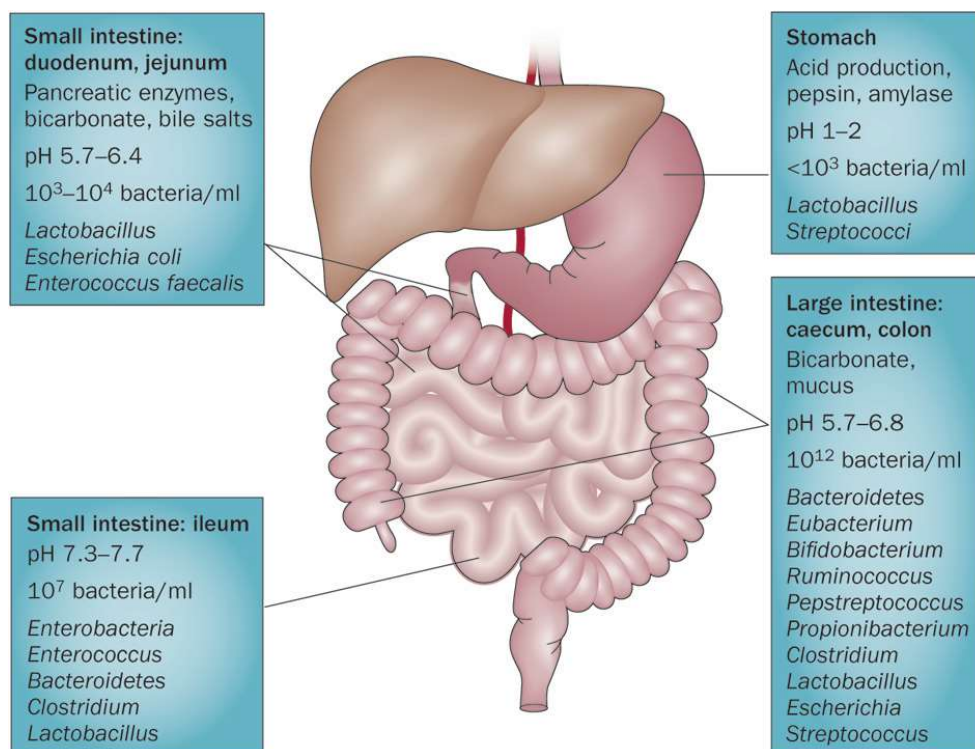


Figure 1.1 Bacterial characteristics in different regions of the human GI tract. Diagram showing the conditions, bacterial abundance and types of bacteria colonising in each part, taken from Aron-Wisniewsky *et al.* (2012).

Numerous scientific studies note that bacterial cells in the body outnumber human cells by 10:1 (Gill *et al.* 2006, Turnbaugh *et al.* 2007, Round and Mazmanian 2010). This figure has been found to originate from one historic estimate from the 1970s that was based on crude assessments of the volume of the whole GI tract (Luckey 1972). However, a recent review has re-evaluated the total bacterial numbers against total human cells, a revised human to bacterial cell ratio has been proposed to be 1:1, with 10^{13} bacterial cells mostly dominated by colon bacteria and 10^{13} human cells, when red blood cell numbers are taken into account (Sender *et al.* 2016).

1.1.2 The role of human gut microbiota in health

Physiological functions of the gut microbiota

In the physiological state, the microbiota establishes a relatively stable ecosystem within the GI tract and is one of the most important factors in the maintenance of normal physiological function (Rooks *et al.* 2014). Apart from the minimal bacterial gut genome that allows bacteria to survive in the gut, genes that are involved in the homeostasis of the ecosystem which is called the minimal gut metagenome have two functional clusters of genes. Those involved in the housekeeping of bacteria include functions that contribute to metabolic pathways such as amino-acid synthesis, central carbon metabolism and essential protein complexes such as DNA and RNA

polymerase. Other functions are gut-specific such as sugar harvest and adhesion to host proteins i.e. fibrinogen, collagen and fibronectin (Qin *et al.* 2010).

One of the main metabolic functions of the gut microbiota includes the fermentation of a range of polysaccharides and oligosaccharides including unabsorbed sugars and carbohydrates from mucus glycoprotein derived from the host, which will otherwise be lost in the faeces. The predominant products from carbohydrate metabolism include hydrogen, carbon dioxide, ethanol and short chain fatty acids (SCFA) (Gallo *et al.* 2016). The gut microbiota also influences the synthesis of vitamins and amino acids (LeBlanc *et al.* 2013), caloric extraction efficiency from food (Turnbaugh *et al.* 2006) and the absorption of iron, calcium and magnesium. SCFA, comprising butyrate, propionate and acetate, are a vital energy source for colonocytes and help maintain tissue integrity (Conlon and Bird 2015). Gaseous products such as hydrogen sulphide (H₂S), carbon monoxide and nitric oxide have been regarded as signalling molecules to maintain the mucosal integrity. Moreover, in mammalian cells, H₂S-driven energy production occurs most efficiently in the epithelial cells of the GI tract (Wallace *et al.* 2017).

The fermentation products of gut microbiota are responsible for the modulation of gut peptide secretion involved in the energy homeostasis, food intake and pancreatic function (Cani and Delzenne 2009). The metabolism of fermentable non-digestible dietary fibres also helps the development of microvilli and in turn increases nutrient absorption and the anaerobic metabolism of peptides and proteins resultant from host energy-conversion (Nicholson *et al.* 2005). The host metabolic status may also be influenced by the GI tract microbiota, as it contributes to the metabolism of bile acids, SCFA and breaking down non-digestible polysaccharides and fibres (Backhed *et al.* 2004), as shown in Figure 1.2 a. The gut microbiota exerts a protective function on the host by preventing the colonisation of pathogens and modulating the host immune-system (Roeselers *et al.* 2013). The gut microbiota is also responsible for the modulation of hormone release in the GI tract and there is increasing interest on how the gut microbiota regulates brain behaviour via the gut-brain axis (Carabotti *et al.* 2015).

Core microbiota

It is of great interest to identify whether there is a common core microbiome catalogue that is shared among individuals. Using 16S ribosomal RNA (rRNA) gene sequencing methods, it was found that there are larger similarities in gut microbiota at phylum level between individuals, as the Firmicutes and Bacteroidetes made up over 90% of the distal gut microbiota of known phyla; other minor phyla that are shared amongst individuals include Actinobacteria, Fusobacteria,

Proteobacteria and Verrucomicrobia (Eckburg *et al.* 2005, Duncan *et al.* 2007, Tremaroli and Backhed 2012).

It was proposed that there is a discrete core microbial community with high temporal stability of microbiome for each individual, which is dependent on health, age, diet, antibiotic use and other environmental factors (Caporaso *et al.* 2011a, Huttenhower C 2012, Maurice *et al.* 2013). However, the inter-individual variations between adult gut microbiota are huge, as demonstrated in an identical-twin study, where participants were found to have less than 50% homology in species phylotypes (Turnbaugh *et al.* 2010). Nonetheless, some species were identified as key species in the human gut microbiota, including *Bacteroides uniformis*, *Faecalibacterium prausnitzii* and *Roseburia intestinalis* (Qin *et al.* 2010).

Metagenomic sequencing has allowed us to analyse the genomes of complex bacterial communities. The Metagenomics of the Human Intestinal Tract (MetaHIT) project has collaborated with scientists all over Europe to gather metagenomic data from eight countries (Ehrlich 2011). One of the studies investigated the gut microbiome of 39 individuals from four countries, demonstrating that individuals fall into three distinctive clusters called enterotypes (Arumugam *et al.* 2011), distinguished by the variation in levels of genera in *Bacteroides* (enterotype 1), *Prevotella* (enterotype 2) and *Ruminococcus* (enterotype 3), with phylogenetic and functional difference in vitamin biosynthesis and the pathways they use to generate energy. However, it was shown that the three enterotypes are not a representative sample of microbiota classifications (Le Chatelier *et al.* 2013), as most studies showed only the *Bacteroides* and *Prevotella* clusters, and *Ruminococcus*-driven enterotype seemed less evident (Claesson *et al.* 2012, Yatsunenko *et al.* 2012), suggesting that they form part of the *Bacteroides* enterotype (Wu *et al.* 2011). Furthermore, in a recent study that sequenced more than 1200 adults' gut microbiota, enterotypes were found to lack distinct boundaries of classification. As a continuous gradient of bacterial abundance is present within body sites (Koren *et al.* 2013), this suggests that discrete enterotypes may not exist at all. Conflicting opinions on the distinctiveness in enterotypes remain debatable (Koren *et al.* 2013, Ding and Schloss 2014, Moeller and Ochman 2014). As *Bacteroides* and *Prevotella* both belong to *Bacteroidales*, functional groups were found to be continuous and overlapping between the two groups and were clustered in term of functions, the lack of distinct metabolotypes between the groups may be explained by the likelihood that they perform similar functions in the gut (Holmes *et al.* 2012).

To better understand the intestinal bacteria that regularly live in the healthy gut, large scale studies have since been performed to identify the composition of the gut microbiomes with 110

and 1135 participants respectively (Falony *et al.* 2016, Zhernakova *et al.* 2016). Out of the 664 genera present in the gut microbiota, a 14-genera core microbiota composition has been identified from the combination of the above studies (Falony *et al.* 2016). These 14 genera include *Roseburia*, *Faecalibacterium*, *Dorea*, *Coprococcus*, *Blautia*, *Bacteroides*, *Ruminococcus*, *Prevotella*, *Parabacteroides*, *Oscillibacter*, *Bifidobacterium*, *Barnesiella*, *Anaerostipes* and *Alistipes*. Genus richness has also been shown to correlate positively to age and negatively to total core abundance. Furthermore, markers for the gut microbiota composition and diversity have been revealed via population-based metagenomic analyses, of which 110 factors have been associated to 125 species (Zhernakova *et al.* 2016). In particular, faecal chromogranin A (CgA) has been found to be negatively correlated to microbiome diversity. It was also suggested that factors such as diet, smoking, drugs and disease explains 18.7% of the variations in the gut microbiota (Zhernakova *et al.* 2016). These factors will be further discussed in the next section.

1.1.2 The role of human gut microbiota in disease

As the composition of microbial communities plays a major role in maintaining health, minor changes of the microbial population could have substantial repercussions, either good or bad, on human health. When structural disruption has occurred to the commensal gut microbiota, known as dysbiosis (Petersen and Round 2014), the microbiota becomes inefficient at performing their main functions such as energy and vitamin production and defending against pathogens, which in turn increases the chance of downstream complications including immunological and metabolic defects as the host becomes more predisposed to infection (Langdon *et al.* 2016).

The disruption of the gut microbiota has been shown to strongly associate with diseases such as inflammatory bowel disease (IBD) and metabolic diseases including diabetes, obesity (Zak-Golab *et al.* 2014), cancer (Ohtani *et al.* 2014) and cardiovascular diseases. Dysbiosis associated with these diseases are triggered by low-grade chronic inflammation (Wellen and Hotamisligil 2005); the main factors contributing towards the alteration of gut microbiota were established to be social- and cultural-dependent, instead of hereditary-dependent. As bacterial colonisation happens rapidly after birth, environmental variations from the microbiome have a greater role in the pathogenesis of diseases than the variations occurring in the human genome (Madan *et al.* 2012) and implies that the microbiota have an important role in the development of disease. To identify the underlying gut microbiota variations that characterise various diseases, the change in the Firmicutes and Bacteroidetes ratio was frequently highlighted. While there is an increased Firmicutes:Bacteroidetes ratio associated with obesity (Turnbaugh *et al.* 2006), Firmicutes were dramatically reduced in Crohn's disease (Finucane *et al.* 2014).

Diet is one of the biggest factors that rapidly and repeatedly alters the gut microbiome (David *et al.* 2014). It was shown that a strict vegetarian diet reduces the Firmicutes:Bacteroidetes ratio in the gut microbiota, whereas the bacterial diversity and enterotypes remains unchanged (Backhed *et al.* 2004). Levels of pathobionts such as *Enterobacteriaceae* were decreased and commensals such as *Bacteroides fragilis* and *Clostridium* species in clusters XIVa and IV were increased. These collectively lead to a significant reduction of faecal lipocalin-2, a biomarker for intestinal inflammation (Chassaing *et al.* 2012), and short chain fatty acids levels, which are signatures of obesity diseased-phenotypes. High-animal based diets contribute to the development of inflammatory bowel disease; the overgrowth of the sulphate-reducing pathobiont *Bilophila wadsworthia* increased faecal bile acid concentration and increased sulphite reductase expression (David *et al.* 2014), and is associated with a pro-inflammatory T helper type 1 immune response and subsequently increased incidences of colitis in a genetically susceptible mouse model (Devkota *et al.* 2012). The diseased state associated with bile acid and short chain fatty acid metabolism is shown in Figure 1.2 b.

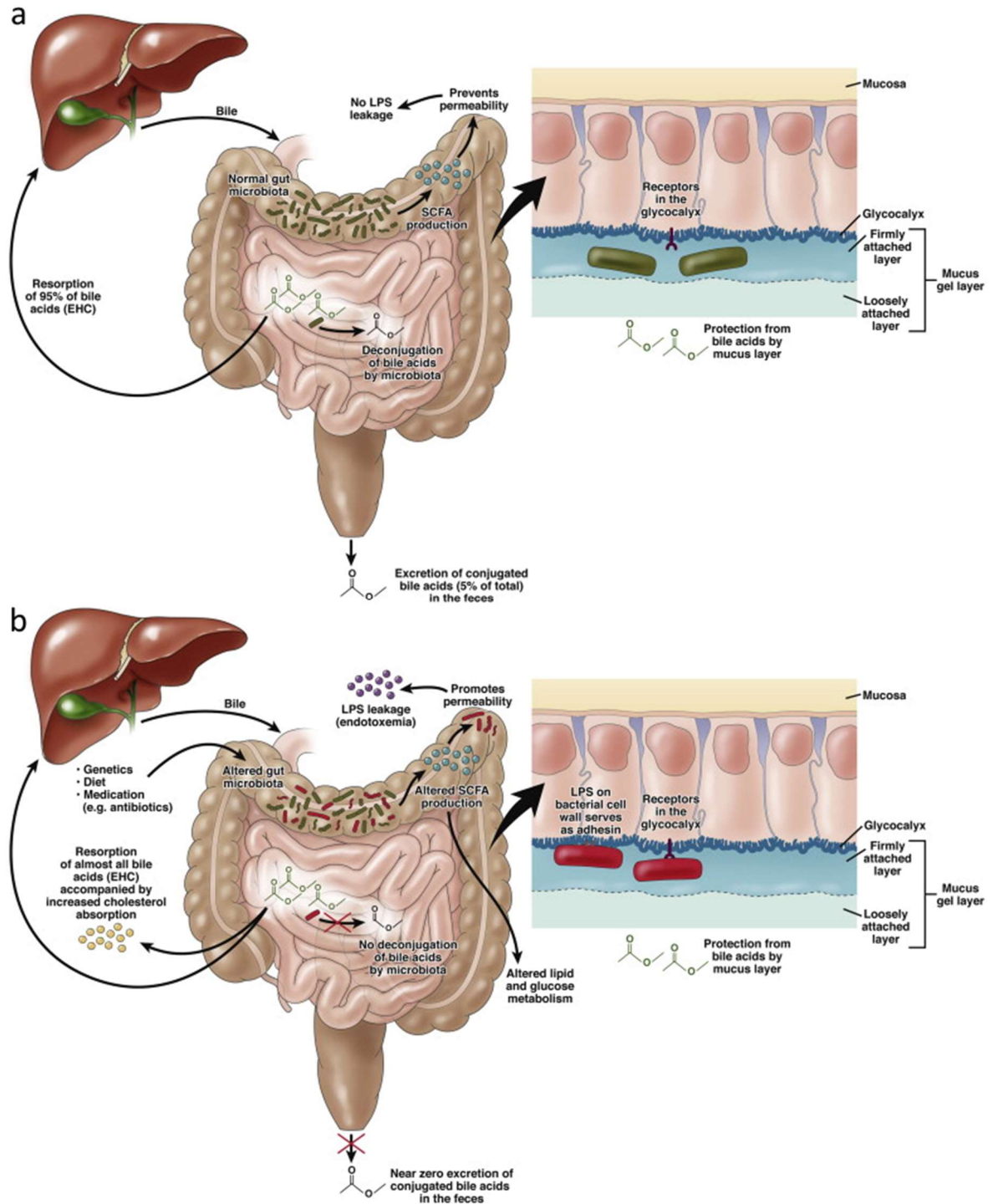


Figure 1.2 Metabolism of bile acid and SCFA and their mechanism in the a) physiological and b) pathophysiological state. Alteration in SCFA production results in increased intestinal permeability which leads to worsened metabolic endotoxemia, followed by low-grade inflammation. Figure taken from Nieuwdorp *et al.* (2014).

Dietary fibre or plant-based food intake is important as they are the primary source of carbohydrate fermentation in the gut microbiome (Conlon and Bird 2015). Evidence has been

shown that the lack of fibre in the diet encourages the degradation of the mucus layer in a gnotobiotic mouse model colonised with synthetic human gut microbiota. This leads to susceptibility to pathogens and the development of colitis (Desai *et al.* 2016). The understanding of nutritional, biliary and microbial dynamics is therefore crucial to establishing links for diet-related diseases.

Conditions such as Crohn's disease and obesity are both associated with lower bacterial diversity, where pro-inflammatory species e.g. *Bacteroides* and *Ruminococcus gnavus* that are associated with IBD are more frequently found in low bacterial gene count of individuals. It was discovered that some metabolic markers correlate with the richness of human gut microbiome and could be used to differentiate individuals with high or low bacterial richness (Koren *et al.* 2013). The microbial diversity is reduced both in abundance and biodiversity in Crohn's disease. The levels of *Faecalibacterium prausnitzii* – an anti-inflammatory commensal bacterium – is reduced in Crohn's disease patients (Sokol *et al.* 2008).

Some bacterial genes are enriched in obese individuals (when compared to lean individuals), of which 75% of these obesity-associated genes are from Actinobacteria and 25% from Firmicutes. Moreover, lean individuals contain 42% of enriched genes from Bacteroidetes (compared to 0% for obese individuals) (Turnbaugh *et al.* 2009). These genes indicate their role in carbohydrate, amino acid and lipid metabolism. Germ free mice receiving a gut microbiota transplant from an obese mouse resulted in increased body fat compared to mice receiving a gut microbiota transplant from a lean mouse (Turnbaugh *et al.* 2006). Since the majority of the obese-enriched genes derive from Actinobacteria, a more detailed understanding of whether certain bacteria or transcripts are causative of obesity would identify these as targets for the development of treatments.

However, there are conflicting results between patient studies and mouse-model data on the role of gut microbiome and obesity. A study has analysed publicly available data from the Human Microbiome Project (HMP) and MetaHIT and concluded that there is no simple taxonomic signature of obesity, as the inter-study variation is much greater than the taxonomic difference between lean and obese individuals within each study (Manichanh *et al.* 2006). This further supports the need to understand the function of the microbiota as well as the taxonomic structure, as different bacteria or genetic pathways could contribute to the increased carbohydrate and lipid functions observed with obese individuals (Turnbaugh *et al.* 2009).

Bacterial lipopolysaccharide (LPS) present in Gram-negative bacteria has been shown to be an inflammation trigger for high-fat-induced obesity and type 2 diabetes, potentially through a

mechanism termed metabolic endotoxaemia (Cani *et al.* 2007a). The composition of the microbiota clearly affects the concentration of LPS, which was found to be inversely correlated to the level of *Bifidobacterium* spp. (Cani *et al.* 2007b). Also, increased *Escherichia coli* (*E. coli*) levels are linked with active ulcerative colitis (UC) (Petersen *et al.* 2009) and an increased intestinal inflammation burden in UC patients (Mirsepasi-Lauridsen *et al.* 2016), highlighting how commensal bacteria could be pathobionts and induce disease progression in an already susceptible host.

1.1.3 Current tools for the study of gut microbiota

To study the human gut microbiota, an *in vitro* batch culture model is often utilised as a fermentation model of the colon with pH and temperature controls (Mandalari *et al.* 2007, Avendano-Perez *et al.* 2015). The composition of the gut microbiota is often characterised by conventional bacterial culturing techniques and 16S rRNA gene sequencing for metataxonomic analysis. Metabonomic analysis can also be incorporated to enhance the understanding of the metabolic changes subject to a treatment intervention.

To evaluate changes in the gut microbiota in an *in vivo* setting, a murine model is the most commonly used model for gut microbiota studies. It has a similar gastrointestinal structure and anatomy to humans which allows a better evaluation of the host-microbiota interaction. Both human and mouse microbiota are dominated by the Bacteroidetes and Firmicutes phyla, with similar abundance in genera such as *Clostridium*, *Bacteroides* and *Blautia*, though genera such as *Prevotella*, *Faecalibacterium* and *Ruminococcus* are more abundant in human and *Lactobacillus* is more abundant in mice. The human and mouse microbiota are nonetheless functionally similar (Nguyen *et al.* 2015); the treatment response in mice is often representative of the impact and the microbiota shifts in humans by antibiotics (Becattini *et al.* 2016). Mouse microbiota are therefore a comparable model to study the potential impact of human gut microbiota subject to antimicrobial treatment. The use of germ free mice transplanted with human gut microbiota is also a valuable tool to investigate the direct link between the human gut microbiota within a host. However, the lack of a native homeostatic gut microbiota may impact on the evaluation of the structural changes in the commensal bacteria following a targeted intervention (Laukens *et al.* 2016).

The composition of the gut microbiota is often characterised by conventional bacterial culturing techniques and 16S rRNA gene sequencing for metagenomic analysis (Gallo *et al.* 2016). The technology available for the understanding the gut microbiota has progressively increased in

recent years. Whole genome shotgun sequencing is becoming increasingly popular and allows the interpretation of functionality of the gut microbiota and increasing taxonomical resolution at genus and species level (Jovel *et al.* 2016). However, in terms of assessing community ecology and biodiversity, 16S rRNA gene sequencing is still more robust and allows notably better identifications of bacterial communities at different taxonomic scales including the phylum and family levels (Tessler *et al.* 2017). Metabonomic analysis has also been incorporated to study the modulation of gut microbiota, which allow the identification of metabolic profiles and help explain the possible metabolic pathways involved (Vernocchi *et al.* 2016).

1.2. Modulation of the gut microbiota

1.2.1 Existing agents available for the rebalancing/modulating of the gut microbiota

Non-specific therapeutics

Antibiotics are the most common treatment readily available to treat microbial infections. Various types of antibiotics act by different mechanisms to allow different spectrums of antimicrobial activity (Langdon *et al.* 2016). Broad spectrum antibiotics such as ampicillin and gentamycin, as well as the rise in multidrug resistant pathogens, often have a large impact on the microbiota including damage to the composition and diversity of the gut microbiota leading to dysbiosis.

Since antibiotics are readily tested for their safe therapeutic use, modifications of vancomycin with the hope of combating and delaying antibiotic resistance are underway. They showed increased potency with synergistic action that work via several mechanisms, including different ways of interfering with the bacterial cell wall (Okano *et al.* 2017). However, even though vancomycin has narrow-spectrum activity and is designed to target Gram positive bacteria, Gram negative bacteria can also be depleted and the commensals perturbed (Ubeda *et al.* 2010) and this can lead to increased susceptibility to secondary infections in both humans and mice (Lewis *et al.* 2015). This is likely due to the great magnitude of interdependence between bacterial taxa (Becattini *et al.* 2016).

To target the microbiota using transcription as a therapeutic target, rifamycins are a good example as they are a successful class of antibiotics. They work by inhibiting bacterial RNA polymerase resulting in the prevention of RNA elongation (Campbell *et al.* 2001). The broad spectrum antimicrobial activity spans from staphylococci to *Listeria* spp. (Thornsberry *et al.* 1983). The results from clinical trials have shown that, by targeting the gut microbiota, the non-systemic

antibiotic rifaximin can significantly relieve the general symptoms of irritable bowel syndrome (IBS) compared to placebos (Pimentel *et al.* 2006, Di Stefano *et al.* 2011, Pimentel *et al.* 2011, Pimentel *et al.* 2014). This increases our confidence that targeting the bacterial transcription mechanism can be used as a drug to treat gastrointestinal conditions.

Faecal Microbiota Transplantation (FMT)

To alleviate the impact of dysbiosis, faecal microbiota transplantation has been a popular idea as a means of rebalancing the gut microbiota. It has been shown in a randomised clinical trial that FMT is effective in treating recurrent *C. difficile* infection (Cammarota *et al.* 2015) and is widely regarded as an effective treatment option for *C. difficile* related dysbiosis (Bibbo *et al.* 2017), with a success rate of over 90% (Kelly *et al.* 2016).

Some evidence has been shown that it helps with the management of metabolic disorders and IBD. To treat IBD, donors with a healthy microbiota were used who could increase protective commensals including Clostridia and *Bacteroides* and decrease pathogenic or opportunistic commensals e.g. adherent-invasive *E. coli* (AIEC) and *Mycobacterium* in a patient's microbiota (Khajah 2017). Meta-analysis systematic review has indicated that short term use of FMT facilitates remission in active UC (Narula *et al.* 2017). However, more supporting evidence from clinical trials are needed in order to review whether or not FMT will be suitable for routine clinical use for IBD or metabolic disorder (Bakker and Nieuwdorp 2017).

Even though successful reversal of gut microbiota by FMT has been reported for multiple conditions, the efficacy of FMT treatment is still variable against IBD and dependent on donor and also the time of UC (Moayyedi *et al.* 2015). The long term effects are not fully understood and safety is still a major concern. Risks include the transfer of antibiotic resistance genes, the transmission of unknown infectious agents, and also possible microbiota-induced diseases that may further aggravate the patient's clinical outcome, as the patient is already a susceptible host (van den Elsen *et al.* 2017). This procedure will require standardisation and needs its safety and efficacy to be evaluated to ensure that FMT can be used effectively in regular clinical practice.

There are also issues concerning donor-recipient compatibility, this indicates that there may be significant differences in efficacy of the same faecal transplant between different patients (Li *et al.* 2016). Since associated bacterial strains (Lawley *et al.* 2012, Reeves *et al.* 2012, Buffie *et al.* 2015) and metabolites (Buffie *et al.* 2015) have been identified to provide protection against *C. difficile*, FMT may eventually be replaced by selective probiotic strains and effector molecules (Becattini *et*

al. 2016), which allow a more accurate reconstruction of gut microbiota with minimal adverse side effects and with reduced safety concerns (Wang *et al.* 2017).

Prebiotics, probiotics and polyphenols

Dietary interventions including probiotics, prebiotics and polyphenols are amongst the most accessible ways to modulate gut microbiota composition or to improve metabolic activity. Probiotics are microorganisms that can confer health benefits to the host, when adequate amounts are administered (Hill *et al.* 2014). Due to the variability in activity between different strains, probiotics are often not well characterised. There is limited comparable strain-matched data available for meta-analysis (Marchesi *et al.* 2016). It was proposed, in a systematic review of randomised control trials, that a probiotic does not primarily work by altering the gut microbiota's composition (Kristensen *et al.* 2016), but instead it was suggested that it may promote health benefits by maintaining stability and functionality of the gut microbiome, e.g. by reducing the perturbation of the gut microbiota or to confer a quicker recovery following antibiotics and poor diet (Sanders 2016).

Prebiotics are fermented ingredients that selectively stimulate growth and/or activities of microbial organisms in the gut microbiota and promote health benefit to the host (Gibson *et al.* 2004). In a randomised, double-blind, placebo-controlled cross-over trial, inulin-type fructans modulate the gut microbiota including an increase in *Bifidobacterium* and a decrease in *Bilophila* abundance, which led to improvement in constipation symptoms (Vandeputte *et al.* 2017). Although some evidence has been shown to demonstrate health benefits, more large scale human studies will be required to provide the consistent evidence for their long-term health effects.

Polyphenols are another dietary food group that have been generally regarded to have modulatory effects on the balance of the gut microbiota, including the increase of *Lactobacillus* spp. and *Bifidobacterium* spp. and of reducing pathogenic bacteria to maintain intestinal health, acting in a way similar to probiotics (Duenas *et al.* 2015). Researchers have attempted to modulate the microbiome and reverse the adverse effects of obesity. One study has examined a gastrointestinal microbiome modulator (GIMM), which consists of prebiotics and polyphenols. GIMM improved blood glucose tolerance in obese patients but showed insignificant changes in the metabolic and gut microbiota markers to indicate successful microbiome modulation (Rebello *et al.* 2015).

1.2.2 Target-specific therapeutic agents

Utilisation of bacterial and bacteriophage systems

Bacteriophages are capable of infecting and replicating within a selected bacterium and can be exploited for target-specific antimicrobials. Bacteriophages have been used to decrease the levels of AIEC associated with the intestinal mucosa in Crohn's disease patients. It was found that AIEC were significantly decreased in the faeces and also in the adherent intestinal flora following treatments with a bacteriophage cocktail (Galtier *et al.* 2017). However, such technology is limited to finding a bacteriophage that can infect specific bacteria of interest. Also, as large amount of bacteriophages will be required to treat an infection, they may trigger an immune response leading to secondary health impacts, which may interfere with the treatment (Reardon 2017).

Clustered Regularly Interspaced Short Palindromic Repeats-associated (CRISPR)-CRISPR-associated (Cas) system has been found to have critical roles regulating bacterial physiology during environmental stress. The Type II system containing cas9 endonuclease in particular, has been exploited for binding nucleic acid sequence or cleaving specific sequence for their targets (Barrangou and van Pijkeren 2016). RNA-guided Cas9 has been used in conjugation with bacteriophage to kill virulent *Staphylococcus aureus*, but not non-virulent ones by targeting the virulence genes (Bikard *et al.* 2014), and successful antimicrobial activity against *Staphylococcus aureus* was also observed *in vivo*. RNA-guided nucleases have allowed specific drug resistant bacteria to be killed by targeting drug-resistance genes (Citorik *et al.* 2014) and showed a selective reduction of targeted strains.

Another approach has discovered the ability to re-sensitise antibiotic resistant *E. coli* using a modified CRISPR-Cas9 mediated system (Kim *et al.* 2016), suggesting that the CRISPR-cas9 system can be used to target bacterial virulence and also reverse drug-resistance with sequence specificity. CRISPR-based antibiotics have been commercially pursued by companies in France and USA.

Oligonucleotide-based targeting

The use of nucleic acid based antimicrobials for narrow-spectrum activity has been described as selectively inhibiting the translational initiation of pathogenic bacteria in mixed bacterial cultures (Mondhe *et al.* 2014), suggesting that the use of oligonucleotides as inhibitors may allow a tuneable spectrum of activity. The first ribosomal RNA synthesis inhibitor was described in a recent study, whereby a small chemical molecule inhibitor was found to bind to NusB and prevented the formation of NusB-NusE heterodimer, which regulates the assembly of rRNA

transcription antitermination complex to allow transcription of rRNA genes (Yang *et al.* 2017). Such an inhibition in turn reduced the synthesis of rRNA and affected cell viability. Inhibition of *Staphylococcus aureus* was observed when compared to other ESKAPE pathogens whilst showing no significant toxicity to mammalian cell lines, though NusB/E are also highly conserved among bacteria (Yang *et al.* 2017). An antivirulence agent of Ebselen targeting major *C. difficile* virulence factor toxin B was shown to reduce disease pathology in host tissues against an *in vivo* mouse model of *C. difficile* infection (Bender *et al.* 2015) via multiple mechanisms of action. For the above studies, further testing on a native mixed bacterial community is required to evaluate their target specificity and their impact on the commensal bacteria.

A *staphylococcus*-selective antimicrobial designed to inhibit key components in the fatty acid synthesis of *Staphylococcus* spp. has shown minimal disturbance of the gut microbiota abundance and composition compared to an antibiotic control (Yao *et al.* 2016). This highlights the target-specific approach that can be utilised as an alternative to broad spectrum antibiotics and thus may minimise disruption of the microbiome.

Other groups have also been studying nanoparticle delivery to target bacteria; magnetic nanoparticles encapsulated with broad spectrum antimicrobial peptides have been studied for an infection site-targeted approach (Maleki *et al.* 2016). Furthermore, silver nanoparticles have been coupled with siRNA gene silencing to demonstrate siRNA-driven activity against *Bacillus subtilis* targeting bacteraemia (Sun *et al.* 2016). Though this approach is theoretically target specific, the total bacterial profiles were not evaluated in the mouse model.

Antibiotic resistance is one of the most serious health threats we face as a society. Factors that influence successful treatment of microbial infection includes the host, the bacterial target or the constituent gut microbiota, and the drug itself (Nemeth *et al.* 2015). The extensive use of antibiotics over the last 80 years has progressively lead to an increased rate of drug resistance and also deaths related to drug-resistant pathogens. Taken together with the negligible amount of new antibiotic discovery and the rate of bacteria developing antibiotic resistance, we will run out of effective antibiotics soon (Langdon *et al.* 2016).

The development of bactericidal compounds with higher specificity is needed to minimise collateral damage to commensal gut microbiota. The potential to develop DNA-based antimicrobials with a narrow spectrum is a novel way to engineer the gut microbiota with predictive effects on human health. Specifically targeting a narrowly selected group of the bacterial population by blocking transcription of genes, and also to minimise the alteration of

bacterial composition and diversity could be an effective approach in the future for selective antimicrobial targeting, which will be further discussed in the next section.

1.3. Antimicrobial system used in this thesis

1.3.1 Transcription Factor Decoys (TFDs)

A transcription factor (or sequence-specific DNA-binding factor) is a protein that controls the rate of transcription of genetic information from DNA to messenger RNA by binding to a specific DNA sequence. In turn, this helps to regulate the expression of genes near that sequence. Transcription factors work alone or with other proteins in a complex by promoting (as an activator), or blocking (as a repressor) the recruitment of RNA polymerase to specific genes. A defining feature of transcription factors is that they contain at least one DNA-binding domain (DBD) which attaches to a specific sequence of DNA adjacent to the genes that they regulate.

Transcription factor decoys (TFDs) are nucleic acids that contain the binding site for a transcription factor. When introduced into cells, they act as competitive inhibitors for the binding of the transcription factor to its genomic target and so modify the regulation of a targeted gene (Mann and Dzau 2000) (Figure 1.3).

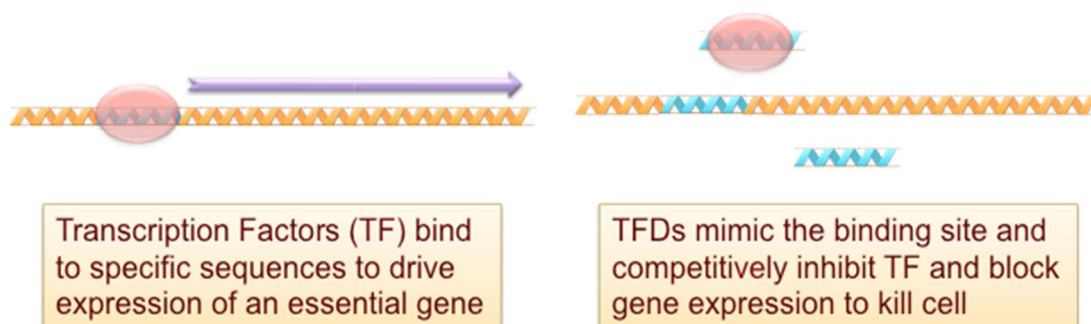


Figure 1.3 The mechanism of Transcription factor decoy (TFD) acting on transcription factors of interest. TFD competitively inhibits the transcription factor binding sites to block gene expression, resulting in the destruction of bacteria cells (McArthur 2009b).

TFDs have distinct advantages over other DNA-based therapeutics including plasmids containing transgenes for gene therapy, oligonucleotides for antisense and antigene applications (Crooke 1998), ribozymes, DNazymes, aptamers, and small interfering RNAs (siRNAs) (Stull and Szoka 1995, Patil and Burgess 2003). The mechanism of action for TFDs is simple and predictable - they control gene expression by sequestering transcription factors, preventing the latter from binding to promoters by flooding the cell with sufficient copies of the specific binding sequences (hence,

the term “decoys”). This is in contrast to antisense strategies where targets are difficult to define due to the complex secondary structure of mRNA. In comparison to antisense approaches, TFDs have the further advantages in that they act rapidly, preventing the expression of genes, whereas antisense approaches deal with the consequences of expression. As a result, TFDs are effective at much lower concentrations, because a single TFD-transcription factor interaction can block the transcription of a single gene that otherwise may have given rise to many thousands of copies of mRNA, which constitute the targets for the antisense approach.

TFDs also have advantages over both traditional antibacterial and other types of biologics, including antibodies and antisense molecules, because they act on multiple, novel targets. The novelty of the targets ensures that the treatments will not be susceptible to extant resistance mechanisms nor can resistance be readily acquired by the pathogen due to horizontal gene transfer. They can act on multiple targets (sets of co-ordinately regulated genes) hence they greatly reduce the chance of resistance arising as it would require the acquisition of multiple mutations at each, or the majority, of targets.

TFDs have been previously developed to inhibit a number of pathogens, most notably treatment of MRSA sepsis infections and also to prevent growth of the Gram-negative *Pseudomonas aeruginosa in vitro* (McArthur 2014). A transcription factor decoy (TFD) is an oligonucleotide designed to bind to and sequester targeted transcription factors and to prevent the expression of essential genes, ultimately leading to death of the targeted cell or organism. Gram-negative bacteria are of particular concern because their outer cell wall protects them against most of the antibiotics, detergents and chemicals used as treatments. This outer cell wall consists of a lipid bilayer and is a selective permeable barrier that excludes compounds with molecular weights above 800. However, many small molecules can pass through the outer membrane via various types of pores. As a result, many commonly used antibiotics are not effective against Gram-negative bacteria. Fortunately, there are a few antibiotics which do work against them, but these are a small number of therapies – and the clinical pressure to deliver treatments, in consideration of a concomitant danger of misuse – makes the rise of resistance more likely to happen and thus it will be more difficult to cope with when it does (Rice 2009).

1.3.2 TFD designed against *Enterobacteriaceae*

Enterobacteriaceae are a family of Gram-negative bacteria that are of particular relevance to the present thesis. Indeed, several *Enterobacteriaceae* strains have been isolated which are resistant to antibiotics including carbapenem, which are often claimed as "the last line of antibiotic defence" against resistant organisms. A couple of TFDs with varying antimicrobial spectrum has been designed that could exert antimicrobial activity against *Enterobacteriaceae*.

The first one being Gram negative sigma factor (GNSig) TFD, which competitively inhibits alternative sigma factor 54 in Gram negative bacteria, including *Enterobacteriaceae*. Alternative sigma factor is an RNA polymerase sigma subunit that is highly conserved throughout the bacterial genome, which is critical for the initiation of gene expressions. It contributes to virulence in Gram negative pathogens (Kazmierczak *et al.* 2005) and has been found to have an important role in regulating stress resistance (Riordan *et al.* 2010). The inhibition of such transcription would, for example, reduce viability during osmotic stress. However, the antimicrobial spectrum of the TFD span a variety of Gram negative bacteria (Kazmierczak *et al.* 2005) and may not show *Enterobacteriaceae*-selective reduction, though this TFD can be used initially for the establishment of methods and techniques.

Another TFD was designed to competitively inhibit the fumarate and nitrate reductase (FNR) transcription factor of *E. coli*, which is a homologue of the cAMP receptor protein (Crp), which coordinates the switch between aerobic and anaerobic respiration. An internal hexaethylglycol linker is used for this TFD. The FNR transcription factor also coordinates numerous virulence factors (Barbieri *et al.* 2014). The N-terminal sensory domain of the transcription factor binds either a $[4\text{Fe-4S}]^{2+}$ or a $[2\text{Fe-2S}]^{2+}$ cluster (Beinert and Kiley 1999). Under anaerobic conditions, $[4\text{Fe-4S}]^{2+}$ predominates and this drives the formation of FNR dimers that bind to their genomic consensus site 5'- TTGATnnnnATCAA-3' (Spiro 1994) to control expression of up to 115 operons involved in anaerobic respiration (Constantinidou *et al.* 2006). Expressed in another way, the FNR TFD targets facultative anaerobic bacteria (Figure 1.4). This group of bacteria makes adenosine triphosphate (ATP) by aerobic respiration if oxygen is present, but is capable of switching to anaerobic respiration if oxygen is absent. In contrast, an obligate aerobe cannot make ATP in the absence of oxygen and obligate anaerobes die in the presence of oxygen.

The FNR transcription factor is highly conserved in *Enterobacteriaceae* and other γ -proteobacteria. For example, in *Pseudomonas aeruginosa* two homologues exist, ANR and DNR that share the *E. coli* binding site (Winteler and Haas 1996), and are similarly involved in anaerobic respiration, particularly bacterial denitrification as they sense the level of nitrogen oxides directly

(Giardina *et al.* 2008). These homologues are involved in determining the virulent characteristic of the pathogen by regulating quorum sensing and biofilm formation (Fink *et al.* 2007) which are key properties. The transcription factor is also involved in the switch of the bacteria to a virulent character and is upregulated in infection models of cystic fibrosis (Platt *et al.* 2008). Homologues of the Crp-FNR superfamily occur in most bacterial families, including those containing obligate anaerobes, although both the binding site and regulatory function of these transcription factors have changed in comparison to the *E. coli* FNR (Matsui *et al.* 2013).

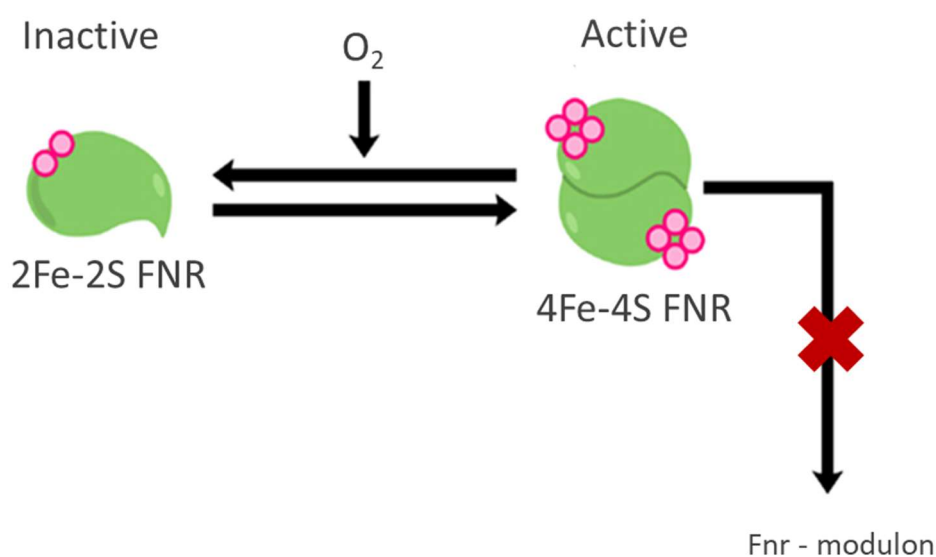


Figure 1.4 FNR is involved in the switch between aerobic and anaerobic respiration in facultative anaerobic bacteria. Under anaerobic conditions, 4Fe-4S FNR is active and drives the *fnr* modulon. FNR TFD is designed to inhibit the growth of *Enterobacteriaceae* by blocking the transcription of these genes. Figure was adapted from Förster *et al.* (2014).

1.3.3 Delivery molecule

While it may be possible to deliver a bacterial TFD to its intended target, the bacterial TFD may be part of an antibacterial complex that includes one or more delivery components. Delivery of a TFD through the bacterial cell wall is a considerable challenge, although transfection of bacteria with oligonucleotides poses notably different and fewer challenges than it does for eukaryotes. In the case of *Staphylococcus aureus*, delivery through a 20-40 nm peptidoglycan layer and a single phospholipid bilayer is required (Silhavy *et al.* 2010), both of which are typically negatively charged, whereas for *C. difficile* the outer capsule consists of a dense proteinaceous shell, termed the S-layer, which in Atomic Force Microscopy (AFM) images resembles a closely woven matrix. Cationic peptides have previously been used to deliver modified and neutrally charged antisense oligonucleotides to various bacteria (Ghosal and Nielsen 2012, Järver *et al.* 2012). However,

because TFDs may be synthesised with an unmodified backbone, they may retain their negative charge which is an important component driving DNA-protein interactions. Such molecules will readily precipitate if mixed with cationic delivery peptides, making their formulation difficult. An appropriate delivery particle for TFDs needs to protect a non-modified oligonucleotide from degradation in blood and other fluids, bind the oligonucleotide with high efficiency and selectively transfect bacteria.

Ideally, the delivery moiety is, or is part of a nanoparticulate delivery system consisting of a quaternary amine compound or a bis-aminoalkane and unsaturated derivatives. The term aminoalkanes refers to amino groups (preferably tertiary amino groups) that form part of a heterocyclic ring. The delivery component associates with the phosphate backbone of the TFD to shield the TFD's charge and to protect it from degradation in biological fluids, whilst allowing passive transport across bacterial membranes to deliver the TFDs into the cytoplasm of the cell.

As with all oligonucleotide therapeutics, delivery is a challenge: a large and negatively charged molecule must be delivered to the bacterial cytoplasm, through the negatively-charged bacterial cell envelope. Previous work has used nanoparticles formed from a bolaamphiphilic lipid (Fuhrhop and Wang 2004), 12-bis-THA. This molecule consists of two tetrahydroacridinium (THA) head groups, with delocalized cationic charge, connected by linear aliphatic chain of 12 methylene groups (Figure 1.5). THA binds tightly to and condenses DNA, presumably through a combination of electrostatic forces and intercalation (Kuruvillea *et al.* 2005). Additionally THA, and other similar compounds, bind to anionic phospholipids typical of prokaryotic membranes, most typically cardiolipin (Weissig *et al.* 2000, Mamusa *et al.* 2016), as part of the delivery mechanism to the bacterial cytoplasm. The poor aqueous solubility of these compounds drives self-assembly to sub-micromolar particles that bind oligonucleotides with high affinity to protect them against degradation (Mamusa *et al.* 2016, Marín-Menéndez *et al.* 2017). However, a key property of these particles that needs to be improved is their stability, as currently they readily form aggregates. To this end a structure activity relationship study was performed to better understand the key parts of the molecule driving the formation of the particles. A similar bolaamphiphile, dequalinium, was studied; it is a recognised antibacterial agent and also has been investigated as a gene delivery agent to mitochondria, which also harbour anionic phospholipids (Weissig *et al.* 2000, Montis *et al.* 2014). However, the particles formed by dequalinium showed a high polydispersity index (PDI) and their colloidal stability was compromised by dilution. A key improvement was extending the polycyclic system of the head group from a 2-ring quinolonium to a 3-ring THA. The resultant molecule was found to have approximately a 60-fold higher binding capacity for plasmid DNA and

is six-fold better than the commercially available transfection agent Lipofectamine (Weissig *et al.* 2001).

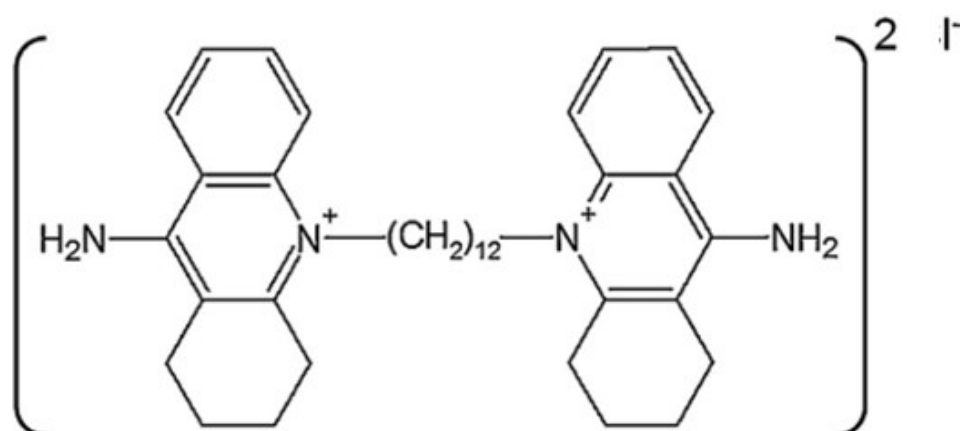


Figure 1.5 Chemical structure of bolaamphiphilic lipids, 12,12'-(dodecane-1,12-diyl)bis(9-amino-1,2,3,4-tetrahydroacridinium), referred to as 12-bis-THA, used for the assembly of nanoparticles (McArthur 2009b), figure was adapted from Mamusa *et al.* (2016).

1.3.5 Functional interaction between the delivery particle and Transcription Factor Decoy

To protect TFD from rapid degradation by biological nucleases for successful delivery, TFDs are encapsulated in bolaamphiphilic molecules. The encapsulation transcription factor decoys (TFD) with 12-bis-THA were achieved through self-assembly, referred to as loaded nanoparticles (LNPs) (Figure 1.6). TFDs are condensed in a nanoparticulate complex which improves stability in biological fluids and crucially transfects the bacterial cell membrane in order to deliver TFD to the bacterial cytoplasm (McArthur 2009b). By coupling TFD with the delivery molecule 12-bis THA (i.e. LNPs), they have shown successful transfection activity *in vivo* (McArthur 2014). They were potent and active against a wide range of pathogens, including multi-drug resistance strains. It has been shown that nanoparticulate delivery triggers a genetic response mediating cell wall stress in the bacteria; it is these genes which the TFDs are designed to block giving a rapid, bactericidal effect.



Figure 1.6 Loaded nanoparticles are comprised of transcription factor decoy oligonucleotides that define the antimicrobial spectrum, which are encapsulated by delivery nanoparticles to target bacteria.

From recent studies on bacteria and synthetic membrane models, it was shown that the mechanism of TFD delivery to bacterial cytoplasm is connected to cardiolipin (CL), an anionic lipid that is abundant in prokaryotic membranes (Marin-Menendez *et al.* 2017). Cardiolipin content has been shown to be related to osmotic stress. As osmotic stress is imposed upon *E. coli*, cardiolipin level increases as the phosphatidylglycerol (PE) levels decrease on the bacterial membrane (Romantsov *et al.* 2009). It was hypothesised that as bacterial membrane reorganises itself, membrane permeability increases, which allow TFD to be released from the nanoplexes into the cytoplasm.

1.3.6 Established knowledge on TFD antimicrobials on toxicity and in vivo animal studies

DNA-based therapy has emerged as a new class of therapeutic agents of high potential, as oligonucleotides are designed to be highly specific to sequencing data from the bacteria target, with low predicted toxicity and can be manufactured relatively inexpensively through chemical synthesis and biological replication (McArthur 2009b). Since DNA is a ‘natural’ compound, research and development on target identification, lead compound discovery and medicinal chemistry phases of a conventional drug development are truncated and allow rapid discovery of new drugs.

The nanoparticulate antimicrobials are currently undergoing preclinical development for several indications, including a treatment for *Clostridium difficile* infection. It was shown in animal studies that the NPs could be delivered to the stomachs of Golden Syrian Hamsters and maintain good activity to the extent that TFD antibacterials successfully cleared a severe gut infection equivalent to vancomycin activity (McArthur 2009a), which provide good evidence that NPs are well suited to the treatment of gut disorders.

1.4 Potential bacterial targets for microbiota engineering for TFD antimicrobials

Given the scarcity of treatment against Gram negative bacteria e.g. *Salmonella* and *E. coli* in the gastrointestinal tract, the development of a novel treatment against Gram negative bacteria is highly desirable. Unlike Gram positive bacteria, the lipopolysaccharides and proteins present on the outer membrane of Gram negative bacteria, forming a low permeability barrier, and thus make it difficult for antimicrobials to penetrate the bacterial cell (Zgurskaya *et al.* 2015). The discovery of new antimicrobials effective against Gram negative bacteria is therefore a major challenge and an urgent advancement of new antimicrobial agents is required (World Health Organisation 2017). TFD technology has shown successful delivery to a wide range of Gram positive bacteria including MRSA and *C. difficile* (McArthur 2014). It would be worthwhile to investigate whether our nanoparticulate delivery system could penetrate the Gram negative cell walls and successfully deliver the transcription factor decoy within Gram negative bacteria (see Section 1.3.2).

1.4.1 Enterobacteriaceae

Enterobacteriaceae are key members of the gut microbiota; a vast variety of genera within the family are gastrointestinal pathogens (e.g. *Salmonella* and *Shigella*) and commensal bacteria (e.g. *Klebsiella*, *Enterobacter* and *Escherichia*) that could be opportunistic and associated with disease when occasion arises (Hooper and Gordon 2001).

E. coli is a Gram negative, non-sporulating, facultative anaerobe that is commonly found in the human intestinal tract (Eckburg *et al.* 2005), where it is most abundant in the small intestine (Zoetendal *et al.* 2012). Though it only constitutes 0.1% of the human colon microbiota, *E. coli* provides a protective effect to the healthy balance of the gut microbiota by preventing the colonisation of pathogens in the intestinal mucosa and supplying supplementary nutrients and enhancing the acquisition of nutrition in humans (Reid *et al.* 2001). It is the most-studied bacterial organism and has played a pivotal role in microbiology and biotechnology following extensive studies of its genome.

Certain pathogenic strains of *E. coli* can be opportunistic and can cause disease when the body's immunological tolerance is compromised (Belkaid and Hand 2014); pathogenic commensals such as adhesive invasive *E. coli* are found in high quantities in IBD patients (Khajah 2017) and Enterocytotoxic strains of *E. coli* in persistent diarrhoea (Sarker *et al.* 2017). An increase in

Enterobacteriaceae has also been observed in diarrhoea-dominant IBS patients (Carroll *et al.* 2012). Dysbiosis was shown in antibiotic-associated diarrhoea where Proteobacteria (including *E. coli*) were notably increased; the subsequent reduction of Proteobacteria following faecal transfer resolved the clinical complications (Shahinas *et al.* 2012, Shankar *et al.* 2014). The increase in *E. coli/Enterobacteriaceae* population may have a role in dysbiosis and disease phenotypes associated with the gut microbiota (Figure 1.7), as the alteration of *E. coli* composition has been observed to be associated with intestinal inflammatory disorders in both human and mice (Thornsberry *et al.* 1983, Campbell *et al.* 2001).

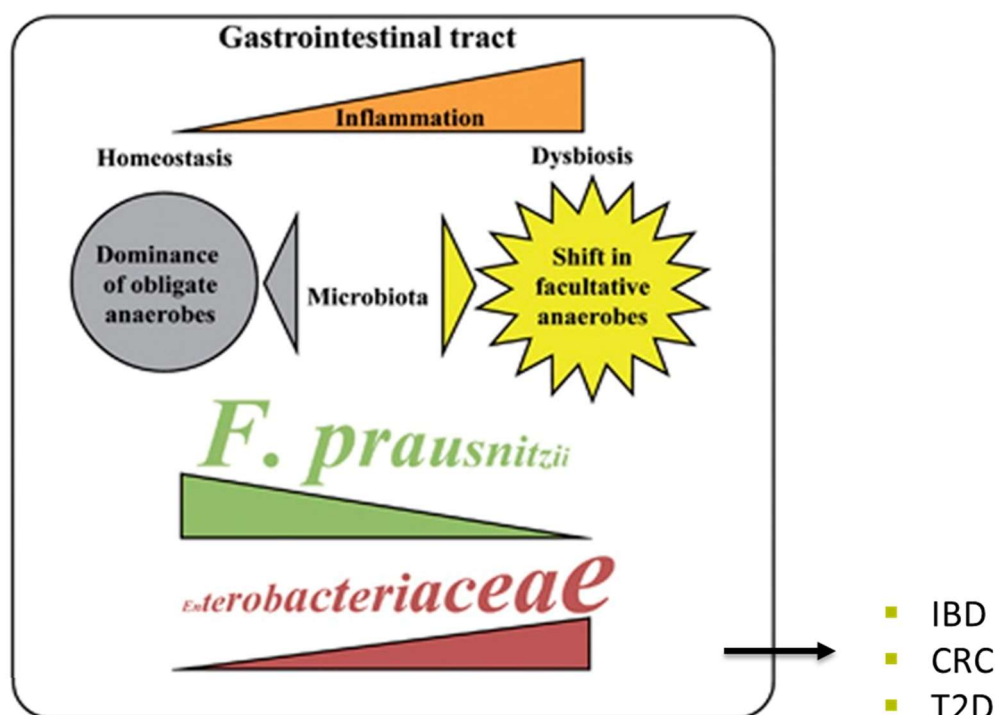


Figure 1.7 Increase in facultative anaerobes (*Enterobacteriaceae*) is associated with dysbiosis and disease development including inflammatory bowel disease (IBD), colorectal cancer (CRC) and Type 2 diabetes (T2D). Figure was adapted from Rigottier-Gois (2013).

Pathogenic strains such as AIEC are associated with Crohn's disease and colorectal cancer, and it was discovered that the common expression of haemagglutinins in AIEC correlates with its properties to adhere and invade the intestinal epithelium (Prorok-Hamon *et al.* 2013). *Enterobacteriaceae* undergo an increase in levels at the onset of Crohn's disease along with *Fusobacteriaceae*, *Pasteurellaceae*, *Veillonellaceae*, whilst Bacteroidales and Clostridiales are greatly reduced (Gevers *et al.* 2014).

A hallmark for IBD – dysbiosis, often lead to increase of Enterobacteria as other bacterial groups levels plummet (Galtier *et al.* 2017). The selective growth advantage of *E. coli* due to an increased host-derived nitrate availability has been proposed as the leading cause for inflammation-related dysbiosis (Winter *et al.* 2013).

As drug resistant bacteria become more widespread, antibiotics have become less effective. According to the World Health Organisation, *Enterobacteriaceae* is one of three bacterial groups that is considered a critical threat to human health, and which requires the highest priority in finding effective antibacterial treatment (World Health Organisation 2017). It is of interest to see if *Enterobacteriaceae* can be reduced specifically in the gut microbiota for future gut microbiota association studies.

1.4.2 Sulphate reducing bacteria

Sulphate reducing bacteria (SRB) are obligate anaerobic bacteria, although phylogenetically diverse, they share a common function in sulphur metabolism. They are capable of reducing sulphate ion for energy through sulphite reduction. This results in the formation of hydrogen sulphide (H_2S) as a by-product of respiration.

H_2S can permeate the cell membrane and has physiological importance for the gastrointestinal tract at non-toxic concentrations (Fiorucci *et al.* 2006). Though at higher concentrations, H_2S could have a negative impact on the colonic epithelial cells by inhibiting butyrate oxidation, the energy source of colonic epithelial cells (Roediger *et al.* 1993a), and by degrading the mucus layer (Ijssennagger *et al.* 2015). SRB's pro- and anti-inflammatory properties range from the promotion of inflammation in UC (Pitcher *et al.* 2000) to the resolution of colitis (Wallace *et al.* 2009) maintaining the balance of H_2S levels within physiological level is therefore important for the integrity of the gut (Feng *et al.* 2017).

Increased H_2S has been associated with UC (Rowan *et al.* 2009), increased SRB populations were also observed in faecal samples of UC patients (Pitcher *et al.* 2000). It has been shown that SRB preferentially colonises the ileal pouches of UC patients than familial adenomatous polyposis patients (Duffy *et al.* 2002). H_2S is also found to be genotoxic and causes DNA strand breakage (Attene-Ramos *et al.* 2007), cell cycle arrest at G1 and p53-induced apoptosis (Baskar *et al.* 2007). Tight regulation of the colonic H_2S level is therefore crucial to maintain intestinal integrity. *Desulfovibrio piger*, a common Gram negative SRB in the human gut, could be another possible bacterial target for IBD (Loubinoux *et al.* 2002).

1.5 Aims and objectives of the research

The aim of this project is to investigate the possibility of rebalancing the gut microbiota by selectively reducing certain bacterial groups using TFD coupled with the nanoparticulate delivery system, with minimal disruption to the rest of the gut microbiota.

Main objectives:

- 1) Investigate whether LNP loaded with TFD can act as specific antimicrobials to target *Enterobacteriaceae*.
- 2) Determine whether TFD will have minimal disruption in the commensal bacterial community.
- 3) Explore whether TFD activity *in vitro* can be translated to an *in vivo* model.
- 4) To design TFDs for other bacterial targets with functional similarities e.g. SRB and evaluate their antimicrobial activity.

General Materials and Methods

Chapter 2

Chapter 2: General Materials and Methods

2.1 Culturing bacteria

All materials were purchased from Sigma-Aldrich unless stated otherwise. Molecular biology methods are as described in Sambrook *et al* (1989) unless stated otherwise.

2.1.1 Culture media

The compositions of media used for bacteria cultures are described as follows, and dissolved in ultra pure (UP) H₂O:

Luria (L) medium (Lennox): 10 g/l Tryptone, 5 g/l Yeast extract, 5 g/l NaCl, 1 g/l D-glucose.

Luria-Bertani (LB) medium: 10 g/l Tryptone, 5 g/l Yeast extract, 10 g/l NaCl.

Solid media were prepared by adding 15 g/l agar to the appropriate medium before autoclaving.

Postgate medium C: 6 g/l sodium lactate, 4.5 g/l Na₂SO₄, 1 g/l NH₄Cl, 1 g/l Yeast Extract, 0.5 g/l KH₂P₄, 0.3 g/l sodium citrate tribasic, 0.06 g/l MgSO₄·7H₂O, 1 ml/l FeSO₄·7H₂O and 0.04 g/l CaCl₂·2H₂O. Adjust pH to 7.5 then add 0.5 g/l cysteine HCl and 4 ml/l 0.02% resazurin before autoclaving.

2.1.2 Bacterial strains and growth conditions

All bacterial strains used in this thesis are listed in Table 2.1, *E. coli*, *Desulfovibrio piger* (*D. piger*), *Desulfovibrio simplex* (*D. simplex*) and *Desulfovibrio vulgaris* (*D. vulgaris*) were obtained from in-house culture collections (QIB, Norwich, UK); some *D. piger* were isolated from human faeces in this study. Identity of bacterial strains was confirmed by 16S rRNA gene sequencing and Ribosomal Database Project for sequence match.

Table 2.1 List of organisms and growth conditions used

Strain name	Growth condition	Media
<i>E. coli</i> DH5 α	37°C, Aerobic, 250 rpm	L medium
<i>D. piger</i> UC15	37°C, Anaerobic, Static	Postgate medium C
<i>Desulfovibrio simplex</i>	37°C, Anaerobic, Static	Postgate medium C
<i>Desulfovibrio vulgaris</i>	37°C, Anaerobic, Static	Postgate medium C
SRB isolates from the human gut	37°C, Anaerobic, Static	Postgate medium C

The *E. coli* strain was stored at -80°C in 20% glycerol and grown in L media at 37°C. Sulphate reducing bacteria (SRB) were stored as freeze dried cultures at 4°C and revived before use in Postgate medium C. Cultures were then kept at 4°C in Postgate Medium C liquid media and/ or agar stab for short term storage (within 3 months).

Anaerobic bacteria were incubated in an anaerobic chamber (Don Whitney, UK), materials were generally pre-reduced overnight, except for SRB-related experiments, where materials were pre-reduced for 48 h before use, at an atmosphere of 5% CO₂, 10% H₂ and 85% N₂.

Cell density was measured with a UV/ Vis spectrophotometer at a wavelength of 600 nm.

2.2 Biological characterisation of LNPs

2.2.1 Making TFD and NPs

All reagents were filtered-sterilised (FS) with 0.2 μ m filter (Millipore) unless stated otherwise.

TFD preparation

Hairpin

10 μl of oligonucleotide was suspended in UP H₂O to a final concentration of 250 μM . It was vortexed for 5 s in a 1.5 ml microcentrifuge tube before annealing the hairpin by incubating at 95°C for 5 min and allowing to cool to room temperature. The oligonucleotide was precipitated by adding 1.5 μl of 1 mg/ml glycogen per 100 μl of sample. NaCl was added to give a final concentration of 0.5 M followed by 2 volumes of 100% ethanol (pre-chilled at -20°C). The sample was mixed and incubated at -20°C for 2 h before being spun at 16000 x g for 30 min. The supernatant was discarded and the pellet was washed with 200 μl of 70% ethanol, before further centrifugation at 16000 x g for 15 min. The supernatant was discarded and the pellet was air-dried before it was resuspended in UP H₂O. The concentration of the oligonucleotide was adjusted to 1 $\mu\text{g}/\mu\text{l}$ based on Nanodrop ND-1000 spectrophotometer analysis (Thermo Scientific) (see Section 2.6.4). The final product was checked for size and integrity by gel electrophoresis using 2% agarose with 100 bp DNA ladder as a marker before staining in ethidium bromide (1 mg/l).

Dumbbell

The two complimentary oligonucleotides were resuspended in UP H₂O to a concentration of 25 μM and annealed by incubating the mixture at 95°C for 5 min. They were allowed to cool at 1°C/min to form the dumbbell. This structure was annealed with T4 DNA Ligase (NEB) at room temperature overnight, the un-ligated oligonucleotides were removed by T7 Exonuclease digestion, before being subjected to HPLC purification. The TFD was precipitated by the addition of 0.1 volumes of NaClO₄ and 3 volumes of acetone. This mixture was vortexed before being incubated at -20°C for 15 min and pelleted. The TFD pellet was washed with 1 ml of ice-cold acetone before being washed with 1 ml of ice-cold 100% ethanol, and air-dried at room temperature. The TFD pellet was resuspended in UP H₂O at a stock concentration of 1 $\mu\text{g}/\mu\text{l}$.

Nanoparticle preparation

Nanoparticles were formed with a proprietary bolaamphiphilic lipid, developed by the industrial partner, Procarta Biosystems Limited (Mamusa *et al.* 2016, Marin-Menendez *et al.* 2017). The chemical is 12,12'-(dodecane-1,12-diyl)bis(9-amino-1,2,3,4-tetrahydroacridinium) (termed 12-bis-THA hereafter) with iodide/chloride counter ion and was synthesized by Shanghai ChemPartner.

To form nanoparticles for *E. coli*, [12-bis-THA]₂ was dissolved in dimethyl sulfoxide (DMSO) at 10 mg/ml, diluted in 50 mM MES buffer (pH 5.5) supplemented with 0.1% hydroxypropyl methylcellulose (HPMC), resulting in [12-bis-THA]₂ at a final concentration of 180 μM . To form

nanoparticles for SRB, [12-bis-THA]Cl₂ dissolved in UP H₂O at a final concentration of 180 µM and supplemented with 0.1% HPMC. The molecule spontaneously self-associated to form empty nanoparticles (ENPs). To obtain a homogenous dispersion, vigorous vortexing was performed for 30 s. The TFD-loaded nanoparticles (LNPs) were obtained by adding the TFD to MES buffer (50 mM, pH 5.5) at a concentration of 10 µg/mL before the ENP dispersion (180 µM) mentioned above.

2.2.2 Minimum inhibitory concentrations (MIC) and minimum bactericidal concentrations (MBC)

To set up MIC assay plates, 160 µl of media and 40 µl of NPs were added and mixed in the first column of wells (i.e. total volume of 200 µl) in a 96-well plate (Greiner Bio-One Ltd). For the rest of the wells, 100 µl of media was added. 100 µl of the mixture from the 1st column was added to the wells in the 2nd column (to perform a 1:2 serial dilution), samples were serially diluted across the columns until the 11th column. 100 µl of bacterial inoculum (overnight culture subcultured at 2% just before experiment) were added to the sample wells. Positive and negative controls were placed in the 12th column including media only control, bacterial inoculum with media negative control, and antibiotic positive control (25 µg/ml carbenicillin against *E. coli*, or 100 µg/ml spectinomycin against SRB). The remaining inoculum were used to determine the total viable count at the start of the experiment by 1:10 serial dilution and plating 20 µl in triplicates per dilution. The MIC assay plate were incubated with the following conditions depending on the bacterial inoculum: at 37°C at 140 rpm overnight for *E. coli*; and at 37°C anaerobic incubator, without shaking for 48 h for SRB.

For MBC, the experiment was set up as described above, the wells with no growth were plated on L agar (for *E. coli*) and incubated at 37°C overnight. Sample with the lowest concentration of NPs with no growth was considered the MBC.

2.3 Physical characterisation of LNPs

2.3.1 Dynamic light scattering for NP size measurement

Dynamic light scattering signals were detected by an EMI 9863B/350 photomultiplier on a Brookhaven Instruments Apparatus (BI 9000AT correlator and BI 200SM goniometer) as described previously (Marin-Menendez *et al.* 2017). The hydrodynamic diameter of the particles was

measured by placing 450 μl in a 1 ml plastic cuvette and a value for the polydispersity index (PDI) was derived. $\text{PDI} < 0.2$ were considered monodispersed, and the z-average was used as the measurement for particle size using cumulative fitting. $\text{PDI} \geq 0.2$ were considered polydispersed, the distribution fit method was used instead to measure the particle size obtained from size peak by intensity.

2.3.2 Flow cytometry and fluorescence-activated cell sorting (FACS)

To look at the amount of LNPs that were successfully bound to TFDs, TFD-bound NPs (NP for *E. coli* was used, see Section 2.2.1) and were sorted against the unbound equivalent by gating the populations with or without TFD (fluorescence originates from Alexa Fluor 488-TFD max excitation/emission 490/525 nm); or TFD were stained with DNA dye SYBR green (0.1X, diluted in TAE) (Life Technologies) or Acridine Orange (0.1 $\mu\text{g}/\text{ml}$) (Life Technologies) on the SH-800 cell sorter (Sony). Samples were sorted according to the 2 defined gates (mode: ultra purity, regular cell) and collected in 2 separate tubes, the sorted populations were re-run on the flow cytometer for further NP characterisation such as the amount of aggregation in the sample. The data were analysed using FlowJo software v10 (FlowJo, LLC).

2.3.3 Time course stability study using exonuclease treatment against TFD

Fetal bovine serum (FBS) was made up at 5% with UP H_2O . Different GN Sig TFD structures (5 μl) including hairpin, dumbbell and duplex were added to 495 μl of 5% FBS and incubated for 0 min, 30 min, 60 min, 90 min, 2 h, 3 h, 4 h, 5 h, 6 h and 3 days at 37°C, before analysis by 2% agarose gel electrophoresis by running 15 μl of sample with 8 μl of 2x loading buffer.

2% agarose gel was made up with 1X Tris acetic EDTA (TAE) buffer (Fisher Scientific). Gels were run at 80 V until the loading dye was two-thirds down the gel, before the ethidium bromide-stained gel was viewed under UV light.

2.3.4 Pendant Drop to measure surface tension of NPs

Theta OneAttension Optical Tensiometer was used to perform surface tension measurements. ENPs were prepared by a dispersion of DMSO solution of [12-bis-THA] I_2 or [12-bis-THA] Cl_2 in H_2O to obtain a final concentration of 0.18 mM and 0.40 mM respectively, further dilutions were performed to obtain 0.18 mM, 0.018 mM, 0.0018 mM and 0.00018 mM samples. A minimum of 2 repeated measurements were done on each sample at 25°C. For each repeat, images of an ENP droplet were recorded in a size-controlled manner at 1 frame per second for 900 s to obtain surface tension data against time using the Young-Laplace equation (Berry *et al.* 2015).

2.4 Confocal microscopy

2.4.1 Sample preparation

Bacterial cultures were grown in their appropriate media, until *E. coli* reached OD_{600 nm} 0.3-0.5 in L broth or SRB OD_{600 nm} 0.2-0.3 in Postgate medium C (Section 2.1).

Fluorescent LNPs were freshly made according to Section 2.2.1, except green fluorescent Alexa488 (max excitation/ emission 501/519 nm)-labelled hairpin TFD was used.

A ratio of 1:1 bacterial cultures and fluorescent LNPs were mixed (200 µl + 200 µl) in a 1.5 ml microcentrifuge tube and incubated in the dark while shaking for 1 h and 1 h 30 min respectively for *E. coli* and SRB (SRB incubations were performed inside the anaerobic cabinet), see Table 2.2 for details of confocal sample preparation (Marin-Menendez *et al.* 2017).

Tetramethylrhodamine conjugate of wheat germ agglutinin (TMR-WGA) (max excitation/emission 555/580 nm) (Life Technologies) and FM464-FX (max excitation/emission 565/744 nm) (Life technologies) were used to stain *E. coli* and SRB cell walls respectively at a final concentration = 10 µg/ml per 400 µl of bacteria/LNP mixture, then incubated for 30 min while shaking. Water was used as a negative control to substitute fluorescent LNPs to determine base-line fluorescence.

Samples were smeared on poly-L-lysine coated microscopy slides (Sigma-Aldrich) in quadruplicate with boundaries pre-defined with a wax pen.

Additional fixation step for SRB samples only – samples were taken out of the anaerobic cabinet and formaldehyde (at 4% final concentration) was added to the sample on the slide.

Slides were kept in the humid chamber (a box filled with wet tissues) and allowed to settle at room temperature in the dark for 30 min or 1 h respectively for *E. coli* and SRB. The slides were gently washed with FS phosphate buffered saline (PBS) and air-dried before the addition of Fluoroshield™ mounting media (Sigma-Aldrich). They were allowed to set horizontally for 15 min in the dark, at room temperature, before being stored at 4°C prior to confocal microscopy analysis. All confocal slides were analysed within 24 h of sample preparation.

Table 2.2 Difference between *E. coli* and SRB confocal sample preparation.

	<i>E. coli</i>	SRB
NPs used	[12-bis-THA] ₂	[12-bis-THA]Cl ₂
Incubation time after adding fluorescent LNP and bacteria	1 h	1.5 h
Incubation temperature after adding fluorescent LNP and bacteria	Room temperature	37°C
Membrane dye added	TMR-WGA	FM464-FX
Incubation time in humid chamber at room temperature	30 min	1 h
Fixation	NO	YES (4% formaldehyde final concentration)

2.4.2 Confocal microscopy analysis

Confocal samples were viewed on a confocal microscope (Leica SP5 II) with a 63x magnification lens in the presence of Zeiss Immersol 518F oil. A I3 filter and N21 filter were used to visualise green and red fluorescence respectively. Sequential scans were used to prevent fluorescence bleeding when more than 1 laser was used to excite the samples. All images had a format of 512x 512, zoom factor of 8 and pinhole size of 0.5 airy unit and frame average of Accu 1 unless otherwise stated. All samples were stored as .lif files on LAS AF software and images were exported as .tif files.

2.4.3 Data analysis

LAS AF-Lite and Fiji (JAVA based freeware from bioimaging website) software were used to add scale bars and to analyse confocal images by measuring the size of the bacterial cell.

2.5 Batch culture fermentation

2.5.1 Preparation of media solutions and selective agar

Batch culture fermentation were performed using a method described previously (Mandalari *et al.* 2007).

Chemostat medium: per 1 l of medium, add peptone water (2 g), yeast extract (2 g), NaCl (0.1 g), K₂HPO₄ (0.04 g), KH₂PO₄ (0.04 g), MgSO₄·7H₂O (0.01 g), CaCl₂·2H₂O (0.01 g), NaHCO₃ (2 g), Tween 80 (2 ml), vitamin K (10 µl of 0.5 v/v, dissolved in ethanol), cysteine.HCl (0.5 g), bile salts (0.5 g) and Hemin (0.02 g dissolved in 400 µl 1 M NaOH). 10 g glucose was added to the autoclaved media before use as a carbon source.

Wilkin Chalgren solid medium: 43 g/l Wilkins Chalgren Anaerobic agar (Oxoid).

Bacteroides solid medium: 28 g/l Brucella Broth (Oxoid), 15 g/l agar bacteriological (Agar No. 1) (Oxoid) and 10 ml/l hemin solution (0.5 mg/ml) were mixed before autoclave. After cooling, 200 µl/l vitamin K solution (0.5 v/v, dissolved in ethanol), 3 ml/l kanamycin (25 mg/ml), 7.5 ml/l vancomycin (1 mg/ml) and 50 ml/l laked horse blood (Thermo Scientific) were added.

Beerens solid medium: 39 g/l Columbia Agar Base (Oxoid), 0.5 g/l Cysteine HCl, 5 g/l Agar and 5 g/l glucose were boiled to dissolve ingredients. After cooling, 5 ml/l propionic acid was added and 40 ml/l NaOH was used to adjust to pH 5. No autoclaving was required.

Clostridia solid medium: 43 g/l Wilkins Chalgren Anaerobic agar (Oxoid); after autoclaving and cooling, 8 ml/l novobiocin (1 mg/ml) and 8 ml/l colistin (1 mg/ml) were added.

MRS solid medium: 52 g/l MRS broth (Oxoid) and 15 g/l agar.

MacConkey No. 3 solid medium: 51.5 g/l MacConkey Agar No. 3 (Oxoid).

Antibiotics were dissolved in UP H₂O before filter-sterilisation as follows: 1 mg/ml novobiocin, 1 mg/ml colistin, 25 mg/ml kanamycin and 1 mg/ml vancomycin and then stored at -20°C before use.

2.5.2 Inoculation of media solutions with faecal bacteria

Aliquots of 135 ml of chemostat media were added to the batch fermentation vessels and were pre-reduced by oxygen-free nitrogen with a gentle stirring overnight. Vessels were connected to water jackets filled with 37°C water for temperature control. An optimal pH of 6.8 was maintained

with an automated pH controlled system. The pH ranged between of 6.6 to 7.0 and was adjusted using 1 M NaOH and 1 M HCl.

A freshly voided faecal sample was diluted to 1:10 in a pre-reduced PBS and placed into a Seward stomach bag, before being homogenised in the Stomacher 400 circulator at 230 rpm for 45 s. 15 ml of the resulting faecal slurry was then added to each of the vessels. LNP was added to the faecal inoculum as a target-specific oligo-based antimicrobial against *E. coli*, along with control treatments scrambled LNP (SLNP) and vehicle control (containing all the components in LNP except that TFD and [12-bis-THA] was omitted), at a 2% final volume. Samples were taken at predose (before the addition of treatments), 0 h, 4 h, 8 h for viable colony counts, DNA extraction for downstream 16S rRNA gene sequencing and NMR analysis. Colonies from MacConkey No. 3 plates were also picked for 16S rRNA gene colony PCR (Chapter 2.7) to confirm the identity of the bacteria present in the sample.

2.5.3 Quantification of bacteria and analysis

Viable bacterial cell counting

Agar plates were pre-reduced in the anaerobic cabinet overnight before use. Faecal slurries were serial diluted from 10^{-1} to 10^{-7} in PBS and 20 μ l were plated at each dilution in triplicates. The colony forming units (CFU) were calculated using the formulation:

$$\text{CFU/ml} = \text{no. of colonies} \times \text{dilution factor} / \text{volume plated}$$

Dilution of selective and/or differential agar were plated at the dilutions as stated in Table 2.3.

Table 2.3 Experimental details for bacterial viable count in batch model fermentation.

Type of agar	Selective for	Incubation (days)	Dilution
Wilkins Chalgren (WC)	Anaerobes	1	-4 to -7
<i>Bacteroides</i>	<i>Bacteroides</i>	1	-4 to -7
Beerens [#]	<i>Bifidobacterium</i>	1	-4 to -7
Clostridia	<i>Clostridium</i>	1	-3 to -6
MRS	<i>Lactobacillus</i>	1	-3 to -6
MacConkey No. 3*	<i>Enterobacteriaceae</i> Pink colour: coliforms straw colour: non-lactose fermenter	1	0 to -7

* incubate at aerobic conditions

Beerens were not measured in the mouse experiment

2.5.4 NMR sample processing

For batch experiment

Samples (13 ml) were taken from the *in vitro* batch model at predose, 0 h, 4 h and 8 h. Samples were centrifuged at 5000 x g for 15 min at 4°C, then 900 µl of supernatant was transferred to 1.5 ml microcentrifuge tube (performed in triplicates for each sample), followed by the addition of 100 µl NMR phosphate buffer (0.51 g NaH₂PO₄·H₂O, 2.82g K₂HPO₄, 34.5 mg Trisodium phosphate, 100 mg NaN₃, dissolved in 200 ml D₂O). The mixtures were vortexed briefly before being frozen at -20°C until analysis.

For mouse experiment

Faecal slurry samples (diluted 1:10 in PBS) were centrifuged at 16000 x g for 15 min at 4°C. 90 µl of supernatant and 810 µl of PBS were added to each 1.5 ml microcentrifuge tube (performed in

triplicates), before 100 µl of NMR buffer was added to each of 900 µl of supernatant. The mixtures were vortexed briefly before being frozen at -20°C until analysis.

2.6 Phylogenetic analysis of bacterial communities using 16S rRNA gene sequencing

2.6.1 Propidium monoazide treatment to differentiate live and dead bacteria

Propidium monoazide (PMA) (Biotium), a cell membrane impermeable DNA intercalating agent, was used to discriminate between live and dead bacterial DNA (Lai *et al.* 2016), so that only DNA from live bacteria were amplified for downstream 16S rRNA gene sequencing. Faecal slurry diluted in 1:10 pre-reduced PBS was centrifuged at 5000 x g for 15 min at 4°C and resuspended in 500 µl of PBS. An aliquot of 1.25 µl of PMA (20 mM) was mixed with each sample in a 1.5 ml microcentrifuge and incubated on a shaker at 195 rpm in darkness for 5 min at room temperature. PMA photoactivation was performed on a Phast blue light apparatus (GenIUL) or BLU-V system (Qiagen) for 15 min. The samples were then centrifuged at 10000 x g for 8 min, and then the supernatant was removed, before the resuspension of the pellet in 978 µl of sodium phosphate buffer (buffer taken from the FastDNA SPIN kit for soil (MP Biomedicals, UK)). Samples were stored at -80°C before DNA extraction.

2.6.2 DNA extraction for bacterial community (16S rRNA gene) profiling

Genomic DNA was extracted for bacterial community (16S rRNA gene) sequencing after PMA photo-activation (section 2.6.1.) using a FastDNA SPIN Kit for soil (MP Biomedicals, UK). After each faecal suspension was being thawed, they were mixed with 122 µl of MT buffer and allowed to settle at 4°C for 1 h. Each mixture (1 ml) was next transferred into a Lysing Matrix E Tube and then lysed 3 times at 6.5 m/s with a CY: 24*2 adaptor. There were cooling for 2 and 4 min between the lysis steps respectively, using a FastPrep instrument (MP Biomedicals, UK), before next being centrifuged for 1 min at 16800 x g. Following this, the supernatant was transferred into a clean 1.5 ml microcentrifuge tube, before being mixed with a 250 µl protein precipitation solution (PPS) reagent by vigorously inverting the tube by hand for 10 times in total. Each sample was then precipitated out using centrifugation at 16800 x g for 5 min, before the supernatant was transferred into a sterile 15 ml tube. An addition of 1 ml of binding matrix was used before the tube was inverted by hand for 2 min, before being allowed to stand in a rack for 3 min, to allow the silica matrix to settle. 1 ml of supernatant was then discarded before the binding matrix was resuspended into the remaining supernatant. 600 µl of the mixture was then transferred into a

SPIN filter tube, before being centrifuged for 1 min at 14500 x g. The flow through was discarded. DNase-free salt/ethanol wash (SEWS-M) solution (500 µl) was added to the SPIN filter tube and centrifuged for 1 min at 14500 x g before the flow through was discarded, this step was performed a total of 3 times. The SPIN filter was centrifuged for a further 2 min at 14500 x g to remove residual SEWS-M wash solution and then air-dried for 5 min. For efficient DNA elution, 50 µl of Dnase/Pyrogen Free DNA elution solution (DES) was gently stirred with the matrix; each sample was left for 1 min at room temperature and centrifuged at 14500 x g for 1 min before storing the DNA at -20°C.

2.6.3 Gel electrophoresis of nucleic acids

Agarose gels were made up at a concentration of 0.8-1% (Melford), dissolved in 0.5 x Tris borate EDTA (TBE, Fisher). 2-10 µl of samples were loaded into the gel and then run against 0.5 x TBE, a final concentration of 1X gel loading buffer was then added to the sample when required. HyperLadder 1 (Bioline) or 2-Log DNA Ladder (NEB) was used whenever appropriate. The gels were run until the loading dye was two-thirds down the gel, and then stained in 1 mg/l ethidium bromide for 30 min, before being rinsed briefly in deionised H₂O, prior to being viewed under UV light on a transilluminator (302 nm). Images were then captured using the Alphaimager (Alpha Innotech).

2.6.4 Measurement of DNA concentration

Nanodrop

Nanodrop ND-1000 spectrophotometer (Thermo Scientific) was used to determine DNA using UV spectrophotometry under the nucleic acid option, measuring the absorbance at 260 nm. After the sampler was cleaned with UP H₂O, initialised and blanked, 1 µl of the sample was used for the measurement to obtain concentration in ng/µl. The quality of DNA can be confirmed by the 260/280 ratio of > 1.7.

Qubit

To make up the Qubit™ working solution (Life Technologies), Qubit™ reagent and Qubit™ buffer were mixed in a ratio of 1:200 and then kept away from light beneath foil. Standard 1 and standard 2 (10 µl) were then added to 190 µl of working solution for the calibration and 2 µl of samples were next added to 198 µl of working solution using 0.5 ml clear thin wall PCR microcentrifuge tubes. Samples were then vortexed for 2-3 s before being incubated at room temperature for 2 min before measuring the DNA concentration using Qubit.

2.6.5 Illumina Miseq sequencing settings

Paired-end 16S rRNA gene community sequencing was performed using the Illumina Miseq platform at the Earlham Institute (Norwich, UK). After genomic DNA had been extracted from faecal slurry, the 16S small subunit rRNA gene region V4 was amplified using degenerate primers 515F (AATGATACGGCGACCACCGAGATCTACACGCT XXXXXXXXXXXXX TATGGTAATT GT GTGYCAGCMGCCGCGGTAA) and 806R (CAAGCAGAAGACGGCATAACGAGAT AGTCAGCCAG CC GGACTACNVGGGTWTCTAAT), based on literature (Caporaso *et al.* 2011b, Caporaso *et al.* 2012) with modification on primer degeneracy (Aprill *et al.* 2015, Parada *et al.* 2016) and using redesigned forward-barcoded constructs (Walters *et al.* 2016). On the forward primer, the adaptor sequence was then linked to the Golay barcode, which allows identification unique to each sample. Platinum Taq polymerase (ThermoFisher) was used to amplify ribosomal gene regions (with amplicon size ~ 390 bp) using the following conditions: 94°C for 3 min; 35 cycles of 94°C for 45 s, 50°C for 60 s, 72°C for 90 s; followed by 72°C for 10 min before leaving at holding temperature of 4°C. Amplicons were quantified using Quant-iT PicoGreen dsDNA assay Kit (ThermoFisher). The amplicons were purified using MoBioUltraClean PCR Clean-Up Kit, before the concentration and A260/A280 ratio were measured for quality assurance.

2.6.6 Bioinformatic analysis of 16S rRNA gene sequencing

Quantitative Insights Into Microbiological Ecology (QIIME) was used to analyse the bacterial community (Kuczynski *et al.* 2012) extracted from faecal origin after Illumina Miseq sequencing (Section 2.6.5.). Forward and reverse reads of the samples were joined and sequences were filtered so that the sequences were between 200 bp and 1000 bp using prinseq lite. Other criteria to be met included: having an average quality score of at least 25 within a 50 bp length, read length between 200 and 1000 bp, and having an Illumina quality digit of > 0. Chimeric sequences were detected and eliminated using Usearch 6.1 (Edgar 2010) and prinseq-lite (Schmieder and Edwards 2011). Greengenes 13.8 were used to assign bacterial taxonomy among phylum to species level from the operational taxonomic units, also enabling reverse strands to be searched against the Greengenes database by uclust, with the confidence value of 50% as threshold and OTU clustered from trimmed reads at 97% identity level. Beta-diversity PcoA plots were generated by weighted and unweighted Unifrac distances and visualised in the Emperor tool (Kuczynski *et al.* 2012).

2.7 Polymerase Chain Reaction (PCR)

2.7.1 PCR preparation and conditions

To make DNA templates, single colonies were picked from an agar plate and resuspended in 10 μ l of sterile UP H₂O and heated at 95°C for 5 min before taking 1 μ l as template in each 50 μ l PCR reaction. PCR reaction were set up using GoTaq G2 polymerase (Promega) according to the manufacturer's recommendation.

For 16S rRNA gene amplification

The following primers (Sigma-Aldrich) were used to yield a 1500 bp amplicon: AMP_F 5' GAG AGT TTG ATY CTG GCT CAG T_m 60.6 or 62.9°C; AMP_R: AAG GAG GTG ATC CAR CCG CA T_m 69 or 71.4°C (Baker *et al.* 2003). Components of the PCR reaction and the PCR conditions are described in Table 2.4. A negative control was used by replacing a DNA template with UP H₂O. When the PCR reaction was completed, 10 μ l of PCR products were analysed on 1% agarose gel electrophoresis (Section 2.6.3) to check for the presence of a 1500 bp PCR product. Successfully amplified PCR products were purified by the QIAquick PCR purification kit (QIAGEN) following manufacturer's instructions and DNA was quantified by Nanodrop (see Section 2.6.4) and sequenced using the Mix2Seq kit (Eurofins) following manufacturer's guidelines.

Table 2.4 Composition of PCR reactions and PCR cycling conditions.

PCR reaction components		Quantity
DNA Template		1 μ l
5X GoTaq Reaction Buffer		10 μ l
dNTP (25 mM each) (Bioline)		0.4 μ l
Primer F (20 μ M)		1 μ l
Primer R (20 μ M)		1 μ l
GoTaq DNA Polymerase		0.25 μ l
UP H ₂ O		36.35 μ l
Total		50 μ l
PCR reaction conditions		
Temperature	Duration	No. of cycles
95°C	2 min	1
95°C	30 s	20 [#]
55°C*	30 s	
72°C	30 s**	
72°C	5 min	1

* Annealing temperature (T_A) were adjusted according to the primer T_m i.e. [MAX T_A = T_m (of the lowest pair) -3°C]

** Extension step durations were generally calculated based on 1 min/kb; for 16S rRNA gene PCR, 30 s is sufficient for a 1.5 kb elongation

20 cycles were used as a default, however, when PCR amplification was low, 25 cycles were used instead

For amplification from SRB

PCR primer *dsrB* were used to amplify SRB to obtain DNA template of the *dsrB* gene, before qPCR primers (*dsrB_Human* or *Human_desulfov*) were used for qPCR standard curve (primer details can be found in Section 2.8.3). PCR settings are described in Table 2.5.

Table 2.5 PCR conditions for different SRB primers.

	dsrB_Human F and R	Human_desulfov F and R	dsrB_F1 and R1 for UC15	dsrB_F1 and R1 for isolate 6 and 19	dsrB_F2 and R1 for UC15	dsrB_F2 and R1 for isolate 6 and 19
*Annealing temperature	49°C	52°C	62°C	62°C	55°C	55°C
**Elongation duration	20 s	20 s	54 s	43 s	54 s	43 s
No. of cycles	25	25	25	25	25	25

* Annealing temperature (T_A) were adjusted according to the primer T_m i.e. [MAX $T_A = T_m$ (of the lowest pair) - 3°C]

** Extension step durations were generally calculated based on 1 min/kb

2.7.2. Identification of bacterial isolates

After the purified PCR products were sent off for 16S rRNA gene sequencing (Section 2.7.1), data were obtained from Eurofins website and the chromatograms were checked from the .ab1 file using FinchTV software (Geospiza, Inc.). High quality sequences were trimmed, copied to Editseq (DNASTAR) and saved as .seq files; before assembling the paired forward and reverse sequence as a single contig on SeqMan (DNASTAR, Inc.) as .fas files where appropriate. The consensus sequences or single sequences (if no overlapping was possible) were exported to the Ribosomal Database Project (RDP release 11) (http://rdp.cme.msu.edu/seqmatch/seqmatch_intro.jsp) for

sequence match, using the following search options: Strain= Type and Non Type; Source= Isolate; Size= ≥ 1200 bp and Quality= good. Sequence identity of the bacterial isolates was determined based on the highest S_{ab} score (Cole *et al.* 2014).

2.8 SRB related experiments

2.8.1. Isolation and identification of human SRB

To preserve anaerobic bacteria, all reagents, apparatus and media in contact with bacteria were pre-reduced for 24-48 h prior to use. The inner region of the human faecal sample was scooped and diluted 1:10 in PBS and homogenised using a pellet pestle motor in the anaerobic cabinet. 100 μ l of the resulting faecal slurry was placed in anaerobic Postgate medium C (Section 2.1). The samples were incubated until a black precipitation was developed, indicating the presence of Fe₂S (Butlin *et al.* 1949). Serial dilution was performed on these samples from 10⁰ – 10⁷, 100 μ l of each dilution was then spread on a pre-reduced Postgate medium C agar plate. When black colonies were grown, individual colonies were streaked on a 25-grid Postgate medium C plate. Gram-staining was performed, and their morphologies were recorded. Colonies were subcultured 3 times by streaking until pure and single isolates were obtained. The SRB were stabbed in Postgate medium C agar vials for short term storages and were then freeze dried for strain archiving.

2.8.2. SRB identification

Colony identification using 16S rRNA gene

16S rRNA gene PCR was performed on isolates (Section 2.7.1), and plated on agar to check for contamination. This was performed on Wilken Chalgren (for anaerobic bacteria) and Nutrient agar (for aerobic bacteria). The identity of the SRB isolates was then analysed following steps described in Section 2.7.2. The 16S rRNA gene sequences that had the same species identity were then further aligned to check whether they were the same strain using Seqman, and finally, the level of confidence in the nucleotide matcher was cross-checked with the original .abi file.

Aligning *dsrB* gene sequences of SRB human isolates

Clustal omega was used to align nucleotide sequences from human SRB isolates, then alignments were imported to Genedoc for visualisation. The nucleotide sequence was then translated to amino acid sequence in Editseq in three different frames, before being searched for on Blastp to examine their identity against known proteins. The amino acid sequences were also uploaded to Genedoc to compare any difference in protein sequence for different SRB strains.

Gram staining

Gram staining was performed to visually distinguish whether the human SRB isolates were Gram-positive or Gram-negative depending on the difference in the cell walls. Working in the anaerobic cabinet, a loopful of water was spread across a clean glass slide. A single colony was selected using a disposable sterile loop and emulsified, before the slides allowed to air dry. The slides were then taken out of the anaerobic cabinet and the dried films were passed through the Bunsen flame briefly for heat fixation without direct contact with the flame. The samples were stained with Gram stain reagents (Remel Europe Ltd) as follows: first, samples were stained in crystal violet solution by flooding the slide for 1 min, before being washed briefly with tap water for no more than 5 s and then drained. Slides were then flooded with Gram's Iodine solution and allowed to mordant for 1 min before being washed off with water and then drained. Excess water on slides was removed with blotting paper, before the slides were next flooded with 95% ethanol for 10 s for decolourisation. This was then being washed off with tap water before being drained. For counterstaining, slides were flooded with safranin solution for 30 s before being washed off with water and then drained. Samples were blotted dry using lens paper (Kimberly-Clark Professional) and care was taken not to rub the samples. The slides were then examined with a 100X 1.35 oil immersion lens on an Olympus BX60 light microscope (Olympus) using bright field illumination.

2.8.3. qPCR Primer Design

PCR primers which amplify the near-full length *dsrB* gene were designed using Primer 3 <http://primer3.ut.ee> based on *dsrB* gene from *D. piger* UC15, default settings were used except for product size range= 301-1000 to cover the full length of *dsrB* gene. The prospective primer sequences were checked against the human_*desulfov* alignment to see if it would amplify other *Desulfovibrio* species. Oligo Calc <http://biotools.nubic.northwestern.edu/OligoCalc.html> and Sigma-Aldrich OligoEvaluator <http://www.oligoevaluator.com/Login.jsp> were used to predict primer properties e.g. the presence of hairpin formation and secondary structures. The general criteria included avoiding runs of three nucleotides; having GC rich 3' ends for both the forward and reverse primer for the last three nucleotides (i.e. no more than five nucleotides); having a 100% matched sequence especially on the 3' end of the primer and avoiding degenerate nucleotides if possible; avoiding primer-dimer by making sure the last three nucleotides at the 3' of the two primer sequences were not complementary to one another; having optimal primer length of ~18-22 bp and optimal T_m at 52-58°C with GC content at 40-60%. For the purpose specific to these primers, the PCR amplicon had to flank and allow extra nucleotides on either side

of the PCR amplicon result from the SYBR green qPCR primers as described above. Primers were ordered from Sigma-Aldrich, resuspended in sterile UP H₂O and stored at -20°C.

PCR primers used to amplify the whole *dsrB* gene is as follows:

dsrB_F1: 5' TACAATCCCGCCAAACCGAT 3'; T_m 68.2°C

dsrB_F2: 5' ACCATGTCCATCACCCACA 3'; T_m 65.1°C

dsrB_R1: 5' GGAGGTTTCGTTGGGGATGTA 3'; T_m 65.9°C

Several SYBR green-based qPCR primers were designed to amplify the *dsrB* gene in SRB found in humans. A literature search was performed to look for common SRB found in human gut microbiota (Loubinoux *et al.* 2002, Jia *et al.* 2012, Nava *et al.* 2012, Rey *et al.* 2013).

The National Center for Biotechnology Information (NCBI) protein database was then used to obtain *dsrB* gene sequences from SRB. Complete sequences were picked and the coding nucleotide sequences were selected and aligned using clustal W2 (<http://www.ebi.ac.uk/Tools/msa/clustalw2/>). The sequence similarity was manually checked and alignment improved using Genedoc (Nicholas *et al.* 1997). Based on the alignment of the (i) common SRB in human gut; and (ii) common *Desulfovibrio* spp. in the human gut, qPCR primers were designed with the following criteria: Primers were designed based on the regions with the highest sequence similarity between the bacterial species, one from the forward strand and one from the reverse strand. Wherever possible, primers sequence were at least 18 nucleotides long (with a minimum of 15 nucleotides), with an amplicon size of 40 – 300 bp. Whenever appropriate, nucleotides with less degeneracy were preferred, with no more than 6 degenerate nucleotides in a primer sequence. Primers were ordered from Eurofins Genomics and resuspended in sterile UP H₂O and stored at -20°C.

qPCR primers used to quantify SRB are described below:

Human_desulfov F: 5' TGCGACATCGCCGACAA 3'; T_m 55.2°C

Human_desulfov R: 5' CGCACATGTTKATGCAGC 3'; T_m 55.6°C

Or

dsrB_Human F: 5' TGCGAYATYGBGACAA 3'; T_m 52.0°C

dsrB_Human R: 5' RCACATGTTBAKGCAGCA 3'; T_m 52.9°C

2.8.4. Quantitative PCR (qPCR)

To quantify SRB from human faeces using qPCR (Fuller *et al.* 2007), PCR primers dsrB_F1 and dsrB_R1 (Section 2.7.3) were used to first amplify the *dsrB* gene following the method as described in Section 2.7.1 above, except PCR products were eluted using sterile deionised H₂O following PCR purification, quantified by Qubit (Section 2.6.4) and then the copy number was adjusted to 10¹⁰ using Copy Number Calculator <http://scienceprimer.com/copy-number-calculator-for-realttime-pcr>. After a serial 10-fold dilution, they were then used as the qPCR template to have copy numbers between 10⁰- 10¹⁰. SYBR green-based primers dsrB_Human and Human_desulfov (see Section 2.7.3) were used to generate standard curves against different SRB strains on the qPCR machine (ABI7500 Taqman). The qPCR standard curved experiment were performed using QuantiFast SYBR Green PCR kit (Qiagen); the qPCR reaction mix and reaction conditions are listed in Table 2.6. The standard curves were analysed using 7500 Software v2.0.6 using the auto threshold cycle (C_t) value. The C_t value at the auto threshold were plotted against the log₁₀ copy number of the starting template to deduce the r² value of the linear regression and efficiency of the primers for each bacterial strain using the formula efficiency= 10^(-1/slope)-1.

Table 2.6 a) qPCR reaction mix and b) reaction conditions.

a

Reagents	volume added
SYBR green master mix (Qiagen)	5 μ l
Human_desulfov forward primer (10 μ M)	0.5 μ l
Human_desulfov reverse Primer (20 μ M)*	0.5 μ l
UP H ₂ O	2 μ l
DNA template	2 μ l
Total	10 μl

*20 μ M of reverse primer was used to ensure equal molar of Human_desulfov forward and reverse primer with 100% match.

b

Reaction temperature	Duration	No. of cycles
95°C	5 min	
95°C	10 s] x 40
60°C	35 s	
95°C	15 s	
60°C	1 min	
95°C	15 s	
60°C	15 s	

2.8.5. Genomic DNA extraction of SRB

After bacterial cultures were grown, cells were centrifuged at 3000 x g for 10 min before performing genomic DNA extraction using the chloroform method (Bruce M. Pearson, personal communication). Supernatants were discarded and the pellets were resuspended in 1 ml of PBS before being transferred to a 2 ml screw-cap tube. The cell suspensions were further centrifuged at 13000 x g for 3 min at 4°C. Supernatants were discarded and the pellets resuspended in 400 µl elution buffer (EB) (10 mM Tris-Cl, pH 8.5). 70 µl 10% (w/v) sodium dodecyl sulphate (SDS) and 5 µl 10 mg/ml proteinase K were then added to the resuspension, and then mixed by inversion before incubating at 65°C for 10 min. 100 µl 5M NaCl was mixed in to the samples and 100 µl of 65°C -preheated 10% cetyltrimethylammonium bromide (CTAB) in 0.6 M NaCl was next added. The samples were vortexed until white suspensions were formed, and were then incubated at 65°C for 10 min. Chloroform/isoamyl alcohol (24:1) (500 µl) was next added to the samples, vortexed for 10 s and then centrifuged at 13000 g for 5 min at 4°C. The upper aqueous phase was transferred to a fresh microcentrifuge tube, to which a 0.6 volume of isopropanol was added. Samples were mixed and incubated for at least 30 min before a 10 min centrifugation at 13000 g. The supernatant was discarded, and the pellet was washed with 500 µl of 70% (v/v) ethanol (precooled at 4°C). The samples were centrifuged again briefly, to remove the residual supernatant with a pipette. The pellet was air-dried and resuspended in 50 µl EB supplemented with 1 µl of 10mg/ml RNase A, and incubated at 37°C for 30 min. 5 µl of 3 M sodium acetate pH 8.0 and 100 µl of ice-cold ethanol (pre-cooled at -20°C) were gently added at the side of the tube, and gently mixed by flicking the tube. The DNA was spooled onto a fine glass pipette tip and lightly dipped into a tube filled with 70% ethanol to wash the pellet. The pellet was then dissolved in 50 µl of fresh EB and the resulting DNA was stored at -20°C.

2.9 Mouse model experiment

2.9.1. Animal Model and experimental design

The animal work was done under approved home office animal licence and was performed by a personal license holder (Devina Divekar). Consideration of animal welfare was conformed under home office guidelines to minimise harm on animals.

Wild type C57BL/6J mice littermates were bred and caged at the Disease Monitoring unit (University of East Anglia, Norwich) until 8 weeks old before the experiment commenced. Faecal pellets were collected three days before the start of experiment to record baseline *E. coli* levels.

On the day of the experiment, 100 μ l of LNPs were administered using oral gavage tubes (Linton Instrumentation) both at 0 h and 2 h, faecal samples were collected at each time point according to the dosing regimen (Table 2.7); faecal pellets were diluted 1:10 by pre-reduced PBS and vortexed for 60 s to obtain faecal slurry. The resultant samples were used for viable bacterial plate counting (Section 2.5.3), faecal water preparation for metabonomic analysis (Section 2.5.4) and phylogenetic analysis of bacterial communities using 16S rRNA gene sequencing (Section 2.6).

Table 2.7 Details for each mouse experiments including treatment group, dosing regimen and faecal pellet collection.

Mouse experiment	Treatment groups	Time points of oral gavage (100 μ l)	Time points for faecal pellet collection
Experiment 1	Vehicle control (0.7% (w/v) saline); Scrambled LNP (15 μ g/ml); LNP (15 μ g/ml)	0 h and 2 h	0 h, 2 h, 4 h, 6 h, 24 h
Experiment 2	Vehicle control (0.7% (w/v) saline); LNP (3 μ g/ml); LNP (15 μ g/ml)	0 h and 2 h	0 h, 4 h, 6 h, 8 h, 24 h

2.9.2 Sample processing and storage conditions

When the experiment ended at 24 h, mice were euthanised and dissected. Colon tissues were collected and stored appropriately for further analysis. Colon intestine was stored in Neutral buffer formalin (NBF) for paraffin tissue sectioning. Storage methods for each samples are described in Table 2.8.

Table 2.8 Sample processing for mouse experiment.

Samples	Storage	Pre-fill with
Faecal pellet collection	Room temperature	-
Colon for histological analysis	Shake O/N, then changed to 70% ethanol, rock for 30 min before changing 70% ethanol again and shake O/N, then store at 4°C until paraffin embedding	4 ml 10% NBF

Colon were dehydrated after initial fixation from NBF (see Table 2.8 above) and encased in tissue cassettes (Thermo Fisher Scientific), labelled using lead pencil and placed in metal racks. Tissues were then immersed in 70% ethanol to prevent them from drying out. Cassettes were left in the tissue processor (Leica ASP300S) overnight where tissues were cycled through 70%, 80%, 90% and 100% ethanol, before xylene and paraffin wax (Paraplast) (Sigma-Aldrich), details of steps and duration can be found in Table 2.9.

Table 2.9 Reagents used for paraffin tissue processing.

Reagents used to immerse tissues	Duration
70% Ethanol	1 h
80% Ethanol	1 h 30 min
90% Ethanol	2 h
100% Ethanol	1 h
100% Ethanol	1 h 30 min
100% Ethanol	2 h
Xylene	30 min
Xylene	1 h
Xylene	1 h 30 min
Paraffin wax	1 h
Paraffin wax	2 h
Paraffin wax	2 h

The processed tissues were transferred to the embedding station (Leica EG1150H), cut into sections, positioned and then embedded in paraffin wax. The samples were cooled and stored at 4°C before tissue sectioning.

Cross sections of tissues embedded in paraffin were prepared with a thickness of 5 µm with a rotary Microtome (Leica RM2235) using disposable microtome blades (Thermo fisher Scientific), for downstream histological analysis.

Haematoxylin and eosin staining

Cross sections of the tissues having been cut were then placed in a glass slide container and stained by being immersed in solutions for a set period as follows: Briefly, samples were de-waxed in two separate containers containing HistoClear (National Diagnostics), for 5 min each, then the

tissue sections were rehydrated by using descending concentrations of ethanol (100%, 80% and 70% respectively) for 2 min each. Slides were subsequently immersed in distilled water for 5 min. Slides were then stained in Haematoxylin (Sigma-Aldrich) for 5 min and the bluing step was performed by washing slides under running distilled water to allow haematoxylin colour to develop. Samples were then treated in 1% HCl (dissolved in 70% ethanol) for 15 s, then briefly rinsed in distilled water. Slides were then incubated in 0.1% sodium bicarbonate, and were gently rinsed under running distilled water for 5 min, before being stained with Eosin (Sigma-Aldrich) for 30 s. The slides were dehydrated with ascending ethanol concentration (i.e. 70%, 80% and 100%) for 2 min each, before being immersed in Histoclear solution for 5 min twice in two separate containers. Excess Histoclear was tapped and wiped off on the slide without touching the tissues. A drop of Neo-Mount[®] mounting medium (Merck Millipore) was used on each tissue section before it was left to dry for a few hours, prior to being viewed on microscope.

2.10 Statistical analysis

GraphPad Prism 5.04 (GraphPad Software) was used to perform all statistical analyses in the thesis. All statistical analyses, unless stated below, were performed using one way ANOVA to compare the data across treatment groups, and Tukey-Kramer post test to compare all pairs of data, with the threshold for statistical significance set at $P \leq 0.05$.

Figure 3.5b

Paired T-test (2-tailed) was performed with a threshold for statistical significance set at $P \leq 0.05$.

Figure 5.1 and 5.2

Our primary hypothesis was that the effect of LNP's antimicrobial activity against *Enterobacteriaceae* would be evident at 6 and 8 hours. Change scores from time 0 to 6 (or 8) hours were calculated for each mouse by subtracting the log CFU/g value at 0 h from the value at 6 (or 8) h. Log transformation was used to stabilise variances across groups and ensure normal distribution of scores within groups. One way ANOVA was used to compare the change scores across treatment groups, and Tukey-Kramer post test was used to compare all pairs of data, with the threshold for statistical significance set at $p < 0.05$.

Characterisation of nanoparticulate TFDs

Chapter 3

Chapter 3: Characterisation of nanoparticulate TFDs

3.1. Introduction

A new type of oligonucleotide-based antimicrobial is being developed by Procarta Biosystems Limited called Transcription factor decoy (TFD) (McArthur 2009b, McArthur 2014, McArthur 2015, McArthur 2017). They consist of a short sequence of synthetic oligonucleotides that comprise the binding site for an essential bacterial transcription factor. When introduced within a bacterial cell, TFDs competitively inhibit the transcription factor from binding to its designated site on the bacterial DNA to alter the expression of the targeted gene (Mann and Dzau 2000) (Figure 3.1).

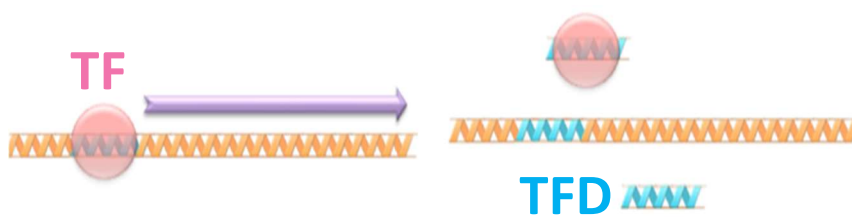


Figure 3.1 The mechanism of transcription factor decoy (TFD) acting on transcription factors (TF) of interest. Transcription factors control gene expression by binding to specific sequences in the bacterial genome. TFD mimics the binding site and competitively inhibits the transcription factor to change gene expression, resulting in the killing of bacterial cells.

As the negatively charged and sizable TFDs could not pass through the bacterial membrane into the cytoplasm by itself, the delivery is facilitated by forming self-assembling nanoparticles (NPs) using a bolaamphiphilic molecule called 12-bis-THA (Mamusa *et al.* 2016) (Figure 3.2), which effectively binds to TFDs (resulting in a complex termed loaded nanoparticle (LNP) hereafter) and protects TFDs against nuclease degradation (Marin-Menendez *et al.* 2017). The NPs transfect bacteria by binding to the prokaryotic-specific anionic phospholipids, cardiolipin and phosphatidylglycerol. In particular, cardiolipin has a crucial role in the structural integrity of the respiratory chain, as cardiolipin rafts are responsible for anchoring them in the membranes (Arias-Cartin *et al.* 2012). These lipids are highly conserved among bacteria and were shown to be consistently present in the membrane of pathogenic clinical isolates (Sohlenkamp and Geiger 2016), making these lipids good targets for bacterial delivery.

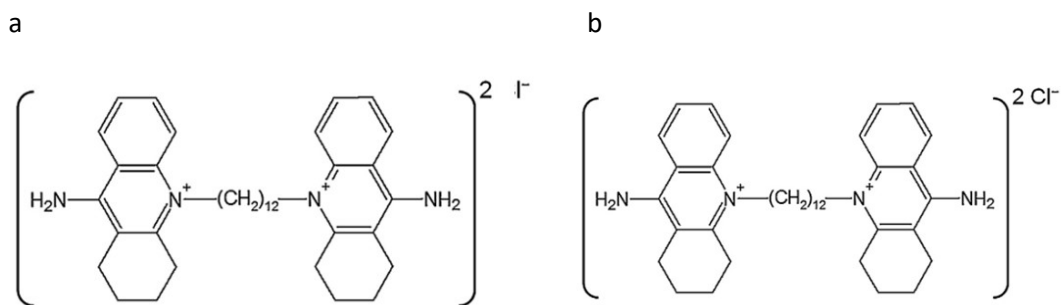


Figure 3.2 Chemical structure of bolaamphiphilic lipid, bola-amphiphile a) 12,12'-(dodecane-1,12-diyl)bis(9-amino-1,2,3,4-tetrahydroacridinium) iodide ($[[12\text{-bis-THA}]]\text{I}_2$); b) 12,12'-(dodecane-1,12-diyl)bis(9-amino-1,2,3,4-tetrahydroacridinium) chloride ($[[12\text{-bis-THA}]]\text{Cl}_2$) (Mamusa *et al.* 2016), used for the assembly of nanoparticle (NP). It consists of two identical polar head groups with delocalised cationic charges and associated with a quaternary ammonium joined by a dodecane chain.

A TFD was designed to competitively inhibit Gram-negative sigma factor 54 (GNSig) from binding to RNA polymerase (Wigneshweraraj *et al.* 2008), transcription of genes that are essential for bacteria's survival is therefore not activated and this in turn leads to cell death. Another TFD was designed to competitively inhibit the cyclic adenosine monophosphate receptor protein- fumarate and nitrate reductase (Crp-FNR) transcription factor of *E. coli*, which are highly conserved among *Enterobacteriaceae* (Korner *et al.* 2003) to control gene expression related to anaerobic respiration (Constantinidou *et al.* 2006).

Structures of TFD

To improve the stability of TFDs, TFDs are designed as different structures such as dumbbell (DB), hairpin (HP) and duplex, as different means of slowing down *in vivo* exonuclease degradation to prolong their efficacy within the bacterial cytoplasm (Figure 3.3). DB forms a monomeric circle with two stem-loops, and duplex contains phosphorothioate nucleotides (i.e. one of the non-bridging oxygens is replaced by sulphur at the phosphate backbone) on both ends of the oligonucleotide of each linear strand to prevent degradation and minimise the chirality effect from the duplex (Dias and Stein 2002). Whereas HP contains one stem loop and free 5' and 3' ends that are protected by phosphorothioate nucleotides.



Figure 3.3 TFD structures including dumbbell, hairpin and duplex with modifications to resist nuclease degradation. Asterisk, phosphorothioate nucleotides.

For the purpose of this thesis, empty nanoparticle (ENP) consists of the delivery NP 12-bis-THA; loaded nanoparticle (LNP) consists of both 12-bis-THA and TFD; and scrambled LNP (SLNP) consists of 12-bis-THA and a non-functional TFD. Hydroxypropyl methylcellulose (HPMC) is added to the nanoparticles (NPs) as an excipient and to prevent aggregation.

To better understand the properties of these NPs, dynamic light scattering was used to evaluate the particle size of ENP and LNP. Minimum inhibitory concentration (MIC) experiments were conducted to investigate the minimal dose needed to have a biologically relevant antimicrobial effect on the targeted bacteria. To minimise NP aggregation and improve antimicrobial activity, amount of excipient used in the NP formulation was explored, as larger particle size prevents NPs from transfecting the bacterial cell. To further determine the ratio of LNPs that are non-aggregated for efficient antimicrobial activity, flow cytometry was performed to investigate the proportion of individual NPs incorporated with TFDs present in the NP formulation. The pendant drop technique is often used to characterise a surfactant's ability to form particles. It is done by measuring the change in surface tension to determine the critical micelle concentration (CMC) - the minimum concentration of surfactants needed to form micellar/ aggregate structures (Burlatsky *et al.* 2013). To characterise NP's biological stability against DNases degradation, the robustness of different TFD structures will be tested by a time course study to determine the TFD structure to take forward for future *in vitro* testing.

3.2 Materials and Methods

Protocols used in this chapter are described in Chapter 2 Section 2.1 Culturing bacteria, 2.2.1 Making TFDs and NPs, 2.2.2 Minimum inhibitory concentrations (MIC) and minimum bactericidal concentrations (MBC), 2.3.1 Dynamic light scattering for NP size measurement, 2.3.2 Flow cytometry and fluorescence-activated cell sorting (FACS), 2.3.3 Time course stability study using exonuclease treatment against TFD and 2.3.4 Pendant Drop to measure surface tension of NPs. For Section 3.3.1- 3.3.3, [12-bis-THA]₂ was used for making NPs.

3.3 Results

3.3.1 Dynamic light scattering for NP size measurement

To investigate the size distribution of NPs and their respective monodispersity, dynamic light scattering (DLS) was performed from 4 separate batches of NPs. DLS measures Brownian motion and relate this to particle size (Weatherbee *et al.* 2017). A typical distribution is shown in Figure 3.4, plotting correlation coefficient against time, and demonstrated the presence of aggregation as the base line did not touch the y-axis (Figure 3.4).

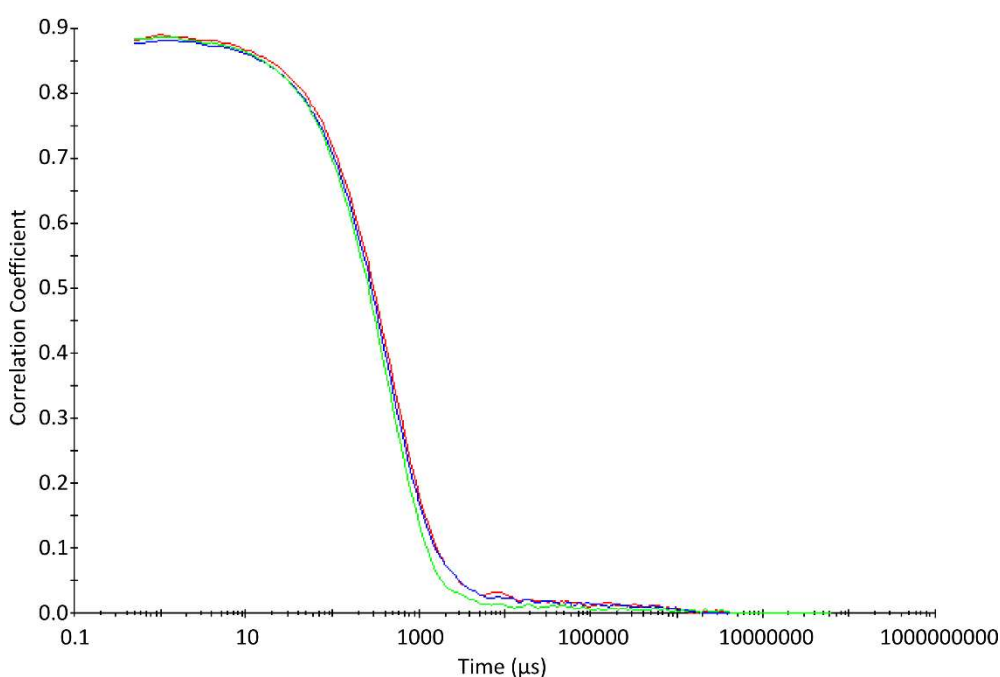


Figure 3.4 Representative correlation curve of 12-bis-THA with 0.1% hydroxypropyl methylcellulose (HPMC) complexing with transcription factor decoy (TFD), forming loaded nanoparticles (LNPs).

Using the NP formula with 0.1% HPMC, empty nanoparticles (ENPs) and loaded nanoparticles (LNPs) had polydispersity indexes (PDI) of 0.41 nm and 0.33 nm respectively. As the PDI value is > 0.2 , the particle size peak with the highest intensity was used to estimate the NP size due to indication of polydispersity. The particle sizes of ENPs and LNPs were measured from the hydrodynamic diameter, the diameter of a hypothetical sphere that mimics the way the measured sample diffuses, of the size 477.79 ± 53.47 nm and 291.58 ± 51.52 nm (Table 3.1); the particle size peak with the highest intensity was used to determine the size of the NPs to represent the majority of the sample.

Table 3.1. Particle size measured by DLS Malvern Zetasizer Nano ZS. Average of 4 batches of NP made from 12-bis-THA were used for the analysis. Particle size is obtained from size peak intensity as polydispersity index > 0.2. ENP, empty nanoparticles; LNP, loaded nanoparticles; HPMC, hydroxypropyl methylcellulose; GN Sig HP TFD, Gram negative sigma factor hairpin TFD.

Sample	Polydispersity index		Particle Size Peak	
	Mean (nm)	S.D.	Mean (nm)	S.D.
ENP + 0.1% HPMC	0.41	0.12	477.79	53.47
LNP + 0.1% HPMC (GN Sig HP TFD)	0.33	0.18	291.58	51.52

3.3.2. Minimum inhibitory concentration and minimum bactericidal concentrations of LNPs

Minimum inhibitory concentration

To investigate the efficacy of LNPs in exerting antimicrobial activity, the minimum inhibitory concentration (MIC) of LNPs were tested against *E. coli*, whereby a fixed ratio of TFDs were added to 12-bis-THA.

LNPs were tested with and without the addition of bulking agent/excipient hydroxypropyl methylcellulose (HPMC) to determine the optimum formulation of NPs with the highest antimicrobial activity. The use of GN Sig TFDs did not show significant difference in MIC between each NP pair (i.e. ENPs and LNPs with the same amount of HPMC), and was only significant reduced ($P \leq 0.05$) when HPMC-containing LNPs were compared to ENP (Figure 3.5 a). No significant difference ($P > 0.05$) in MIC was observed between LNPs with 1% and 0.1% HPMC, implying 0.1% HPMC is sufficient to improve LNP formulation.

To improve specificity against *Enterobacteriaceae*, Crp-FNR TFD was used against *E. coli* instead in a separate experiment. Also, to assess the TFD-specific activity with comparable NP structure/size, an LNP loaded with a scrambled sequence of TFD i.e. scrambled-TFD loaded nanoparticle (SLNP) was tested instead of ENPs as a more appropriate control to assess the TFD specific activity. It was shown that LNPs with 0.1% HPMC had a significantly lower MIC ($P \leq 0.01$) compared to SLNPs with 0.1% HPMC (Figure 3.5 b), confirming the LNP activity was specific to the functional sequence of TFD against *E. coli*. As LNPs with 0.1% HPMC was more stable than with 1% HPMC (Michael McArthur, unpublished data), the LNP

formula containing 0.1% HPMC was taken forward for future *in vitro* tests along with SLNPs as a control.

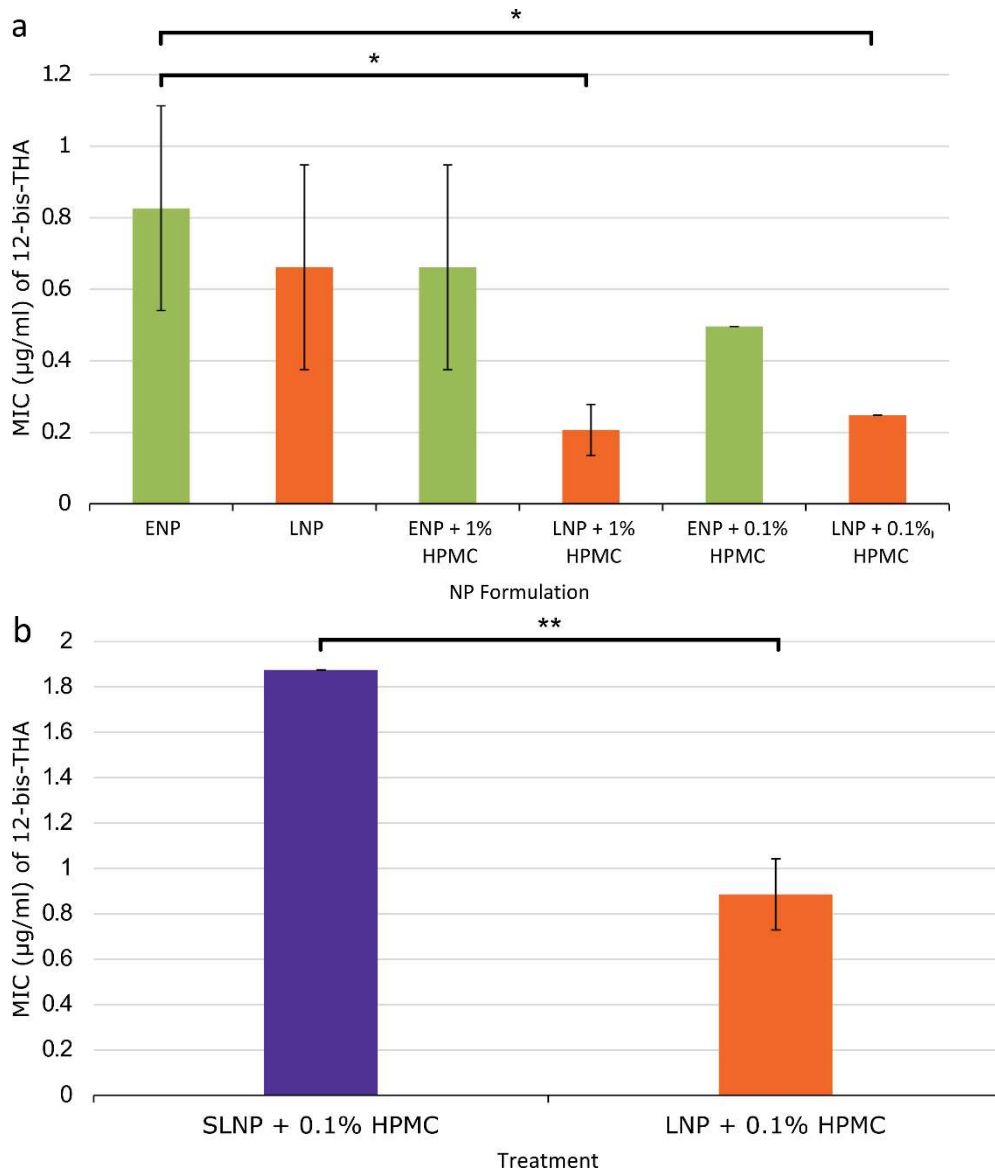


Figure 3.5. Minimum inhibitory concentration of empty nanoparticles (ENPs), loaded nanoparticles (LNPs) and scrambled loaded nanoparticles (SLNPs) to exert antimicrobial activity. A fixed volume of *E. coli* DH5 α cells were added to each of the wells of a microtitre plate and were incubated at 37°C with shaking overnight, after which the visible growth/no growth in each well was recorded. a) A representative MIC experiment of ENPs and LNPs loaded with Gram negative sigma factor (GN Sig) TFD in formulation with and without excipient HPMC. Means of 3 biological repeats were calculated \pm standard deviation (SD); b) Minimum inhibitory concentrations of 12-bis-THA of SLNP and LNP using formulation with 0.1% HPMC (loaded with Crp-FNR TFD) against *E. coli* DH5 α . The results are means of 3 technical repeats with 3 biological repeats in each were calculated \pm SD. Single and double asterisks denote $P \leq 0.05$ and $P \leq 0.01$ respectively.

Minimum bactericidal concentration

Minimum bactericidal concentration (MBC) was performed to determine the mechanism by which the NPs work, whether they act by preventing further bacterial growth (i.e. bacteriostatic) or by killing the cell (i.e. bactericidal). It was shown that ENP, SLNP and LNP (using formulation with 0.1% HPMC) were all bactericidal at 0.9275 $\mu\text{g}/\text{ml}$, as there was a $> \log_{10} 3$ significant decrease in viable cell counts (Figure 3.6) compared to untreated samples ($P \leq 0.001$), indicating that the NPs' antimicrobial mechanism of action were bactericidal.

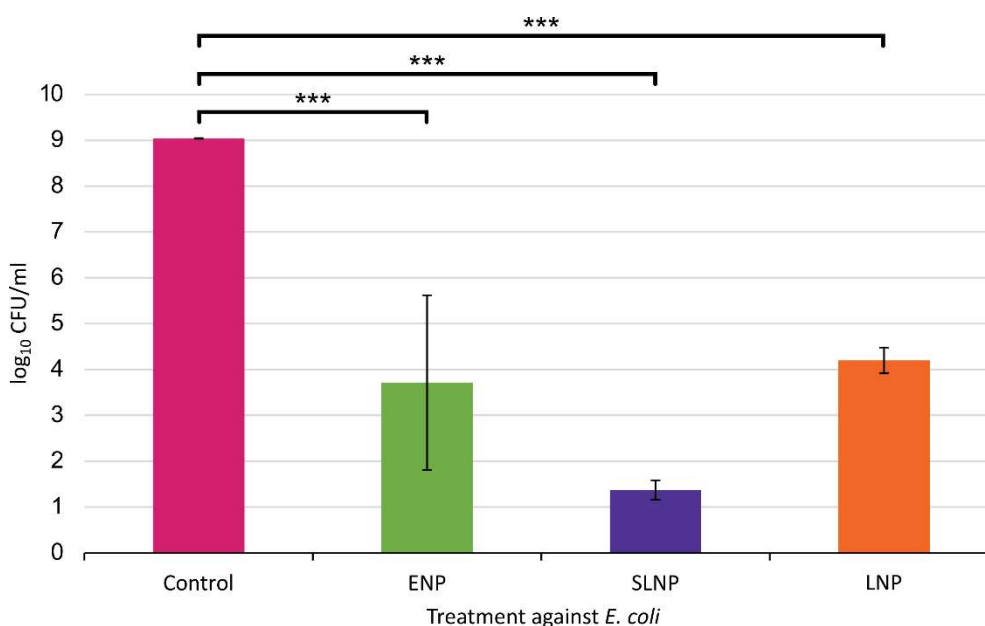


Figure 3.6. Minimum bactericidal concentrations of NPs. Colony counts of *E. coli* significantly decrease ($P \leq 0.001$) from different NP treatments compared to untreated *E. coli* control. ENP, SLNP and LNP treatments were bactericidal at 0.9275 $\mu\text{g}/\text{ml}$ using NP formulation with 0.1% HPMC. ENP, empty nanoparticles; SLNP, scrambled nanoparticles; LNP, loaded nanoparticles. Means of at least 2 repeats calculated \pm SD. Triple asterisks denote $P \leq 0.001$.

3.3.3. Flow cytometry and fluorescence-activated cell sorting (FACS) of LNP formulations

To investigate the formulation that yields the highest theoretical biological activity, the aggregation of NPs should be minimised. Different NP formulations were explored and physically characterised via flow cytometry to elucidate the scattering characteristics between aggregates and non-aggregates in different NP formulations. FACS was used to investigate the yield of TFD-bound LNPs and determine amount of aggregates and their properties once they were segregated from the non-aggregated population. Furthermore,

FACS was also performed to determine the efficiency of Acridine Orange and SYBR green to fluorescently stain TFD as an alternative to using fluorescent-labelled TFDs.

The fluorescence profiles of LNPs loaded with fluorescent-labelled TFDs were compared between two NP formulations, LNP and LNP + 0.1% HPMC, by the presence of high fluorescein isothiocyanate (FITC) fluorescence indicating aggregation of NPs. ENP and ENP + 0.1% HPMC had a small amount of low level auto-fluorescence on the FITC and Brilliant Violet scale (Figure 3.7 a) due to the presence of 12-bis-THA. Less aggregated NPs were detected in the LNP + 0.1% HPMC compared to the LNP formulation, as indicated by a higher percentage of particles with low FITC intensity (particles with increased FITC intensity denote aggregation); LNPs + 0.1% HPMC had almost double the amount of non-aggregated NPs compared to LNPs (Figure 3.7 b), indicating the presence of HPMC in the NP formulation markedly reduced the amount of NP aggregation.

The effects of time on the aggregation of NPs were also studied by leaving the NPs to stand overnight, before repeating flow cytometry analysis the following day. LNPs + 0.1% HPMC had twice the amounts of non-aggregated particles compared to the results from the same sample obtained the day before, confirming the disaggregation of NPs over a 1-day period (Figure 3.7 c). To analyse the non-aggregated and aggregated NP population individually, FACS was performed to separate the two populations and they were re-analysed on the flow cytometer. It was shown that, after sorting, the aggregated NPs can disaggregate into smaller, non-aggregated particles, whereas non-aggregated NPs mostly remained in the non-aggregated gated area, with only a very small portion shifting to the aggregated-gate. This finding showed that NPs were dynamic and the aggregation status was reversible, with the tendency for the aggregated NP population to disassemble into individual particles.

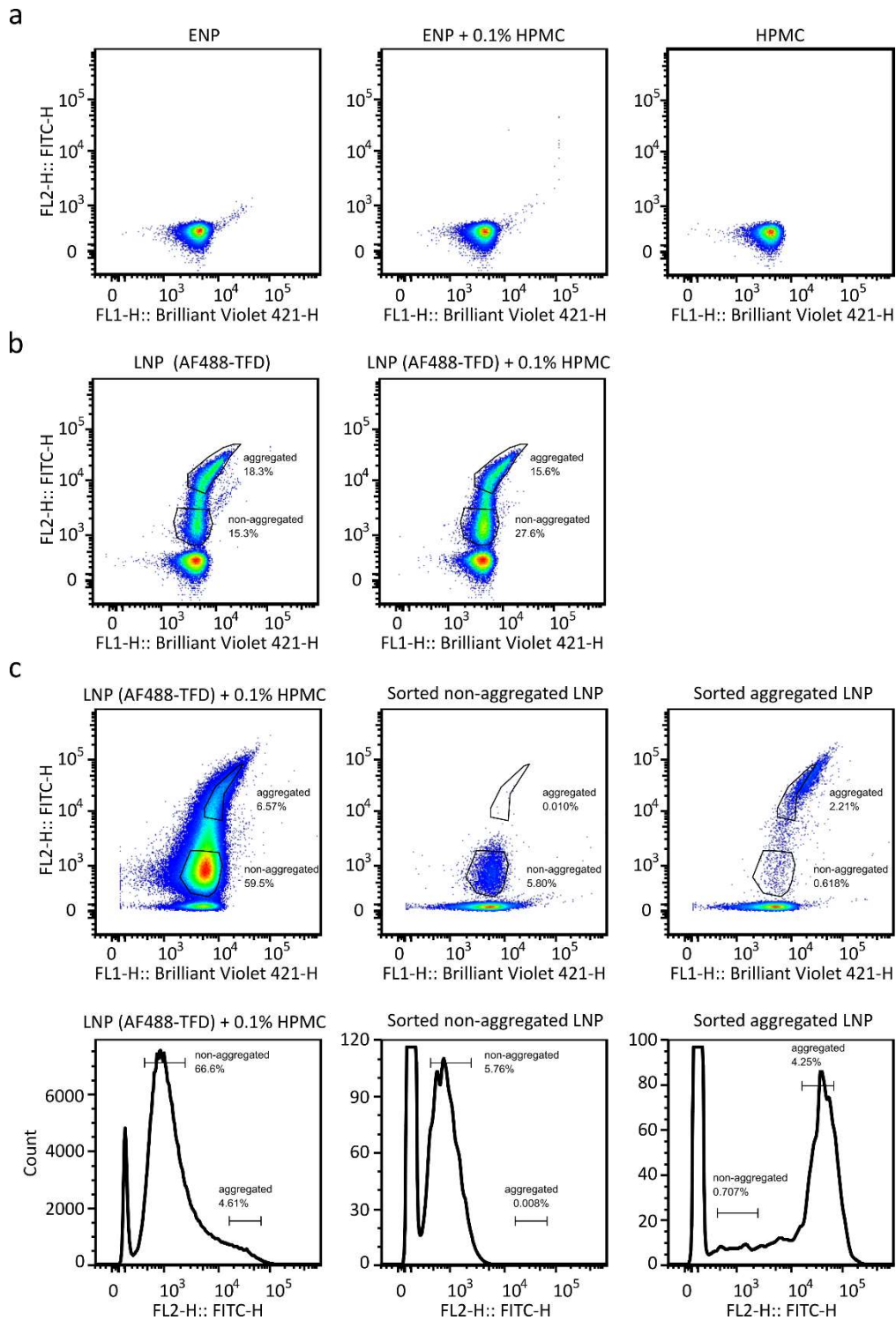


Figure 3.7 HPMC decrease LNP aggregation in flow cytometry and fluorescent activated cell sorting (FACS). a) controls showing ENPs contain low levels of autofluorescence b) comparison of LNPs and LNPs + 0.1% HPMC fluorescence profile loaded with alexa488-flourescent TFD; c) left: Profile of LNPs + 0.1% HPMC (loaded with alexa488-flourescent TFD) after 24 h; the populations gated within the aggregated and non-aggregated gates were sorted by FACS in HPMC-lined collection tube) and reanalysed using flow cytometry; middle: sorted cells originated from the non-aggregated gate; and right: sorted cells originated from the aggregated gate. Gates show location of particles before sorting.

When collecting the sorted population from FACS, it was noticed that when the sample collection tube was coated with HPMC (Figure 3.7 c) or bovine serum albumin (BSA) (Figure 3.8 a), the number of sorted LNPs were higher than when samples were sorted with foetal bovine serum (FBS)-coating (Figure 3.8 b), as HPMC and BSA act as a buffer and exert a protective effect against NP degradation as they enter the collection tube with force.

In contrast, when NPs were sorted into FBS-coated collection tubes, fewer NPs were collected compared to HPMC-or BSA-lined tubes. From the TFD stability experiment, FBS was used as a source for exonuclease for TFD degradation, it is therefore expected that TFDs were degraded by FBS as they came in contact with the NPs.

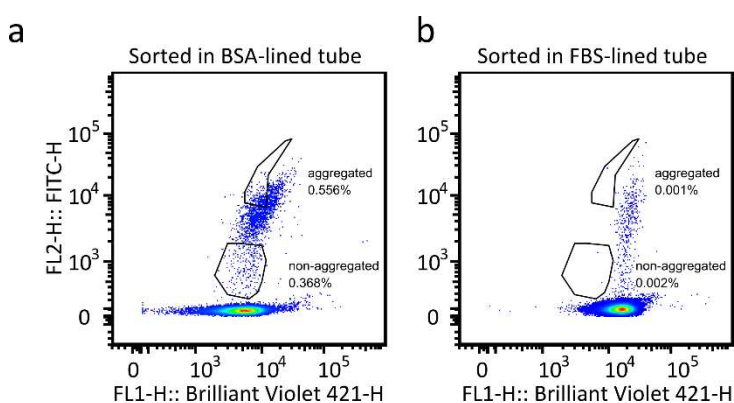


Figure 3.8 Aggregates profile of LNPs with Alexa-488-fluorescent TFD in 0.1% HPMC, a) sorted in BSA-lined tube b) sorted in FBS-lined tube. Gates show location of particles before sorting, showing changes in the fluorescent profile of the aggregates.

Apart from using fluorescently labelled TFDs, other methods of TFD staining, DNA dye SYBR green or Acridine Orange (with positive fluorescence on the FITC scale), were compared to see whether they would bind specifically to TFD. SYBR green did not show any fluorescence profile with TFD. It was shown that Acridine Orange bound strongly to TFD (Figure 3.9 a) and had some non-specific binding to ENPs (Figure 3.9 b), though Acridine Orange's fluorescence profile for TFD and ENP can be differentiated, characterised by a lower intensity of Acridine Orange fluorescence for TFD and higher fluorescence for ENP. Interestingly, LNP's FITC-fluorescence profile closely resembled those in ENP (Figure 3.9 c) and not a combined profile of TFD and ENP, suggesting that Acridine Orange either cannot get into the NP to interact with TFD or that the TFD-Acridine Orange fluorescence profiles were masked by the TFD-NP complex.

To determine which hypothesis was correct, LNPs were treated with sodium taurocholate (NaTC) to break the NPs apart in the hope to reveal separate TFD and NP fluorescence

profile within LNP. The TFD and ENP population could be differentiated on the histogram of the broken LNP sample, revealing two distinct FITC-positive peaks for TFDs and ENPs (Figure 9 d). This finding suggests that Acridine Orange could be used as a green fluorescent marker for NPs and TFDs for further characterisation in the future.

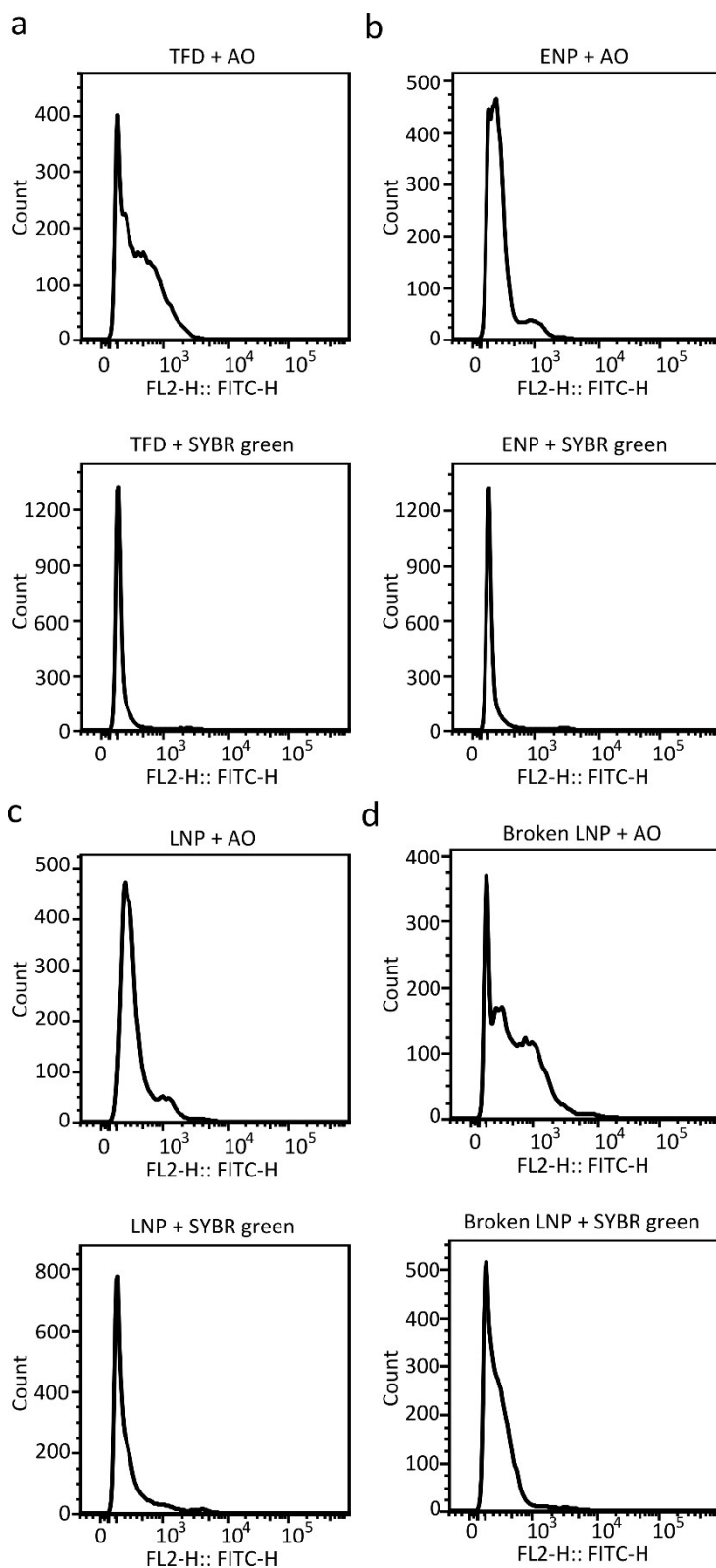


Figure 3.9 Characterisation of ENP and LNP using flow cytometry. SYBR green and Acridine Orange were used to stain DNA and NP to comparatively assess suitability for fluorescently stained TFDs. Acridine Orange and SYBR green fluorescence profile of a) TFD; b) ENP; c) LNP; d) LNP broken by sodium taurocholate.

3.3.4. Measurement of surface tension of 12-bis-THA by pendant drop analysis

To characterise the concentration of 12-bis-THA needed to form NPs for TFD encapsulation, critical micelle concentration (CMC), the concentration of surfactant above which 12-bis-THA starts to form NPs, was measured via changes of surface tension with time at different concentrations of ENPs.

At low concentration, the amphiphilic molecules arrange themselves near the surface of the water, with the hydrophobic end held above the surface while submerging hydrophilic head in the water, showing only little changes in surface tension (Chakraborty *et al.* 2011). The surface tension begins to decrease as the concentration of surfactant increases until the surface become saturated with surfactants. At this point, surface tension no longer decreases and reaches a stable level i.e. when 12-bis-THA begin to self-aggregate into NPs. CMC is defined as the concentration at which increased surfactants i.e. 12-bis-THA levels no longer reduces the surface tension when the surface is saturated (Burlatsky *et al.* 2013), which indicates the concentration at which 12-bis-THA is needed to form NPs. As surfactants at higher concentration reaches surface saturation within a short period compared to diluted samples, 12-bis-THA at various concentrations were measured through a fixed period to determine the CMC.

Two versions of ENPs, ENP_I and ENP_Cl (made from amphiphilic molecules [12-bis-THA]₂ and [12-bis-THA]Cl₂ respectively) were tested. As water has a surface tension of ~72.6 millinewton (mN)/meter (m) (Chakraborty *et al.* 2011), a decrease in surface tension value indicates surface activity in the samples. Large variations in surface tension measurements were seen between repeat measurements when the samples were measured sequentially.

To address this problem, the needle that dispense the sample drop was washed thoroughly between each measurement to remove the remains of all surface active materials. Also, the volume of sampling drop was considerably decreased by evaporation through time, leading to invalid measurement of surface tension (Picknett and Bexon 1977). To reduce the rate of evaporation, the sampling drop was encased in a lidded-cuvette and held close to the meniscus of the water filled within the cuvette to create a humid atmosphere (Berry *et al.* 2015). The experiments were conducted under a temperature-controlled environment to reduce the effects of temperature fluctuation during long sampling period

and the additional insulation controls were in place to prevent the expansion and contraction of the glass syringe to ensure the size of the sampling drop is consistent.

In Figure 3.10 a, the surface tension of ENPs_I at 0.18 mM decreased from 70 mN/m to 65.4 mN/m within a 15 minute period, implying the presence of surface active material at this concentration. However, when the ENPs_I were diluted no surface activity was observed. In Figure 3.10 b, 0.4 mM and 0.18 mM of ENPs_Cl had the same decline rate in surface tension, which may indicate that, at these concentrations, the surface was close to being saturated. It was predicted that the surface tension would plateau within 1.5 h, but the surface tension continued to decline even after 4 h (data not shown). ENPs_I only showed surface active properties at the highest concentration possible (0.18 mM), indicating [12-bis-THA]I₂'s poor surface activity. However, this concentration of NPs was not enough to obtain a flat base line surface tension level to determine CMC.

Comparing [12-bis-THA]I₂ and [12-bis-THA]Cl₂, the latter was more surface active as indicated by the decrease in surface tension at lower concentration, suggesting a lower concentration of [12-bis-THA]Cl₂ may be needed to form NPs. Even though the control parameters improved surface tension measurements and the repeatability of measurements, the point at which the surface tension no longer decreased was still not observed in both ENPs_I and ENPs_Cl before excessive evaporation took place, the CMC value therefore could not be deduced from the current experimental setting. This may suggest that [12-bis-THA]I₂ and [12-bis-THA]Cl₂ were not very surface active and a prolonged sampling period is required for surface tension to reach a stable level to obtain the CMC value. The measurement of surface tension to identify the CMC may not be suitable for the characteristics of 12-bis-THA.

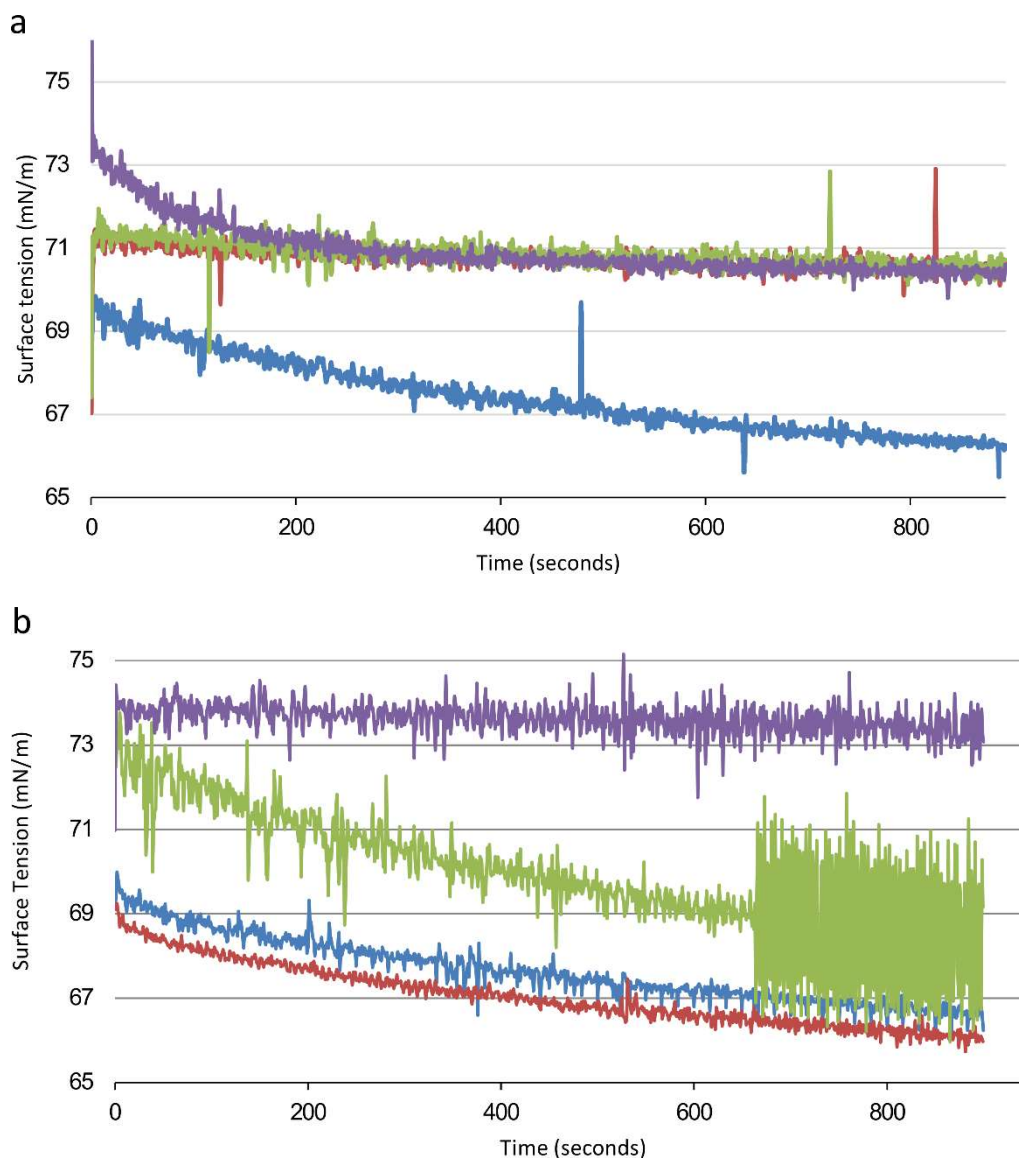


Figure 3.10 Surface tension of a) ENP_I and b) ENP_Cl samples using Pendant drop with minimum 2 repeats at different dilutions over time, each line is an average of duplicate data. Blue: 0.4 mM; Red: 0.18 mM; Green: 0.018 mM; Purple: 0.0018 mM.

3.3.5. Time-course stability study using exonuclease treatment against TFD

To investigate the duration over which the TFDs were resistant against biological degradation, foetal bovine serum (FBS) containing exonucleases was used as a source for non-specific digestion to mimic physiological conditions. The stability of different TFD structures was tested via a time-course degradation; it was shown that the dumbbell structure was the most robust TFD structure, as DB had the strongest band intensity compared to HP and duplex in the presence of FBS at 300 minutes (Figure 3.11). The second most robust structure was HP while duplex was the structure most prone to degradation. This indicated that under physiological conditions, TFDs were robust enough

to withstand enzymatic degradation for 6 h to prolong efficacy. TFDs were degraded after 3 days in the presence of FBS, whereas the control TFDs without FBS treatment remained intact, indicating the structures were stable and robust at 37°C.

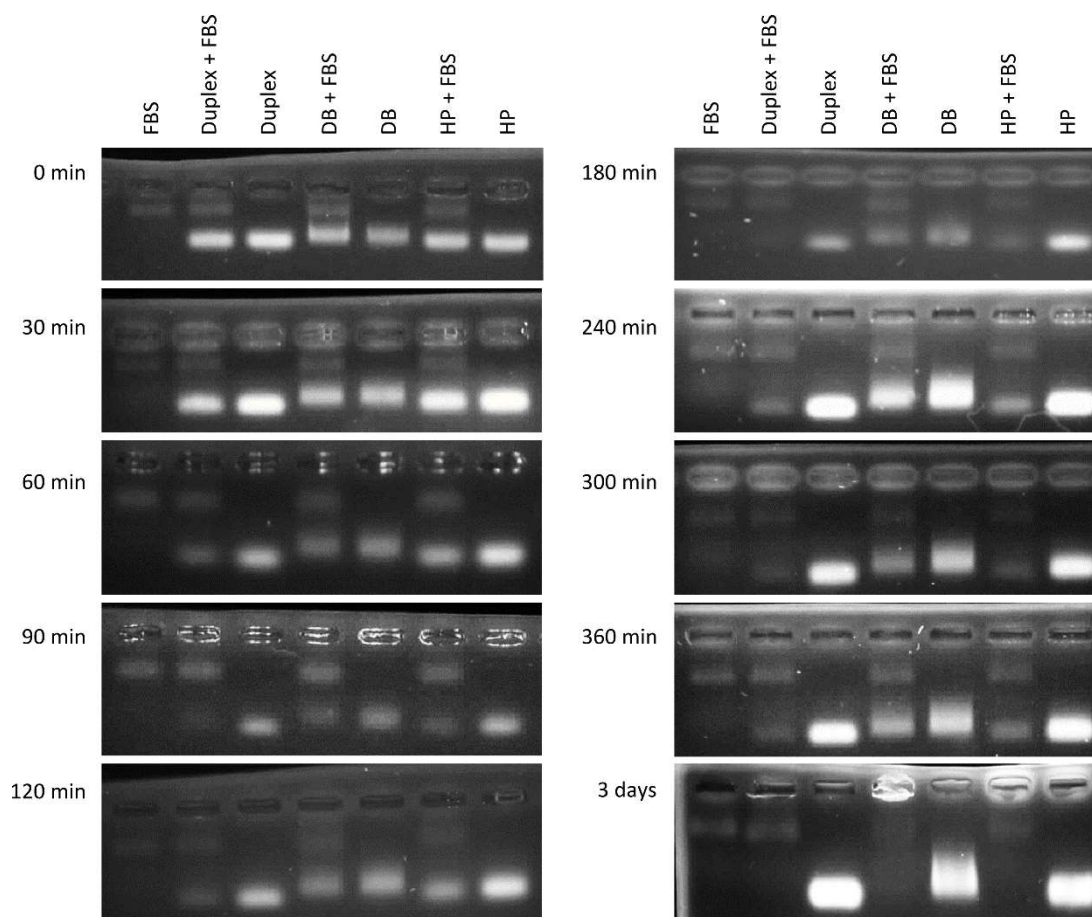


Figure 3.11 Agarose gel image of time course susceptibility study of TFDs Duplex (with phosphorothioate oligodeoxynucleotides terminal modifications), Dumbbell (DB) and Hairpin (HP) in the presence of fetal bovine serum (FBS) (which degrades TFDs). It is shown that DB survived up to 360 min in the presence of FBS, followed by HP which has a more visible band from 60 min onwards compared to duplex.

3.4 Discussion

Determination of NP size for targeted delivery in the human body

Size determination is an important physical characteristic to consider as NP size affects absorption and increases target efficiency in the human body (Youshia and Lamprecht 2016). Smaller particles (10-100 nm) tend to be absorbed within the bloodstream and accumulate within the liver and spleen with wider organ distribution (De Jong *et al.* 2008), whereas larger particles (300 nm or more) do not penetrate the blood stream and remain

in the intestine and colon (Jani *et al.* 1990, Bergin and Witzmann 2013). Having the correct particle size for the intended target location is therefore crucial for effective delivery. As *E. coli* reside in the lower intestine (Katouli 2010), the desirable size would be around 300 nm (Bergin and Witzmann 2013), which matches the hydrodynamic diameter of LNPs + 0.1% HPMC measured in DLS, suggesting LNPs made with [12-bis-THA]_{I2} were appropriate for oral administration into the GI tract.

Comparing LNPs made with [12-bis-THA]_{I2} in this study to those made with [12-bis-THA]_{Cl2} (Marin-Menendez *et al.* 2017), the LNPs_{Cl} were much smaller in size at 180 ± 10 nm. [12-bis-THA]_{I2} is soluble primarily in DMSO and methanol and scarcely soluble in water, whereas [12-bis-THA]_{Cl2} is readily soluble in water and implies increased biological activity (Mamusa *et al.* 2016). [12-bis-THA]_{I2} tends to precipitate and form crystal as it become saturated when dispersed in water after vigorous shaking. Nonetheless, as the [12-bis-THA]_{I2} formulation was already established, it was used for the *E. coli* related experiments; [12-bis-THA]_{Cl2} was then utilised in new LNPs designed specifically against sulphate reducing bacteria (Chapter 6).

Due to electrostatic interactions between the anionic nanoparticles and TFDs (Marin-Menendez *et al.* 2017), the LNPs are smaller in size compared to ENPs as expected, which evidently showed successful formation of TFD and [12-bis-THA]_{I2}. NP polydispersity was indicated as the PDI value was > 0.2, though a PDI between 0.3-0.4 often indicates good NP synthesis when made by injection method with little aggregation, it can be assumed that the NPs were quality assured for the use in downstream biological experiments such as MIC/MBC and batch model experiments (see Chapter 4). Although no correlation has been found between particle size and biological activity for NPs from Procarta™ (unpublished data), DLS measurements are done routinely after NPs are made in order to provide information about their physical characteristics.

TFD-specific activity was observed against both GN Sig and Crp-FNR TFD against *E. coli*

As indicated by the MIC results, TFDs evidently exert specific antimicrobial activity against *E. coli* comparing LNPs with ENPs and SLNP controls. Apart from particle size, drug-to-polymer ratio was also important to the drug formulation (Maderuelo *et al.* 2011). It was shown that HPMC decrease the MIC of LNPs, indicating the effectiveness of HPMC in increasing LNPs' antimicrobial activity. This is as expected as the concentration of the polymer can hugely influence the physiochemical properties of the drug formulation (Agarwal and Murthy 2015). Even though LNPs with 1% HPMC and 0.1% HPMC had similar

MIC, LNPs with a lower ratio of HPMC at 0.1% were found to be more stable and allow more rapid release of drug content with less swelling for optimal drug release rate (Michael McArthur, unpublished data). LNPs made with 0.1% HPMC and FNR TFD was therefore selected to be used in the *in vitro* batch culture fermentation experiments (see Chapter 4).

As the NPs are prepared manually using the injection method, variations can occur between runs, which may explain why the TFD-specific activity may be seen in some sample runs and not others. Relatively small changes in LNP MIC values could be due to batch to batch variation and handling difference in NP preparation. However, it is still a good basis for the improvement of TFD specificity. Investigating continuous growth curve data may be a good alternative method to elucidate any differences in the modes of action between ENPs and LNPs.

HPMC improved LNP_I by reducing aggregation

By comparing LNP_I formulations with and without the HPMC via flow cytometry, it was shown that LNPs + 0.1% HPMC consisted of fewer aggregates compared to LNP. This is as expected as HPMC is a known excipient and a component widely used for controlled-delivery in oral formulations in pharmaceutical industries (Osorio *et al.* 2011, Nokhodchi *et al.* 2012). HPMC is generally considered safe for human consumption as it is also used in the food and cosmetic industries, with desirable properties including being chemically inert and physically stable in normal conditions (Joshi 2011). This makes HPMC a great NP stabiliser (Ghosh *et al.* 2013) to be used in conjunction with the active ingredients in LNPs – 12-bis-THA and TFDs – to improve stability and prevent aggregation in this antimicrobial formulation.

Aggregation of NPs was reversible in FACS

When the samples were passed through FACS to separate the NP aggregates from the non-aggregated population, it was surprising that there was a change in the fluorescence profile in the aggregated population; some of the aggregates have in turn fallen into the non-aggregated population. This could be explained by the fact that as aggregates could be small enough to be identified as one distinct cell in flow cytometry, there may be a larger majority of aggregates compared to the non-aggregated population; some aggregates may have disaggregated during the process of being sorted and mixed with the sheath fluid, the dilution and mixing action in the FACS machine could lead to further dissociation of NPs.

The presence of different linings of the collection tube result in different NP recovery; the recovery of NP events from HPMC and BSA-lined tubes were higher than those lined with FBS, as FBS are known to degrade TFD. From the fluorescence profile of the sorted aggregate population, it was suggested that NP aggregation is reversible; NP aggregates tend to dissipate into individual NPs instead of aggregating over time. This may provide an explanation to why NPs may increase antimicrobial activity over time.

Acridine Orange can differentiate TFD and LNP fluorescence profile with NaTC treatment

TFD was only released when LNP were broken by NaTC treatment, showing that TFDs were intact within LNPs and complexed with [12-bis-THA]₂ without signs of segregation from the [12-bis-THA]₂. When comparing different DNA-binding fluorescent dyes i.e. SYBR green and Acridine Orange, Acridine Orange appeared to bind to both TFD complexed with LNPs (at higher fluorescence intensity) and TFD released from NaTC treatment (at lower fluorescence intensity in comparison). The presence of distinct fluorescence profiles between the two groups would make Acridine Orange a suitable fluorescent marker for NPs and TFD for flow cytometry in the future.

It is interesting that we were not able to see a distinct shift in fluorescence profile with SYBR green when staining TFD. Being an intercalating agent that is designed to bind double stranded DNA, it was expected to have specific binding activity with TFD, as previously tested on gel electrophoresis. This could be due to low intensity of fluorescence that is not distinct enough to differentiate from the background against the non-fluorescent cells.

Pendant drop is not suitable for the CMC measurement of 12-bis-THA

CMC is an important parameter for drug characterisation as this allows us to determine the minimum concentration of 12-bis-THA to form NPs, to ensure the integrity and functionality of LNPs in *in vitro* and *in vivo* settings. Despite trying different experimental settings and incorporating better controls to maintain temperature and prevent evaporation, it was not possible to obtain the baseline surface tension value to determine CMC of ENPs using the pendant drop method, as they showed no signs of surface saturation.

The measurement of surface tension to evaluate CMC appeared to be unsuitable due to the properties of ENPs, as similar results were obtained by Procarta™ when determining CMC of NPs using surface tension (unpublished data). The surface activity was so low that we cannot derive the CMC before other factors e.g. evaporation/draught become a

dominating factor that further decreases surface tension. Changes in the structural arrangement of 12-bis-THA on the surface of the drop may explain why, as the volume of drop decreases, the surface tension continued to decrease (i.e. the surface still hasn't been saturated). It was only possible to get similar results for the first two repeats of a sample (except samples with no surface activity), and has been shown repeatedly with different batches of ENP. ENPs may have rapid changes in surface properties over a short period of time and it was therefore not possible to obtain reproducible results within the sampling period.

Relating the ENP_I data to the CMC results obtained previously from Nanosight (CMC at 0.0018 mM) and DLS (CMC at 0.075 mM) by Procarta Biosystems Limited (unpublished data), it is surprising that no surface activity was shown at 0.018mM ENPs_I with pendant drop as particles were formed previously at this concentration. We would expect 0.18mM ENPs_I to be saturated with surfactants with no further decrease in surface tension but it was not the case.

Publications from a different research group have found similar difficulty in obtaining CMC or critical aggregate concentration (CAC) from bolaamphiphiles in solution (Menger and Wrenn 1974, Yiv *et al.* 1976). The unique properties of Dequalinium makes determining the precise point of transition between monomer to aggregate difficult using methods such as isothermic titration calorimetry, laser light scattering and Monte Carlo simulations (Lasch and Hildebrand 2002). When a similar pendant drop experiment was repeated by coworkers (Mamusa *et al.* 2016), the results confirmed with our experimental finding that the equilibrium plateau was not obtainable within the experimental time frame despite a decrease in surface tension being observed. Other techniques such as DLS, static light scattering were also used to determine CMC yet no conclusive results had been drawn.

The preferred HP TFD structure was stable against exonuclease degradation

The structures of the TFDs were also investigated for their essential stability against nuclease degradation within the bacterial cell. DNA structures including dumbbell (Escaja *et al.* 2003), hairpin (Bikard *et al.* 2010) and duplex containing phosphorothioate nucleotides (Eckstein 2014) were found naturally in bacterial DNA, which made them good candidates for antibacterial therapy. However, they are also likely to experience bacterial degradation as there are mechanisms in place to recycle the damaged host material.

We were pleasantly surprised that the TFD structures can withstand prolonged degradation to both exo- and endo-nuclease contained within FBS (Keum and Bermudez 2009). As the TFD structures were designed to protect against exonucleases degradation, the general degradative effect of FBS was regarded to be caused by endonucleases.

In vitro digestion studies have demonstrated that dumbbell TFDs (a closed monomeric circle) had better structural integrity than the hairpin and duplex structures. The curvature of the loops act as a means of protection as this prevents degradation from the 3' end (Wittig *et al.* 2002), this may explain why the dumbbell structure is the most resistant against enzymatic attack as 3' ends were not available for exonucleases to act upon. However, dumbbell formation is time consuming and may lead to large amounts of wastage on malformed byproducts, and are therefore not preferred.

On the contrary, the TFD duplex containing only three phosphorothioate internucleotide linkages on each end, was least resistant against degradation, as serum consists of heat-stable nucleases (von Kockritz-Blickwede *et al.* 2009) that can degrade oligonucleotides (Segal *et al.* 1992). Furthermore, phosphorothioate-containing unmethylated CpG nucleotides can trigger mammalian immune response (Hacker *et al.* 2002) as prokaryotic DNA contains CpG dinucleotide at a much higher frequency than eukaryotic DNA (Cardon *et al.* 1994, Bode *et al.* 2011). The duplex TFD is therefore counterproductive for treating microbiome dysbiosis if repeat dosing were to be given and was therefore not taken forward for further testing.

Although the TFD hairpin, containing a stem loop and phosphorothioate linkages, was less stable than the dumbbell, it was more resistant to degradation than the duplex as it had substantial resistance due to containing both modifications. Overall, hairpin is the preferred TFD structure due to the ease of formation, less wastage and relatively good stability, therefore was used in future experiments. Being biodegradable also makes TFD advantageous as there will be less concerns about the adverse effect of undigested DNA within the host body (Kawane *et al.* 2014). The ability for LNPs to survive in harsh acidic and enzymatic environment through the gastrointestinal tract before reaching its bacterial target is also an important consideration. It would be interesting to determine LNPs' stability in bodily fluids such as amylase, pancreatic acid and stomach acid to investigate the likelihood that LNPs would be remain intact when testing *in vivo* experiments.

To conclude, LNPs made with [12-bis-THA]₂ + 0.1 % HPMC, with an appropriate hydrodynamic diameter to target the colon, were the most biologically and physically

optimal formulation. The preferred HP TFD structure was robust against nuclease degradation for up to 6 h. TFD-specific activity was observed compared to ENP and SLNP against *E. coli*, whereby SLNP was considered a better matched control for LNP in future *in vitro* experiments. The current experimental set up was not suitable to obtain CMC of 12-bis-THA. Combining the flow cytometry and MIC data, a lower concentration of 0.1% HPMC was therefore used instead of 1% HPMC to reduce aggregation and enhance biological activity. LNP_I + 0.1 % HPMC will be used for downstream *in vitro* and *in vivo* experiments e.g. batch model fermentation against *E. coli*.

TFD specific targeting against *E. coli*

Chapter 4

Chapter 4: TFD specific targeting against *Enterobacteriaceae*

4.1. Introduction

Antimicrobial resistance incidence has become more prevalent and there is an ever-increasing need for new antimicrobials (Penchovsky and Traykovska 2015). One of the novel approaches is oligonucleotide therapeutics, to which selected bacteria are targeted at the genetic level within the cytoplasm. The use of antisense technology allows the inhibition of bacterial mRNA from being translated, however, a very high concentration is required for efficacy. The inhibition of transcription by blocking a transcription factor from binding to its consensus site is therefore a more attractive option. Oligonucleotide copies of the DNA binding site, named Transcription Factor Decoys (TFDs) (McArthur 2009b, McArthur 2014, McArthur 2015, McArthur 2017), competitively inhibit transcription factors from turning on essential bacterial genes in order to exert antimicrobial activity. A delivery system is also utilised to facilitate TFD delivery by encapsulating them with a lipid molecule (12-bis-THA) to form loaded nanoparticles (LNPs). These protect the TFDs from enzymatic degradation and deliver the bulky oligonucleotides to the bacterial cytoplasm (Marin-Menendez *et al.* 2017).

Gram-negative bacteria have become a major concern to the general public as complexity of the bacterial outer membrane makes it difficult for antimicrobials to penetrate. As *Enterobacteriaceae* is a family of bacteria that include some of the most challenging species of pathogenic bacteria that require urgent attention including the development of new antimicrobial treatments (World Health Organisation 2017). In this study, *E. coli* was used as a model organism for *Enterobacteriaceae* infection, which is commonly found in the healthy gut microbiota in human (Hooper and Gordon 2001) and its overgrowth is associated with Crohn's disease (Lupp *et al.* 2007, Garrett *et al.* 2010). The aim of the study was to determine whether a TFD can be developed to selectively remove *E. coli*, and other *Enterobacteriaceae*, as a demonstration of microbiome engineering.

A TFD that binds and competitively inhibits cyclic AMP receptor protein- fumarate and nitrate reductase (Crp-FNR) transcription factor was used in this study. It is highly conserved amongst *Enterobacteriaceae* (Korner *et al.* 2003) to regulate respiration and its stress response against host immune response (Unden and Schirawski 1997). Moreover, even though homologues of Crp-FNR exist in other bacterial families, including those comprise obligate anaerobes, the

corresponding binding site sequences are different to those in *Enterobacteriaceae* and have different functions all together, making Crp-FNR a good genomic target to selectively modify *Enterobacteriaceae* levels in the gut microbiota (Matsui *et al.* 2013).

The three main aims of the study were to 1) investigate TFD internalisation within *E. coli*, 2) to identify the optimum dose of LNP for bespoke bacterial targeting and 3) to test the TFD efficacy in the *in vitro* gut microbiota setting. The main experimental approach for each aim is detailed below.

Confocal scanning microscopy experiment

To visualise whether TFDs can penetrate bacteria cell membrane and transfect *E. coli*, confocal laser scanning microscopy was used to explore different cross-sections of the bacterial cell with adjustable depth of field. Confocal microscopy is a superior technology to wide field microscopy for biological samples as dichroic mirrors not only separate the excitation and emission light, they also allow the separate detection of light of different wavelengths (Jonkman and Brown 2015). The presence of a pinhole eliminates background haze and allows only the focal point to be visible on the objective, while the scanning mirrors rapidly and repeatedly scan one pixel at a time to produce a complete scanning image of the sample at the same depth of field (Prasad *et al.* 2007). Together this allows the build-up of 3-dimensional samples by scanning through the sectioning depths of the sample layer by layer to visualise intact bacterial cells *in situ* without physically slicing the bacterial cell.

Dosing determination experiment

In chapter 3, we determined the MIC of LNP + HPMC formulation against *E. coli*. In order to translate the dosage needed from a single culture to an *in vitro* batch model, experiments to ensure the LNP dose is high enough to exert antimicrobial activity were performed. Transitional experiments were designed that looked at the dosing proportions, different doses of LNPs were added to human faecal microbiota samples to estimate dosing required by altering the NP: human microbiota ratio. As a control, scrambled loaded nanoparticles (SLNPs), which are NPs loaded with TFD with a matching but non-functional scrambled sequence, were used to compare TFD-specific activity against LNPs. Whereas 'control' was composed of all the reagents used in the formulation of LNP except the NP and TFD as a base line control.

In the dosing determination experiment, the 1x dose equates to 0.66% (v/v) dose of total batch media volume, with doses up to 90x being tested in triplicate in order get a better idea of the optimal dose for the batch model experiment. The experiments were set up to mimic the batch

model in a smaller scale but without the pH control and stirring. Samples were taken at predose, 0 h, 8 h and 24 h to evaluate the viable counts of coliforms and total anaerobes in the sample by plating serial dilutions on selective media.

Batch culture fermentation

To investigate the gut microbiota's response to LNP treatment in an anaerobic, temperature- and pH- controlled system, *in vitro* batch model fermentation experiments were conducted (Mandalari *et al.* 2007). Samples were collected at selected time points for viable counts of different bacterial populations and the identity of the colonies on the MacConkey no. 3 plates (selective and differential agar that support *Enterobacteriaceae* growth) were subsequently confirmed using 16S rRNA gene PCR based sequencing. Cell pellets were processed both with and without propidium monoazide (PMA) to differentiate live/dead cells (Fujimoto *et al.* 2011) prior to Illumina Miseq sequencing to enrich our knowledge of the viable bacterial community (including non-culturable organisms) that were present in each treatment. 16S rRNA gene sequencing using the Illumina Miseq platform was then performed to determine the taxa of the gut microbiota community upon LNP treatments, PCoA plots were analysed to detect any structural changes occurring between different time points and treatments. Metabonomic analyses were also performed to identify any possible metabonomic changes to gain further insight into how LNP impact upon the gut microbiota function.

4.2. Materials and Methods

For methods relating to confocal microscopy, see Section 2.4; for batch culture fermentation, see Section 2.5. Methods for propidium monoazide treatment, DNA extraction for bacterial community profiling and subsequent 16S rRNA gene analysis can be found in Chapter 2.6.

4.2.1. LNP dosing determination experiment

To explore which NP: bacteria ratio is most effective against *E. coli* from human faecal slurry, different types and doses of NPs (i.e. control, SLNP and LNPs) and faecal bacteria ratios were used to achieve 1x (equivalent to 0.66% NP dose v/v in batch fermentation model), 1.65x, 3.36x, 12.5x and 90x dose compared to the standard ratio used in batch model. These were added to 1.35 ml of pre-reduced chemostat media and incubated without stirring in an anaerobic cabinet (see Table 4.1). Samples were taken at predose, 0 h, 8 h, 24 h for viable counts. In the scaled up experiment, volume of all components was 100x higher as stated below.

Table 4.1 Experimental details for dosing determination experiment.

	original dose (1x)	1.65x dose	3.36x dose	12.5x dose	90x dose
media (ml)	1.35	1.35	1.35	1.35	1.35
faecal dilution % in PBS	10%	6%	6%	6%	3.33%
faecal volume (μ l)	150	150	150	100	50
total faecal %	0.99%	0.60%	0.59%	0.40%	0.11%
NP added (μ l)	10	10	20	50	100
NP %	0.66	0.66	1.32	3.33	6.67
NP (ml): faeces (g) ratio	1: 1.5	1: 0.9	1: 0.45	1: 0.12	1: 0.0167

4.3 Results

4.3.1 TFD delivery in *E. coli* using confocal microscopy

LNPs formed with a fluorescently labelled TFD (Alexa-488 (green)) were used to determine whether they could transfect *E. coli*. Bacterial cell wall was labelled with TMR-WGA (red) when visualised with laser scanning confocal microscopy. TFD had been internalised or was associated with the outside of the bacterial cell. In Figure 4.1a, an *E. coli* cell control showed red fluorescence signal only on the surface of the bacterial cell, with no green fluorescence in the green channel; demonstrating that red fluorescent dye only causes fluorescence on the surface of the bacteria. When LNPs with green fluorescent-labelled TFDs were added to the bacteria (Figure 4.1b), green fluorescence can be seen within the boundaries of the red-fluorescently labelled bacterial cell wall, revealing that TFDs had successfully incorporated into the bacterial cell after 1.5 h incubation with LNPs (Figure 4.1 c).

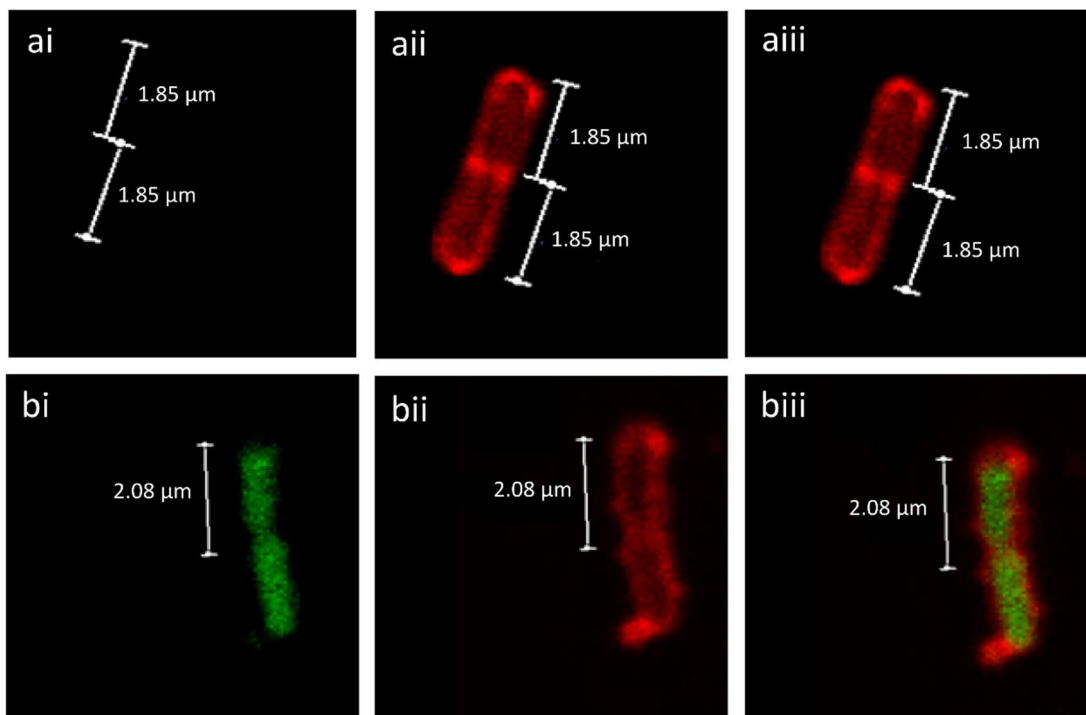


Figure 4.1 Confocal scanning images of (a) *E. coli* control and (b) *E. coli* cells with loaded nanoparticles in L media. The incorporation of Transcription Factor Decoy (TFD) from the LNP was shown in (biii) but not when TFD is absent in (aiii). Red: *E. coli* cell wall; Green: TFD. i) green channel; ii) red channel; iii) red and green channel overlay.

To compare the efficiency of TFD incorporation within *E. coli* when used in physiologically relevant *in vitro* conditions, *E. coli* cells were treated with the NP formulation of choice, LNP + 0.1% HPMC in the presence of chemostat media, to imitate the conditions used in the batch model fermentation.

When LNP-treated *E. coli* were incubated in chemostat media and a water control, both treatments showed successful delivery after 1.5 h of TFD incubation with delivery increasing at 4 h; more TFD incorporation was observed when incubated in water (Figure 4.2 c) compared to those in chemostat media at both 1.5 h (Figure 4.2 a) and 4 h (Figure 4.2 b). This showed that LNPs incubated in different solution i.e. Luria (L) broth (Figure 4.1), water (Figure 4.2 c) and chemostat media (Figure 4.2 a) can be transfected within the same time frame of 1.5 h; though the transfection efficiency is lower when incubated in chemostat media compared to the water control. In summary, LNP were able to incorporate within *E. coli* in L broth and chemostat media for nanoparticle delivery, and 4 h of LNP incubation result in optimal nanoparticle delivery with the current experimental settings (Figure 4.2 b and d).

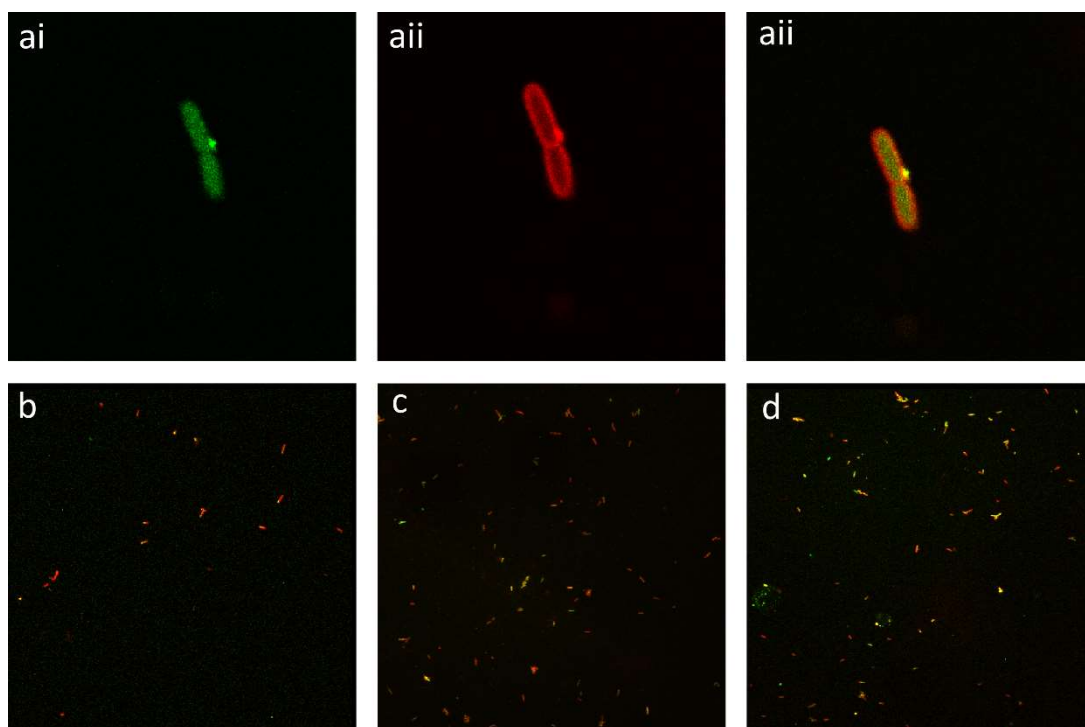


Figure 4.2 Confocal scanning images of a) *E. coli* with LNP + 0.1% HPMC in chemostat media incubated for 1.5 h; i) green channel; ii) red channel; iii) red and green channel overlay; b) broad view of *E. coli* + LNP + 0.1% HPMC incubated in chemostat media for 4 h; c) broad view of *E. coli* + LNP + 0.1% HPMC incubated in water control for 1.5 h; d) broad view of *E. coli* + LNP + 0.1% HPMC incubated in water control for 4 h. Red: *E. coli* cell wall; Green: TFD.

4.3.2. Analysis of viable microbial community in human faecal bacteria cultures in dosing determination experiments

Bacteriostatic activity was achieved at 1x LNP dose in triplicate experiments

As NPs will likely adhere to other bacteria in the gut microbiota, to ensure successful NP delivery to the *Enterobacteriaceae*, it is important to adjust the NP dosage accordingly to allow efficient targeting. To investigate the amount of LNPs needed to show antimicrobial effect in a mixed faecal bacterial community, different ratios of NPs: faecal microbiota (including 1x, 1.65x, 3.36x, 12.5x and 90x dose) were tested in triplicate experiments to determine the minimum NP dose needed to display antimicrobial activity (see dosing scheme in Section 4.2.1). To achieve bacteriostatic antimicrobial activity ($> 1 \log_{10}$ and $< 3 \log_{10}$ decrease in colony forming units) (Pankey and Sabath 2004, Basri *et al.* 2014), as little as 1x dose was needed repeatedly when comparing the experimental observations from the triplicate experiments (Figure 4.3). At this minimum 1x dose, sufficient antimicrobial activity against coliforms was observed with LNP + 0.1

% HPMC, while anaerobic bacteria were unaffected with all treatments (control, SLNP + 0.1% HPMC and LNP + 0.1% HPMC). SLNP treatment did not reduce coliforms level, indicating the antimicrobial activity in LNP treatment was TFD-specific. LNPs were effective against coliforms in the triplicate experiments, despite there were large variations in the efficacy ranging from $\log_{10} 1$ to $> \log_{10} 5$ CFU/ml decrease in the coliforms viable counts.

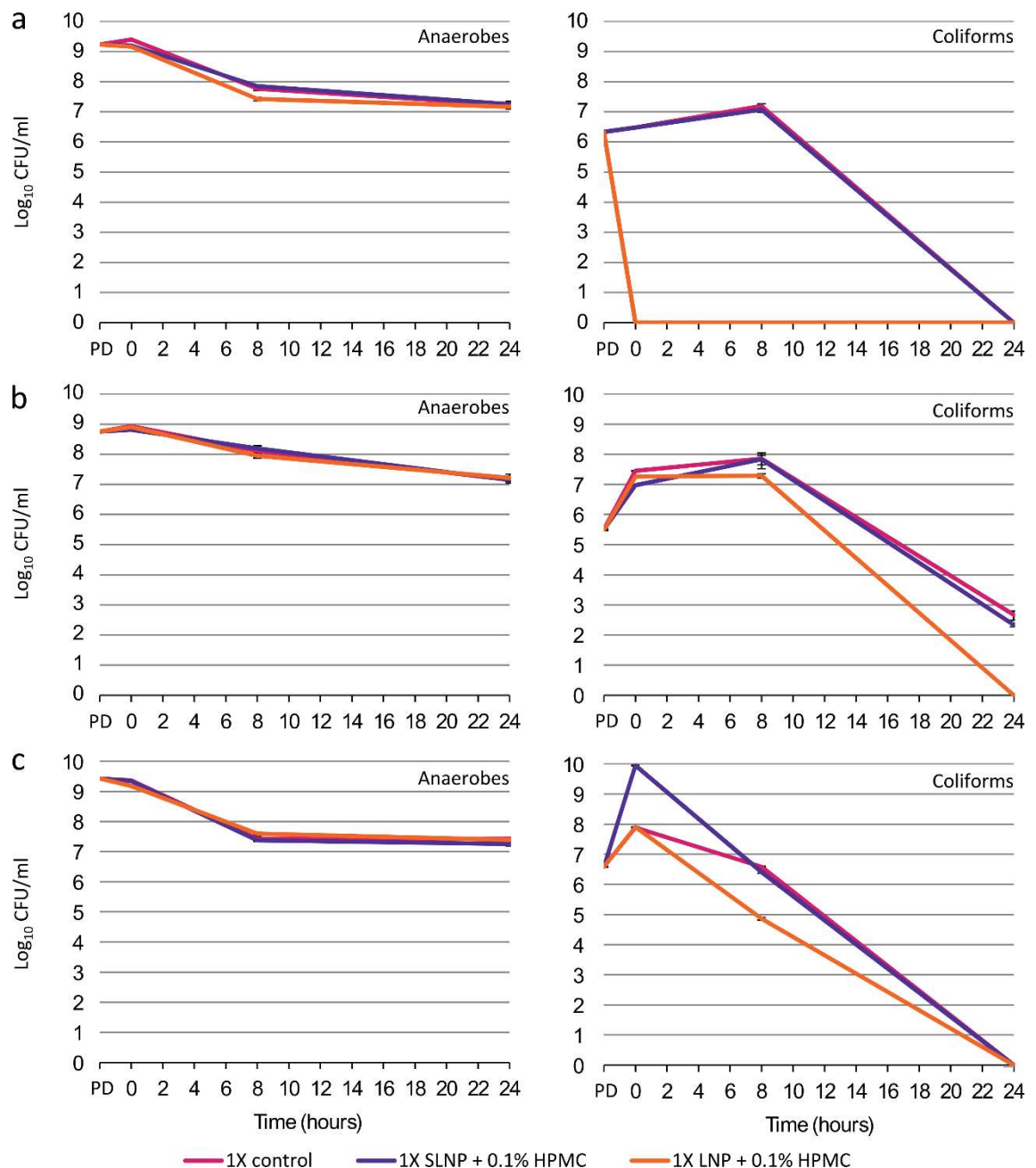


Figure 4.3 Bacterial viable counts of anaerobes (left) and coliforms (right) in dosing determination experiments at 1x NP dose in a) experiment 1; b) experiment 2; c) experiment 3. Same donor was used in all 3 experiments.

Variation in minimum bactericidal dose in triplicate dosing determination experiment

Unlike bacteriostatic activity, the minimum LNP dose required for bactericidal antimicrobial activity ($\geq 3 \log_{10}$ decrease in CFU) (Lee and Burgess 2013) differed between experimental runs. A minimum of 1x, 3.36x and 12.5x LNP doses were needed in the triplicate experiments respectively (Figure 4.4). As there was a 12.5x difference in the minimum LNP dose required for bactericidal activity, large variation in LNP dose required to target sufficient quantities of coliforms were noted even though the freshly void faecal samples originated from the same donor. In general, minimal changes in the viable bacterial counts of total anaerobes were observed from LNP treatment compared to control and SLNP in most LNP doses for all 3 experiments, suggesting LNP were mostly TFD-specific against coliforms and did not reduce the population in the rest of the gut microbiota samples as indicated by total anaerobe viable counts. Non-specific antimicrobial activity was observed at 90x LNP dose in experiment 1; a \log_{10} 3 CFU/ml decrease in total anaerobe viable counts were observed in LNP treatment compared to control and SLNP from 8 h onwards (Figure 4.4 a). However, non-specific damage to the total anaerobes at 90x were only observed in one out of three experiments, suggesting that large quantities of LNP (90x more than the minimum bactericidal dose) was needed to cause non-specific antimicrobial effect on the rest of the gut microbiota.

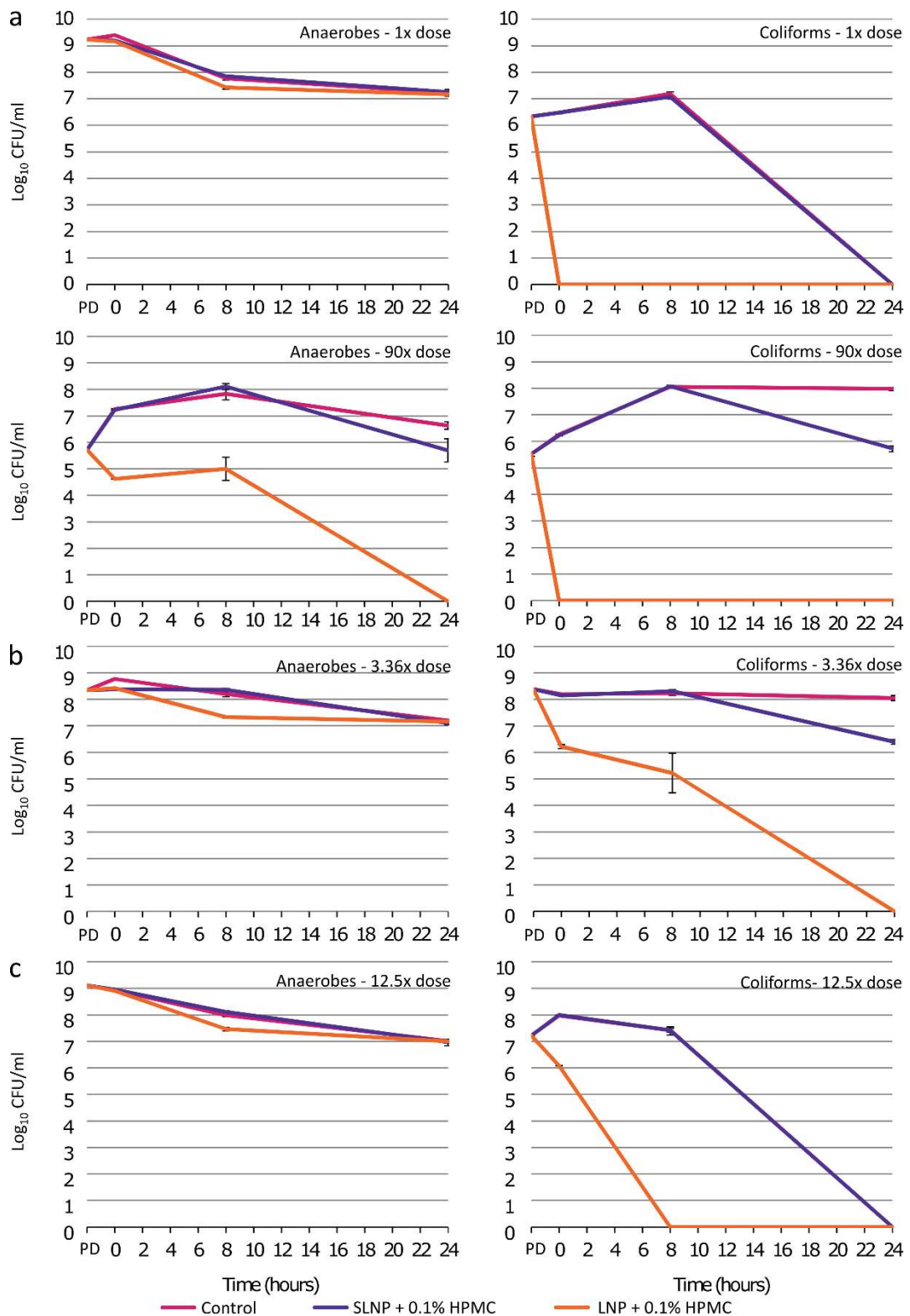


Figure 4.4 Bacterial viable counts from anaerobes (left) and coliforms (right) for dosing determination experiment a) experiment 1 - 1x dose is already enough for significant antimicrobial activity specific to *E. coli*, however 90x dose showed some sign of broad spectrum effect on the rest of the gut microbiota; b) experiment 2 - 3x dose is needed for significant antimicrobial activity specific to *E. coli*; c) experiment 3 - 12.5x dose is needed for significant bactericidal ($\geq \log_{10} 3$ decrease in CFU/ml) antimicrobial activity specific to *E. coli*.

Dosing determination at a larger volume

To determine whether the NP dosage needed is scalable for future batch culture fermentation experiments, a scaled-up experiment with a larger total volume (150 ml instead of 1.5 ml) was run in parallel with dosing determination experiment 2 and 3.

In dosing determination experiment 2, 1x dose was tested in the scaled up experiment (without stirring just like the dosing determination experimental set up), there were no differences in viable bacterial counts for total anaerobes and coliforms (Figure 4.5 a). Both the scaled up 1x dose and the 1x dose from the dosing determination experiment (Figure 4.3 b) did not show bactericidal activity as expected.

Even though no bactericidal activity was observed at 1x dose in dosing determination experiment 3 (Figure 4.3 c), a minimum of 12.5x LNP dose was needed for bactericidal activity (Figure 4.4 c). When the experiment was scaled up with stirring, a $\geq \log_{10} 5$ decrease in coliforms viable counts was observed with 1x LNP dose at 8 h compared to control (Figure 4.5 b). Suggesting bactericidal activity was enhanced and the minimal bactericidal dose needed was lowered (i.e. from 12.5x to 1x) when scaled up with stirring. Combining the results from Figures 4.3, 4.4 and 4.5, it was decided that a 3x dose was a feasible LNP dosage that could provide sufficient antimicrobial activity against *Enterobacteriaceae* without collateral damage to the rest of the gut microbiota when scaling up for the batch culture fermentation experiments which involves stirring, the results will be detailed in the next section (Section 4.3.3).

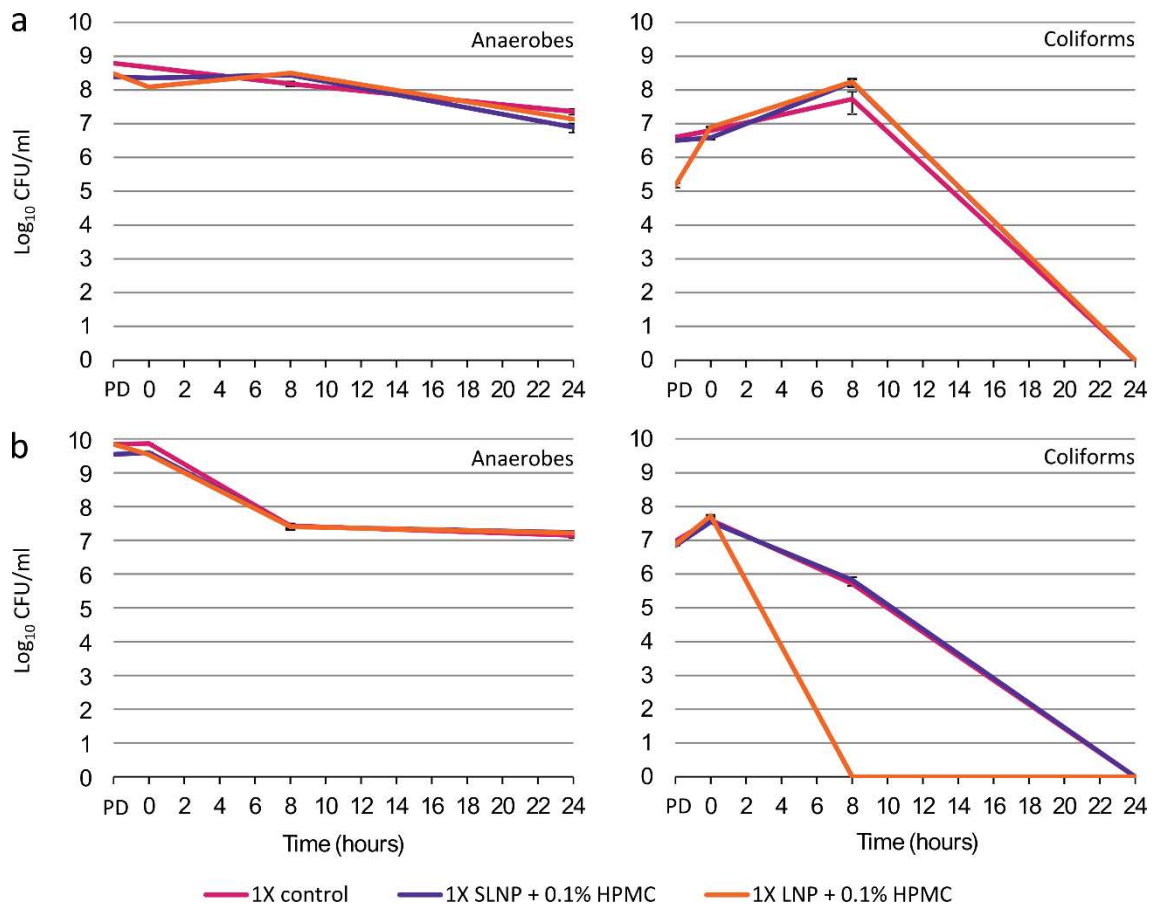


Figure 4.5 Bacterial viable counts of anaerobes (left) and coliforms (right) in a scaled up study of a) dosing determination experiment 2; b) dosing determination experiment 3, in 150 ml vessels (with no pH control).

4.3.3 Assessing effects of LNPs in human faecal bacterial cultures mimicking colon condition *in vitro*

After determining the predicted dosing range suitable for the mixed human gut microbiota samples, 3x dose (equivalent to 2% of total volume in the batch culture fermentation) were used to determine whether LNP can efficiently reduce the coliforms population without affecting the rest of the gut microbiota communities in a temperature- and pH- controlled anaerobic environment mimicking conditions in the human colon, using different faecal donors in experiment 1 to 4.

Batch culture fermentation experiment 1

In the first batch culture fermentation experiment, the bacterial viable counts were at similar levels at predose for all the bacterial groups examined. The composition of the overall viable total anaerobe and *Lactobacillus* community treated with control, SLNP and LNP were similar over the

8 h period (Figure 4.6). This shows that LNPs did not damage the overall gut microbiota or the beneficial *Lactobacillus* population.

Total *Enterobacteriaceae* viable bacterial counts were decreased by \log_{10} 3 CFU/ml with LNP treatment at 0 h, whereas there was a \log_{10} 2.5 CFU/ml decrease at 4 h compared to the control, a \log_{10} 3 CFU/ml drop was also observed at 8 h with SLNP treatment. The viable coliforms population were \log_{10} 5 CFU/ml at predose for all treatments. Notably, immediately after the addition of LNPs at 0 h, a significantly decreased were observed with LNP treatment, whereby no coliforms were detected (limit of detection < 16 CFU/ml), compared to \log_{10} 6.5 CFU/ml in control and SLNP treatments. The lack of detectable coliforms in LNP-treated sample was maintained for 8 h until the end of the experiment, as compared to the control which had \log_{10} 8.5 and \log_{10} 9 CFU/ml of coliforms at 4 h and 8 h respectively. For SLNP, the coliforms levels were similar to those in control up to 4 h, before the levels decrease to \log_{10} 6 CFU/ml.

Bifidobacterium population was not shown as no detectable colonies were present (limit of detection < 1.67×10^5 CFU/ml). In general, control and SLNP treatments had similar bacterial counts at 0 h and 4 h for the bacterial groups examined, though some decrease has been observed across all groups in the vessels containing SLNP at 8 h. A higher final volume was observed in the sample vessel containing SLNP treatment compared to the control and LNP, this is due to automated pH buffer addition. This may have diluted the samples in the SLNP vessel leading to a reduction in countable colonies in a given volume.

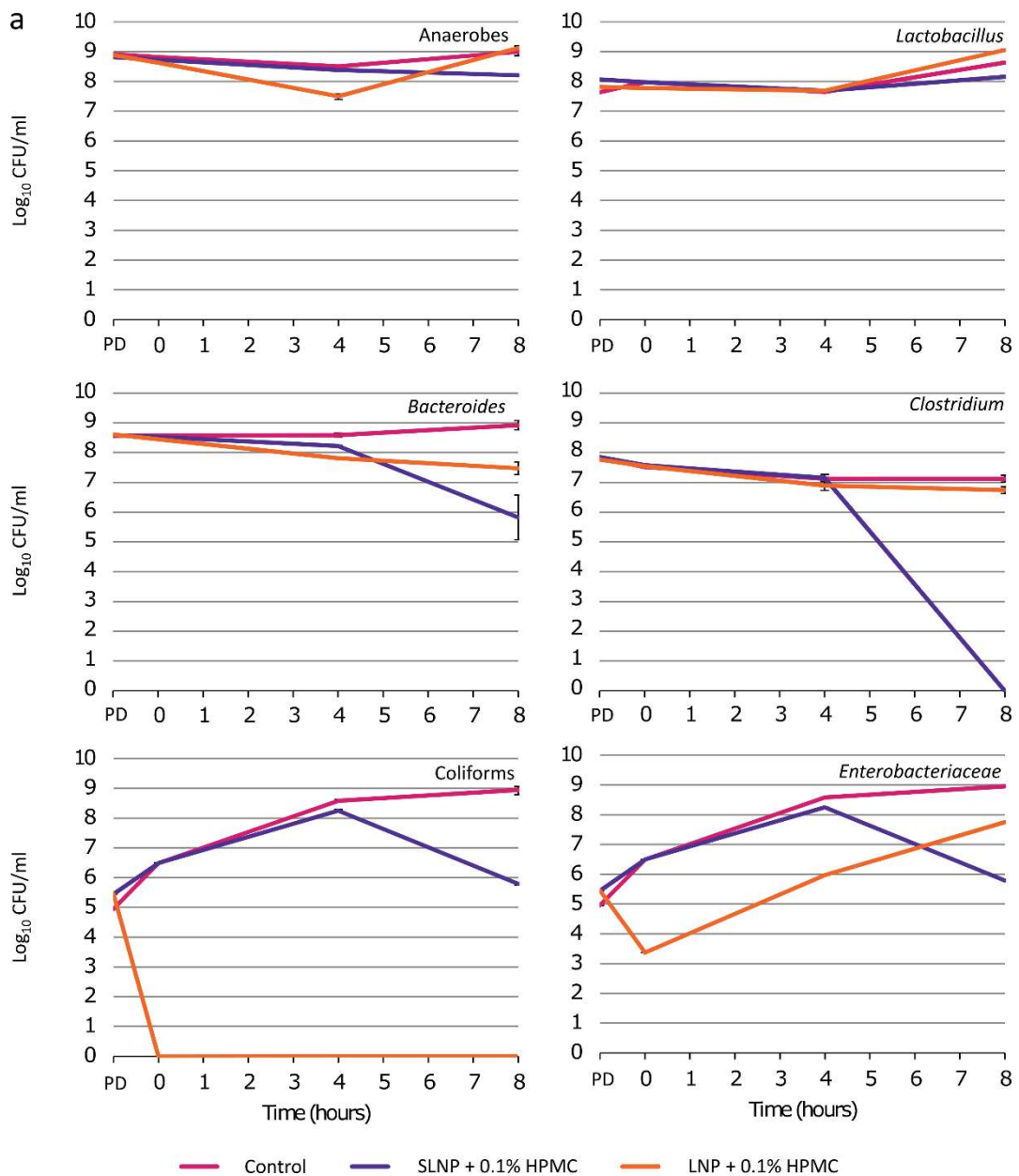


Figure 4.6 Bacterial viable counts for anaerobes, *Bacteroides*, *Clostridium*, *Lactobacillus*, coliforms and *Enterobacteriaceae* for control, SLNP and LNP treatments at 2% doses in batch culture fermentation experiment 1. PD, predose-treatment; treatments were added at 0 h prior to sampling.

Colonies on MacConkey no. 3 plate with LNP treatment at 0 h, 4 h and 8 h (bright pink coloured with lots of bile precipitation) were notably different to the samples from other treatments and time points (pink coloured) (Figure 4.7), suggesting the change in the *Enterobacteriaceae* population subject to LNP-treatment from 0 h was effective until the end of the experiment at 8 h. By comparing the identity of 10 randomly selected MacConkey no. 3 colonies from each of SLNP and LNP treatment, sequencing results from 16S rRNA gene colony PCR suggests the presence of *E. coli* (pink) with SLNP treatment, whereas 8 colonies were suggested as *Klebsiella*

pneumonia (bright pink) and 2 colonies were identified as *E. coli* (pink) in LNP-treated samples at 4 h (Table 4.2). This suggests that *E. coli* levels were reduced by LNP though *Klebsiella* spp. appeared less sensitive.

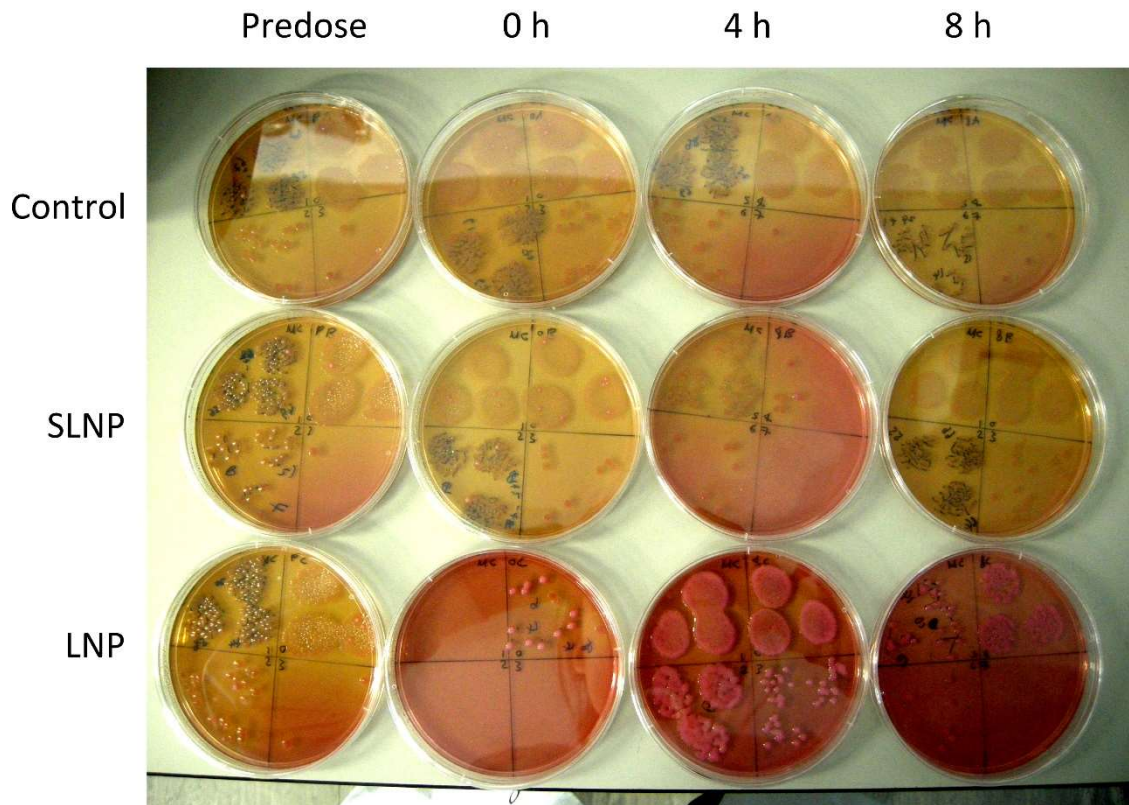


Figure 4.7 *Enterobacteriaceae* colonies on MacConkey no. 3 plates for batch culture fermentation experiment 1. Pink colonies were mostly present at predose for all treatments and in control and SLNP treatments at 0 h, 4 h and 8 h, whereas bright pink colonies were mostly present with LNP at 0 h, 4 h and 8 h.

Batch culture fermentation experiment 2

The second batch culture fermentation experiment was performed using a different donor (Figure 4.8). While the viable counts of the total anaerobic microbiota were similar between control and SLNP throughout the course of the experiment, the total anaerobes level were lowered in LNP-treated samples by $\log_{10} 2$ CFU/ml at 8 h compared to the controls. *Bacteroides* viable levels for all 3 treatments corresponded with the trend seen in total anaerobes. *Bifidobacterium* had similar levels across all 3 treatments at each of the time points, while *Clostridium* were at relatively similar levels across treatments up to 4 h and had around $\log_{10} 2$ decrease from LNP treatment compared to the control.

Lactobacillus levels were similar between SLNP and control up to 4 h, levels were decrease in SLNP approximately \log_{10} 2.5 CFU/ml at 8 h compared to the control; whereas for LNP-treatment lactobacillus level decreased by \log_{10} 2 CFU/ml at 4 h and 8 h compared to the control treatment.

Total *Enterobacteriaceae* viable bacterial counts were decreased to an undetectable amount (< 16 CFU/ml) with LNP treatment at 0 h. Although some growth was observed from 4 h onwards, there was still a \log_{10} 4 and \log_{10} 2.5 CFU/ml decrease at 4 and 8 h respectively compared to their controls.

The coliforms viable levels with control and SLNP treatment had similar trends to total anaerobes and *Bacteroides*; immediately after the addition of LNPs at 0 h, viable coliforms levels decreased to an undetectable amount (< 16 CFU/ml) up to 4 h, before levels recovering at 8 h to \log_{10} 6.5 CFU/ml. This evidently suggests LNP's ability to exert antimicrobial activity against *Enterobacteriaceae* without disrupting other commensal bacterial communities in the microbiome.

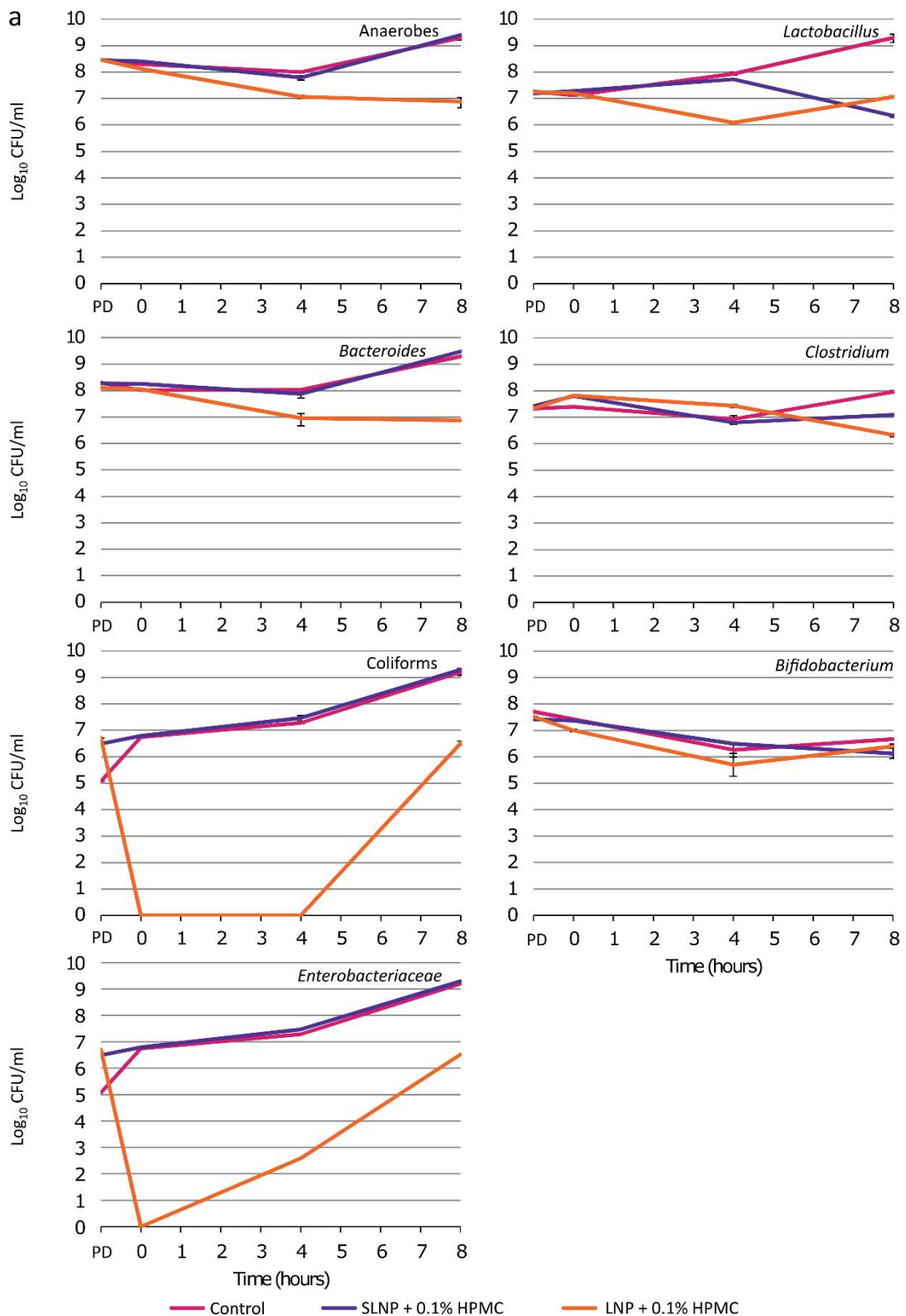


Figure 4.8 Bacterial viable counts for anaerobes, *Bacteroides*, *Clostridium*, *Lactobacillus*, coliforms and *Enterobacteriaceae* for Control, SLNP and LNP treatments at 2% doses in batch culture fermentation experiment 2. PD, predose-treatment; treatments were added at 0 h prior to sampling.

Colonies on MacConkey no. 3 plate with LNP treatment at 4 h (straw coloured) were notably different to the samples from other treatments and time points (pink coloured) (Figure 4.9), suggesting LNP treatment changed the population of *Enterobacteriaceae* present in the gut microbiota 4 h after the treatment; the *Enterobacteriaceae* colonies with LNP at 8 h again had similar morphology as the corresponding samples presented in control and SLNP. Ten colonies from each of the coliforms no. 3 agar plates with LNP- and SLNP-treated samples were processed with 16S rRNA gene colony PCR and sequenced via 16S rRNA gene sequencing. This identified the colonies taken from plates with SLNP treatment as *Escherichia/Shigella* spp. (pink colonies). Only *Pseudomonas aeruginosa* (straw-coloured) colonies were present with LNP treatment, suggesting *Escherichia/Shigella* species was reduced with LNP treatment between 0 h and 4 h (Table 4.2).

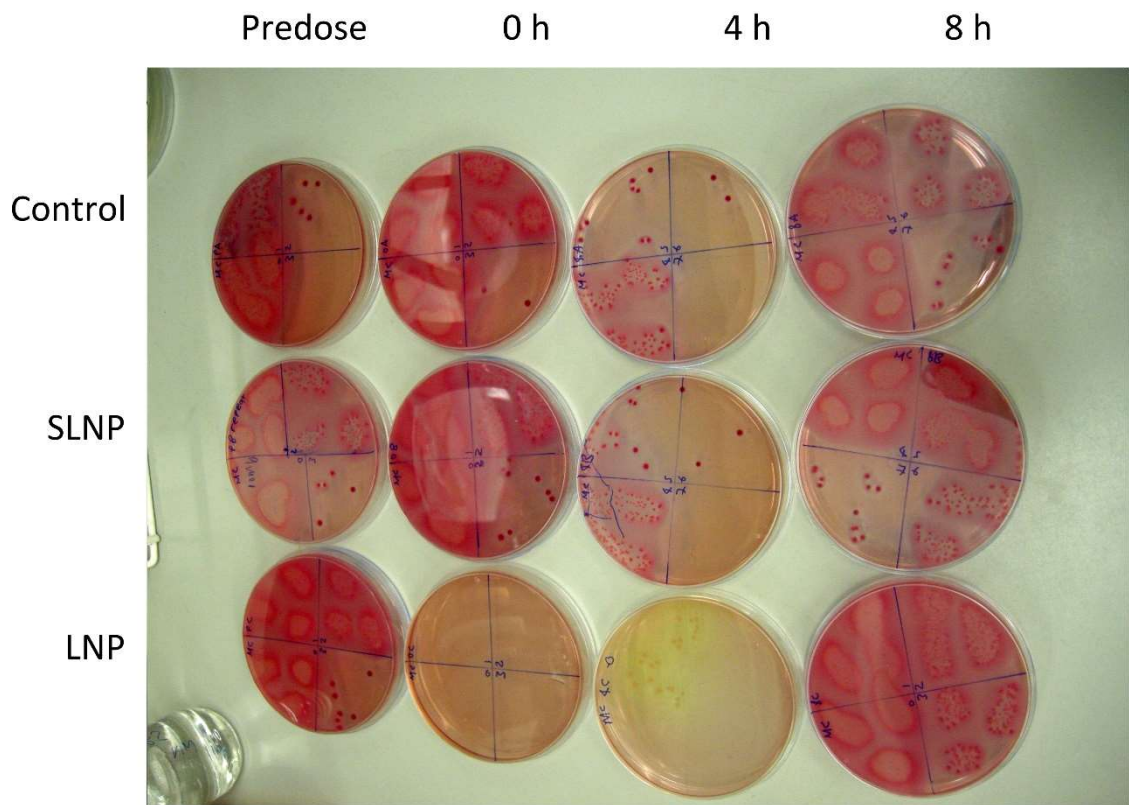


Figure 4.9 *Enterobacteriaceae* colonies on MacConkey no. 3 plates for batch culture fermentation experiment 2. Pink colonies were mostly present at predose for all treatments and in control and SLNP treatments at 0 h, 4 h, 8 h and with LNP at 8 h, whereas straw-coloured colonies were mostly present with LNP treatment at 0 h and 4 h.

Batch culture fermentation experiment 3

In the third batch culture fermentation experiment, no difference in the viable counts in the anaerobes, *Lactobacillus*, *Bacteroides*, *Clostridium*, *Bifidobacterium*, *Enterobacteriaceae* and coliforms population were observed between control, SLNP and LNP from predose to 8 h (Figure 4.10). As the NPs activity were tested against *E. coli* pure cultures in parallel of the batch fermentation, we were able to determine whether LNPs contributed towards the lack of antimicrobial activity against the gut microbiota. The LNPs used in experiment 3 showed $> 3 \log_{10}$ decrease in CFU/ml of *E. coli* compared to the control, suggesting bactericidal antimicrobial activity was present in the LNPs. Furthermore, it was also noticed that the starting coliforms bacterial population of this faecal sample were higher than those observed in the previous two experiments ($\log_{10} 7$ CFU/ml as opposed to $\log_{10} 6$ CFU/ml previously), thus suggesting other factors such as bacterial load could contributing towards the lack of notable antimicrobial activity from LNP treatment against coliforms. A higher dose may therefore be required to show sufficient antimicrobial activity against coliforms in the mixed human gut microbiota sample in future experiment.

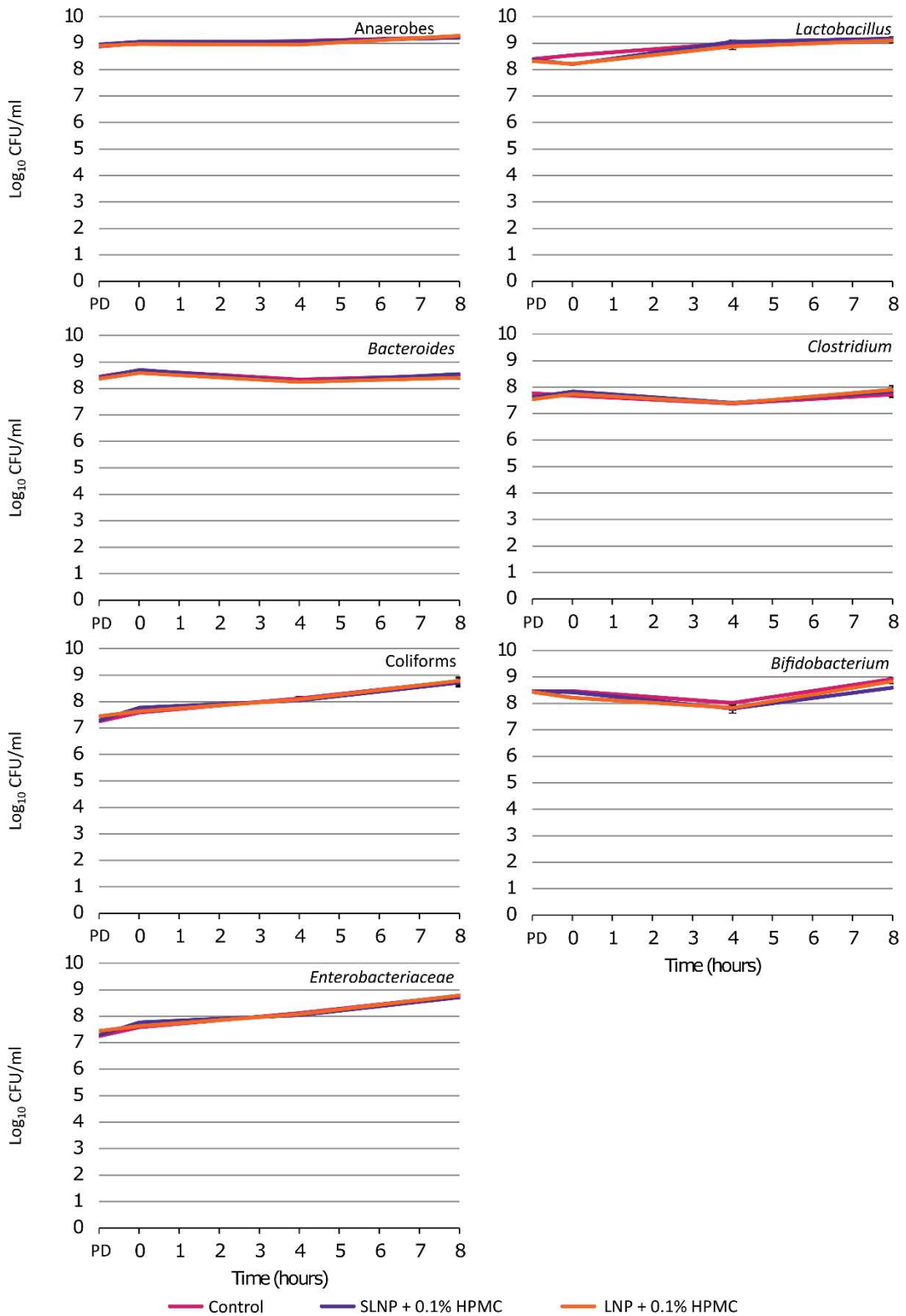


Figure 4.10 Bacterial viable counts for anaerobes, *Bacteroides*, *Clostridium*, *Lactobacillus*, coliforms and *Enterobacteriaceae* for control, SLNP and LNP treatments at 2% doses in batch culture fermentation experiment 3. PD, predose-treatment; treatments were added at 0 h prior to sampling.

Batch culture fermentation experiment 4

Following the lack of antimicrobial activity against coliforms in the third batch culture fermentation experiment, both 2% (i.e. 3x dose, the original dose also used in experiment 1 and 2) and 10% (i.e. 15x dose) doses of NPS were administered in parallel in the fourth batch culture fermentation experiment using the same faecal sample. At the usual 2% NP dose (Figure 4.11), viable bacterial counts were similar between SLNP, LNP and the control for *Bacteroides* and *Clostridium* population throughout the course of the experiment. Only small decrease in viable counts ($\leq \log_{10} 1$ CFU/ml) were observed with LNP treatment in total anaerobe, *Lactobacilli*, total *Enterobacteriaceae* and coliforms population at 4 h compared to the control and SLNP, while having similar viable counts between all treatments at predose, 0 h and 8h. Just like the third experiment, no bactericidal activity was observed against coliforms with 2% LNP treatment.

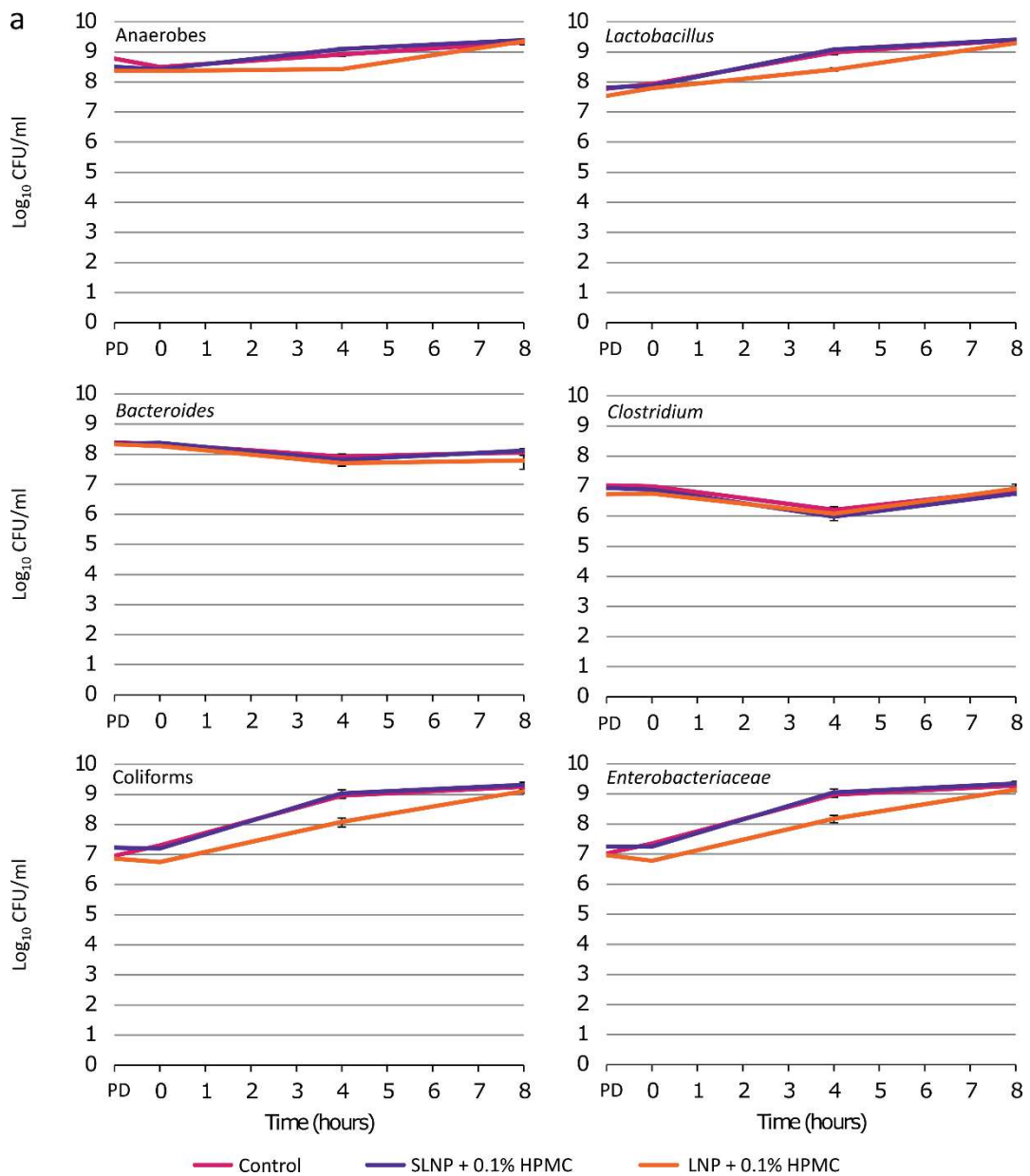


Figure 4.11 Bacterial viable counts for anaerobes, *Bacteroides*, *Clostridium*, *Lactobacillus*, coliforms and *Enterobacteriaceae* for control, SLNP and LNP treatments at 2% doses in batch culture fermentation experiment 4. PD, predose-treatment; treatments were added at 0 h prior to sampling.

In contrast, with 10% LNP a log₁₀ 3 CFU/ml decrease in *Enterobacteriaceae* and coliforms was observed at 0 h and 4 h compared to the control (Figure 4.12), indicating that the LNP targeted antimicrobial approach is dose dependent. The levels of total *Enterobacteriaceae*/ coliforms with LNP treatment grew to similar levels to those with control and SLNP treatment at 8 h. A log₁₀ 2 CFU/ml decrease in viable bacterial counts for total anaerobes and *Lactobacillus* population were observed at 4 h with LNP treatment, though they returned to similar levels to those in the control

and SLNP treatment after 8 h, suggested the temporal disturbance in the mentioned bacterial groups against a high LNP dose were reversible. *Bacteroides* and *Clostridium* viable bacterial counts were decreased by about \log_{10} 1 CFU/ml with LNP at 4 h compared to the control, and remained similar levels at 8 h.

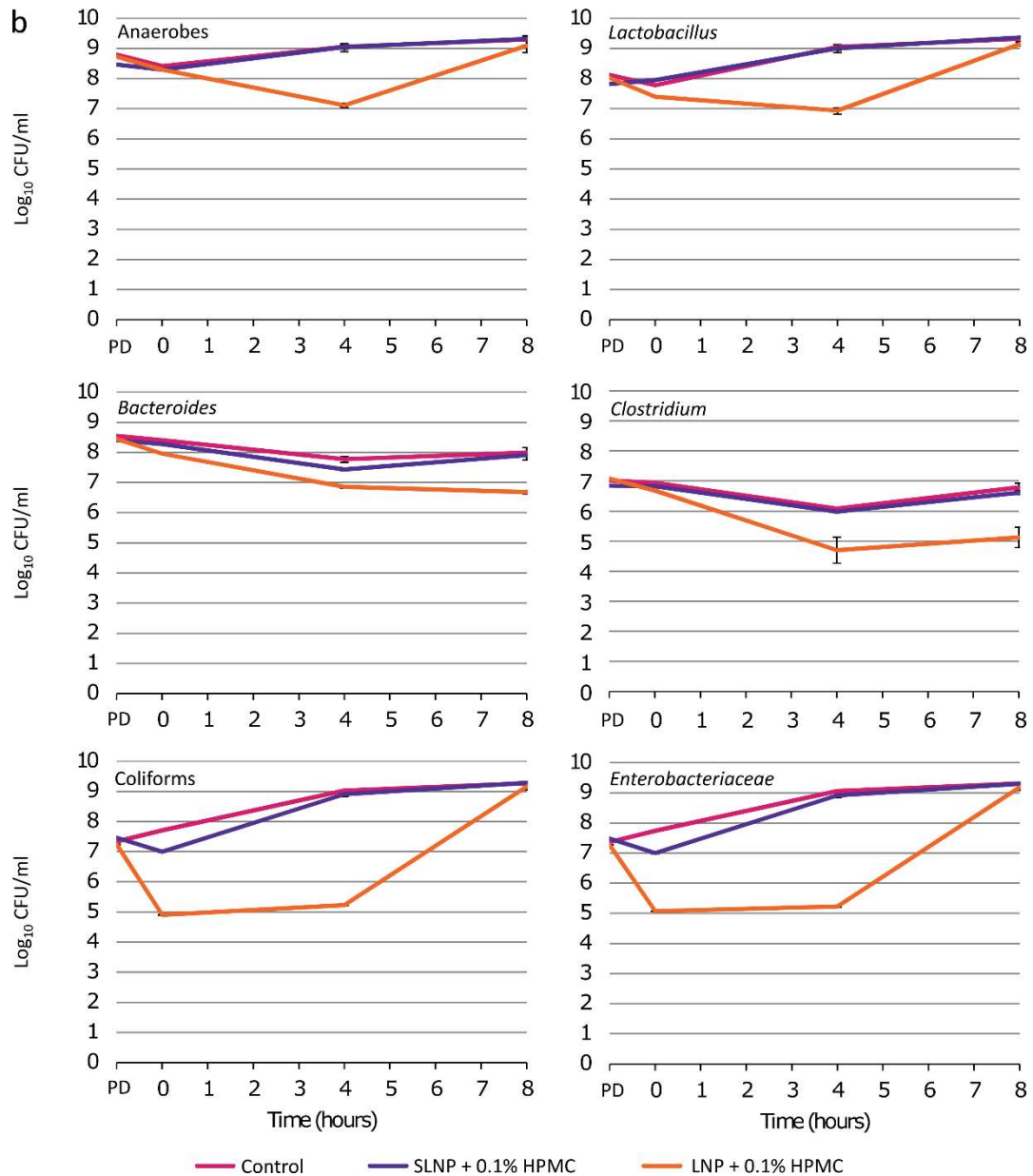


Figure 4.12 Bacterial viable counts for anaerobes, *Bacteroides*, *Clostridium*, *Lactobacillus*, coliforms and *Enterobacteriaceae* for control, SLNP and LNP treatments at 10% doses in batch culture fermentation experiment 4. PD, predose-treatment; treatments were added at 0 h prior to sampling.

16S rRNA gene sequencing confirmed that selected colonies present in both 10% SLNP and 10% LNP treated samples (10% dose) on MacConkey no. 3 agar were *Escherichia/Shigella* spp. and *Klebsiella* spp., suggesting that there were little difference in the composition of *Enterobacteriaceae* population subject to 10% SLNP and LNP treatments even though the viable population were sufficiently decreased (Table 4.2).

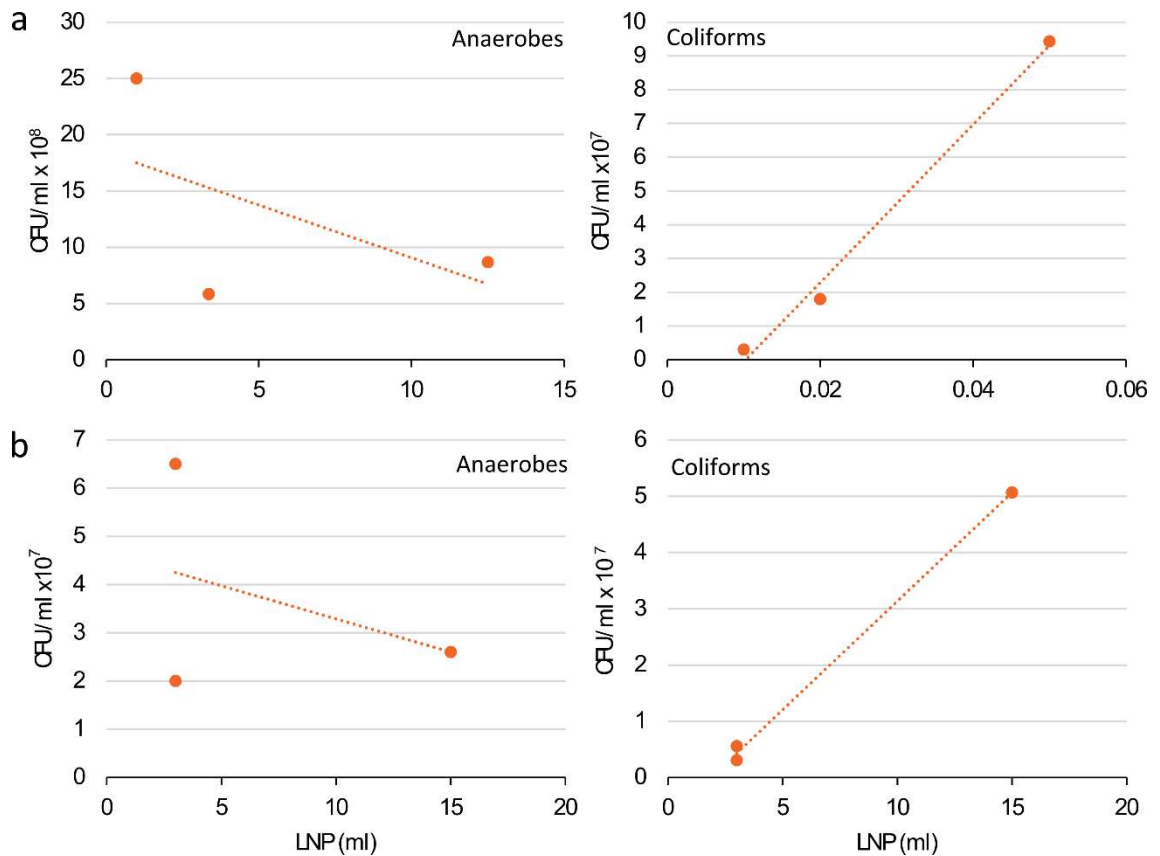
Table 4.2 Summary 16S rRNA gene colony PCR sequencing identity of MacConkey no. 3 colonies from Batch culture fermentation model.

	<i>Escherichia/Shigella</i> spp.		<i>Klebsiella pneumonia</i>		<i>Pseudomonas aeruginosa</i>	
	<u>SLNP</u>	<u>LNP</u>	<u>SLNP</u>	<u>LNP</u>	<u>SLNP</u>	<u>LNP</u>
Experiment 1	10	2	-	8	-	-
Experiment 2	9	-	-	-	-	10
Experiment 4	9	8	1	2	-	-

We did not see coliforms-targeting antimicrobial activity in batch culture fermentation experiment 3 (at 2% LNP) and in experiment 4 antimicrobial activity was exerted only at 10% but not 2% dose. Therefore there may be a dose dependant effect relating to the quantity of bacteria presented in the faecal sample against the amount of NPs administered. To determine whether the density of the inoculum affects response to LNP, the starting viable count for anaerobes and coliforms in control treatment were plotted against LNP dose added at 0 h. There were no linear correlations when the total anaerobe colonies were plotted against the volume of LNP (Figure 4.13), either from the dosing range ($R^2= 0.302$) or batch culture fermentation experiments ($R^2= 0.152$). However, when the quantity of starting coliforms were plotted against the volume of LNP, a positive linear regression was obtained with R^2 of 0.992 and 0.998 respectively for LNP dosing determination (Figure 4.13 a) and batch model experiments (Figure 4.13 b), suggesting the successful exertion of LNP antimicrobial activity is associated with the starting coliforms quantity, but not total anaerobes, at the time of NP administration from preliminary data.

The correlation equation was applied to some experiments that did not show antimicrobial activity against *Enterobacteriaceae*. By inserting the starting *Enterobacteriaceae* levels in to the equation, the volume of LNP required for antimicrobial activity was predicted. As expected, the LNP dose used was lower than the predicted effective dose (Figure 4.13 c), which further suggests

the importance of the starting coliforms population in defining the effective dose of LNPs to exert bactericidal antimicrobial activity.



c

Relative LNP dose used (%)	2%	2%	2%	2%
LNP dose used (ml)	3	3	3	3
Starting coliforms in control when LNPs were added at 0 h (CFU/ml)	9.18x10 ⁶	3.50x10 ⁷	3.85x10 ⁷	2.02x10 ⁷
Predict LNP dose needed for sufficient bactericidal activity with $x=(y+7 \times 10^6)/4 \times 10^6$ (ml)	4.05	10.50	11.38	6.79
Is the LNP dose used sufficient for bactericidal activity from the prediction?	No	No	No	No

Figure 4.13 Linear relationship between starting coliforms quantity and LNP dose for a) dosing determination experiment; and b) batch model fermentation; c) prediction of minimum dose required for sufficient antimicrobial activity in the batch model with different gut microbiota samples.

To elucidate growth (or the lack of) at later time points upon NP administration, the change in CFU compared to their respective predose value were used for statistical analysis. LNP only significantly reduced ($P \leq 0.001$) the CFU of *Enterobacteriaceae* and coliforms at 0 h, when compared to their respective controls, when data from experiment 1,2 and 4 at 2% LNP dose were combined. When viable count data from batch experiments 1, 2 and 4 were combined (based on a bactericidal dose of 2%, 2% and 10% NPs respectively), it was suggested that while coliforms viable counts were reduced by $> \log_{10} 3$ CFU/ml at 4 h, other bacterial groups such as *Bacteroides*, *Bifidobacterium*, *Clostridium* and *Lactobacillus* and the total anaerobes were maintained, with small decrease in total anaerobes as expected from the decrease in coliforms population (Figure 4.14). This suggests that overall, given the LNP dose were appropriately administered according to the starting quantity of coliforms, LNPs has the ability to exert antimicrobial activity targeting coliforms specifically without altering the rest of the gut microbiota community.

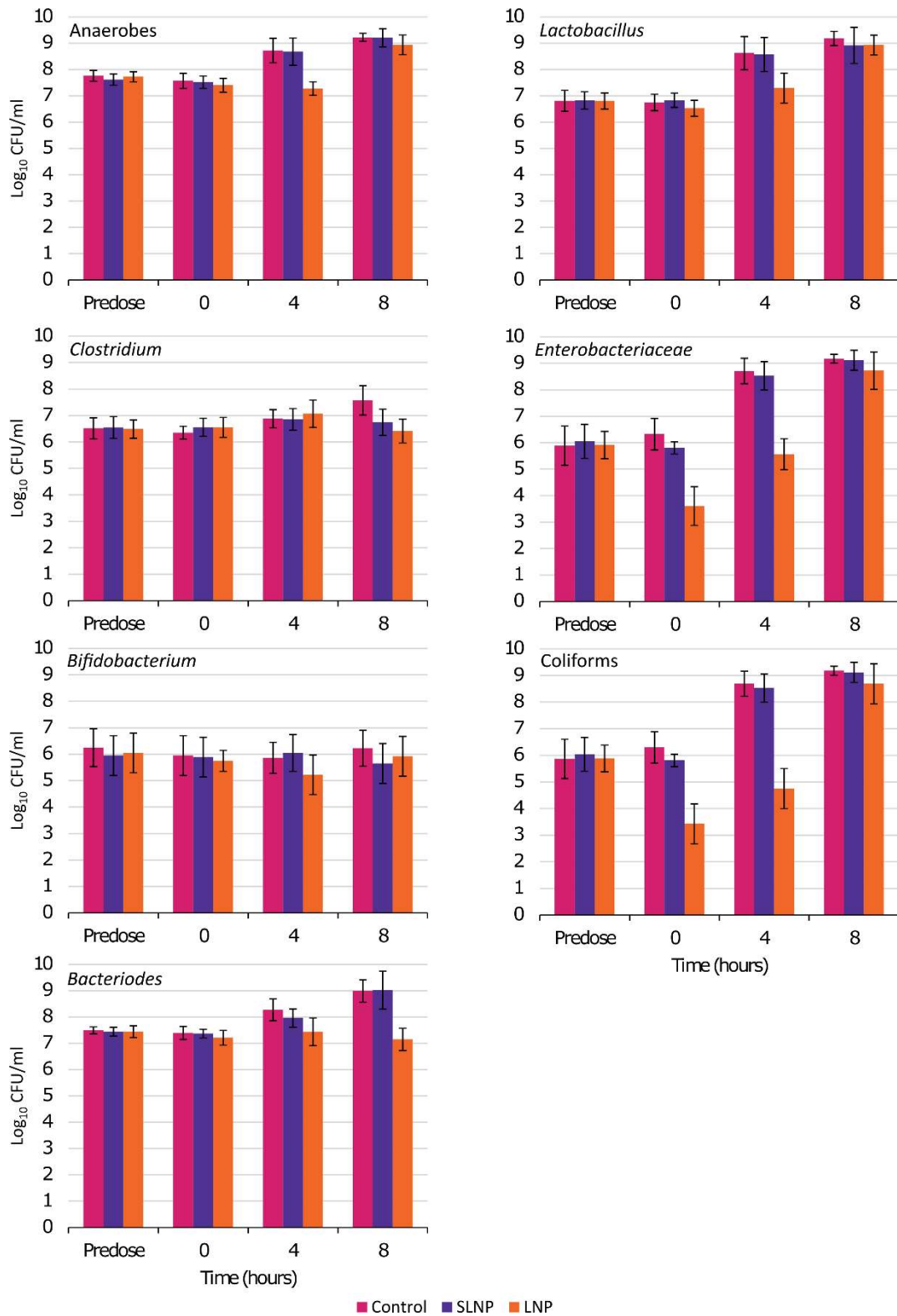


Figure 4.14 Averaged viable bacterial colony counts for *in vitro* batch culture fermentation experiments 1, 2 and 4. Bacterial viable counts for anaerobes, *Bacteriodes*, *Clostridium*, *Lactobacillus*, coliforms and *Enterobacteriaceae* with control, SLNP and LNP treatments were calculated from bactericidal dose of 2%, 2% and 10% respectively.

4.3.4. Metataxonomic analyses of microbial community in human faecal bacteria cultures

To determine the viable numbers of *Enterobacteriaceae* in the 16S rRNA gene community analysis, it is important to only take account of the live bacteria in the sample and omit the dead community to elucidate the antimicrobial effect in the viable portion of the gut microbiota community. Samples taken from the batch culture fermentation were treated with propidium monoazide (PMA) that was photo-activated. This photo-activation causes intercalation of double stranded DNA from dead bacteria to prevent PCR amplification for subsequent 16S rRNA gene sequencing (Fujimoto *et al.* 2011). The comparison between untreated and PMA-treated samples are shown in Figure 4.15 a and b respectively. The PMA-treated samples more closely resembled the viable *Enterobacteriaceae* trend in the viable bacterial counting results (Figure 4.6) compared to the untreated sample and was used for the determination of viable populations for all 16S rRNA gene analysis thereafter.

16S rRNA gene sequencing data obtained from the Illumina Miseq platform showed that while bacterial communities at the family level were similar at predose for all 3 experiments, a notable decrease in the proportion of *Enterobacteriaceae* out of the total bacterial community were seen in LNP-treated samples at 4 h in batch model experiments 1, 2 and 4 individually (Figure 4.15, 4.16 and 4.17 respectively). Due to the variations in the microbiota composition from different donors, it is not possible to make statistical comparisons.

In batch culture fermentation experiment 1, samples were dominated by *Lachnospiraceae*, *Bacteroidaceae* and *Ruminococcaceae* in descending proportions at predose and 0 h. *Enterobacteriaceae* only form a small percentage of the whole gut microbiota community at predose and 0 h, only making up 5.92%, 2.64%, 1.73% at predose, and 2.8%, 2.7% and 0.1% at 0 h in control, SLNP and LNP respectively (Figure 4.15 b), indicating LNPs were reducing *Enterobacteriaceae* at 0 h. At 4 h, abundance of *Enterococcaceae*, *Bacteroidaceae*, *Bifidobacteriaceae*, *Streptococcaceae* and *Lachnospiraceae* were greatly increased when *Enterobacteriaceae* levels declined to 3.46% with LNP treatment compared to the control (83.76%) and SLNP (73.38%). While SLNP had slightly lower levels of *Enterobacteriaceae* compared to the control at 4 h, there were increased abundance of *Bacteroidaceae* and *Bifidobacteriaceae*. At 8 h, both SLNP- (3.32%) and LNP-treated (4.72%) samples both had reduced the proportion of *Enterobacteriaceae* compared to the control (69.56%) (Figure 4.15 b), the reduction in *Enterobacteriaceae* by SLNP may suggest non-TFD specific disruption occurring at 8 h. Large increases in proportions of *Enterococcaceae* were shown in LNP (59.19%) and SLNP

(75.59%) compared to the control (11.52%). A smaller increase in *Bifidobacteriaceae* and *Streptococcaceae* with decrease in *Bacteroidaceae* levels were observed in SLNP and LNP compared to the control respectively. Similar diversity between family levels were seen across all time points with all three treatments, suggesting LNP did not cause overall damage to the gut microbiota in general.

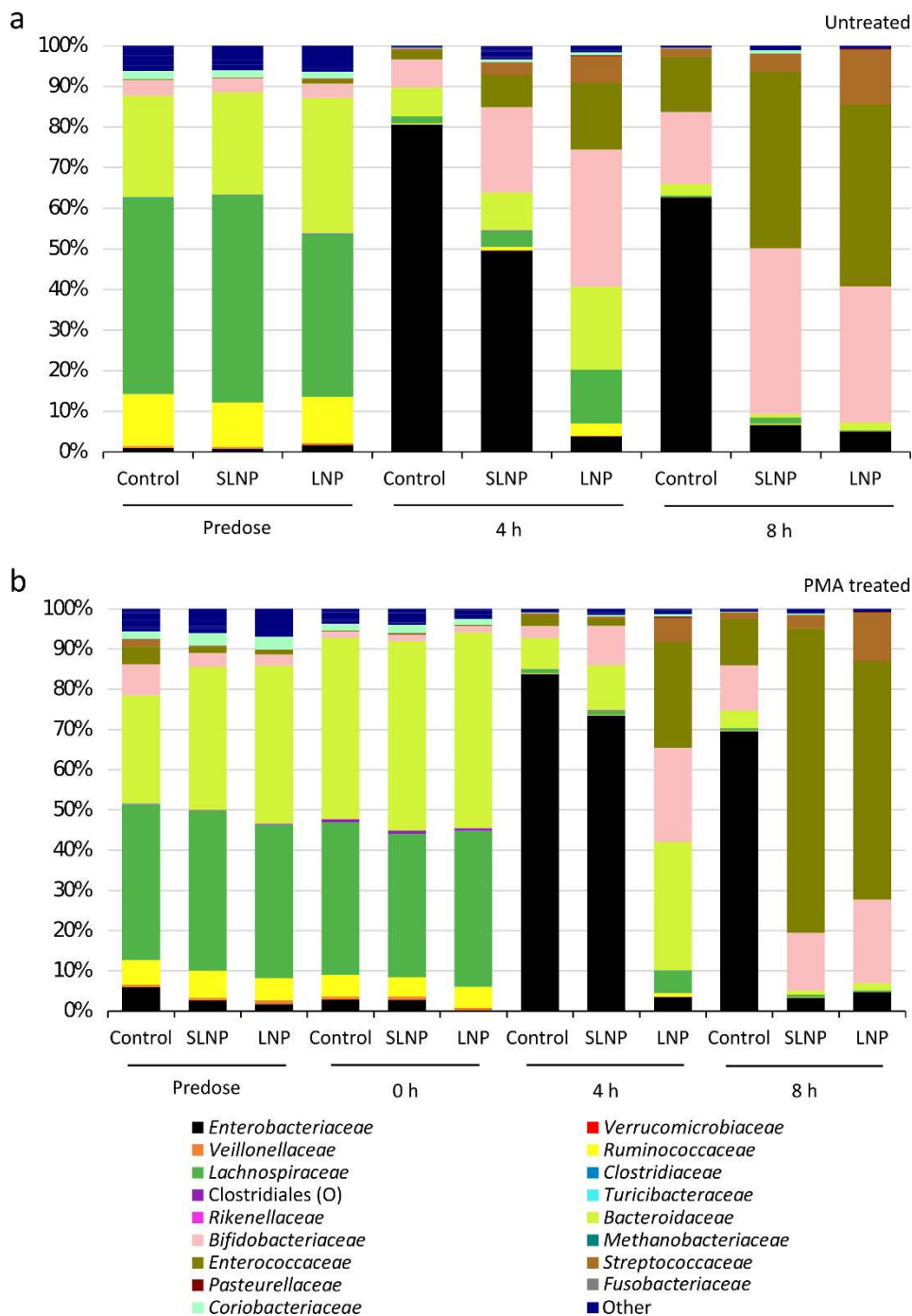


Figure 4.15 Bacterial community analysis of 16S rRNA gene sequencing at family level for *in vitro* batch culture fermentation experiment 1; a) live and dead bacterial community in untreated samples; and b) live bacterial community in PMA treated samples.

In batch culture fermentation experiment 2, samples at predose and 0 h showed similar proportions of bacterial group at the family level, consisting mainly of *Lachnospiraceae*, *Bacteroidaceae*, *Ruminococcaceae*, *Bifidobacteriaceae* and *Coriobacteriaceae* in descending proportions. Large proportions of *Enterobacteriaceae* were shown in control (33.76%) and SLNP

(78.81%) at 4 h compared to 0 h; though interestingly, the overall bacterial composition of the LNP-treatment at 4 h largely resembled those at 0 h, with only 0.2% of *Enterobacteriaceae* in LNP-treated samples. The control sample at 4 h and 8 h also showed a large increase in *Fusobacteriaceae* (Figure 4.16) which was absent in the SLNP and LNP sample.

Enterobacteriaceae levels with LNP (18.21%) remained lower than the controls at 8 h, while the SLNPs-treated sample was largely composed of *Enterobacteriaceae* (97.76%) compared to the control (42.66%). The diversity of bacterial groups were higher in LNPs compared to the control and SLNP as the constituents resembled more closely to the bacterial community at the start of the experiments i.e. *Bacteroidaceae*, *Ruminococcaceae* and *Lachnospiraceae*, suggesting LNP were able to maintain the diversity of the gut microbiota while targeting *Enterobacteriaceae*. Increase proportions of *Pasteurellaceae*, *Streptococcaceae*, *Bifidobacteriaceae* and *Coriobacteriaceae* were also observed at 8 h in LNP compared to the control and SLNP.

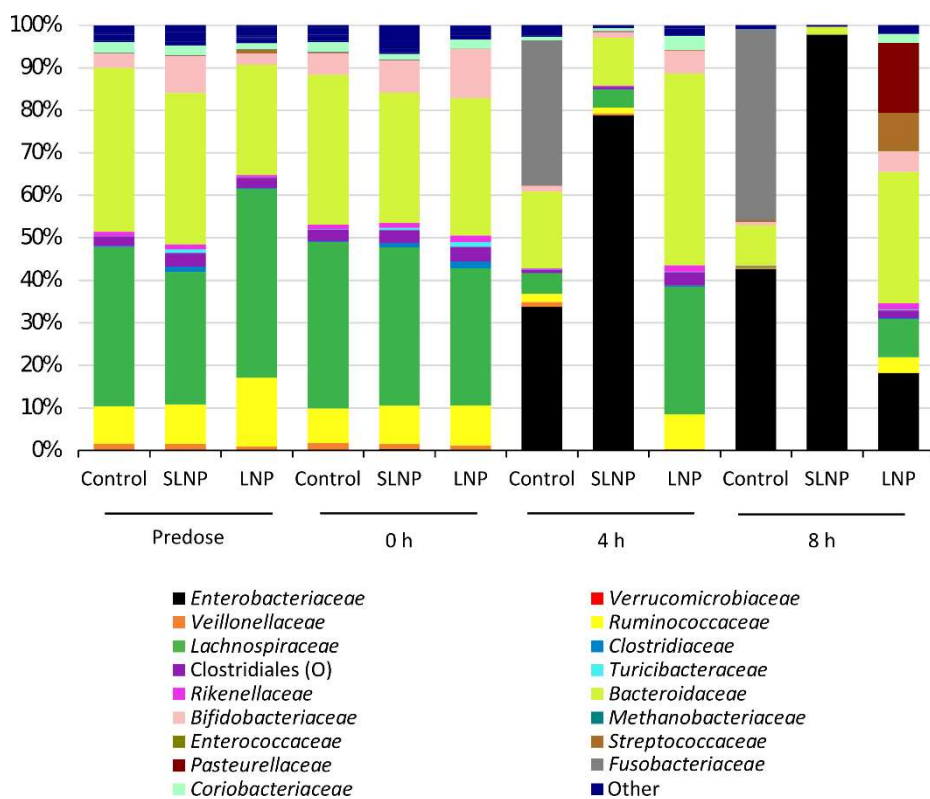


Figure 4.16 Live bacterial community analysis of 16S rRNA gene sequencing at family level for *in vitro* batch culture fermentation experiment 2 (PMA-treated) at 2% NP dose.

In batch experiment 4, the gut microbiota predominantly comprises *Enterobacteriaceae*, *Verrucomicrobiaceae*, *Ruminococcaceae* and *Bacteroidaceae* at predose in descending order. While no notable difference in the composition of the gut microbiota community was observed at

each time point between treatments at 2% NP dose (Figure 4.17 a), changes in the proportion of *Enterobacteriaceae* were shown with 10% LNP treatment as described below. *Enterobacteriaceae* was markedly decreased at 0 h from 16.27% in the control and 31.26% with SLNP to 0.86% with LNPs, with increased Clostridiales (in the order level) and *Clostridiaceae* at 0 h (Figure 4.17 b). At 4 h, *Enterobacteriaceae* levels with LNP treatment (16.06%) were still notably lower than those in control (92.17%) and SLNP treatment (93.76%). *Verrucomicrobiaceae* were increased from 2.55% and 1.87% in control and SLNP respectively to 29.65% with LNP at 4 h; *Turicibacteraceae*, *Rikenellaceae*, *Bacteroidaceae*, *Bifidobacteriaceae* and *Methanobacteriaceae* were also increased proportionally with LNP compared to the controls.

At 8 h, all treatments were consisted mainly of *Enterobacteriaceae* at 95%, 95% and 97.78% for control, SLNP and LNP respectively, with decreased proportions of *Bacteroidaceae* and *Bifidobacteriaceae* in LNP. The above data suggested that while 2% LNP had no effect on the gut microbiota, *Enterobacteriaceae* was inhibited by 10% LNP from 0 h to 4 h, with growth observed 8 h after LNP treatment.

LNP-treated gut microbiota maintained similar diversity of bacterial groups compared to the samples at the start of the experiment. LNP-treated samples were also more diverse compared to the control and SLNP at the same time points, suggesting LNP did not reduce the diversity of the gut microbiota, unlike traditional antibiotic treatments.

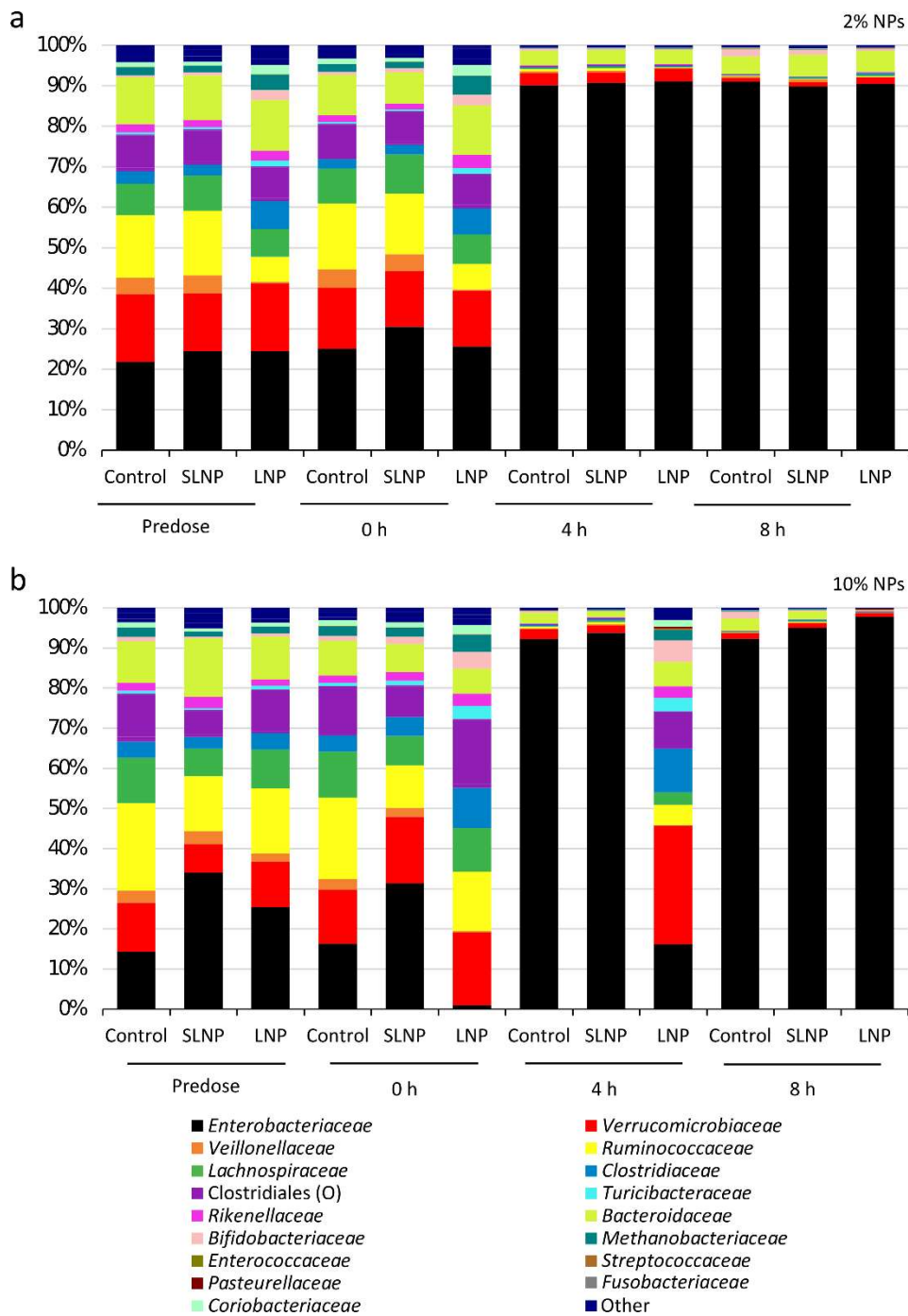


Figure 4.17 Live bacterial community analysis of 16S rRNA gene sequencing at family level for *in vitro* batch culture fermentation experiment 4 (PMA-treated) at a) 2% dose and b) 10% dose.

Principal Coordinates Analysis

To determine the community structures of the gut microbiota samples upon LNP treatment, weighted unifracs Principal Coordinates Analysis (PCoA) plots were used to look at the spatial relationship between different samples in the same experiment run.

For PCoA plots from experiment 1 (Figure 4.18), predose samples all clustered together before the addition of NP treatments. At 4 h the LNP sample was spatially closer to all predose samples and were further away from 4 h control and SLNP on the PC1 axis (which accounts for 57.81% of the variability), indicating community structure had more similarity to the predose samples than the control treatments at 4 h. The samples at 8 h shifted further away from their previous time points, suggesting a structural shift associated with time. Overall, LNPs had shifted less on the PC1 axis compared to the control and SLNP treatment, suggesting the shift in the gut microbiota structure in LNPs were less than those associated with control and SLNP over time, suggesting LNP structurally resembled the gut microbiota from the predose samples.

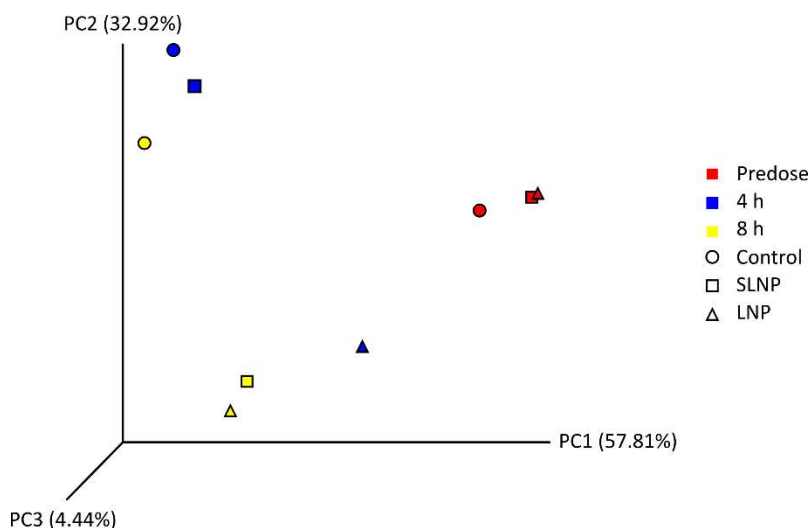


Figure 4.18 Principal coordinates analysis (PCoA) plots of Illumina sequence data for *in vitro* batch culture fermentation model experiment 1. 3D PCoA plot was generated from weighted UniFrac analysis, where x- and y- and z-axis represents the first, second and third principal coordinates respectively.

For experiment 2 (Figure 4.19), predose and 0 h samples had similar spatial arrangement regardless of treatment. At 4 h, control and SLNP become more distant on the PC1 axis (accounting for 83.34% of the total variability) from the original samples while LNP remain closely clustered with the samples at predose and 0 h. At 8 h, there is a further shift in all treatments, though LNP treatment remain most similar to all samples at predose and 0 h compared to control and SLNP, again suggesting less overall change occurred in the gut microbiota with LNP treatment.

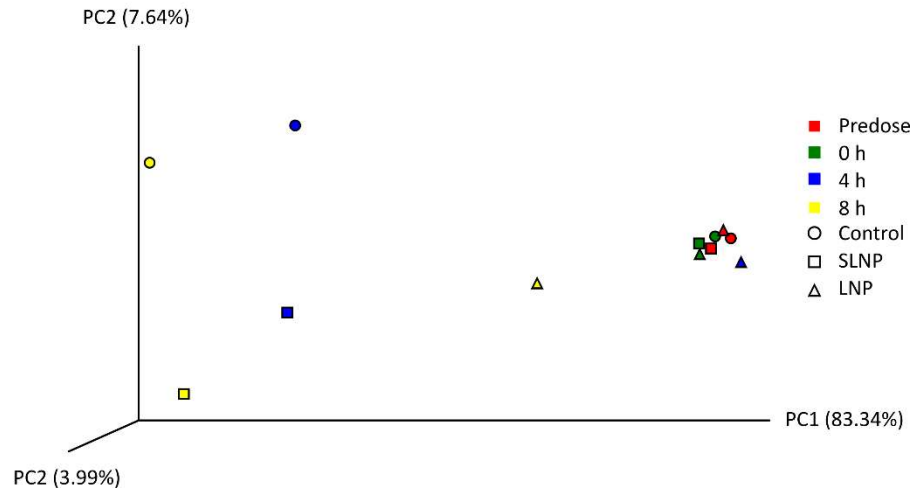


Figure 4.19 Principal coordinates analysis (PCoA) plots of Illumina sequence data for *in vitro* batch culture fermentation model experiment 2; 3D PCoA plot was generated from weighted UniFrac analysis, where x- and y- and z-axis represents the first, second and third principal coordinates respectively.

For experiment 4 (Figure 4.20), all treatments at the same time points clustered together for 2% NP dose, suggesting no notably difference in gut microbiota structure (Figure 4.20 a). At 10% NP dose, sample treated with LNPs at 4 h are more spatially related to all the predose samples than control and SLNP-treated samples on the PC1 axis (accounting for 69.36% of the total variability), suggesting LNPs were structurally more similar to predose and 0 h samples (Figure 4.20 b).

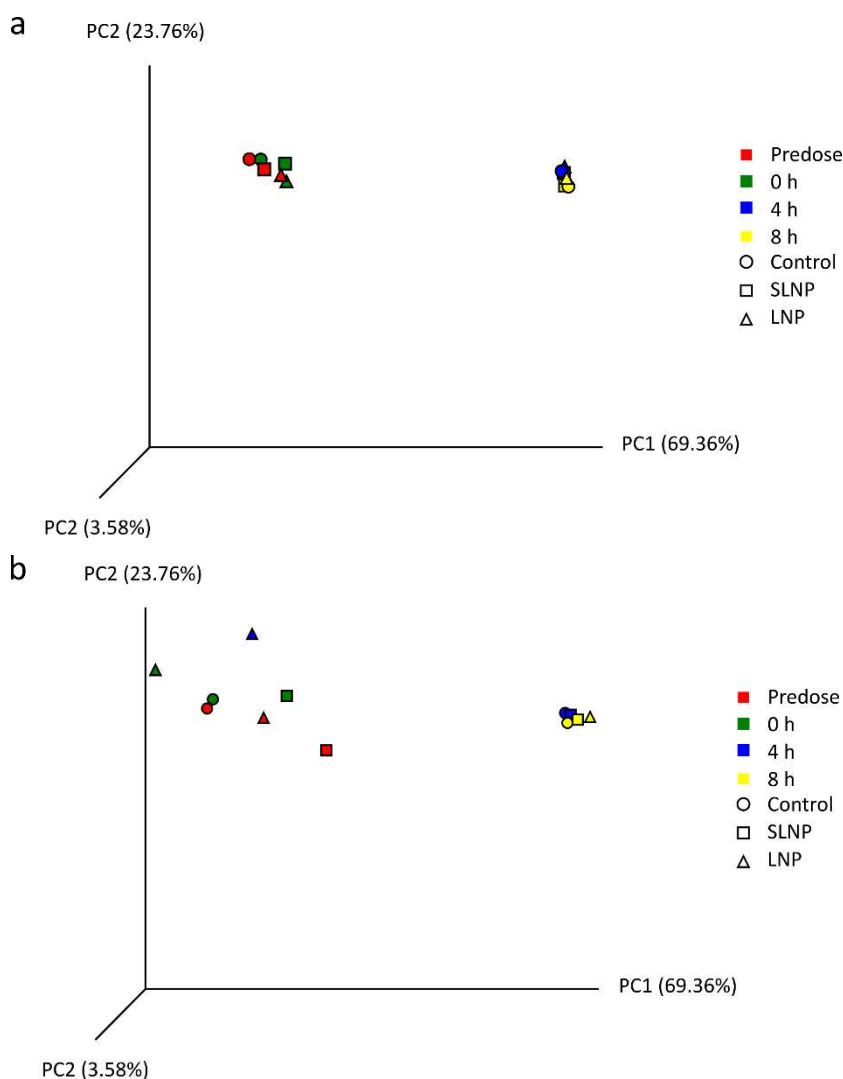


Figure 4.20 Principal coordinates analysis (PCoA) plots of Illumina sequence data for *in vitro* batch culture fermentation model experiment 4. 3D PCoA plot was generated from weighted UniFrac analysis, where x- and y- and z-axis represents the first, second and third principal coordinates respectively. a) at 2% dose; b) at 10% dose.

4.3.5. Metabonomic analysis in the human gut microbiome in the presence of TFD

^1H NMR spectroscopy allowed the examination of the metabolites present in the *in vitro* batch culture fermentation samples with different NP treatments. A representative NMR spectrum, shown from batch model experiment 3 (Figure 4.21), comparing NMR spectra between 2% and 10% LNPs provided insight into the LNP dose response effect on the concentration of metabolites.

In general, not much difference in metabonomic profile was seen between control and SLNP, both at 2% and 10%, indicating the delivery compound 12-bis-THA is not affecting the bacterial community metabolically, suggesting LNPs are good vehicle for drug delivery. The difference in profile derived from SLNP and LNP treatments indicated that the TFD was the driving force of the metabonomic changes.

LNP-treatment resulted in a lower yield of products of anaerobic metabolism (Figure 4.21) such as ethanol and lactate compared to the control and SLNP at 4 h and 8 h. The upward trends for propionate, formate and acetaldehyde production were less prominent compared to the control and SLNP, indicating a reduction in bacterial growth and anaerobic metabolism. This trend is more prominent in 10% than 2% LNP, which may be associated with the discrepancy in antimicrobial activity observed between the doses.

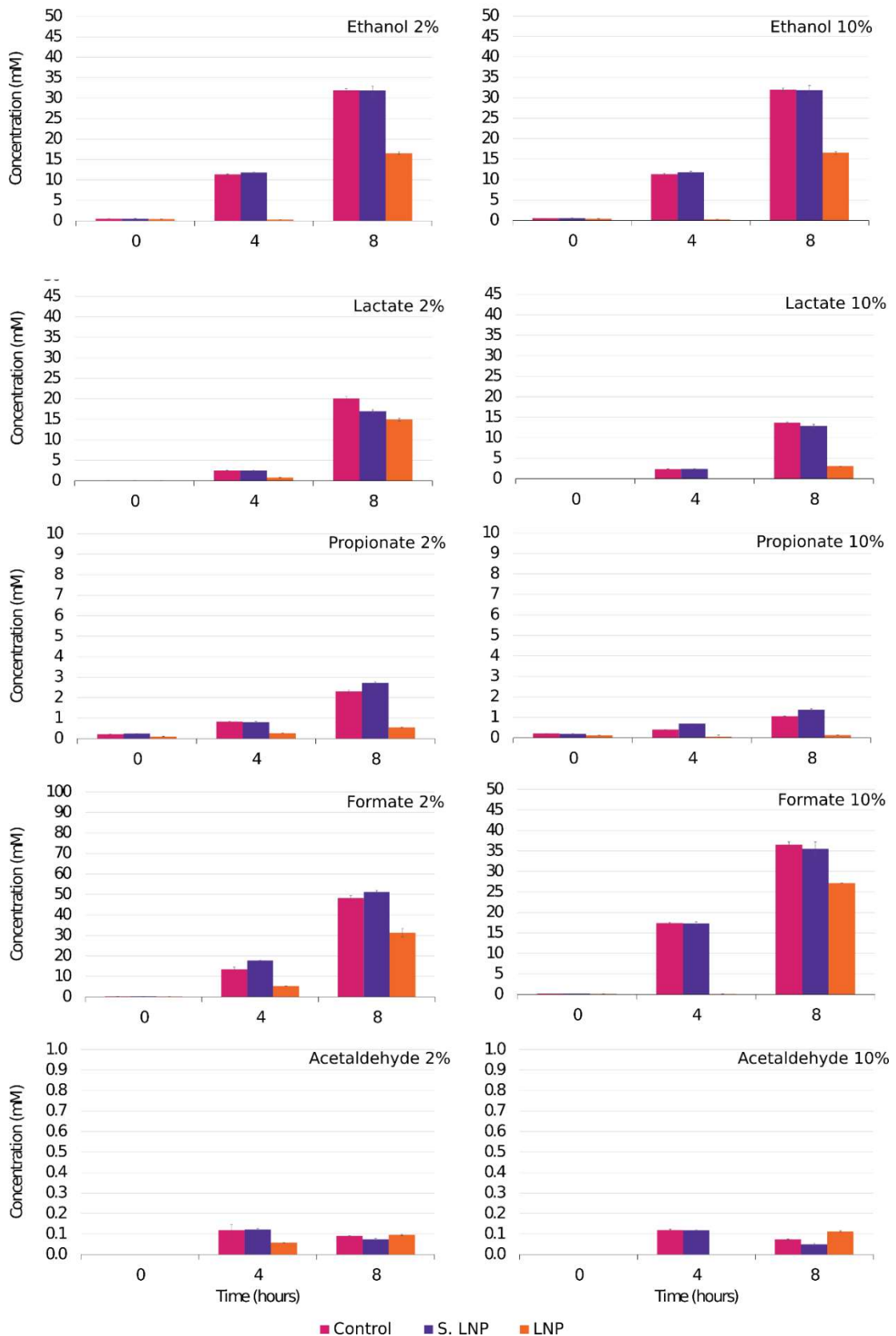


Figure 4.21 Metabolites concentrations involved in anaerobic metabolism. Ethanol and lactate, and short chain fatty acids propionate, formate and acetaldehyde. A minimum of two repeats were analysed and the mean \pm SD were plotted.

Metabolites such as cystine, glucose and glutamate were depleted by control and SLNP batch fermentation vessels at both 2% and 10% dose at 8 h (Figure 4.22), while they were mostly diminished by 2% LNP at 8 h, the levels remained high for 10% LNP samples. This may indicate growth was slower with LNP compared to control and SLNP as the use of these metabolites were delayed in a dose-dependent manner.

Phenylalanine, leucine and isoleucine, valine, tyrosine, histidine and methionine were used at 8 h regardless of dose (Figure 4.23 and 4.24). Asparagine and aspartate levels were depleted in the 2% and 10% treatment vessels (including control, SLNP and LNP), except 10% LNP at 4 h (Figure 4.25).

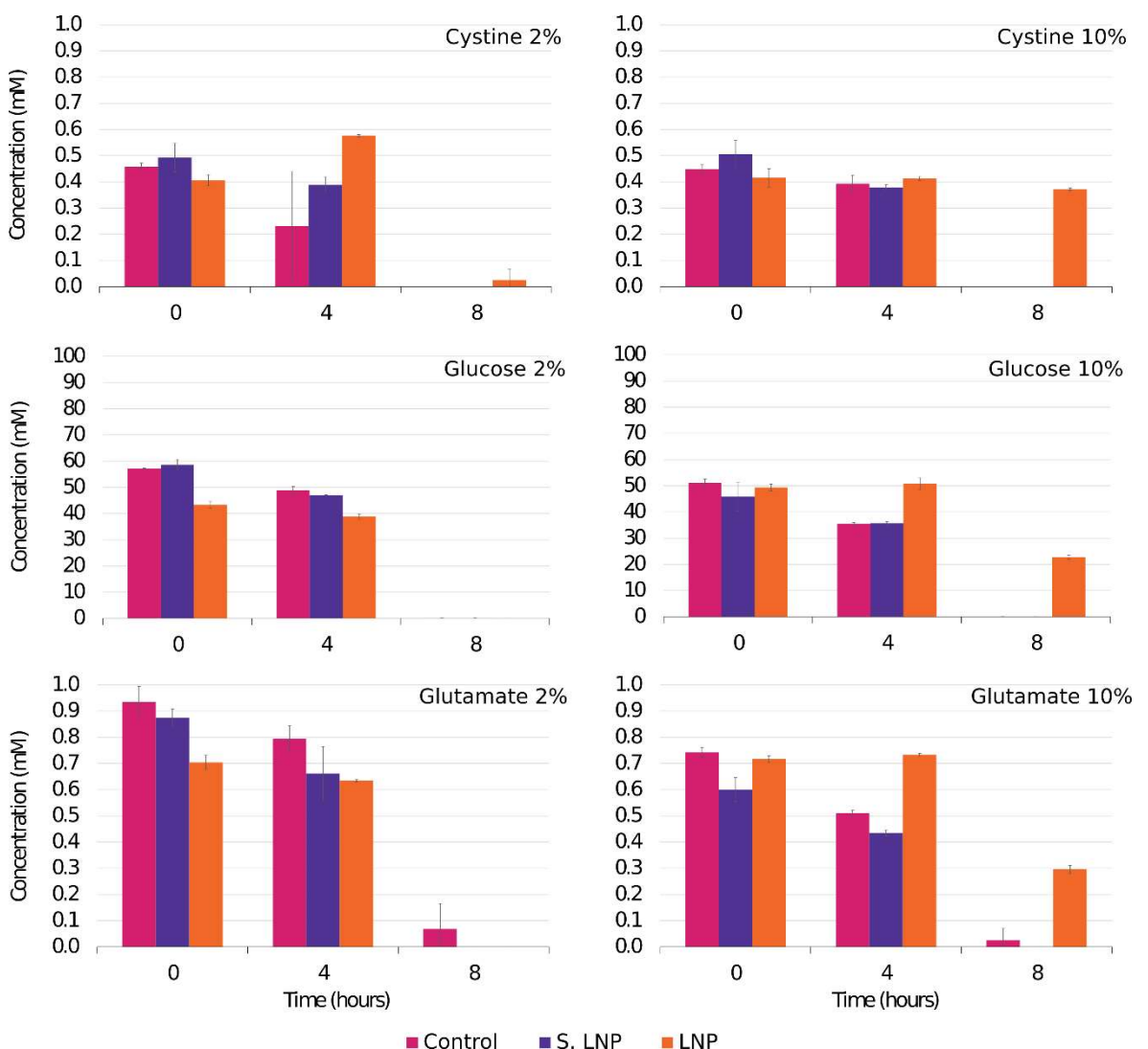


Figure 4.22 Metabolite concentrations of cystine, glucose and glutamate. A minimum of two repeats were analysed and the mean \pm SD were plotted.

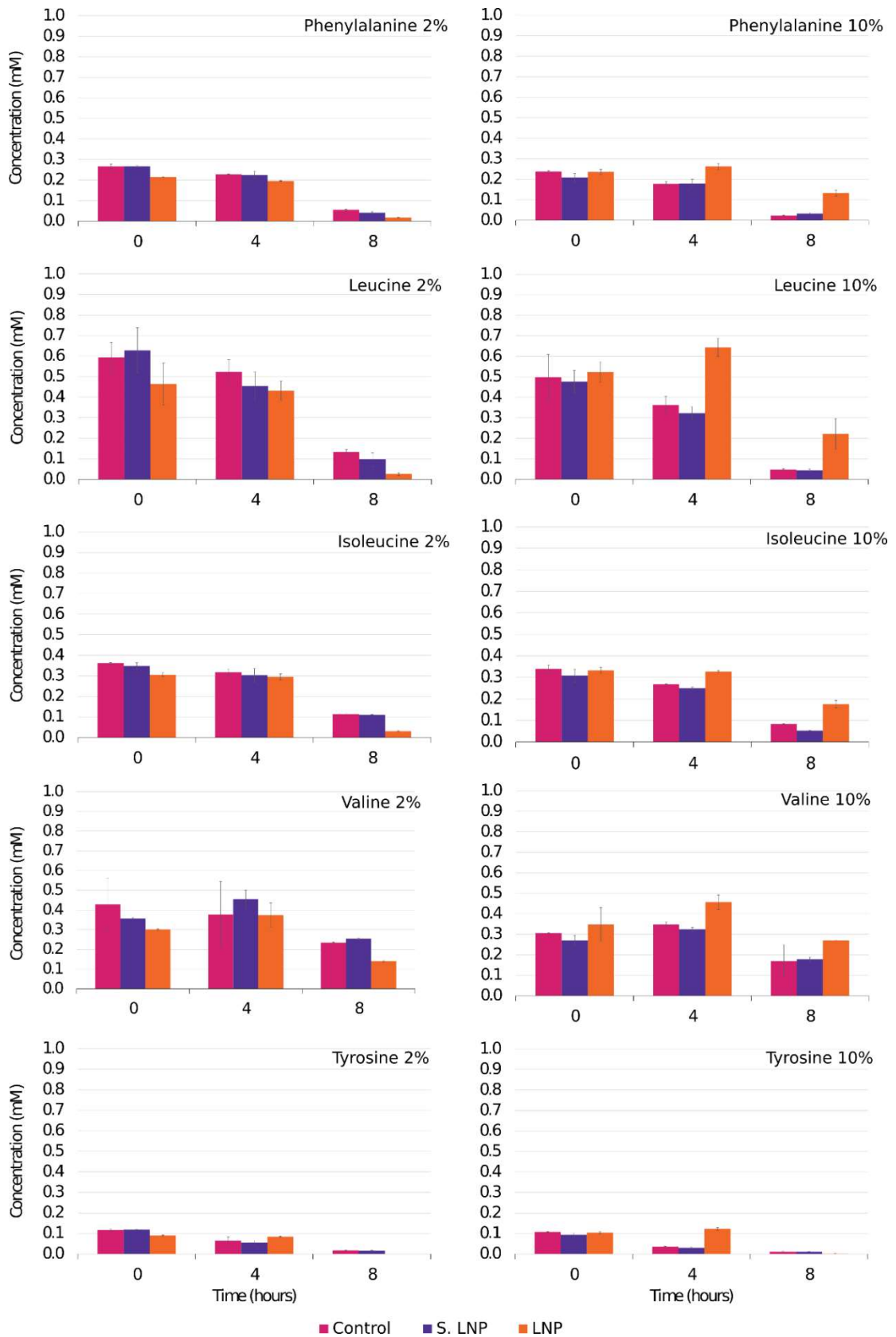


Figure 4.23 Metabolite concentrations of phenylalanine, leucine and isoleucine, valine and tyrosine. A minimum of two repeats were analysed and the mean \pm SD were plotted.

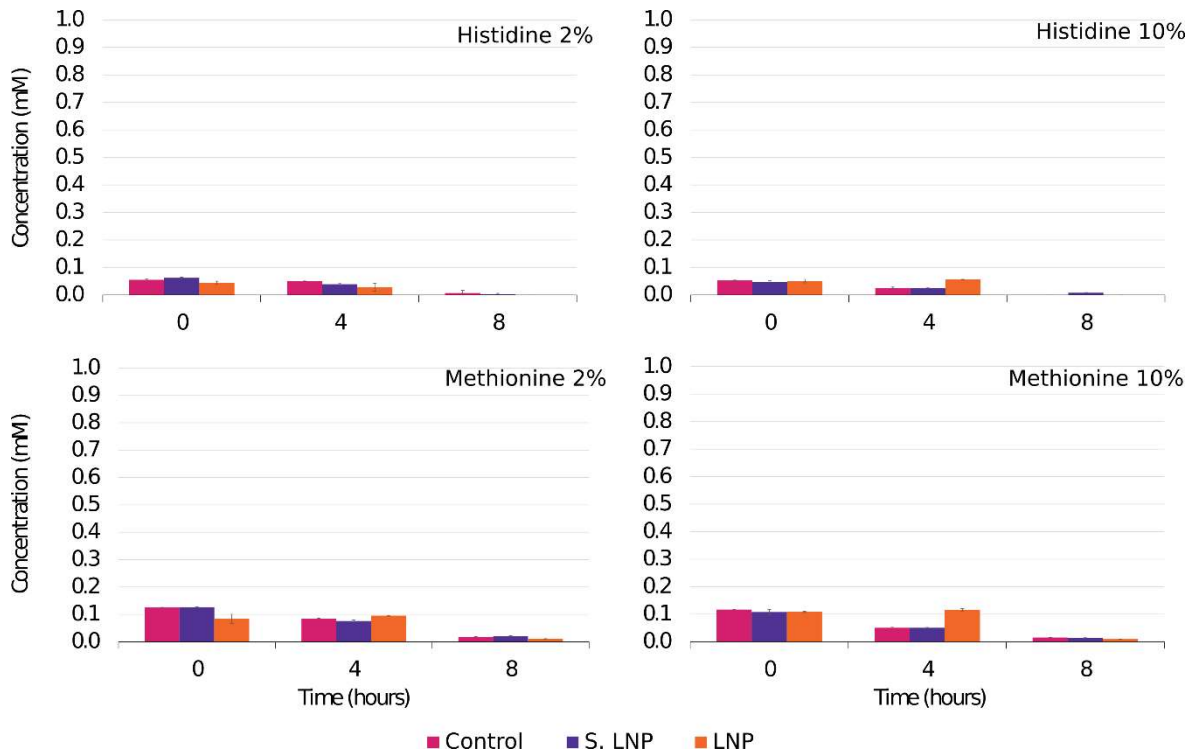


Figure 4.24 Metabolite concentrations of histidine and methionine. A minimum of two repeats were analysed and the mean \pm SD were plotted.

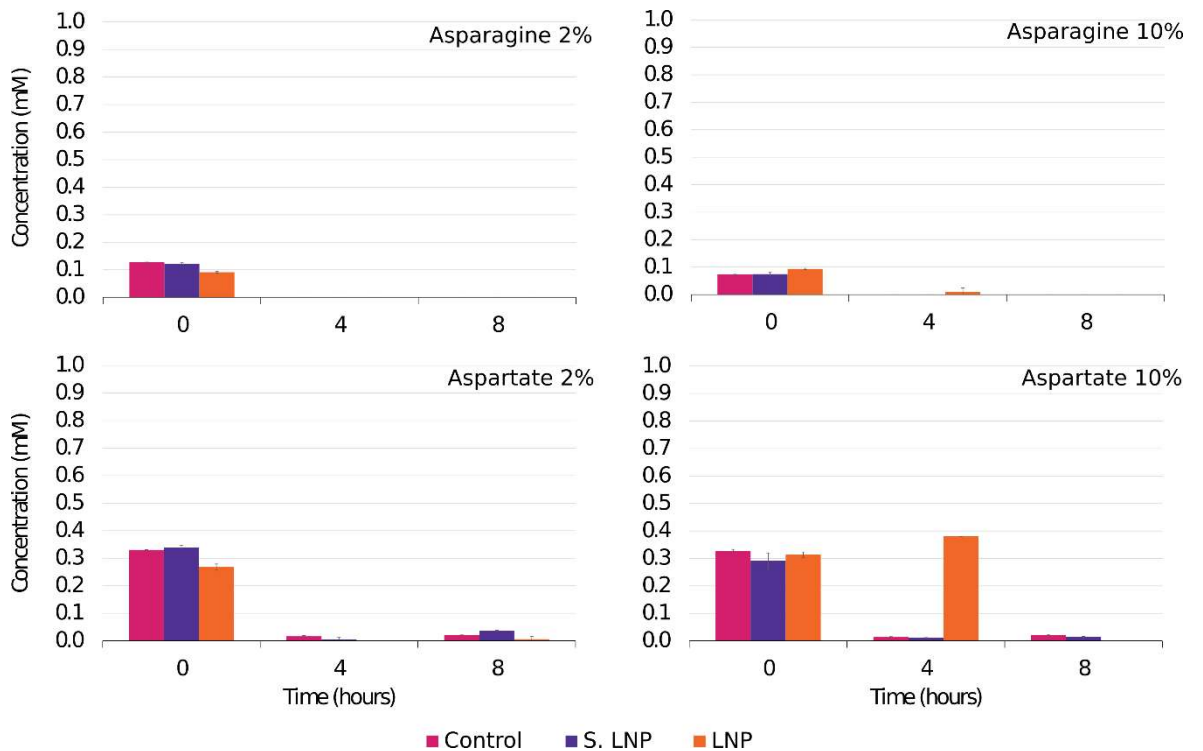


Figure 4.25 Metabolite concentrations of asparagine and aspartate. A minimum of two repeats were analysed and the mean \pm SD were plotted.

Other metabolites were affected differently by LNP treatment (Figure 4.26). Succinate was reduced in line with the LNP dosage. Levels of succinate plummeted at 4 h and reduced by two thirds at 8 h compared to the controls with 10% LNP treatment, whereas succinate levels were higher than the control at 2% dose. The decrease in 3-phenyllactate and 4-hydroxyphenylacetate levels as breakdown products of aromatic amino acids for phenylalanine and tyrosine respectively were seen only with 10% LNP treatment at 8 h. This suggests the impact of LNP dose-response; the 2% LNP treated bacterial communities appeared to be able to adapt to the stress conditions, while the metabolism of amino acids was dampened by the higher LNP dose at 10%.

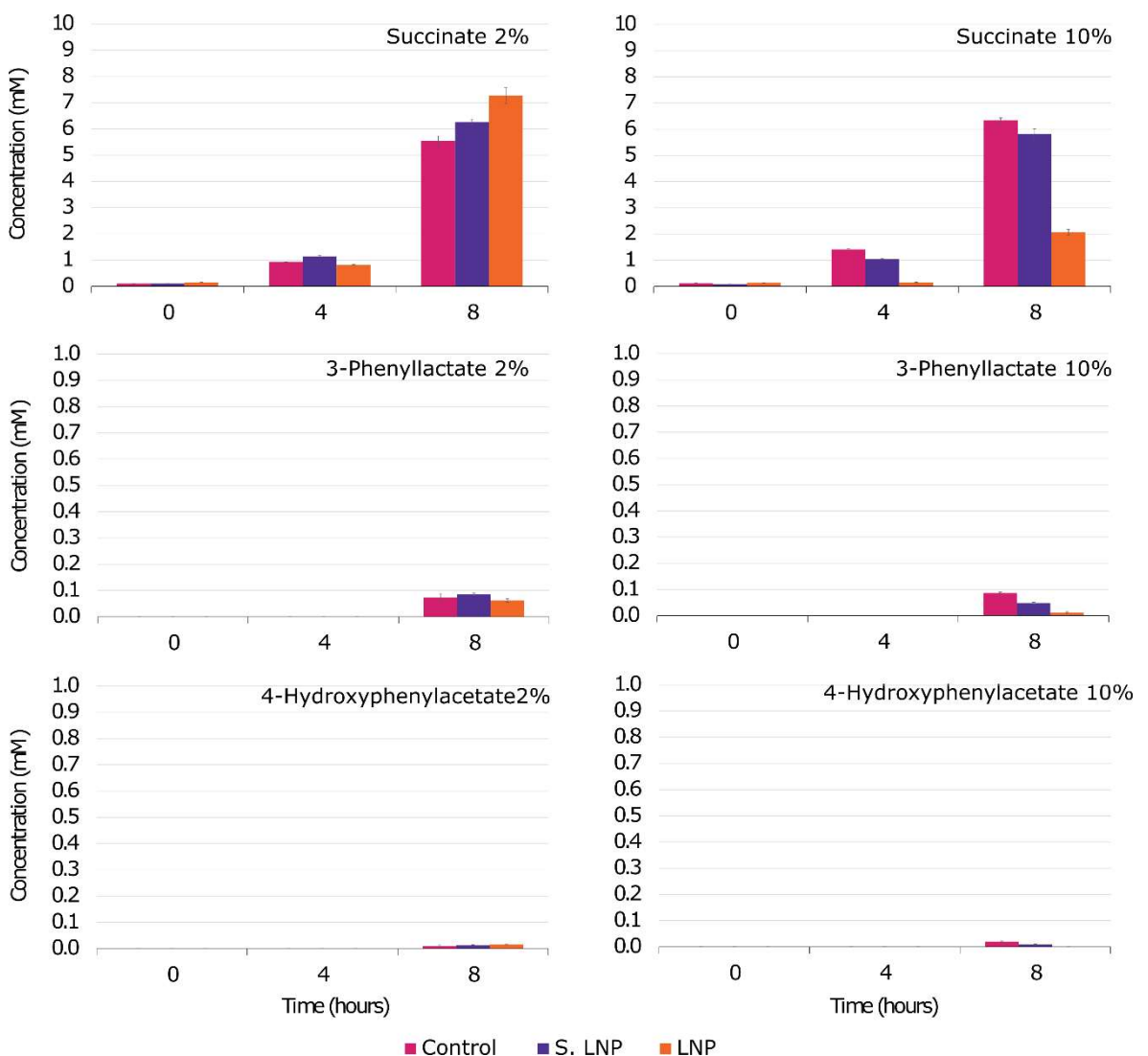


Figure 4.26 Metabolite concentrations of succinate, 3-phenyllactate and 4-hydroxyphenylacetate. A minimum of two repeats were analysed and the mean \pm SD were plotted.

Intermediate metabolites showed a delayed trend compared to control and SLNP (Figure 4.27). Fumarate levels increase with 2% and 10% LNPs at 4 h, but were reduced at 8 h compared to

control, indicating fumarate had higher yield at 4 h and used up at 8 h for both 2% and 10% LNP compared to the control and SLNP at their respective dose. Similarly, pyruvate levels showed a delayed response only with 10% LNP as levels remained high after 8 h, unlike at 2% dose to which pyruvate were used by all treatments. The time delay in the concentrations of these transitional compounds could again be an indication of delayed bacterial growth in the LNP-treated samples, in a dose dependant manner. Also, betaine levels were decreased with 2% LNP at 8 h, while little change was observed with 10% LNP. While uracil levels were increased earlier at 4 h with both LNP treatments compared to control and SLNP (Figure 4.28).

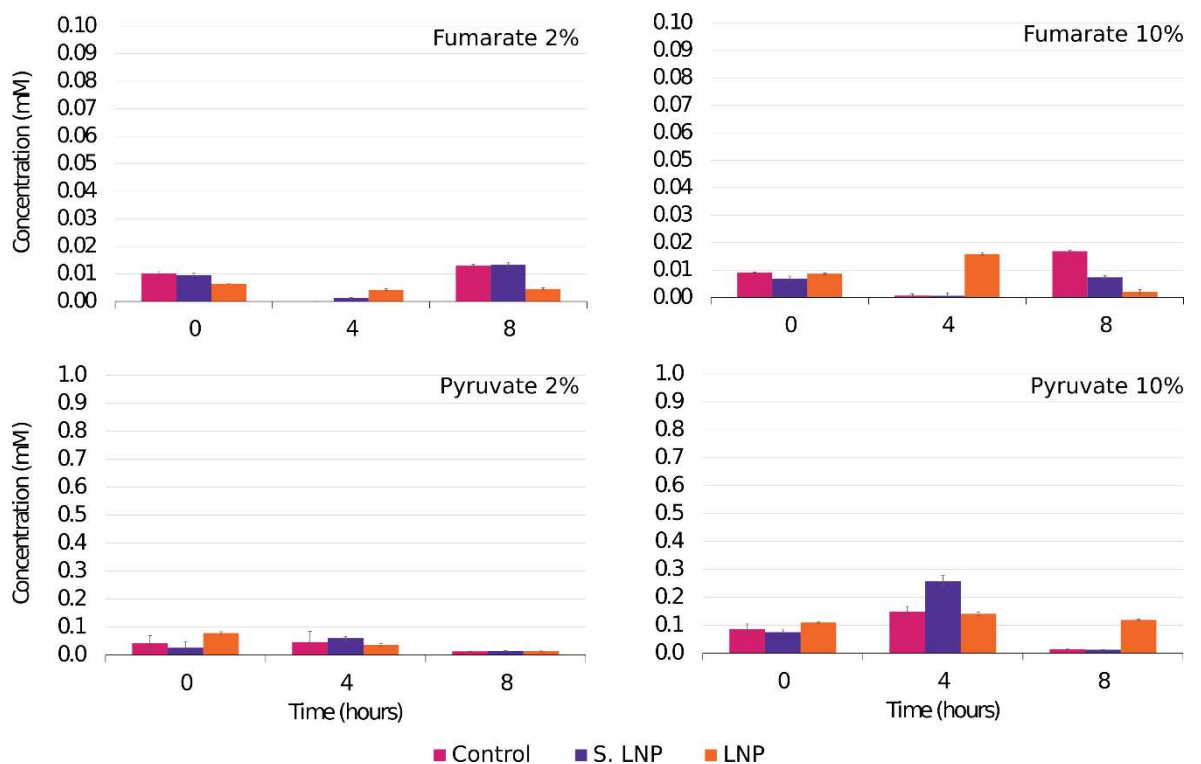


Figure 4.27 Metabolites concentration of fumarate and pyruvate. A minimum of two repeats were analysed and the mean \pm SD were plotted.

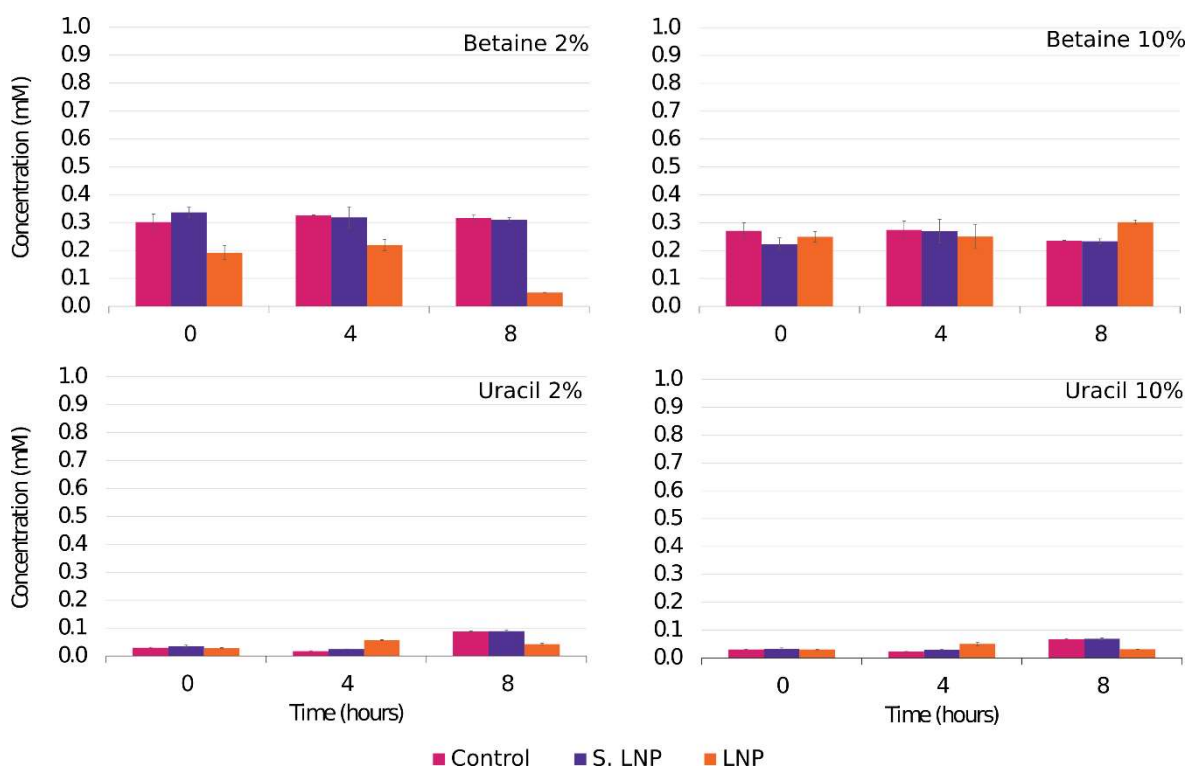


Figure 4.28 Metabolites concentrations of betaine and uracil. A minimum of two repeats were analysed and the mean \pm SD were plotted. Pink, control; purple, SLNP; orange, LNP.

4.4 Discussion

Successful TFD delivery by LNPs within *E. coli*

It has been shown by laser scanning confocal microscopy when formulated with 12-bis-THA TFDs successfully crossed the Gram-negative cell wall and enter the cytoplasm of *E. coli*. This indicates the delivery NP has the ability to penetrate Gram-negative cell wall to introduce TFD to exert the antimicrobial effect. Marin-Menendez *et al.* (2017) have demonstrated 12-bis-THA attached to the polar and septal regions of *E. coli* and biophysical studies have related this to binding to the prokaryotic anionic phospholipid cardiolipin. LNPs have also been shown to enter Gram-positive bacteria including MRSA, *Clostridium difficile*, *Pseudomonas aeruginosa* and even *Mycobacterium smegmatis* which has distinctive cell wall characteristics compared to Gram-negative bacteria (McArthur 2014), suggesting LNP transfection can be applied to both Gram-positive and Gram-negative bacteria. The conical structure of cardiolipin domains are typically present in areas of greater curvature (Fishov and Woldringh 1999, Renner and Weibel 2011) to ensure proper spatial segregation for respiration and cell division of bacteria (Huang *et al.* 2006, Lewis and McElhaney 2009). Therefore, LNPs are designed to be a bacterial-selective delivery system, due to the

absence of cardiolipin in eukaryotic cell membranes and its high degree of conservation amongst all bacteria (Mileykovskaya and Dowhan 2009).

We confirmed that the NP formulation (LNP + 0.1% HPMC) can transfect *E. coli* when incubated in the media used in *in vitro* batch culture fermentation. It was shown that LNPs were able to deliver TFD within the cytoplasm despite the high salt content. Moreover, there were increased proportion of transfected *E. coli* at 4 h compared to 1.5 h, this indicated that TFD delivery occurs in a time-dependent manner and that transfection is still taking place 4 h after the initial LNP administration.

Importance of LNP dosage optimisation for target specific activity

It is worth to notice that in the MIC bioassay, \log_{10} 6 CFU/ml of *E. coli* is present in each well, whereas the *in vitro* batch culture fermentation model found to have \log_{10} 9 CFU/ml of total anaerobes, meaning that there was a 1000-fold increase in bacterial density in the batch model compared to those in the MIC bioassays. To allow the 2 experimental systems to be comparable, the amount of bacteria/TFD had to be readjusted for a direct evaluation of antimicrobial effect. This indicates that a dose-response effect needs to be fine-tuned to ensure sufficient antimicrobial activity, especially in *in vitro* and *in vivo* settings where the starting bacterial load is unpredictable. As LNPs can bind to both Gram-positive and Gram-negative bacteria, sequestration might occur and should be taken into consideration as a factor that could reduce LNP efficacy against *E. coli*.

From the NP dosing determination experiment, a minimum of 1x LNP dose (equates to 1.5 g of faeces/ml of LNPs) was required to achieve bacteriostatic antimicrobial activity (Figure 4.4.). However, to exert a bactericidal effect more LNPs were needed and there were larger variations in the minimum LNP dose required: the effect seen at 1x, 3.36x and 12.5x respectively (Figure 4.5). It indicates a possible 12.5x difference in the minimum dose needed to exert a $\geq \log_{10}$ 3 CFU/ml decrease in coliforms levels, using different faecal samples from the same donor in the space of 4 months. Changes in the microbiota composition and density within the sampling period may account for the intra-individual difference to the LNP responses. Environmental factors such as diet and stress could also change the microbial composition during the experimental period. It has been observed that the amount of total bacteria and Gram-negative bacteria in mice increases under stress conditions (Yoshikawa *et al.* 2016). This may account for why the bactericidal activity is less apparent in the subsequent dosing determination experiments using the same donor during a relatively short period. A higher dose is needed to exert the same antimicrobial effect as there are more bacteria or/and bacteria with the transcription factor target

present in the sample. As the LNPs were freshly made before each experiment, the batch-to-batch variations could also contribute towards the differences in biological activity.

This has highlighted the variability between experiments that could occur, it is important to optimise the dosage accordingly to ensure efficacy. As expected, the more efficacious the LNP doses were, the more likely they are to have non-TFD specific influence on the gut microbiota, though the reduction in other bacterial communities were minimal and did not substantially alter the gut microbiota.

By comparing the viable bacterial counts between SLNP and LNP treatment, the target specificity of TFDs was illustrated as coliforms were mostly affected only by LNP but not SLNP at the minimum dose needed for bactericidal activity for each experiment (Figure 4.5). The total anaerobe levels were similar between all treatments at the minimum dose, further suggesting LNPs' ability to target only the organism of interest as designed.

When the dosing determination experiments were conducted in a larger scale, the antimicrobial activity was enhanced – 1x instead of 12.5x LNP was needed to produce an antibacterial effect when additional stirring was incorporated (Figure 4.6). This may be an explanation for the variability seen in these experiments: as the microcentrifuge tubes in the dosing determination experiments were not shaken while the large scale vessels were mixed using a magnetic stirrer, the LNPs may not have comprehensively mixed with all bacteria to utilise their full antimicrobial activity, therefore creating a discrepancy between the experimental set ups. After considering the practical feasibility and the possible non-specific side effects against the gut microbiota, a 3x dose was used in future *in vitro* batch culture fermentation model experiments.

Non target-specific activity occurs only at very high LNP dose

The dosing determination experiment also allowed us to investigate whether a detrimental effect on the gut microbiota would occur at high doses. At high LNP doses such as 90x dose in experiment 1, non-specific bactericidal activity was observed where there was a \log_{10} 3 CFU/ml decrease in the total anaerobic community from 8 h for SLNP treatment compared to control (Figure 4.5). Coincidentally, this side effect was only observed in experiment 1, where the minimum bactericidal LNP dose was the lowest (hence the highest efficacy) among the 3 experiments; only minimal disruptions to total anaerobes were shown in the other 2 repeats. Inferring only very high concentrations of NPs (90x higher than the minimum LNP dose needed for bactericidal activity) could exert target non-specific damage on the gut microbiota. As 90x dose is unrealistic to use in practical terms, it was decided that 3x dose was to be taken forward for batch model experiment,

as it will likely have minimal effect on the total anaerobe levels and exert the target-specific antimicrobial activity.

Coliforms: LNP dose ratio for successful bactericidal activity

In the batch culture fermentation model experiments (Figure 4.6-4.12), different donors were used and the LNP dose required to reduce coliforms varied. This could be due to differences in bacterial cell density and types in the starting inocula. As freshly voided samples were required for batch fermentation to maintain anaerobic bacteria, it would be difficult to deduce the faecal dry weight without compromising the bacterial community.

The use of a standard dilution series means some samples may fall outside the normal limit due to the dilution by essential pH buffering. This may explain why viable colonies of *Bacteroides*, *Clostridium* and coliforms were decreased at 8 h with SLNP treatment in experiment 1, as there was a greater increase in total volume of the vessel due to pH buffering.

From LNP dosing determination experiment and batch model fermentation experiments, it was demonstrated that the bactericidal LNP dose could be up to 12.5x different between individual runs. To look for possible explanation for these discrepancies, the ratio between the quantity of starting bacterial inoculum: volume of LNPs were compared. While there was no correlation between the total viable bacteria and LNP dosage required at predose and 0 h, interestingly there was a positive linear correlation between the starting coliforms colony forming units in the control treatment at 0 h and the LNP dose needed for bactericidal activity for each of dosing range (Figure 4.13 a) and batch model experiments (Figure 4.13 b) ($R^2= 0.992$ and 0.998 respectively).

We have interpolated the LNP dose required for a bactericidal effect from the known levels of coliforms into the equation from the line of best fit; the predicted bactericidal dose required for the gut microbiota samples which did not show bactericidal activity were notably higher than the experimental dose e.g. batch model experiment 3 at 2% dose and 3 other donors also used for batch model experiments (Figure 4. 13 c); therefore providing an explanation as to why some gut microbiota samples respond to LNP treatment better, as they have lower *E. coli* levels at the point of LNP addition.

More importantly, we have suggested that the LNP dosage effect is not associated with the total anaerobic counts, but has a positive correlation with the coliforms population (Figure 4.13), indicating that the LNPs are more effective in targeting the bacterial group of interest. This gives us confidence that LNP are suitable to be used in a complex bacterial environment to target *E.*

coli, as the antimicrobial response is rapid and LNP dose needed were not affected by the other bacterial community present in the sample, thus minimising the amount of LNPs required for antimicrobial activity.

Potential donors were screened for the levels of *E. coli* before conducting the experiment and preliminary tests were done to have a broad estimation of LNP dose needed. However, it is not always easy to predict the bacterial community in the starting inoculum in batch model fermentation prior to the start of experiment, as the prediction of the LNP dosage response is not always indicative as faecal composition can rapidly change through time by environmental factors such as diet (David *et al.* 2014). Furthermore, the analysis of large population scale studies have identified stool consistency (Vandeputte *et al.* 2016) and medication as major non-redundant covariances which considerably impact on the composition of gut microbiota (Falony *et al.* 2016); these variables should be considered and recorded in future studies involving faecal samples to allow better conclusions to be drawn. These multifactorial relationships need to be explored further to gain a full picture of how the microbiota can be accurately rebalanced.

Also, the formulation of LNP used in this study have limited therapeutic potential, their poor solubility result in large excess of 12-bis-THA to TFD. The use of TFD-conjugates could be another way of increasing the TFD:12-bis-THA ratio to lessen the 12-bis-THA-associated cytotoxicity while increasing TFD-specific antimicrobial activity (Zhao *et al.* 2015).

Impact of non-coliforms *Enterobacteriaceae* on the magnitude of antimicrobial activity

As the TFD was designed to act on *Enterobacteriaceae*, it should theoretically be active also against *P. aeruginosa* if delivery is not limiting. It was therefore interesting to see how the *Enterobacteriaceae* population shifts using differential plating and 16S rRNA gene community sequencing approach following LNP treatment. Using 4 h time point in the batch culture fermentation experiment as an example, different colour colonies of *Enterobacteriaceae* colonies were randomly picked for 16S rRNA gene sequencing for identification at the genus/ species level. The proportional reduction of pink colonies (identified as *E. coli*) were replaced with bright pink colonies (identified as *Klebsiella pneumoniae*) in LNP treatment in batch model experiment 1 (Figure 4.6 b). As *Klebsiella pneumoniae* is a pathogen that has a thick capsule layer (Amako *et al.* 1988), this makes it challenging for particles to penetrate the cell surface (Zgurskaya *et al.* 2015). In experiment 2, *Escherichia/Shigella* spp. was not recovered by sampling for 16S rRNA gene colony PCR with LNP but *Pseudomonas aeruginosa* was; as *Pseudomonas* largely comprises penta-acylated LPS (Pier 2007, Kocincova and Lam 2011), which differs from the hexa-acylated LPS that *E. coli* commonly consists of (Caroff and Karibian 2003). The different compositions of outer

membrane could affect cell permeability considerably; along with the presence of multiple efflux pumps (Ziha-Zarifi *et al.* 1999, Poole and Srikumar 2001, Zgurskaya *et al.* 2015), this may allow *Pseudomonas* to be less prone to LNP treatment. As microbiota composition from different individuals could vary, it was good to have an indication of the impact LNPs have on other closely related organisms in the gut microbiota. Comparing the identity of the *Enterobacteriaceae* colonies from the three batch culture fermentation experiments, it was suggestive that LNP are able to reduce *Escherichia/Shigella* spp. from the gut microbiota repeatedly from three different donors.

Bacterial composition and diversity

From the 16S rRNA gene Illumina sequencing results, by comparing LNP treatment to control and SLNP at the same time point for each experiment, it was confirmed that LNP effectively reduced the *Enterobacteriaceae* abundance while maintaining the diversity of the gut microbiota community for all 3 batch model experiments, at 4 h and 8 h for experiment 1 and 2 and at 4 h for experiment 3. Since PMA excludes the dead bacterial community prior to sequencing, 16S rRNA gene community analysis became more relevant for the evaluation of the viable bacterial community including unculturable bacteria. The decrease in *Enterobacteriaceae* levels from 16S rRNA gene sequencing roughly resembled the trend seen from viable counts (see Section 4.3.3), thus confirming LNP acted on both culturable and non-culturable *Enterobacteriaceae*. For the data that had $> \log_{10} 2.5$ decrease in CFU/ml in the batch culture fermentation experiment, a decrease in *Enterobacteriaceae* was also seen in Illumina sequencing data.

It was unexpected to see *Enterobacteriaceae* as the majority of the gut microbiota community at 4 h and 8 h with SLNP treatment in batch experiment 2, as this trend was not seen in viable colony count results; the presence of non-culturable *Enterobacteriaceae* could be a possible reason why there were discrepancies in the proportion of *Enterobacteriaceae* obtained from viable counts and 16S rRNA gene sequencing. As Illumina sequencing only display results in relative quantity compare to the total bacterial load in each sample, it is difficult to quantify the exact number of bacteria in each sample, let alone compare between different samples. It could be that there is a lower bacterial load in SLNP than in the control sample, therefore for the same amount of *Enterobacteriaceae*, it appeared as a higher % in SLNP due to less bacteria being present than in the control.

Coliforms were the most rapidly growing bacterial group among the colony count results ($\log_{10} 3$ CFU/ml increase compared to the start of experiment) for both control and SLNP in batch culture fermentation experiment 2, there may be food or energy sources that are more favourable for the

growth of *Enterobacteriaceae* than other commensal bacteria. The collective effect of reduced *Lactobacillus*, *Clostridium* and *Bifidobacterium* colony counts in SLNP-treated sample at 8 h may contribute towards the reduction in total bacterial load in SLNP-treated sample compared to control.

To evaluate whether the LNP's preferential antimicrobial activity would fit into categories of Enterotype (Arumugam *et al.* 2011), the donors from experiment 1 and 2 were enriched by *Bacteroides* (Enterotype 1). For the donor in experiment 4, as the levels of *Bacteroides* were marginally higher than *Prevotella* and *Ruminococcus* but the overall *Ruminococcaceae* abundance were higher than *Bacteroidaceae* at the family level. It is hard to define especially when the definition of Enterotypes were found to be less clear than originally thought, with some researchers favouring the concept of having a gradient of species functionality instead (Jeffery *et al.* 2012). Both donors from experiment 1 and 2 with enriched *Bacteroides* were effective against 2% LNP treatment dose showed a preference in reducing *Escherichia/Shigella* spp. over *Klebsiella* or *Pseudomonas*, while donor 4 required a higher LNP dose but did not show observable difference in the presence of *Escherichia/Shigella* spp. or *Klebsiella* spp. As the *Prevotella* and *Bacteroides* groups are functionally overlapping (Holmes *et al.* 2012), the difference in the antimicrobial impact on different donors could be coincidental and are more likely due to a dose-response effect.

Principal coordinates analysis

The overall comparison of the spatial similarity between gut microbiota samples were observed using PCoA of the weighted Unifrac. Similar trends have been observed throughout batch culture fermentation experiments 1, 2, and 4, where PCoA of the weighted Unifrac distances showed that there was a shift in the gut microbiota composition with time for all treatments. For each sample, the principal coordinate shifted in a linear direction for consecutive time points from predose to 8 h, suggesting progressive structural changes occurring through time due to experimental set up.

At early time points e.g. predose, control and SLNP treatment were clustered in close proximity, reflecting these samples have similar microbial community structures. LNPs resembled more closely to the starting gut microbiota community structure compared to the controls, this may give us an insight into the mechanism by which LNPs act against the gut microbiota in a community level; while targeting *Enterobacteriaceae*, treatment with LNP may also minimise or resist change in community structure through time.

Microbiome structural changes were shown to be prominent at certain time points when comparing PCoA results to plate counting results and 16S rRNA gene community taxa plots. Effective LNP treatment resulted in decreased *Enterobacteriaceae* or coliforms in viable counts and 16S rRNA gene community analysis also showed a shift in PCoA plot compared to controls, except for samples at 0 h. Changes in taxa plot proportion were relatively small at 0 h as *Enterobacteriaceae* only made up a very small proportion of all the bacteria in the sample, therefore explaining why it did not lead to major structural changes in the overall gut microbiota. *Enterobacteriaceae* outgrow other bacterial groups in the batch culture fermentation model through time, which made the specific antimicrobial activity of LNPs clearer at later timepoints.

Metabonomic analysis

Anaerobic vs aerobic respiration

Following treatment with an effective dose of LNP i.e. 10% at 0 h and 4 h in experiment 4 (Figure 4.12), the concentration of metabolites lactate and ethanol were reduced at this LNP dose, suggesting decreased anaerobic respiration compared to the controls. The changes in succinate concentration with 10% LNPs differs to those with 2% LNP and therefore may explain the difference in antimicrobial activity. Succinate is primarily produced by the TCA cycle leading to the production of propionate. Though propionate was produced via 3 different pathways by the gut microbiota as an energy source (Reichardt *et al.* 2014), the reduction in its levels suggests a reduced rate of growth. As for formate and acetaldehyde, both levels were reduced in LNP-treated samples regardless of dose.

Fumarate and nitrate reductase (FNR), a transcription regulator that respond to physiological changes depending on environmental and metabolic challenges in *E. coli* (Balletto and Mikulska 2015), has been shown to increase expression as a result of the nanoparticulate delivery (Michael McArthur, unpublished data). While the docking of LNPs on the bacterial membrane is mainly driven by the electrostatic interaction between the cationic LNPs and anionic lipids such as cardiolipin and PG, the membrane destabilisation leads to increased bacterial permeability and allows TFD to be released within the cytoplasm, possibly by formation of transient pores (Marin-Menendez *et al.* 2017). This process is likely to cause stress response within the cell, linking to the destabilisation of respiratory chains as cardiolipin have a structural role in anchoring the respiratory chains in the membranes (Arias-Cartin *et al.* 2012).

The *in vitro* batch culture fermentation is anaerobic, therefore no advantage is expected for facultative anaerobes. Conversely, the batch culture may not be as anaerobic as anticipated and

could be microaerobic in part; also the nanoparticle delivery may have a secondary effects on anaerobic respiration as the physical disruption of membrane-bound respiratory pathways also links to oxidation of iron-sulfur clusters (Beinert and Kiley 1999).

Aerobic respiration is preferable compared to anaerobic respiration then fermentation for facultative bacteria (Crack *et al.* 2004), as the 2 latter are less efficient in yielding ATP compared to aerobic respiration, it would therefore make sense that the bacterial growth is delayed due to the switch in a less efficient metabolic pathway to counteract the stress response. As TCA cycle is part of aerobic respiration, this data is in conjunction with the finding that, as FNR switches to its active, anaerobic form, aerobic respiration ceased and therefore leads to a reduction in aerobic respiration compared to the controls. As fumarate is an intermediate metabolite for several pathways, it is difficult to pin point what the trend of concentration confers. Other metabolites such as glucose and cysteine are also involved in the FNR switch to anaerobic respiration; the levels of these metabolites have also fluctuated, suggesting an indicative, yet undefined role of FNR on the mechanism of how LNP act on the bacterial community.

Insight into how the changes in metabolite might indicate the state of the gut microbiota

Reduction of break down products such as 3-phenyllactate and 4-hydroxyphenyllactate was observed. As *Lactobacillus plantarum* has been found to produce phenyllactate as an antimicrobial agent in high levels (Lam *et al.* 2016), it may indicate that the reduction of 3-phenyllactate was a result of the 2 log₁₀ decrease in lactobacillus viable count at 4 h that was observed only with 10% LNP treatment (Figure 4.12).

In experiment 3, compensating mechanisms have been triggered under stress as suggested by the differential concentrations of betaine present in LNP-treated samples. This is an amino acid known to improve stress tolerance in bacteria (Metris *et al.* 2014), suggesting LNP treatment may be inducing this response. It is speculated that with 2% LNP, there were insufficient amount of LNP to inhibit the stress response from being transcribed as a result of TFD stimulation, betaine levels were decreased with LNP-treatment to combat stress (Sleator and Hill 2002, Wargo 2013, Metris *et al.* 2014) and therefore continued to grow as usual. Whereas in 10% LNP-treated samples, the levels of LNPs were sufficient to completely inhibit the gene expression in response to stress, no stress response was therefore recognised and acted upon from 0 h, which may explain why no difference was observed between betaine levels between treatments at 10% dose, yet the levels of *Enterobacteriaceae* was decreased in viable bacterial counts and 16S rRNA gene Illumina sequencing.

The larger decrease in amino acids i.e. tyrosine, leucine, isoleucine, valine and methionine at 8 h compared to the control and SLNP with 2% LNP, may indicate that even though no visible differences in growth were observed, the bacterial community was more metabolically active to maintain its growth rate. Furthermore, the earlier onset of uracil production for 2% and 10% LNP compared to the controls at 4 h were observed. It could indicate an increase in transcription as a result of stress response with the uracil being converted to RNA by 8 h. Uracil is also found to be synthesised by opportunistic pathogens (but not commensal) to induce reactive oxygen species (Lee *et al.* 2013, Lee *et al.* 2015), although uracil levels were increased earlier in LNP than in the controls, the levels were lower in LNP and was decreased at 8 h to the starting levels, suggesting the effects were only temporal and there is no overall adverse effect from LNPs.

For 10% LNP treatment, the declined use of metabolites i.e. asparagine, aspartate and glutamate at 4 h and phenylalanine at 8 h, which are normally used up by control and SLNP, suggest the delayed growth from 4 h onwards. Other intermediate metabolic products such as pyruvate and fumarate also have a delayed usage compared to control and SLNP may also indicate delayed growth as the control and SLNP most likely have used these metabolites up and arrive at exponential growth phase before LNP reach the same growth phase. Although the gut microbiota struggles to grow, with 2% LNP, it managed to grow regardless as suggested by the decrease of methionine, histidine and glucose as substrates and the production of acetate, propionate and formate. Although samples treated with 10% LNP had difficulty in growth initially, the momentum was also regained at 8 h.

Lower level metabonomic products such as propionate, ethanol, formate, acetaldehyde and lactate suggested that growth occurred at a delayed rate in LNP-treated samples (both at 2% and 10%) compared to control and SLNP. The metabonomic data is concurrent with the 16S rRNA gene Illumina taxa plot and PCoA plot for 10% LNP treatment as the 4 h sample closely resembles the community at predose and 0 h.

Comparing LNPs with currently available antibiotics against Enterobacteria

The side effects of antibiotics also targeting Enterobacteria were compared to LNPs with FNR TFD. Decrease bacterial diversity were observed after Ciprofloxacin (Dethlefsen *et al.* 2008, Dethlefsen and Relman 2011) treatments. This suggests that LNPs may be a better alternative to antibiotics as it reduces disruption to the gut microbiota and maintained microbiota diversity.

To conclude, by combining different experimental approaches e.g. viable bacterial counting, 16S rRNA gene sequencing and NMR metabonomic analysis, this allowed the exploration of how LNPs

interact with the complex gut microbiota and improved understanding of how might LNPs reduce the targeted organisms with minimal disruption to the native microbiota.

**TFD specific targeting against *E. coli*
in mouse model**

Chapter 5

Chapter 5: TFD specific targeting against *Enterobacteriaceae* in mouse model

5.1. Introduction

In vitro experiments in the previous chapter provided insights into how the gut microbiota would respond to LNP treatment. However, they do not account for host-drug or host-microbiota interactions which have an equally important role in evaluating the success of a drug intervention (Kostic *et al.* 2013).

Testing the efficacy of TFD *in vivo* is therefore needed. For this, animal models are often used as the next step to evaluate the drug efficacy before clinical trials are performed (Hughes and Karlen 2014). Murine studies are the easiest and most widely used to evaluate changes to the gut microbiota. They provide insights on how drug intervention can affect both the gut microbiota and the host, allowing comparison of the host-microbiota interaction (Nguyen *et al.* 2015, Grigg and Sonnenberg 2017). The organs of the intestinal tract in mice are anatomically similar to humans and are composed of similar sectional tissues (such as mucosa, lamina propria and submucosa) and cell types (such as absorptive colonocytes, goblet cells and enteroendocrine cells). As such they can be used to monitor changes to the integrity of the intestinal mucosal barrier in the small and large intestine (Ju *et al.* 2017).

Following the validation *in vitro* of LNP's antimicrobial activity against human gut microbiota in the previous chapter, a mouse model was used to determine whether the antimicrobial activity can be translated to a setting *in vivo* and to determine whether any side effects could be observed in mice when LNP are administered. C57BL/6J wild type mice were used to assess the LNP's target-specific efficacy against *Enterobacteriaceae* in the native gut microbiota setting using a physiologically relevant dosing regimen, using similar experimental parameters as the previous chapter such as viable bacterial counts, 16S rRNA gene community analysis and metatranscriptomic profiling. Additionally, the effects of LNP on epithelial barrier integrity were evaluated.

5.2 Methods

Methods specific for mouse experiments are described in Chapter 2, Section 2.9.

5.3 Results

5.3.1 Analysis of viable microbial community in mouse faeces

Experiment 1

An effective way to monitor changes in the murine gut microbiota is to perform microbiological analysis of their faeces. Faecal samples were collected and serially diluted for subsequent quantification by bacterial counts on agar plates, to assess the main bacterial communities including anaerobic bacteria, *Bacteroides*, *Clostridium*, *Lactobacillus* and coliforms. As the transit of materials through the stomach is expected to take 6 h (Padmanabhan *et al.* 2013), decrease in coliforms were observed with LNP treatment at 6 h after the initial treatment as expected, with two oral gavage treatments at 0 h and 2 h. No effect was seen in all other measured bacterial communities in control and SLNP treatments (Figure 5.1), this indicated that the viable bacterial communities were unaffected by the LNP treatment except the targeted coliforms population.

Significant reduction in coliforms at 6 h were observed in LNP treatment compared to the control and SLNP ($P \leq 0.01$). As the coliforms measured at 6 h were below the detection limit (< 200 CFU/ml) with LNP treatment, this equates to a decrease in coliforms numbers of at least $\log_{10} 3.5$ CFU/ml implying a bactericidal effect. Also, a $\log_{10} 2$ CFU/ml decrease in coliforms at 24 h was observed in LNP treatment compared to the SLNP and control.

The control and SLNP colony counts for anaerobic bacteria, *Bacteroides*, *Lactobacillus* and coliforms were similar throughout the mouse experiment, suggesting that the nanoparticles themselves had little effect on the viability of gut microbiota and the antimicrobial activity is mostly TFD specific with the current dosing regimen. Mice with LNP treatment had similar bacterial counts to those with SLNP treatment except coliforms. The *Clostridium* levels in the LNP group mice were higher than the mice in the control and SLNP group before oral gavage treatments, suggesting some intrinsic gut microbiota variation between groups of mice when caged separately. The prevailing trend of *Clostridium* levels between mice in different groups were nonetheless consistent across all time points. This suggests LNP's ability to specifically reduce the coliforms viable population 6 h after the initial drug administration into the stomach, without altering the viability of the rest of the gut microbiota community.

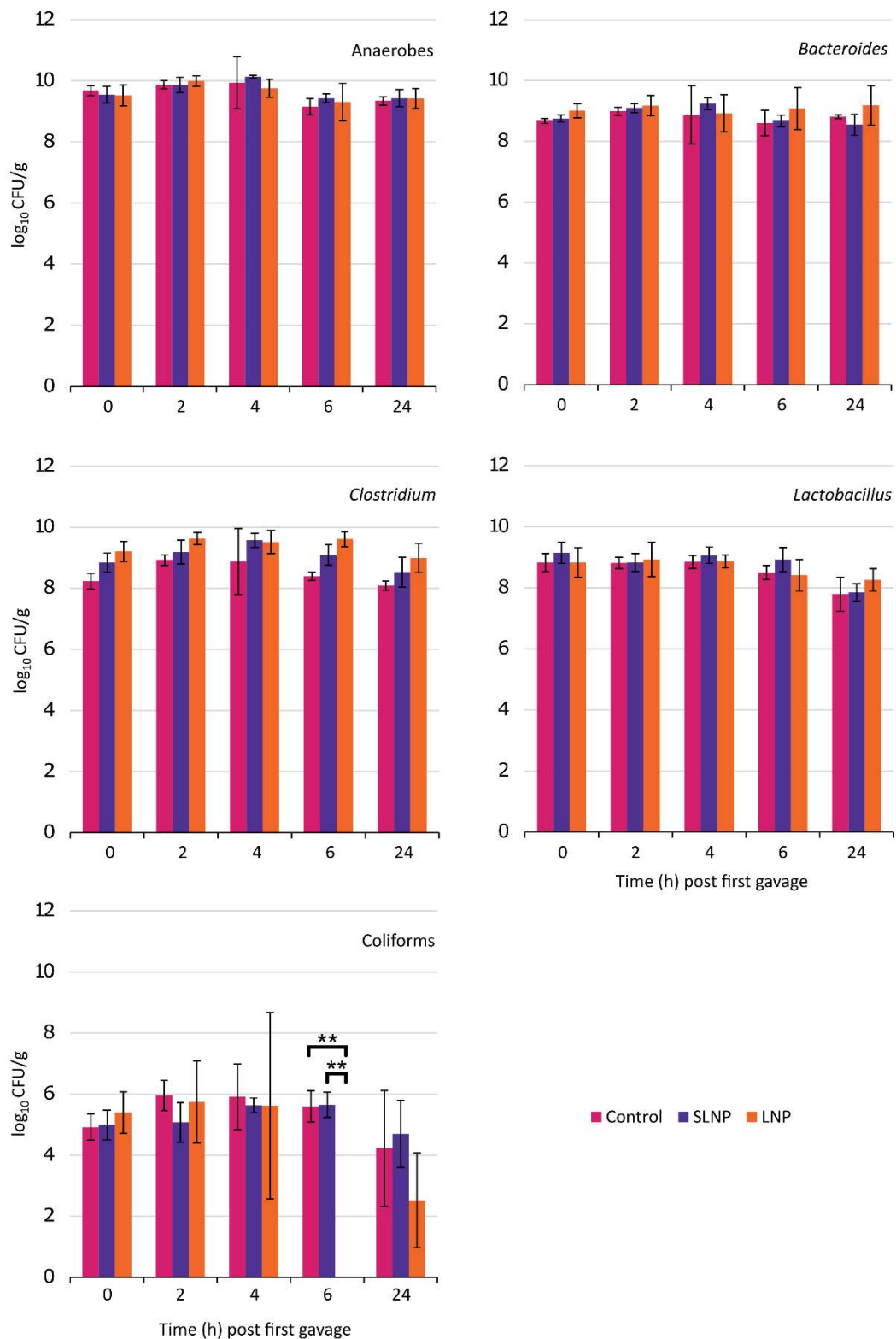


Figure 5.1 Bacterial viable counts for anaerobes, *Bacteroides*, *Clostridium*, *Lactobacillus* and coliforms for mouse experiment 1. Means were calculated from a minimum of 3 samples of faecal pellet (n=3) as some did not produce a faecal pellet at certain time points. Double asterisks denotes $P \leq 0.01$.

Experiment 2

As signs of distress were indicated in mouse experiment 1, faecal sampling at 2 h was omitted to allow the mice to recover from the initial drug administration procedure. As SLNP treatment showed no difference in viable counts compared to LNP in experiment 1, a lower dose of LNP (i.e. LNP diluted 1:5 in vehicle control) was used instead of SLNP to elucidate whether the LNP activity against coliforms was dose-dependent. With this new experimental set up, all mice produced faecal pellets at all the required time points.

Coliforms counts were similar between control and low dose LNP treatment at 0 h, 4 h, 6 h, 8 h, and 24 h (Figure 5.2). The coliforms population significantly decreased by $\log_{10} 2$ CFU/g at 6 h ($P \leq 0.01$) and $\log_{10} 3$ CFU/g at 8 h ($P \leq 0.001$) by LNP treatment compared to control and SLNPs, though the viable colonies returned to similar levels to the control and low dose LNP treatments by 24 h. This indicates a dose dependant response was present with the LNP treatment as only the undiluted LNP treatment showed antimicrobial activity against coliforms. Control, low dose LNP and LNP had generally similar viable colony counts for anaerobic bacteria, *Bacteroides* and *Lactobacillus*. Like experiment 1, variability was seen in the amounts of *Clostridium* at the start of the experiment, though difference were not notable.

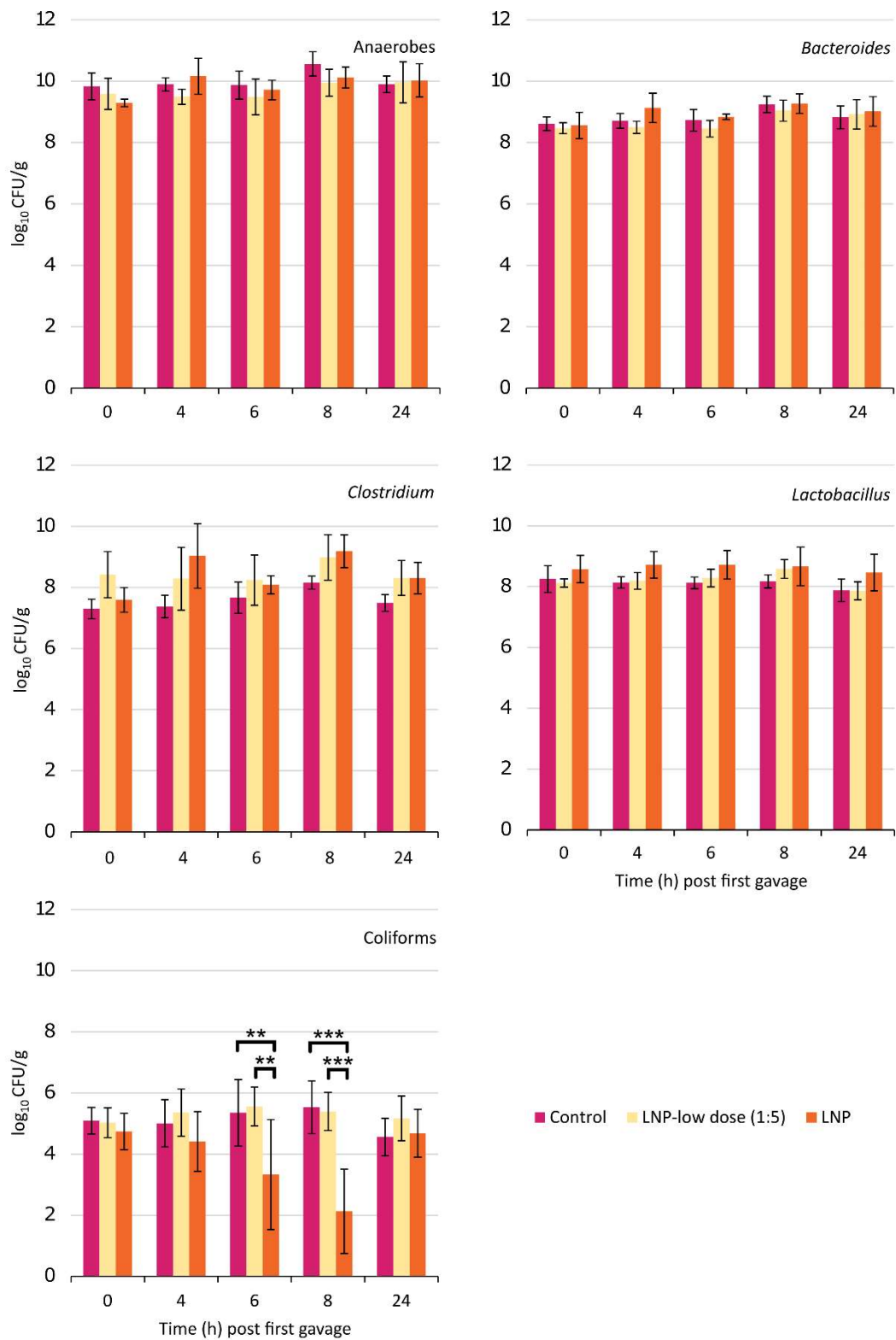


Figure 5.2 Bacterial viable counts for anaerobes, *Bacteroides*, *Clostridium*, *Lactobacillus* and coliforms for mouse experiment 2. Means of colony forming units of 5 mice (n=5) were calculated \pm SD. Double and triple asterisks denote $P \leq 0.01$ and $P \leq 0.001$ respectively.

5.3.2 Metataxonomic analysis of microbial community in mouse faeces

To determine the viable amounts of *Enterobacteriaceae* using 16S rRNA gene sequencing methods, samples were taken from each mouse at each time point and treated with PMA and photo-activation before DNA extraction. The metataxonomic profiles were characterised by sequencing of 16S rRNA gene V4 region from faecal contents.

Despite *Enterobacteriaceae* making up only a low proportion of the total bacterial community, the averaged relative abundances were plotted for each treatment (Figure 5.3). It was shown in experiment 1 that the proportion of *Enterobacteriaceae* was higher in the control sample than SLNP (by > 3 fold) and LNP (by > 5 fold), indicating SLNP and LNP treatments resulted in lower proportions of *Enterobacteriaceae* compared to control. Also, *Enterobacteriaceae* decreased to 0% at 6 h with LNP-treated samples while this group was still present in the control and SLNP-treated samples. Similar trends was seen in experiment 2, where *Enterobacteriaceae* levels were higher in the control than LNP treatment at 4, 6 and 8 h. The similarities observed in both experiments may indicate the increase in *Enterobacteriaceae* levels were inhibited in the presence LNP.

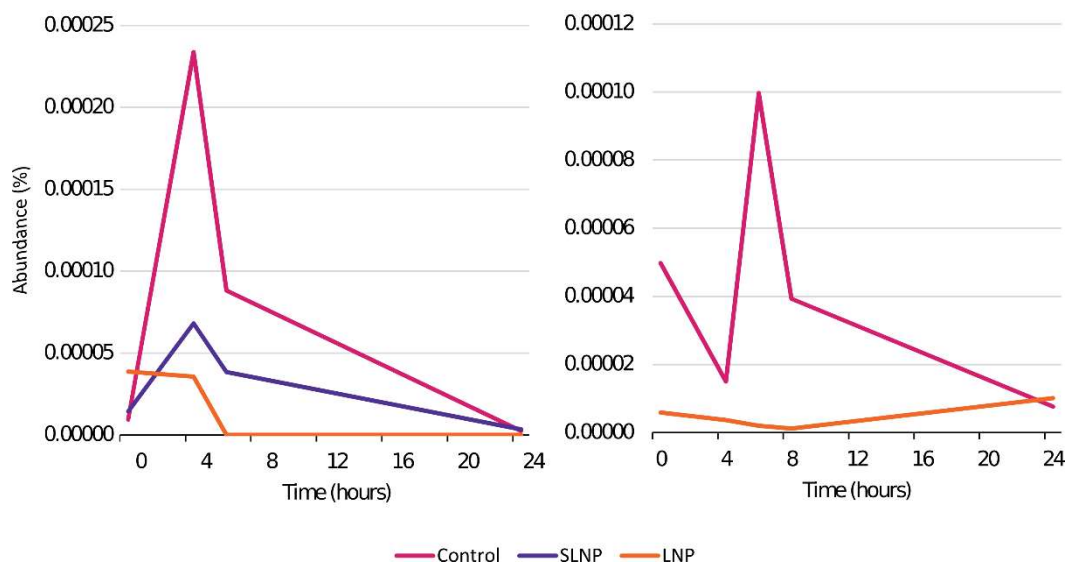


Figure 5.3 Relative abundance of *Enterobacteriaceae* taken from taxa plot from 16S rRNA gene community analysis. Data extracted from taxa plot of community analysis. Left, exp 1; right, experiment 2.

To look at the overall changes in the 16S rRNA gene community, the samples were grouped by treatments at each time point. Samples at 0 h were dominated by the family *S24-7* (from the order Bacteroidales), an unclassified family (in the order Clostridiales), *Lachnospiraceae* and *Ruminococcaceae* and *Rikenellaceae*, with the LNP group mice having proportionally more *S24-7* and less of an unclassified family of Clostridiales, *Lachnospiraceae* and *Ruminococcaceae* than those in the control and SLNP groups (Figure 5.4).

In experiment 1, changes in the bacterial community were seen in the samples treated with saline vehicle control at different time points (especially between 0 h and 4 h), indicating that gut microbiota can rapidly change within the sampling period. Comparing samples at 0 h and 4 h, there is generally a higher relative abundance of family *S24-7* in the control and SLNP and a relative decrease with LNP treatment. LNP-treated samples have in turn increased proportions of an unidentified family (in order Clostridiales), *Lactobacillaceae*, *Lachnospiraceae* and *Ruminococcaceae* at 4 h, with similar community proportions to the 0 h control and SLNP samples.

At 6 h, control samples had a similar trend to that seen at 4 h. With a decrease in *S24-7* family, an unidentified family in Order Clostridiales, *Lachnospiraceae* and *Ruminococcaceae* were in turn increased with SLNP treatment at 6 h. In contrast these communities were decreased with LNP-treated samples with a large increase in *Bacteroidaceae*, *Prevotellaceae* and *Rikenellaceae* abundances.

At 24 h, *S24-7* decreased and *Lachnospiraceae* and *Ruminococcaceae* were increased in all treatment groups. In addition, control samples have decreased *Lactobacillaceae* and increased unidentified family in Order Clostridiales, *Rikenellaceae*, *Prevotellaceae* and *Bacteroidaceae*. SLNP had decreased *Lactobacillaceae* and increased *Rikenellaceae*, *Prevotellaceae* and *Bacteroidaceae* levels. With LNP-treated samples, *S24-7* were hugely decreased with increases in an unidentified family in Order Clostridiales, *Lactobacillaceae*, *Lachnospiraceae* and *Ruminococcaceae*.

In general over the 24 h period, SLNP-treated samples had similar gut microbiota communities and abundances to the control or the SLNP profile at 0 h, suggesting the delivery nanoparticles did not pose obvious change to the gut microbiota. LNP on the other hand, had an overall decrease in the *S24-7* family and increases in unidentified family in Order Clostridiales, *Lachnospiraceae*, *Ruminococcaceae*, *Prevotellaceae*, *Bacteroidaceae* and *Rikenellaceae*.

In experiment 2, similar trends were observed with LNP treatment compared to experiment 1. Samples in experiment 2 were populated by similar bacterial family to experiment 1, with *S24-7*

being the majority, along with Clostridiales order, *Lachnospiraceae*, *Ruminococcaceae* and *Rikenellaceae*.

Like experiment 1, *S24-7*'s relative abundance fluctuated across time points, with some proportional shift of other members in the community consequently. The fluctuation of *S24-7* were consistent in experiment 1 and 2 at 0 h, 4 h and 6 h with LNP treatment compared to the control, the consequential shifts of other communities were also similar. However, the levels of *S24-7* with LNP treatment were higher than the control at 24 h in experiment 2, which is opposite to the trend observed in experiment 1. Instead, relative abundance of *S24-7* is higher than control, with decrease in Clostridiales, *Lachnospiraceae* and *Ruminococcaceae*.



Figure 5.4 Bacterial community analysis of 16S rRNA gene sequencing at family level for mouse experiment with PMA-treatment with average bacterial populations. a) experiment 1; b) experiment 2. (O) indicates an unidentified family in the described order.

Principal Coordinates Analysis

To determine the community structures of the gut microbiota samples upon LNP treatment, weighted unifrac Principal Coordinates Analysis (PCoA) plots were used to look at the spatial relationship between different samples in the same experimental run. For PCoA plots from mouse experiment 1, LNP were structurally more distant from control and SLNP at 0 h on the PC1 scale (which accounted for 45.15% of the variability) (Figure 5.5 a). At 4 h, control and SLNP shifted towards the LNP-treated samples at 0 h (on the right along PC1 axis) whereas 2 out of 3 LNP-treated samples were situated closer to the control and SLNP samples at 0 h (on the left along PC1 axis), suggesting the LNP-treated gut microbiota were structurally similar to the control samples at the start of the experiment. Although all treatments were scattered at 6 h and 24 h, the 6 h samples were on the right half of the PC1 axis. At 24 h, LNP scattered on the left-hand side, SLNP samples were in the middle and controls remained on the right-hand side of the axis. In experiment 2, there was no clustering of samples for each time point, as samples from mice with the same treatment were evenly scattering along the PC1 axis at each time point (Figure 5.5 b). However, there was spatial separation between the two treatment groups since the start of experiment, all the control samples were located at the bottom half of the PC2 axis and the LNP samples were situated at the top half on the axis.

As the structure of the gut microbiota is different in the control and LNP group at the start of both experiments, it is hard to compare the structural dynamics of LNP-treatment compared to the controls from these data.

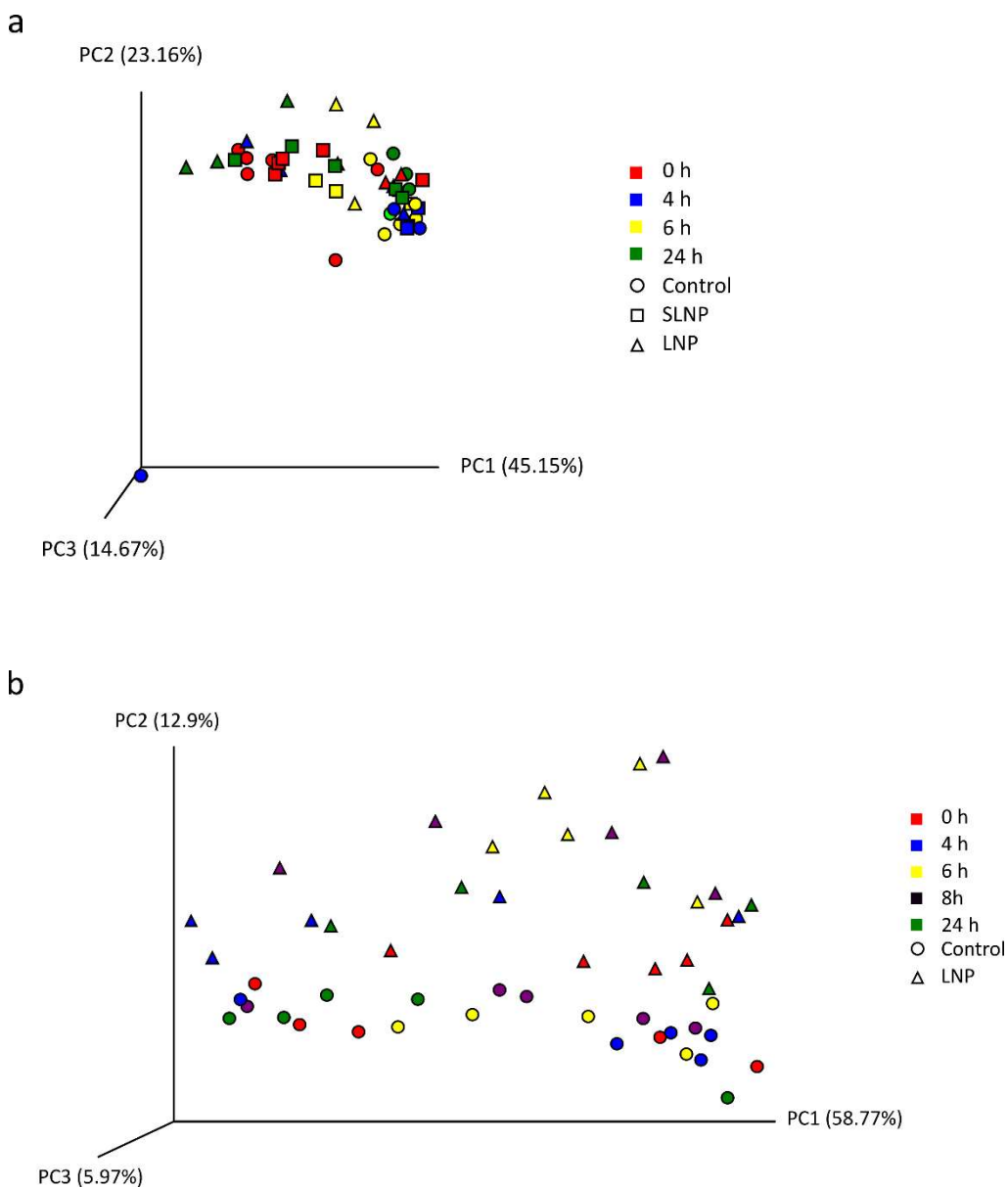


Figure 5.5 Principal coordinates analysis (PCoA) plots from 16S rRNA gene community analysis for *in vivo* mouse model. a) experiment 1; b) experiment 2. 3D PCoA plot was generated from weighted UniFrac analysis, where x- and y- axis represents the first and second coordinates respectively.

5.3.3 Metabonomic analysis of mouse faeces

To determine whether similar metabonomic profiling observed in LNP treatment in the previously chapter can be seen *in vivo* and if they would mirror the changes in the microbial community, ^1H NMR spectroscopy was used to identify the metabolites present in the mouse experiment samples with different NP treatments. A representative NMR spectrum, shown from mouse

experiment 1 (Figure 5.6), is shown to evaluate the profile of metabolites following LNP treatments.

No noticeable difference in metabolite concentration was shown between treatments at different time points, including metabolites butyrate, acetate, propionate, isobutyrate, isovalerate, valerate, ethanol, formate, trimethylamine, putrescine, 3-hydroxyphenylpropionate, 3-hydroxyphenylacetate, 3-phenyllactate, 3-phenylpropionate, glucose, xylose, alanine, aspartate, glutamate, glutamine, glycine, isoleucine, lysine, methionine, tyrosine, taurine, pyruvate, succinate, hypoxanthine and uracil. Large variation were observed within mice and between mice samples, along with limited amount of faeces were available for sampling, making it difficult to draw meaningful deductions from the data.

The metabonomic results from mouse experiment 1 and experiment 2 were comparable, suggesting the lack of notable metabonomic separation between samples with control, SLNP and LNP (low or normal dose) treatments.

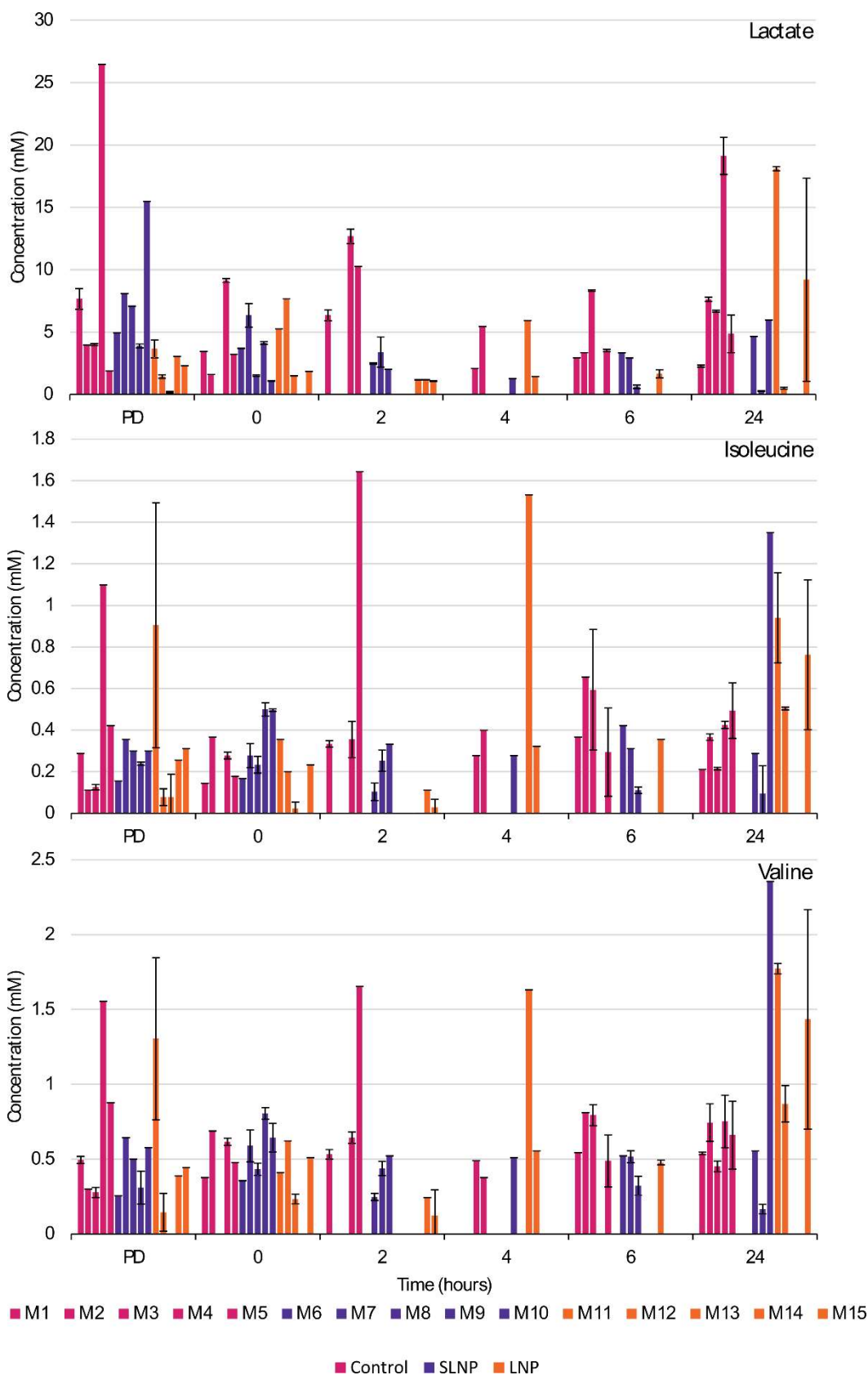


Figure 5.6 A representative of metabonomic profile from mouse experiment 1, showing the large variation within and among mouse faecal samples. M= mouse identification in each group.

5.3.4 Experimental observations of mouse health

Experiment 1

The treatments were administered by two 100 µl oral gavages to the mice at the commencement of the experiment (0 h) and 2 h following. The treatments were the vehicle control and the SLNP and the LNP. The mice were observed throughout the experimental period to monitor early indicators of distress to minimise suffering following the treatments. In addition faecal samples were collected at the following time-points post the experimental start: 0 h, 2 h, 4 h, 6 h and 24 h (see Section 2.9). This process involves handling the mice causing them to defecate. One mouse with SLNP treatment and two mice with LNP treatment were euthanised after the 2 h and 4 h faecal collections respectively, as physical signs of illness were observed followed by the dosing/sampling regimen.

After dissection, tissues from the SLNP and LNP group had abnormal morphology compared to the controls. Shortened small intestine and colon with more liquid faecal pellets were generally observed in mice treated with SLNP. One of the SLNP treated mice also looked ill, had very thin and narrow intestine and a smaller caecum; whereas another mouse had no faecal content in the duodenum, jejunum and ileum and had a smaller cecum. LNP-treated mice had similar observations as seen in SLNP, a shorter small intestine was observed compared to control and faecal pellets were found to be soft in ileum but normal in the colon.

Experiment 2

With the aim to reduce stress of animals, faecal sample collection at 2 h was omitted after the oral gavages and collection was at 8 h instead (see Section 2.9). To determine if there is a dose-dependent effect, the SLNP treatment was replaced with a lower dose LNP that had been diluted in the vehicle (1:5 diluted). At 6 h and 8 h, the mice in LNP treatment group started to show signs of stress, including hunchback posture and piloerection. At 8 h, mice with low dose LNP showed signs of piloerection; one mouse with LNP treatment had unusually narrow faecal pellets. Mice with LNP treatments (both low-dose and normal) had harder stools. No euthanasiation was required before the end of experiment. At the point of dissection, two mice with low dose LNP treatment had very thin small intestines whereas one mouse in the LNP treatment group did not have any colon content.

5.3.5 Histological analysis of mouse intestinal tissues

Haemotoxylin and eosin staining was performed to assess whether any signs of epithelial damage occurred in the colon occurred after LNP treatment. Haemolysin is a purple stains that binds to acidic components in cells such as DNA and RNA. Whereas eosin reacts with basic structures such as protein and cytoplasmic components and stain them pink. Representative histological samples from mouse experiment 1 are shown in Figure 5.7. In control mice, colon samples have normal histological morphology as healthy colonic crypts; colon crypts in LNP- treated mice (either healthy or ill) both had similar morphology to those seen in control mice.

Normal crypt architecture, no observable inflammatory cell infiltration and no muscle thickening were seen, goblet cell depletion was absent, as were crypt abscess, indicating no histological damage typical to colitis was observed according to Kim *et al.* (2012). The lamina propria appears normal and intact, with no signs of inflammations or cell shedding observed as per Erben *et al.* (2014).

Moreover, comparing the histology of LNP-treated mice that remained healthy during the experiment or were culled after 4 h, no histological differences in the healthy or ill LNP-treated mice were observed. This may indicate that, even though some mice showed signs of illness during the experimental period, it could be a transient effect as little difference was observed in their epithelial morphology in the colon.

Overall, no cell shedding or inflammation in colonic crypts observed was upon LNP treatment compared to control mice. This indicated that LNP treatment did not affect the colonic epithelium during the experimental period. While there was no observable difference in colonic crypt lengths between control and LNP-treated healthy mice, the colonic crypts were considerably shorter in LNP-treated mouse that was euthanised before end of experiment compared to the control by about 50%. However, this could be due to sectioning variation in the position of colon, as the sectioning from mouse euthanised prior to the end of experiment (Figure 5.7 c) resembled the proximal colon, as opposed to control and LNP healthy mice (Figure 5.7 a and b) which resembled the distal colon.

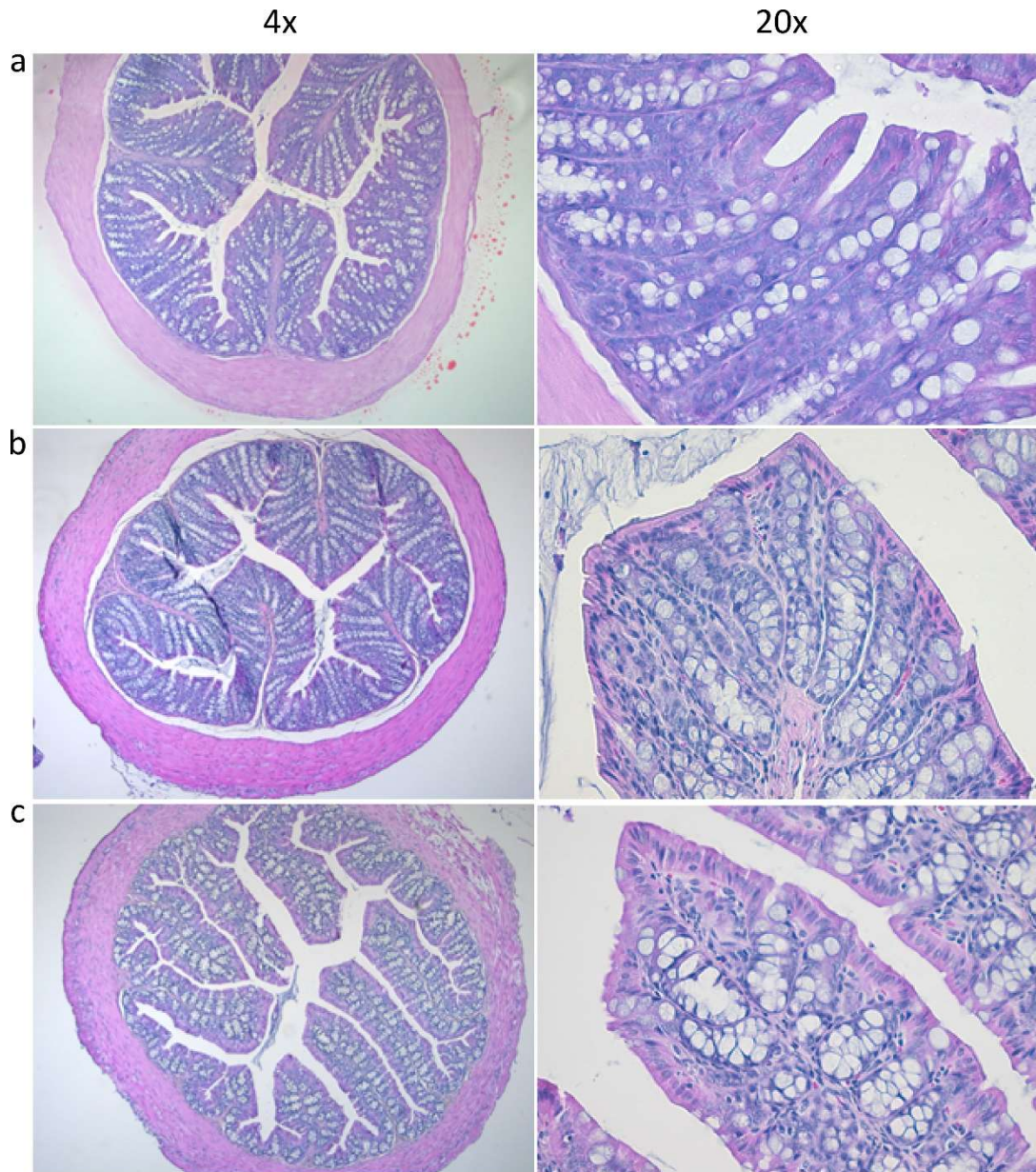


Figure 5.7 Histological photomicrograph of mouse colon stained with haematoxylin and eosin at 4x and 20x magnification from a) saline control mouse; b) LNP-treated healthy mouse; and c) LNP-treated mouse with signs of illness that was euthanised prior to the end of experiment.

5.4 Discussion

Antimicrobial activity was observed when two oral gavages were given in experiment 1 and 2, coliforms viable bacterial counts were specifically reduced at 6 h and 6-8 h with LNP treatment respectively without changing the rest of the commensal bacterial community observed by viable bacterial plate counting, indicating that TFD specific antimicrobial activity against coliforms (which are members of *Enterobacteriaceae*) was observed in the *in vivo* mouse model. Antibiotics norfloxacin and ampicillin was found to significantly decrease anaerobic bacteria by \log_{10} 3 CFU/g of faeces in another mouse study (Membrez *et al.* 2008). The CFU decrease is comparable in the mouse experiments but showed a more selective approach with minimal changes to the rest of the culturable faecal community, suggesting that LNP have a more specific approach on the alteration of the mouse gut microbiota. As most mouse studies typically evaluate antimicrobial activity after a minimal of 1 day (Spees *et al.* 2013, Lackraj *et al.* 2016, Yao *et al.* 2016), the fast acting nature of LNP may be an advantageous to reduce rapidly multiplying bacteria particularly at the start of an infection.

16S rRNA gene community analysis has shown that the bacterial community may be more diverse than expected, as *Enterobacteriaceae* only made up a small percentage of the total abundance in the faecal samples in both experiments. *Enterobacteriaceae* abundance was nonetheless diminished at 6 h with LNP treatment, with temporal fluctuation in the proportion of other bacterial families, but did not affecting the communities present in the samples. The huge relative abundance of unculturable gut microbiota preserved in the samples compared to those detectable from bacterial culturing method may explain the large discrepancy to the expected abundance of *Enterobacteriaceae*.

The main constituents of the gut microbiota at the family/order level in mouse experiments showed some similarities in the microbiota composition in C57BL/6J mouse from the literature, where Bacteroidetes and Clostridiales were the predominant members of the gut microbiota (Zakostelska *et al.* 2016). S24-7 is one of the main members in the 16S rRNA gene analysis of gut microbiota in a C57BL/6 mice model (Yao *et al.* 2016); *Lactobacillaceae*, *Lachnospiraceae* and *Ruminococcaceae* were also seen in other studies at the family level (Steegenga *et al.* 2014, Yao *et al.* 2016). S24-7, an uncultured family in Bacteroidales that dominated the mice gut microbiota from 16S rRNA gene community analysis in both experiments (Figure 5.4), was also previously described as a predominant member of the gut microbiota in mice (Salzman *et al.* 2002) and at lower abundance in other homeothermic animals e.g. humans (Ormerod *et al.* 2016). Increased abundance of S24-7 was found in diabetes-sensitive mice with a high fat diet (Serino *et al.* 2012)

and C57BL/6J male mice with increased exercise when fed a low-fat diet (Evans *et al.* 2014). However, the implication of the fluctuations in this family is still not well studied.

Effects of other antibiotics on the commensal microbiota in mouse models in 16S rRNA gene community analysis

The gut microbiota abundance was not changed by time and treatment over the 24 h period, the only taxon with substantial compositional decrease was *S24-7*, several taxa e.g. Clostridiales order, *Rikenellaceae* family and Bacteroidales order had compensating compositional increase to maintain bacterial abundance when *S24-7* declined. Similar observations (except increase in Bacteroidales) were described in a pathogen-selective treatment with minimal disturbance of the mouse gut microbiota (Yao *et al.* 2016), who demonstrated a recovery of gut microbiota composition 2 days after the treatment had stopped compared to 7 days with antibiotic treatments. As whole genome sequence of *S24-7* is not available, it was difficult to elucidate whether the decrease was due to the presence of Crp-FNR transcription factor. *S24-7* is a member of the Bacteroidales order, therefore it would be rational to speculate other families in this order e.g. *Prevotellaceae* and *Bacteroidaceae* were increased to preserve similar functional roles in the gut microbiota.

As our experimental end point stopped only 24 h after the initial treatment, the assessment of the mice gut microbiota with an extended recovery period is required to fully evaluate the recovery of the gut microbiota post-LNP treatment in the future.

No metabonomic difference has been found between different treatments in both experiment 1 and 2, it was suspected that metabonomic changes due to the specific reduction of *Enterobacteriaceae* may not be observable as *Enterobacteriaceae* only make up a diminutive portion of the total gut microbiota community from 16S rRNA gene analysis. As limited amounts of faecal samples were obtained from the mice to minimise stress, the NMR samples were diluted by nine times compared to the typical protocol to obtain the volume for NMR analysis, this lead to weakening of signals for sugars such as xylose, glucose, arabinose and galactose etc proportionally. The quality of the data was good nonetheless and the substantial dilution of the samples has not affected the quantification of metabolites otherwise.

Antibiotics have been found to result in extensive alterations in the microbial intestinal metabonome, further contributing to the imbalances that interfere with the intestinal homeostasis (Antunes and Finlay 2011, Perez-Cobas *et al.* 2013). It may be of advantage for the antimicrobial to have minimal effect on the metabonomic responses, as they may suggest

minimal disruption to the metabonomic profile of gut microbiota when exerting antimicrobial activity only on a small group of bacteria, implying LNP's selective antimicrobial activity has minimal disruption in the gut microbiota metabonome that would minimise further metabonomic damage to an already imbalanced gut microbiota. However, as there were interindividual differences between the 16S rRNA gene community gut microbiota profile, the metabonomic profile may also differ between mice within the treatment group, making it difficult to pinpoint the typical changes in metabolites following the treatment regimen.

Evaluation of mice's health status

Multiple oral gavage dose of LNPs were administered in Golden Syrian hamster model in a *C. difficile* study and no adverse effect was seen, it was not expected that LNPs would cause harm to animals by multiple gavage dosing (Marin-Menendez *et al.* 2017). A few mice had to be euthanised before the end of the experiment 1 with SLNP and LNP treatment as the extent of poor health reached humane endpoints (National Research Council 2009). The initial experimental design has included collection of a faecal pellet after gavage dosing at 0 h and 2 h, as mouse would usually produce a pellet following a gavage procedure. However, the acquisition of faecal sample was not as easy as expected and may have increased pressure on the mice to provide a faecal sample after gavage was administered.

To improve well being of mice, faecal collection was omitted from 2 h and was changed to 8 h instead in the next experiment. Low-dose LNP (1:5 diluted) was used instead of SLNP to determine whether dose-dependent LNP activity was present. The presence of coliforms specific antimicrobial effect with LNP was consistent with experiment 1, while low dose LNP did not produce any changes in the gut microbiota, this emphasised the dose-response effect of LNP and the higher dose is needed to alter the microbiota given the high density of bacteria. Mice also showed delayed and fewer signs of poor health such as first signs of pain, distress and discomfort compared to experiment 1 and none reached the humane endpoint before the end of experiment, suggesting an improvement in experimental design to relieve stress can avoid adverse health in mice. This may be due to increased time given to mice to recover from the oral gavage before the faecal pellet was demanded. Stress phenotypes were displayed at an earlier time point in LNP compared to low dose LNP in experiment 2, suggesting that the indication of pain-associated behaviour may also be dose-dependent.

From the observations from both experiments, it was suspected that the combination of repeat dosing and faecal pellet collection at 2 h in experiment 1 may be too stressful for the mice. The adverse effect could also originate from the delivery agent. Even though the delivery nanoparticle

is selective for bacterial membranes, it also has some residual activity for eukaryotic membranes as slight haemolysis was previously observed (Marin-Menendez *et al.* 2017). The combination of both factors may exceed the mice's tolerance and accentuate signs of distress after the SLNP and LNP treatment were administered.

It has been found that the oral gavage process can lead to stress in C57BL/6 male mice by increasing systematic stress response (Walker *et al.* 2012). Increased stress and mortality was also observed upon repeated gavage dosing (Arantes-Rodrigues *et al.* 2012). Furthermore, as B57BL/6 males were used in the study, while being more prone to bacterial infection, they have increased stress-related gene expression compared to their female counterparts upon *E. coli* LPS challenge (Everhardt Queen *et al.* 2016), which could explain why stress phenotypes were observed as male mice were used in the experiments.

Effect of LNP on the histological morphology of colon

Even though some LNP-treated mice showed signs of stress and were associated with shortening of intestine and reduced cecum size in experiment 1 and 2, the histological morphology was similar between control- and LNP-treated colon for mice that remained in a healthy physical state. Colonic crypt length was only shortened in the LNP-treated mouse that required euthanasia before the end of experiment 1, suggesting mortality could be affected by stress and/or the extent of tissue damage. The above observations were also noted in other animal models of colitis and inflammatory bowel disease (Siegmond *et al.* 2001, Noti *et al.* 2010, Mishra *et al.* 2013). As only one mouse were euthanised before the end of experiment, it would be difficult to differentiate sectioning variation from the histological damage at the current sample size. The shortening of small intestine with SLNP and LNP treatment may suggest that the delivery nanoparticle could be cytotoxic to mice reaching certain levels and affect tissue morphology with double gavage dose, though the histopathological changes were less severe compared to broad-spectrum antibiotics such as streptomycin (Spees *et al.* 2013). To increase efficacy and reduce side effects from the delivery nanoparticles, TFD-conjugates, which decrease 12-bis-THA: TFD ratio by 1000, were tested by co-workers to have comparable antimicrobial activity as LNP and Levofloxacin in a *in vivo* *Galleria mellonella* model infected with pathogenic *E. coli* (Michael McArthur, unpublished data), this derivative would likely overcome toxicity issues the current LNP formula has experienced.

Lessons learnt and future work

Combining both experiments, we would test for single dose of TFD-conjugate (so more TFD and less 12-bis-THA is used compared to the current LNP formula to reduce toxic effect) using female mice and/ or in a disease model (e.g. DSS-induced colitis) and evaluate antimicrobial activity for a longer period to see if the gut microbiota recover to the control community after treatment (to determine whether any alterations of gut microbiota is transient or long term). The translational potential of a murine model to human terms is limiting as the composition of mice and human microbiota differs. A human-microbiota-associated animal model can be used instead for a more in depth investigation on how the LNP affect the human microbiota *in vivo* (Lundberg *et al.* 2016, Staley *et al.* 2017). Also for the existing mouse experiments, evaluating liver toxicity would be beneficial to determine the presence of a systemic effect of LNP if more time is allowed.

TFD specific targeting against SRB

Chapter 6

Chapter 6: TFD specific targeting against SRB

6.1. Introduction

Sulphate reducing bacteria (SRB) are commensal residents of the human gut microbiota and have been described as having a physiological role in health (Motta *et al.* 2015) and disease (Ijssennagger *et al.* 2016). They are a phylogenetically diverse group of strict anaerobes that are classified by their ability to obtain energy by oxidizing hydrogen while reducing sulphate to hydrogen sulphide (H₂S) as the end product of sulphate reduction (Muyzer and Stams 2008). Gut microorganisms can use H₂S as an energy source (Ley *et al.* 2006, Goubern *et al.* 2007) and it has been reported to play a role in maintaining the integrity of microbiota biofilm and improving colonic mucus production (Motta *et al.* 2015). Endogenous H₂S are produced by host cells at low levels and are used as a signalling molecule in epithelial tissues (Wang 2012), and are carefully balanced to maintain physiological relevant levels to avoid cell toxicity from excess H₂S (Pouokam and Althaus 2016).

However, deleterious mechanisms by which H₂S can degrade the colonic mucus layer (Ijssennagger *et al.* 2015) and induce DNA damage (Attene-Ramos *et al.* 2007, Attene-Ramos *et al.* 2010) have been reported. High levels of H₂S can also induce damage in the intestinal epithelium (Nakamura *et al.* 2010, Medani *et al.* 2011) and are associated with IBD (Roediger *et al.* 1993b, Wallace *et al.* 2009) and colon cancer (Cao *et al.* 2010, Carbonero *et al.* 2012, Ijssennagger *et al.* 2016).

The balance between the interplay of beneficial and detrimental effects of H₂S are crucial for gut health (Feng *et al.* 2017), and the need to develop tools that modulate the levels of SRB and H₂S to improve the understanding of their role in health and to facilitate the investigation of disease association is clear.

As SRB carry non-redundant functions to utilise hydrogen and sulphate and are represented by relatively few species in the gut (Marchesi 2011), mainly members of the genus *Desulfovibrio* in the class of Deltaproteobacteria (Scanlan *et al.* 2009), this makes SRB a good target to reduce the H₂S producing niche that has a pivotal role in human health.

Transcription factor decoy (TFD) has an adaptable spectrum of antimicrobial activity depending on the transcription factor the TFD is designed to target. This system can therefore be explored to

evaluate SRB targeting. Functional genes that are highly conserved among SRB include *dissimilatory (bi) sulphite reductase (dsrB)*, which is essential for the reduction of sulphite to sulphide, and has been utilised as a phylogenetic marker for SRB identification (Geets *et al.* 2006, Giloteaux *et al.* 2013, Guan *et al.* 2014, Gao *et al.* 2015, Tian *et al.* 2017). As SRB are a phylogenetically diverse group, targeting shared metabolic genes is a logical and promising approach.

In the previous chapter, we focused on TFD targeting using *Enterobacteriaceae* as a model organism. In this chapter, we extend the application of the TFD to another GI tract organism, to determine whether TFD could be utilised to selectively reduce SRB that have conserved metabolic functions. SRB were isolated from human faeces and their whole genomes sequenced for future characterisation. Primers were designed to identify human SRB and used to develop an alternative method of quantification using qPCR. Genome mining was performed to identify possible SRB gene targets, their transcription binding sites were used for the design of SRB-targeting TFD before their antimicrobial activities were tested. Confocal scanning microscopy was also utilised to evaluate the TFD delivery within the SRB.

6.2. Materials and Methods

For materials and methods relevant to this chapter, see 2.8.1 for Isolation of human SRB, 2.8.2 for Gram staining, 2.7.1 for PCR conditions, 2.6.3 for gel electrophoresis, 2.6.4 for Measurement of DNA concentration (all samples were measured using Nanodrop except PCR products amplified from gDNA of SRB, which were measured with Qubit), 2.7.2 for identification of bacterial isolates, 2.7.3 for qPCR primer design, 2.7.4 for qPCR, 2.7.5 for genome DNA extraction of SRB, 2.8.4 for Designing TFD to target SRB, 2.2.1 for Making TFD and NPs, 2.2.2 for Minimum inhibitory concentration, and 2.4 for confocal microscopy.

6.3 Results

6.3.1 SRB Isolation of SRB from human faeces

SRB were isolated from human faeces from four different donors using Postgate Medium C to identify human isolates for subsequent experimental analysis. Based on analysis of 16S rRNA gene sequencing, 16 isolates were identified as *Desulfovibrio piger* (S_{ab} score \geq 0.96), 5 isolates were identified as *Veillonella tobetsuensis* (S_{ab} score \geq 0.98), 5 isolates identified as *Veillonella parvula* (S_{ab} score \geq 0.97) and 1 isolate as *Veillonella spp.* (S_{ab} score =1).

One representative Gram staining image for each group is presented in Figure 6.1, the cell wall of *D. piger* (Figure 6.1 a) appeared pink and had rod shaped morphology, confirming that they are Gram-negative bacteria (Beveridge 2001). *V. parvula* (Figure 6.1 b) and *V. tobetsuensis* (Figure 6.1 c) retained the purple crystal violet stain on the cell wall and were identified as Gram-positive cocci. All the above data are summarised in Table 6.1.

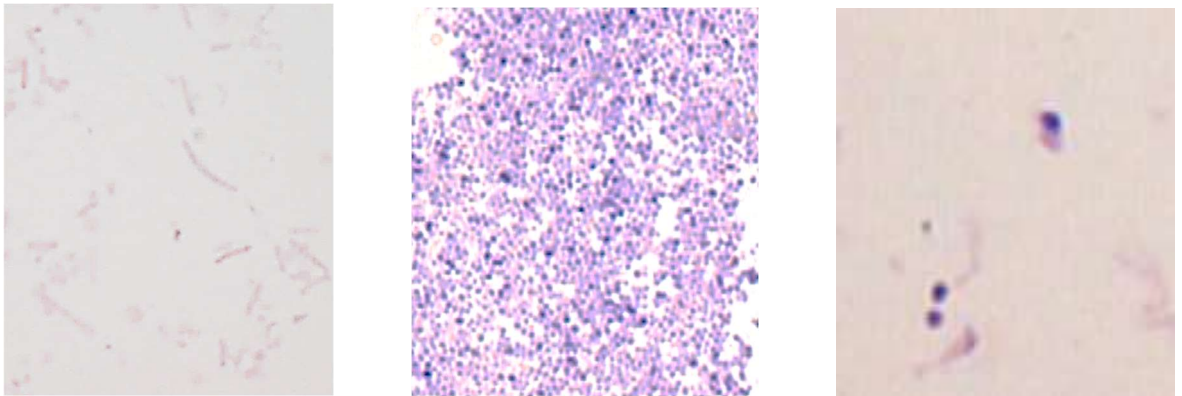


Figure 6.1 Gram staining of human gut SRB isolates. Representative images of isolates as presumptive left) *D. piger* (Gram negative) bacteria; middle) *V. Parvula* (Gram positive) and right) *V. tobetsuensis* (Gram positive).

Table 6.1 Summary table of SRB isolated from human faecal samples. S_{ab} score is the percentage of shared similarity between sequences compared.

16S identification	rRNA gene	S _{ab} score	Isolates no.	Gram stain (+/-)	Cell morphology
<i>Desulfovibrio piger</i>		≥ 0.96	1-10,16-21	-	rod
<i>Veillonella tobetsuensis</i>		≥ 0.98	12,22-25*	+	cocci
<i>Veillonella parvula</i>		≥ 0.97	13-15,25*,26	+	cocci
<i>Veillonella</i> spp.		1	28	+	cocci

*isolate 25 has been identified as both *Veillonella tobetsuensis* and *Veillonella parvula*

6.3.2 Primer designs and qPCR method development

Designing dsrB qPCR primers

To develop a method of quantifying human SRB using qPCR, the coding nucleotide sequence of *dsrB* genes from various SRB species that have been identified in the human gut microbiota from relevant literature (Loubinoux *et al.* 2002, Carbonero *et al.* 2012, Jia *et al.* 2012, Nava *et al.* 2012, Rey *et al.* 2013) were collected from the NCBI database (NCBI 2017). Sequences from *Desulfovibrio* NY682 (EU294503.1), *Desulfovibrio* sp. 6_1_46AFAA (ACWM01000066.1), *Desulfovibrio piger* (ABXU01000058.1), *Desulfovibrio desulfuricans* (CAC09931.1), *Desulfovibrio intestinalis* (BAB55572.1), *Desulfovibrio vulgaris* Hildenborough (U16723.1) were aligned for the design of human_desulfov qPCR primer set (to amplify human *Desulfovibrio* spp.). An addition of *Desulfobacter vibrioformis* (CAB95043.1), *Desulfotomaculum kuznetsovii* (CAC36145.1), *Desulfobulbus rhabdoformis* (CAB95039.1) were also used for the design of dsrB_Human qPCR primer set for the amplification of a wider range of human SRB (Figure 6.2). Based on the alignment, sequences used for Human_Desulfov primer set were F: 5' TGCGACATCGCCGACAA 3', R: 5' CGCACATGTTKATGCAGC 3'. For dsrB_Human primer sets, the sequences F: 5' TGCGAYATYGCBGACAA 3' and R: 5' RCACATGTTBAKGCAGCA 3' were used.

ABXU010000 :	GACATCCC	CGAACTGT	GGGACAT	CGCCGACAA	AGTACT	GCCGCG	CGTTAC	CTCCGCT	GGACC	:	288	
U16723.1 D :	GACATCCC	CGAGATGT	GGGACAT	CGCCGACAA	AGTACT	GCCGCG	CGTTAC	CTCCGCT	GGACC	:	288	
EU294503.1 :	GATATCCG	TGAGTTGT	GGGACAT	CGCCGACAA	AGTACT	GCCGCG	CGCTAT	CTCCGTT	GGACC	:	288	
CAC09931.1 :	CTGATCCG	TGAACTGT	GGGACAT	CGCCGACAA	AGTACT	GCCGCG	CGCTAC	CTCCGTT	GGACC	:	288	
BAB55572.1 :	CTGATCCG	TGAACTGT	GGGACAT	CGCCGACAA	AGTATT	GCCAA	CGCTGT	CTCCGTT	GGACC	:	288	
ACWMD10000 :	GACATCCG	TGAGCTGT	GGGACAT	CGCCGACAA	AGTACT	GCCGCG	CGCTAT	CTCCGCT	GGACC	:	288	
CAB95043.1 :	GACATCAAT	GAAATCT	GGGATATT	GGCGACAA	ACATTG	CCGAC	CGGTAT	CTCCGTT	CGACC	:	288	
CAB95039.1 :	CGTGTAC	GTATAT	TGGCATAT	CGCTGACAA	ATGCT	GCCG	CGTTT	CTCCGTT	CGACC	:	273	
CAC36145.1 :	CACGTGCC	GAAATCT	GGGATATT	GGCGACAA	ATACT	GCCGCG	CGCTAT	GTCCGCT	TCACC	:	297	
ABXU010000 :	ACCCCGA	CAACAT	CGAGTT	CATGGT	CGAAGA	CGAAG	ACACCA	TGAAG	CCCT	CGCC	CC :	348
U16723.1 D :	ACCCGTAA	CAACGT	CGAATT	CATGGT	CGCCGA	CGAG	CTAGCC	TCAAG	CCCT	GAAG	GA :	348
EU294503.1 :	ACCCGTAA	CAACATT	GAATTC	CATGGT	CGACGAC	GAAC	CCACCA	TGAAG	CCCT	CGCG	CA :	348
CAC09931.1 :	ACCCGTAA	CAACATT	GAATTC	CATGGT	CGACGAC	GAAC	CCGCA	TGAAG	CCCT	CGCG	CA :	348
BAB55572.1 :	ACCCGTAA	CAACATT	GAATTC	CATGGT	CGACGAC	GAAG	GGCA	TGAAG	CCCT	CGCG	CA :	348
ACWMD10000 :	ACCCGTAA	CAATAT	CGAATT	CATGGT	CGACGAC	GAAC	CCACCA	TGAAG	CCCT	CGCG	CA :	348
CAB95043.1 :	ACCCGTAA	CAACATT	GAATTC	CATGGT	TGATTCA	AAG	CAATAA	AGTAG	AGC	TTT	GAAGA :	348
CAB95039.1 :	ACCCGTAA	CAACGT	AGAGTT	CATGT	GCGAC	AGTGA	GAA	GGTCT	TGCT	CACT	GAAC :	333
CAC36145.1 :	ACCCCGAA	CAACAT	CGAGTT	TATCGT	CGACAG	CTTG	GAAAG	TGGAA	CCCT	CAAGA	AG :	357
ABXU010000 :	GAGCTCAA	AGCCG	AAGTTC	GACGGCG	CTTCT	TCAAG	TCCCG	CTCGG	CGG	ACCG	CC :	408
U16723.1 D :	GACCTCGC	AGCCG	AAGTTC	GACGGCG	CTCGT	CAAG	TCCCG	ATCGG	CGG	ACCG	CC :	408
EU294503.1 :	GACCTGAA	CTCCG	AAGTTC	CCCGGG	CGCTCT	CAAG	TCCCG	CTCGG	CGG	ACCG	CC :	408
CAC09931.1 :	GACCTGAA	CTCCG	AAGTTC	GACGGCG	CTCGT	TCAAG	TCCCG	CTCGG	CGG	ACCG	CC :	408
BAB55572.1 :	GACTTGAA	CTCCG	AAGTTC	GACGGCG	CTCGT	TCAAG	TCCCG	CTCGG	CGG	ACCG	CC :	408
ACWMD10000 :	GACCTGAA	CTCCG	AAGTTC	CCCGGG	CGCTCT	CAAG	TCCCG	CTCGG	CGG	ACCG	CC :	408
CAB95043.1 :	GATCTGG	CTTCA	CAAG	TTCCCT	GTCT	CGTT	CGTT	CAAG	TCCCG	ATCGG	TA :	408
CAB95039.1 :	GAGCTCGC	AAACCA	AA-----	CGAG-----	ACCT	GCCCA	TCTG	CTT	ACCG	CT	GG :	378
CAC36145.1 :	GATCTGT	GGAG	CCG	CAATTT	TGTTT	CCGG	GAG	CTA	CAAG	TCCCG	ATCGG :	417
ABXU010000 :	GCCCGT	GTCA	GCAAC	ATGGT	TCAC	ACCC	AGGG	CTGGG	TCA	CTGCC	ACAC :	468
U16723.1 D :	GCTGCCG	TGCA	CAAC	ATCGTT	TCAC	ACCC	CAGG	CTGGG	TCA	CTGCC	ACAC :	468
EU294503.1 :	GCCTGCG	TCGCA	CAAC	ATGAT	TCAC	ACCC	CAGG	CTGGG	TCA	CTGCC	ACAC :	468
CAC09931.1 :	GCCGCA	TGCA	CAAC	ATGGT	TCAC	ACCC	AGGG	CTGGG	TCA	CTGCC	ACAC :	468
BAB55572.1 :	GCTGCA	TGCA	CAAC	ATGGT	TCAC	ACCC	CAGG	CTGGG	TCA	CTGCC	ACAC :	468
ACWMD10000 :	GCCTGCG	TCGCA	CAAC	ATGAT	TCAC	ACCC	CAGG	CTGGG	TCA	CTGCC	ACAC :	468
CAB95043.1 :	GCCGAT	TC	CAAT	ATCGTT	TCAC	ACCC	CAGG	CTGGT	TCA	CTGCC	ACAC :	468
CAB95039.1 :	GCTTGT	TA	CAAC	ATCGTT	TCAT	ACCC	CAGG	CTGGG	TCA	CTGCC	ATAC :	438
CAC36145.1 :	GCCAGCA	TCA	CAAT	ATCGT	TCAC	ACCC	CAGG	CTACG	TCA	CTGCC	ACAC :	477
ABXU010000 :	GACGCT	TCCG	CCCCG	TCAAAT	GCCT	CAT	GGAC	CCCAT	GTT	CGAG	CACT :	528
U16723.1 D :	GACGCT	TCCG	CCCCG	TCAAAT	GCCT	CAT	GGAC	CGAAG	CTTT	CGAG	CACT :	528
EU294503.1 :	GACGCT	TCCG	CCCCG	TCAAAT	GCCT	CAT	GGAC	CCCT	GTT	CGAG	CACT :	528
CAC09931.1 :	GACGCT	TCCG	CCCCG	TCAAAT	GCCT	CAT	GGAC	CTTT	GTT	GAG	CACT :	528
BAB55572.1 :	GACGCT	TCT	GGCC	CGTCAA	AGGCT	GT	GAT	GGAC	CCCT	GTT	CGAG :	528
ACWMD10000 :	GACGCT	TCCG	CCCCG	TCAAAT	GCCT	CAT	GGAC	CCCT	GTT	CGAG	CACT :	528
CAB95043.1 :	GATGCT	TCCG	TA	CTG	AAA	GGT	CAC	CA	GGC	CTGTT	GAT :	528
CAB95039.1 :	GACGCT	TCCG	CCCCG	TCAAAT	GCCT	CAT	GGAC	CCCT	GTT	CGAG	CACT :	498
CAC36145.1 :	GACGCT	TCT	CCCT	GGTCAA	AGGCG	T	CAT	GGAT	CA	CTGTT	GACT :	537
ABXU010000 :	CGCCT	GCC	CGG	CCCGT	CGCAT	CT	CCCT	GCC	CTGCT	GCAT	CAAC :	588
U16723.1 D :	CGCCT	GCC	CGT	CCG	GTCC	CT	CCCT	GCC	CTGCT	GCAT	CAAC :	588
EU294503.1 :	CGCAT	GCC	CGAC	CCCGT	CGCGT	GT	CCCT	GCC	CTGCT	GCAT	CAAC :	588
CAC09931.1 :	CGTCT	GCC	CGCC	CCCGT	CGCAT	AG	CCCT	GCC	ATGCT	GCAT	CAAC :	588
BAB55572.1 :	CGTAT	GCC	CGCT	CCCGT	CGCAT	AG	CCCT	GCC	CTGCT	GCAT	CAAC :	588
ACWMD10000 :	CGCAT	GCC	CGG	CCCGT	CGCGT	GT	CCCT	GCC	CTGCT	GCAT	CAAC :	588
CAB95043.1 :	AAAAT	GCC	CGCC	AGCT	CCCT	CTT	CCAT	GCC	ATGCT	GCAT	CAAC :	588
CAB95039.1 :	ACCT	GCT	GC	AG	GT	AG	GT	AT	CG	CT	GG :	558
CAC36145.1 :	ACCT	GCC	CGCA	AG	GT	AG	GG	GT	GG	CT	GCT :	597

Figure 6.2 The *dsrB* gene sequence alignment for the design of qPCR primer sets for Human_*desulfiovibrio* (using the top 6 gene sequences) and *dsrB*_Human (using all gene sequences). Colouring of letters indicates degree of nucleotide conservation between sequences (black, 100%, dark grey, 80%; light grey, 60%). Location for alignment used for the design of primers were marked (green, forward primer; red, reverse primer) for both primer sets.

Design of dsrB primer

To test the quantitative efficiency of the SYBR green-based qPCR primers and to allow absolute quantification using qPCR, primers (named dsrB primer) were designed to amplify the *dsrB* gene. The amplicon of dsrB primer sets are designed to flank the alignment region used in the Human_desulfov or dsrB_Human qPCR primer sets, so the PCR product (amplified by dsrB primer sets) can be used as a DNA template (with known copy numbers of *dsrB* gene) to perform qPCR standard curve for future SRB quantification. The dsrB primers were designed from the dsrB sequence obtained from a human gut *D. piger* UC15 (Wegmann *et al.* 2017) using Primer3 (Koressaar and Remm 2007, Untergasser *et al.* 2012) and searched against the Human dsrB (Figure 6.2 above) to determine which primers had the best matching sequence to other members of human SRB. OligoCalc (Kibbe 2007) was used to check the properties and minimise the occurrence of the hairpin formation, 3' complementary and self-annealing site on the prospective primer sequences before dsrB_F1, dsrB_F2, and dsrB_R1 were designed (Figure 6.3).

```

5' ATGGCTTTTATTTCTTCCGGGTACAATCCCGCCAAACCGATGGAAGGCCGCATTACCGACATCGGCCCCACAAGTACG
ACGAATACTTCCCGCCGGTCATCAAAAAGAATTTTCGGCAAGTGGCTGTACCACGAAATTTCTGAGCCCGCGGTGCTGATGC
ACGTGGCCGAAGGCCGGCACAAGGTGTACACCGTCCGCGTGGGCGGCACCCGCACCATGTCCATCACCCACATCCGCGAGA
TCTGCGACATCGCCGACAAAGTACTGCGCGGCTACCTGCGCTGGACCACCCGTAACAACATCGAGTTCATGGTGAAGACG
AAGCCACCATGAAGGCCCTGCGCGACGACCTGAACAGCCGAAGTTCGACGGCGGTTCCCTCAAGTTCCCCGTGGGCGGCA
CCGGCGCCGGCATCAGCAACATGGTGCACACCCAGGGCTGGGTGCACTGCCACACCCCGCCACCGACGCCTCCGGCCCGG
TGAAATGCGTGATGGACGCCATCTTTGACGACTTCAAGGACATGCGTCTGCCCGCTCCCGTGGCGATCGCCCTGGCCTGCT
GCATCAACATGTGCGGGCGCCGTGCACTGCTCCGACATCGGCCTGGTGGGCATCCACCGCAAACCGCCCATGATCGACCACG
AATGGGCCGACCAGCTGTGCGAAATCCCGCTGGCCGTGGCCGCTGCCCCACCGCTGCCGTCCGTCACCAAGGTGGAAC
ACAACGGCCAGAAGGTGAACTCCATCGCCATCAAGGAAGACCGCTGCATGTACTGCGGCAACTGCTACACCATGTGCCCGG
CCCTGCCCATCGCCGACCACGAAGGCCGACGGCATCGCCATCATGGTGGGCGGCAAGGTGTCCAACCGCATCAGCATGCCCA
AGTTCTCCAAGGTGGTCTGTTGGGCTACATCCCCAACGAACCTCCCCGCTGGCCAGCCTGACCAAGACGGTGAAGCACATCG
TCGAAGTCTACGCCGCCAACGCCAACAGTACGAACGTCTGGGCGACTGGGCCGAACGCATCGGCTGGGAAAGCTTCTTCA
AGCTGACCGGCCTGAAGTTCACCCACCACCTCATCGACGACTTCCGCGACCCGGCGTACTACACCTGGCGCCAGAGCACCC
AGTTCAAGTTCTAG 3'

```

Figure 6.3 The *dsrB* gene sequence for the design of PCR primers from *D. piger* UC15 of human gut origin. Colouring of letters indicate the location of dsrB primer sequences. Grey, dsrB_F1; yellow, dsrB_F2; blue, dsrB_R1. Letters in bold indicate the relative location (but not the sequence of) Human_desulfov and dsrB_Human qPCR primers.

Various PCR conditions including different elongation durations, annealing temperatures and numbers of cycles were tested for the two dsrB primer combinations and optimised for each SRB species/isolate. As the dsrB sequence of the Gram negative isolates differed to those in *D. piger* UC15, we optimised the PCR conditions used in *D. piger* UC15 and the presumptive human gut *D. piger* isolates (see Section 2.7.1).

To produce DNA templates of *dsrB* gene with known copy numbers, gDNA of SRB were used for *dsrB* gene amplification. Primer set *dsrB_F1* and *dsrB_R1* produced more specific PCR products when amplifying *D. piger* UC15 and presumptive *D. piger* (isolate 6 and 19) compared to primer set *dsrB_F2* with *dsrB_R1*. Visible bands of PCR products using gDNA of SRB were present at the expected band size of 911 bp using *dsrB_F1* and *dsrB_R1* primers, indicating that *dsrB* gene of *D. piger* UC15, isolate 6 and 19 were successfully amplified (Figure 6.4). The resulting PCR products were quantified and their copy numbers adjusted to 10^{10} copies, before they were 10-fold serial diluted (10^0 - 10^{10} copies) and used as DNA templates for qPCR standard curves.

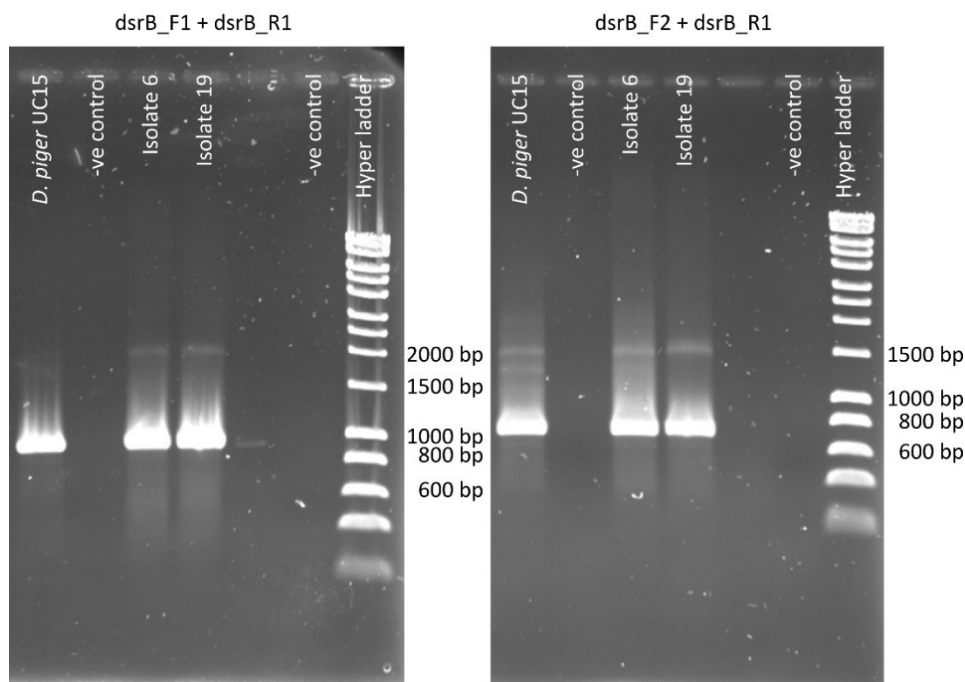


Figure 6.4 Gel electrophoresis of PCR products using gDNA of SRB. Successful amplification was achieved with *D. piger* UC15 and presumptive *D. piger* isolates 6 and 19. PCR products from *dsrB_F1* and *dsrB_R1* primer sets were preferred and used as DNA template for qPCR standard curves. Primer sets a) *dsrB_F1* with *dsrB_R1*; and b) *dsrB_F1* with *dsrB_R1* were used, showing expected band sizes of 911 bp and 719 bp respectively. HyperLadder 1 (Bioline) was used to reference DNA band size.

qPCR standard curve

To determine whether the qPCR primers can accurately quantify SRB, standard curves were performed in triplicates to evaluate the efficiency of the qPCR primers in quantifying SRB (Figure 6.5). It was shown that *D. piger* UC15, isolate 6 and isolate 19 had efficiency of 98.7%, 101.3% and 103.3% respectively, which is within the acceptable efficiency range of between 90-110%. The R^2 value of the slopes are 0.9936, 0.9957 and 0.9954 respectively, indicating good linearity of the PCR assay (≥ 0.985 is acceptable). This qPCR standard curve can be used in future quantification of human SRB.

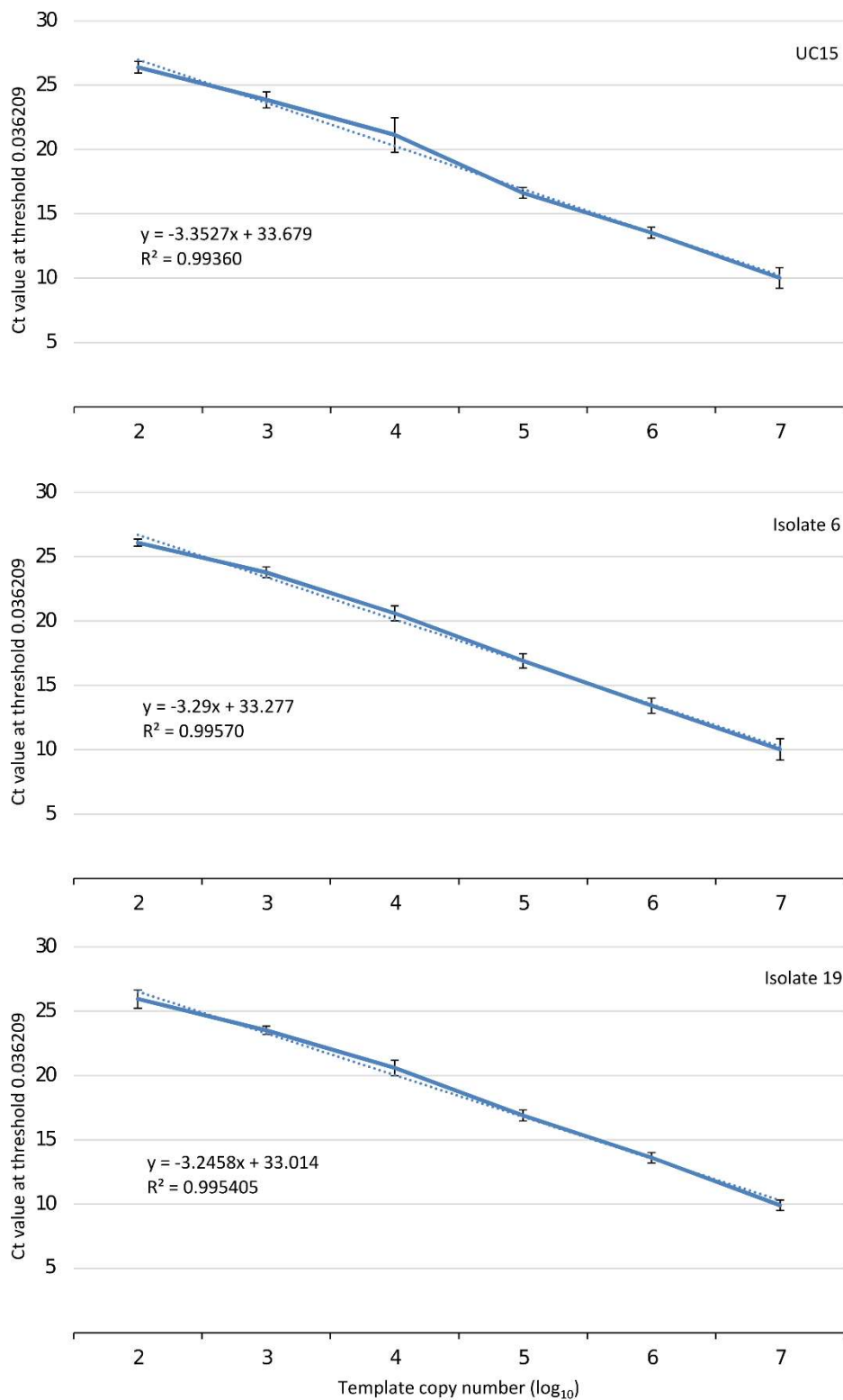


Figure 6.5 qPCR standard curves for *D. piger* UC15, presumptive *D. piger* isolate 6 and isolate 19 using Human_desulfov qPCR primers sets. Strong linear correlation was obtained for absolute quantification of SRB. Means of 3 technical replicates were measured with 3 biological replicates in each experiment \pm SD.

Differentiation of distinct *dsrB* genes between human isolates

To confirm whether the isolated colonies contained the *dsrB* genes, 16S rRNA gene colony PCR was performed to amplify the *dsrB* gene using Human_desulfov and *dsrB*_Human primer sets. All the presumptive *D. piger* isolates were amplified by both *dsrB*_Human and Human_desulfov primers. Comparing amplification of *D. piger* UC15 and presumptive *D. piger* isolates, Human_desulfov primer set produced a single PCR product of the expected size; whereas with *dsrB*_Human primer set, non-specific amplification was also present (Figure 6.6). The presumptive *V. tobetsuensis* and *V. parvula* isolates were not amplified at the expected size (336 bp) by either primer set despite testing them under various experimental conditions. The presence of *dsrB* genes in these isolates was not detected by primers designed from known *dsrB* alignments of SRB, despite the presence of FeS when culturing on Postgate Medium C, indicating H₂S production (Bernardez and de Andrade Lima 2015).

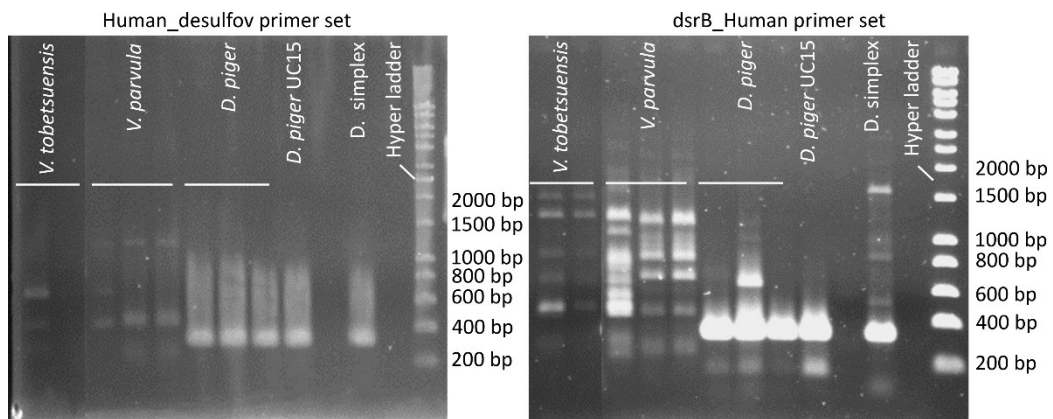


Figure 6.6 PCR amplification using left, Human_desulfov primer set; and right, *dsrB*_Human primer set. Isolates identified as *D. piger* were successfully amplified at 336 bp while isolates identified as *V. tobetsuensis* and *V. parvula* were not. *D. piger* UC15 and *D. simplex* were used as a positive control. HyperLadder 1 (Bioline) was used to reference DNA band size.

To compare the *dsrB* sequence of the Human SRB isolates, *dsrB*_F1 and *dsrB*_R1 primers were used and showed that the human presumptive *D. piger* isolates shared very similar *dsrB* nucleotide sequences from the PCR amplicon and were divided into 2 groups (group 1: isolates 1, 19 and 20; group 2: isolates 4, 6, 8, 10). Two nucleotide differences were observed in *dsrB* genes between the two groups (Figure 6.7), suggesting that they may present 2 different strains of SRB. Also, the qPCR primers sequence human_desulfov matched the *dsrB* gene amplicon from all isolates, indicating that the qPCR primer sequence would amplify these isolates when performing qPCR.

```

iso8 : ~~~~~GCCGGTCATCAAAAAGAAATTTGCGCAAGTGGCTGTACACCGA : 42
iso4 : ~~~~~TTCCC GCCGGTCATCAAAAAGAAATTTGCGCAAGTGGCTGTACACCGA : 47
iso6 : GTACGACGAATACTTCCC GCCGGTCATCAAAAAGAAATTTGCGCAAGTGGCTGTACACCGA : 60
iso10 : ~~~~~GCCGGTCATCAAAAAGAAATTTGCGCAAGTGGCTGTACACCGA : 42
iso20 : ~~~~~GCCGGTCATCAAAAAGAAATTTGCGCAAGTGGCTGTACACCGA : 42
iso19 : ~~~~~ACTTCCC GCCGGTCATCAAAAAGAAATTTGCGCAAGTGGCTGTACACCGA : 49
iso1 : ~~~~~GCCGGTCATCAAAAAGAAATTTGCGCAAGTGGCTGTACACCGA : 42

iso8 : AAATTCCTTGAGCCCCGGCGTGCTGATGCACGTGGCCGAAGGCGGCGACAAGGTGTACACCGT : 102
iso4 : AAATTCCTTGAGCCCCGGCGTGCTGATGCACGTGGCCGAAGGCGGCGACAAGGTGTACACCGT : 107
iso6 : AAATTCCTTGAGCCCCGGCGTGCTGATGCACGTGGCCGAAGGCGGCGACAAGGTGTACACCGT : 120
iso10 : AAATTCCTTGAGCCCCGGCGTGCTGATGCACGTGGCCGAAGGCGGCGACAAGGTGTACACCGT : 102
iso20 : AAATTCCTTGAGCCCCGGCGTGCTGATGCACGTGGCCGAAGGCGGCGACAAGGTGTACACCGT : 102
iso19 : AAATTCCTTGAGCCCCGGCGTGCTGATGCACGTGGCCGAAGGCGGCGACAAGGTGTACACCGT : 109
iso1 : AAATTCCTTGAGCCCCGGCGTGCTGATGCACGTGGCCGAAGGCGGCGACAAGGTGTACACCGT : 102

iso8 : CCGCGTGGGCGGCACCCGCACCATGTCCATCACCCACATCCGCGAACTGTGCGACATCGC : 162
iso4 : CCGCGTGGGCGGCACCCGCACCATGTCCATCACCCACATCCGCGAACTGTGCGACATCGC : 167
iso6 : CCGCGTGGGCGGCACCCGCACCATGTCCATCACCCACATCCGCGAACTGTGCGACATCGC : 180
iso10 : CCGCGTGGGCGGCACCCGCACCATGTCCATCACCCACATCCGCGAACTGTGCGACATCGC : 162
iso20 : CCGCGTGGGCGGCACCCGCACCATGTCCATCACCCACATCCGCGAACTGTGCGACATCGC : 162
iso19 : CCGCGTGGGCGGCACCCGCACCATGTCCATCACCCACATCCGCGAACTGTGCGACATCGC : 169
iso1 : CCGCGTGGGCGGCACCCGCACCATGTCCATCACCCACATCCGCGAACTGTGCGACATCGC : 162

iso8 : CGACAAATACTGCGGGCGTTACCTGCGCTGGACCACTCGTAACAACATCGAATTCATGGT : 222
iso4 : CGACAAATACTGCGGGCGTTACCTGCGCTGGACCACTCGTAACAACATCGAATTCATGGT : 227
iso6 : CGACAAATACTGCGGGCGTTACCTGCGCTGGACCACTCGTAACAACATCGAATTCATGGT : 240
iso10 : CGACAAATACTGCGGGCGTTACCTGCGCTGGACCACTCGTAACAACATCGAATTCATGGT : 222
iso20 : CGACAAATACTGCGGGCGTTACCTGCGCTGGACCACTCGTAACAACATCGAATTCATGGT : 222
iso19 : CGACAAATACTGCGGGCGTTACCTGCGCTGGACCACTCGTAACAACATCGAATTCATGGT : 229
iso1 : CGACAAATACTGCGGGCGTTACCTGCGCTGGACCACTCGTAACAACATCGAATTCATGGT : 222

iso8 : GGAAGACGAAGAAACCATGAAGGCCCTGCGCGACGACCTGAACAGCCGCAAGTTCGACGG : 282
iso4 : GGAAGACGAAGAAACCATGAAGGCCCTGCGCGACGACCTGAACAGCCGCAAGTTCGACGG : 287
iso6 : GGAAGACGAAGAAACCATGAAGGCCCTGCGCGACGACCTGAACAGCCGCAAGTTCGACGG : 300
iso10 : GGAAGACGAAGAAACCATGAAGGCCCTGCGCGACGACCTGAACAGCCGCAAGTTCGACGG : 282
iso20 : GGAAGACGAAGAAACCATGAAGGCCCTGCGCGACGACCTGAACAGCCGCAAGTTCGACGG : 282
iso19 : GGAAGACGAAGAAACCATGAAGGCCCTGCGCGACGACCTGAACAGCCGCAAGTTCGACGG : 289
iso1 : GGAAGACGAAGAAACCATGAAGGCCCTGCGCGACGACCTGAACAGCCGCAAGTTCGACGG : 282

iso8 : CGGTTCTTCAAGTTCCTCCCGTGGGCGGCACCGGCGCTGGTATCAGCAACATGGTGCAAC : 342
iso4 : CGGTTCTTCAAGTTCCTCCCGTGGGCGGCACCGGCGCTGGTATCAGCAACATGGTGCAAC : 347
iso6 : CGGTTCTTCAAGTTCCTCCCGTGGGCGGCACCGGCGCTGGTATCAGCAACATGGTGCAAC : 360
iso10 : CGGTTCTTCAAGTTCCTCCCGTGGGCGGCACCGGCGCTGGTATCAGCAACATGGTGCAAC : 342
iso20 : CGGTTCTTCAAGTTCCTCCCGTGGGCGGCACCGGCGCTGGTATCAGCAACATGGTGCAAC : 342
iso19 : CGGTTCTTCAAGTTCCTCCCGTGGGCGGCACCGGCGCTGGTATCAGCAACATGGTGCAAC : 349
iso1 : CGGTTCTTCAAGTTCCTCCCGTGGGCGGCACCGGCGCTGGTATCAGCAACATGGTGCAAC : 342

iso8 : CCAGGGCTGGGTGCACTGCCACACCCCCGCCACCGACGCCTCCGGCCCCGGTGAAGTGCCT : 402
iso4 : CCAGGGCTGGGTGCACTGCCACACCCCCGCCACCGACGCCTCCGGCCCCGGTGAAGTGCCT : 407
iso6 : CCAGGGCTGGGTGCACTGCCACACCCCCGCCACCGACGCCTCCGGCCCCGGTGAAGTGCCT : 420
iso10 : CCAGGGCTGGGTGCACTGCCACACCCCCGCCACCGACGCCTCCGGCCCCGGTGAAGTGCCT : 402
iso20 : CCAGGGCTGGGTGCACTGCCACACCCCCGCCACCGACGCCTCCGGCCCCGGTGAAGTGCCT : 402
iso19 : CCAGGGCTGGGTGCACTGCCACACCCCCGCCACCGACGCCTCCGGCCCCGGTGAAGTGCCT : 409
iso1 : CCAGGGCTGGGTGCACTGCCACACCCCCGCCACCGACGCCTCCGGCCCCGGTGAAGTGCCT : 402

iso8 : GATGGACGCCATCTTTGATGACTTCAAGGACATGCGTCTGCCCGCTCCCGTGCGCATCGC : 462
iso4 : GATGGACGCCATCTTTGATGACTTCAAGGACATGCGTCTGCCCGCTCCCGTGCGCATCGC : 467
iso6 : GATGGACGCCATCTTTGATGACTTCAAGGACATGCGTCTGCCCGCTCCCGTGCGCATCGC : 480
iso10 : GATGGACGCCATCTTTGATGACTTCAAGGACATGCGTCTGCCCGCTCCCGTGCGCATCGC : 462
iso20 : GATGGACGCCATCTTTGATGACTTCAAGGACATGCGTCTGCCCGCTCCCGTGCGCATCGC : 462
iso19 : GATGGACGCCATCTTTGATGACTTCAAGGACATGCGTCTGCCCGCTCCCGTGCGCATCGC : 469
iso1 : GATGGACGCCATCTTTGATGACTTCAAGGACATGCGTCTGCCCGCTCCCGTGCGCATCGC : 462

iso8 : CCTGGCCTGCTGCATCAACATGTGCGGGCCCGTGCACTGCTCCGACATCGGTCTGGTGGG : 522
iso4 : CCTGGCCTGCTGCATCAACATGTGCGGGCCCGTGCACTGCTCCGACATCGGTCTGGTGGG : 527
iso6 : CCTGGCCTGCTGCATCAACATGTGCGGGCCCGTGCACTGCTCCGACATCGGTCTGGTGGG : 540
iso10 : CCTGGCCTGCTGCATCAACATGTGCGGGCCCGTGCACTGCTCCGACATCGGTCTGGTGGG : 522
iso20 : CCTGGCCTGCTGCATCAACATGTGCGGGCCCGTGCACTGCTCCGACATCGGTCTGGTGGG : 522
iso19 : CCTGGCCTGCTGCATCAACATGTGCGGGCCCGTGCACTGCTCCGACATCGGTCTGGTGGG : 529
iso1 : CCTGGCCTGCTGCATCAACATGTGCGGGCCCGTGCACTGCTCCGACATCGGTCTGGTGGG : 522

```

Figure 6.7 Alignment of a) nucleotide sequences of Gram negative human gut isolates amplified by *dsrB_F1* and *dsrB_R1* primers. Colouring of letters indicates the degree of nucleotide conservation between sequences (black: 100%, dark grey, 80%; light grey, 60%), the marked region indicates the location of *Human_desulfov* and *dsrB_Human* primers. Green, forward primers; red, reverse primers.

The translated amino acid sequence of the 2 groups (using isolate 6 and isolate 19 as representatives) were compared and no differences were observed, indicating the differences were due to codon degeneracy and did not affect the protein (Figure 6.8). The amino acid sequences were searched on blastp (Altschul *et al.* 1997) and were identified as sulphite reductase, a dissimilatory-type beta subunit from *D. piger* (accession WP_040369683.1) with 100% sequence match. Isolates 6 and 19 were sent off for whole genome sequencing for future projects.

```

iso6      : YDEYFPPVIKKNFGKWLYHEILEPGVLMHVAEGGDKVYTVRVGGTRTMSITHIRELCDIA : 60
iso19     : ~~~~~FPPVIKKNFGKWLYHEILEPGVLMHVAEGGDKVYTVRVGGTRTMSITHIRELCDIA : 56

iso6      : DKYCGGYLRWTTTRNIEFMVEDEETMKALRDDLSNRKFDGGSFKFPVGGTGAGISNMVHT : 120
iso19     : DKYCGGYLRWTTTRNIEFMVEDEETMKALRDDLSNRKFDGGSFKFPVGGTGAGISNMVHT : 116

iso6      : QGVVHCHTPATDASGPVKCVMDAIFDDFKDMRLPAPVRIALACCINMCGAVHCSDIGLVG : 180
iso19     : QGVVHCHTPATDASGPVKCVMDAIFDDFKDMRLPAPVRIALACCINMCGAVHCSDIGLVG : 176

iso6      : IHRKPPMIDHEWADQLCEIPLAVAACPTAAVRPTKVEHNGQKVNSIAIKEDRCMYCGNCY : 240
iso19     : IHRKPPMIDHEWADQLCEIPLAVAACPTAAVRPTKVEHNGQKVNSIAIKEDRCMYCGNCY : 236

iso6      : TMCALPIADHEGDGIAIMVGGK : 263
iso19     : TMCALPIADHEGDGIAIMVGGK : 259

```

Figure 6.8 Alignment of translated amino acid sequence of group 1 and group 2 from PCR products amplified by *dsrB_F1* and *dsrB_R1* primers, showing that isolate 6 (representing isolate group 2) and isolate 19 (representing isolate group 1) have the same amino acid sequence in the *dsrB* PCR amplicon. Colouring of letters indicates the degree of nucleotide conservation between sequences (black: 100%, dark grey, 80%; light grey, 60%).

6.3.3 Designing TFD for SRB

To target SRB, a literature search was performed to identify non-redundant genes critical for SRBs' survival under stress conditions. Homologous regulatory components were described among the phylogenetically diverse deltaproteobacteria class which SRB are a member of, ferric-uptake regulator protein (FUR) (Rodionov *et al.* 2004), NrfR (Rajeev *et al.* 2015) and RpoN/ σ^{54} (Price *et al.* 2011) transcription factors were identified as possible TFD targets. To ensure TFD targeting will work against SRB of human gut origin, the locations of genes regulated by these transcription factors were determined from the annotated output of the *D. piger* UC15 genome. -400 bp upstream promoter sequences were selected on Artemis relative to translational start sites of the targeting gene and searched for sequences similar to the predicted binding site sequence motifs shown in Figure 6.9 a and bi. The critical consensus nucleotides of the σ^{54} -dependent promoter *nifH* (Guo and Gralla 1998) with strong binding was also taken into account in the design of the RNA polymerase σ^{54} (RNAP54) TFD (Figure 6.9 b ii). FUR TFD was designed based on predicted palindromic consensus sites GATAATGATnATCATTATC from other *Desulfovibrio* spp. (Rodionov *et al.* 2004). As the transcription factor binding site sequence of FUR

targeting genes in the *D. piger* UC15 genome was not definitive, Softberry BPROM prediction of bacterial promoters (Solovyev and Salamov 2011) and EMBOSS palindrome search (Rice *et al.* 2000) were used to aid the design of TFD. The designed TFD sequences of RNAP54.1, nrfR and FUR TFD and their scrambled TFD sequences are listed in Table 6.2.

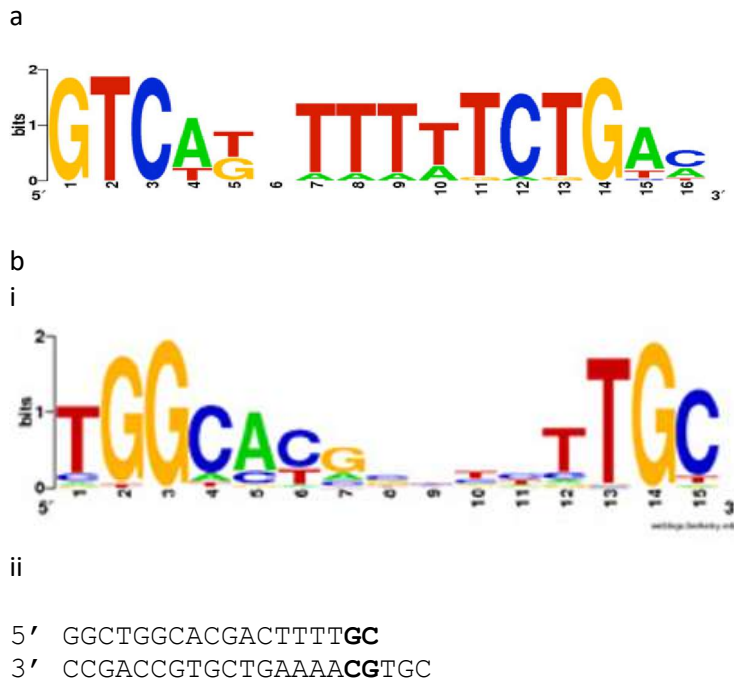


Figure 6.9 Predicted consensus binding site motif for a) NrfR TFD based on upstream regions of *nrfHA* orthologs in *Desulfovibrio* and *Bilophila* genomes (WebLogo taken from Rajeev *et al.* (2015)); b) RNAP54.1 TFD based on i) RpoN (σ^{54}) for alternative *Desulfovibrio* sigma factor 54 (WebLogo taken from Price *et al.* (2011)); ii) DNA fork junction, bold nucleotides indicate critical consensus nucleotides of the sigma 54-dependent promoter *nifH* with strong binding to σ^{54} isolated protein (Guo and Gralla 1998). The height of the nucleotide shown in the sequence logo of each motif is proportional to the information content in bits (Crooks *et al.* 2004).

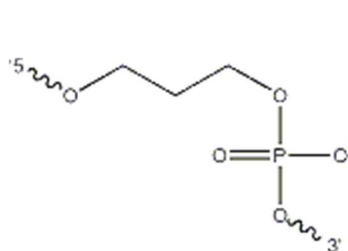
Table 6.2 a) TFD sequences designed to target SRB. Functional and scrambled sequences (including linker and modifications) were included to investigate the sequence-specific antimicrobial activity. Structures of b) internal C3 Spacer (iSpC3); and c) internal dSpacer (iSpPC). TFD sequences were ordered from Integrated DNA Technologies.

a

TFD Sequence Name	Sequence
RNAP54.1	5' C*G*T GCA /iSpC3/T*G*C
Scrambled RNAP54.1	5' G*T*C AGC /iSpC3/G*C*T
nrfR TFD	5' A*A*C AGA AAA TAA CGA T/iSpPC/AT CGT TAT TTT CTG* T*T
Scrambled nrfR TFD	5' A*G*A CTA AAA GAA ATA C/iSpPC/GT ATT TCT TTT AGT* C*T
Fur TFD	5' G*A*A AAT GAT TTT C/iSpPC/GA AAA TCA TTT* T*C
Scrambled Fur TFD	5' A*T*T ATA GTC AAG T/iSpPC/AC TTG ACT ATA* A*T

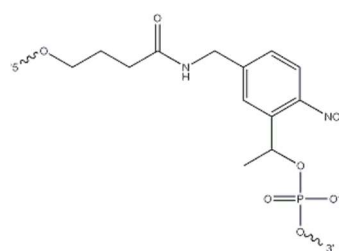
* indicates phosphorothioate bond

b



iSpC3: Internal C3 Spacer

c



iSpPC: Internal dSpacer

6.3.4 Minimum inhibitory concentrations of SRB against TFDs

To test the antimicrobial activity of the designed TFDs, minimum inhibitory concentration (MIC) assays were performed on SRB. The samples were incubated for 48 h inside the anaerobic cabinet to allow sufficient growth for MIC experiments. For method development, preventive measures to avoid sample evaporation were in place, including sealing the assay plates with paraffin, then wrapping in plastic bags before storing within a sealed plastic container.

Different LNPs containing either RNAP54.1, FUR or nrfR TFD were tested against *D. piger* UC15, isolate 6 and *D. vulgaris*. In each technical replicate, three biological replicates were tested for SLNP (with scrambled TFD sequence) and LNP treatments (Figure 6.10). The averaged MIC data showed that TFD-specific antimicrobial activity in LNP was not observed with all three TFDs. TFD-specific antimicrobial activity was only shown in 2 out of 3 biological replicates in an individual

experiment, where LNP with FUR TFD had a 2-fold less MIC value than the ENP and SLNP controls against *D. piger* UC15. This suggests some activity originated from the delivery particles but no TFD-associated activity was observed. A larger amount of LNP is required to inhibit *D. vulgaris* compared to *D. piger* UC15 and presumptive *D. piger* isolate 6, implying that *D. vulgaris* is more difficult for NPs to target than *D. piger*.

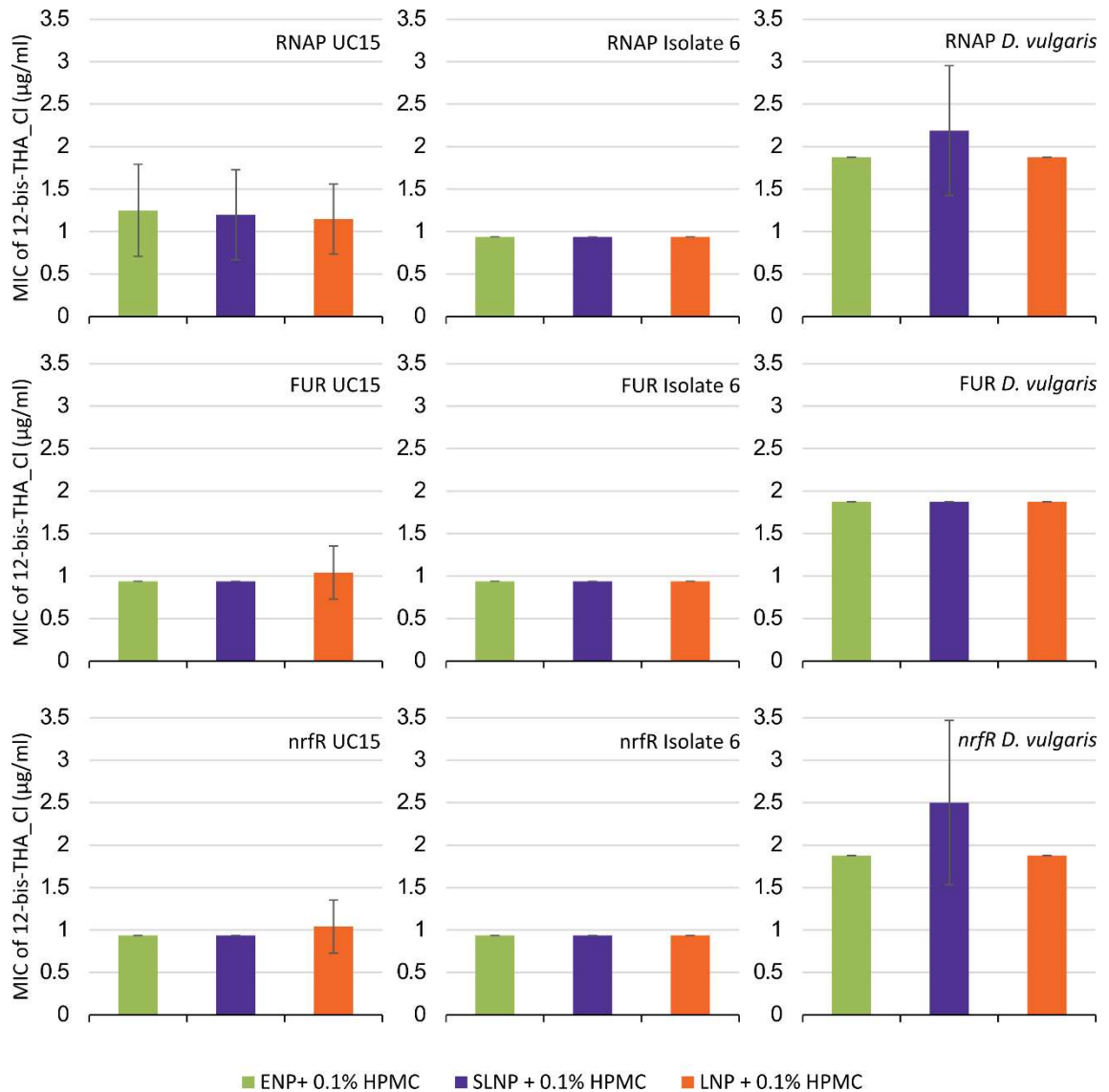


Figure 6.10 Minimum inhibitory concentration of *D. piger* UC15, presumptive *D. piger* isolate 6 and *D. vulgaris*. No TFD-specific antimicrobial activity was observed from LNP compared to ENP and SLNP for all 3 TFD tested. MIC values are means of three technical replicates with three biological replicates in each experiment \pm SD. ENP: empty nanoparticles; SLNP: scrambled loaded nanoparticles; LNP: loaded nanoparticles.

6.3.5 Confocal microscopy to visualise the delivery of TFD in *D. piper*

To investigate whether LNP can successfully deliver TFD to SRB, confocal scanning microscopy was performed. Different cell membrane fluorescent dyes including TMR-WGA, DiD, Mitotracker Deep Red FM and FM464-FX were tested for their ability to stain SRB, FM464 FX was the best in visualising the cell wall of the human SRB isolates and was used for cell membrane fluorescence staining hereafter.

Several isolates representing group 1 and 2 with 16S rRNA gene sequence similarities to *D. piper* (group A and group B) were tested with the usual incubation time of 30 min, but no internalisation was observed in SRB or the positive control *E. coli*. Repeat attempts of increasing 1) incubation time of bacteria with fluorescent TFD-loaded NP, 2) incubation of fluorescent TFD-loaded NP and bacteria with the addition of membrane dye, and 3) the duration of the bacteria and fluorescent TFD-loaded NP mixture were adhered to the confocal microscopy slides before rinsing have been carried out. This showed that these batches of NP required incubation of *E. coli* positive control with fluorescent TFD in LNP for 90 min with 1 h attachment on the confocal slide to visualise successful internalisation and suggests that these batches of delivery NPs required a longer incubation period for TFD-internalisation. Under these conditions, TFD incorporation within most SRB isolates was not seen, TFDs were gathered on the outside of the bacterial cell wall with no clear internalisation observed (Figure 6.11 a and b). However, internalisation was seen in isolate 19 (Figure 6.11 c). TFDs observed within presumptive *D. piper* isolate 19 appeared to attach to the bacterial membrane in spherical structures, even when successfully visualised within the cytoplasm. SRB transfection was rare compared to *E. coli* as only one isolate 19 bacterial cell showed TFD incorporation out of 20 fields of view on 1 out of 4 slides, suggesting *D. piper* may be a more difficult target for LNPs to deliver TFD. This low transfection rate may relate to the lack of positive TFD-specific MIC data.

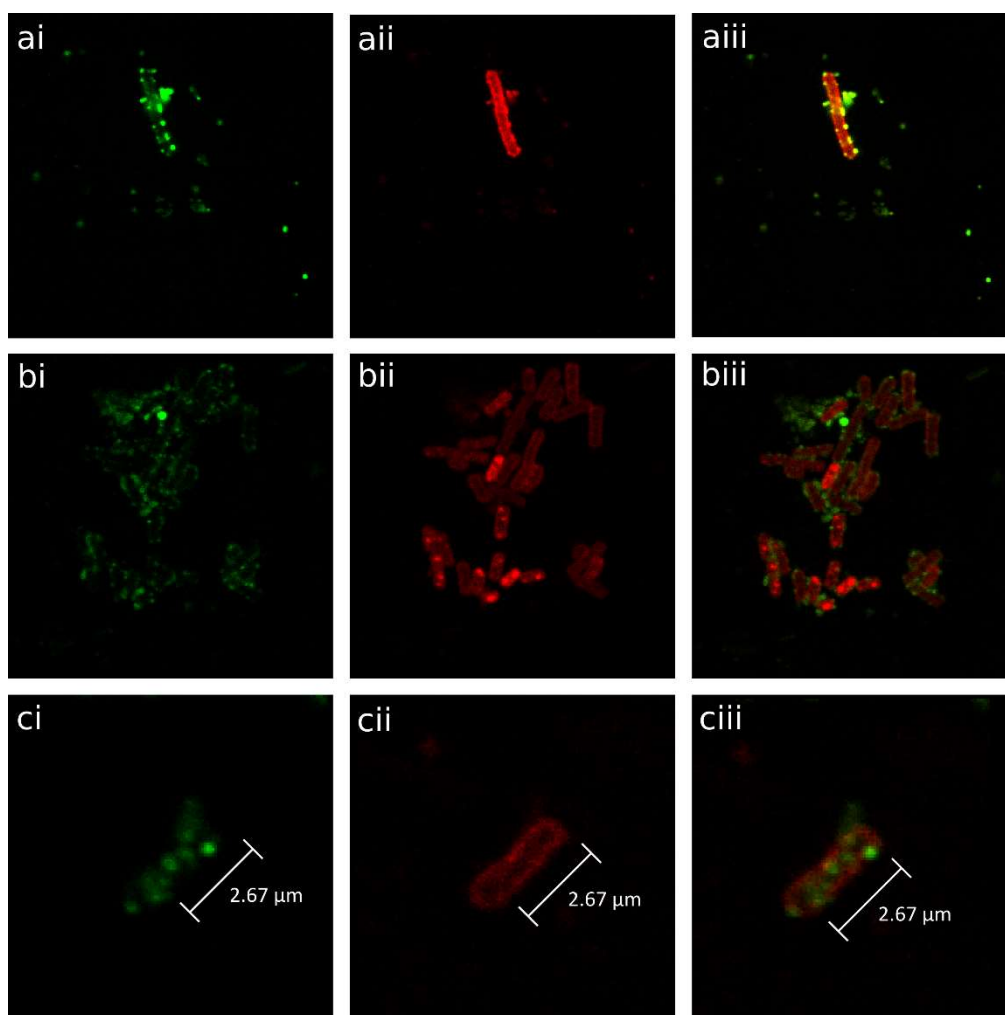


Figure 6.11 Representative confocal scanning microscopy images of Gram negative presumptive *D. piger* isolates. 60 min of LNP incubation of a) isolate 6; and b) isolate 17; c) 120 min of LNP incubation of isolate 19. TFD delivery was observed after prolonged LNP incubation after 120 min. Red: SRB cell wall; Green: TFD. i) green channel; ii) red channel; iii) red and green channel overlay.

6.4 Discussion

Isolation of novel SRB strains

Novel strains of human gut SRB were isolated from human faecal samples, the presence of *dsrB* genes was confirmed in the Gram negative isolates (with $\geq 96\%$ similarities with *D. piger*) showing similar *dsrB* gene sequences to known human SRB from the literature. The genomic DNA of two Gram negative SRB isolates with unique *dsrB* sequences was sequenced and can be used to evaluate the selectivity of SRB TFD for future TFD refinement. In contrast, even though sulfide production was observed in culturing experiments, the Gram positive isolates (with $\geq 98\%$ similarities with *Veillonella* spp.) did not give a product of expected size with *dsrB* primers. There could be differences in nucleotide sequence or codon usage in the *dsrB* gene typical in human gut

SRB. It was found that a strain that belongs to the *Veillonellaceae* family was identified as sulphite reducer and can produce sulphide by utilising sulphite and organic sulphur compounds like cysteine (Feng *et al.* 2017). The Gram-positive sulphide-producing isolates in this study may adopt similar reactions to obtain sulphide.

dsrB primers designed for qPCR may be useful for SRB quantification

To design an accurate quantification method for human gut SRB, several primers were designed and qPCR standard curves were established for future SRB quantification in human gut samples to evaluate TFD activity. Although dissimilatory sulphite reductase primers based on environmental samples e.g. marine/ soil origin were widely investigated (Leloup *et al.* 2007, Bae *et al.* 2015, Pelikan *et al.* 2015), these primers tailored to SRB of human gut origin remained largely unexplored. The design of dsrB primer sets that amplified human gut SRB/ *Desulfovibrio* spp. and demonstration of successful standard curves showed that these primers can be a useful resource to allow future quantification of human gut SRB.

Identification of transcription factor targets

To target human gut SRB, potential TFD targets against transcription factors FUR, nrfR and RNA polymerase σ^{54} were identified in the human gut *D. piger* UC15 genome, and were explored as a proof of principle study to impair SRB growth for TFD development.

Overall MIC data indicated an absence of TFD-specific antimicrobial activity among all 3 TFDs tested against *D. piger* UC15 and two other presumptive *D. piger* (isolates 6 and 19). Although some TFD-specific antimicrobial activity was observed in the first MIC experiment with FUR TFD against *D. piger* UC15, showing a 2-fold decrease in MIC compared to ENP and SLNP in 2 out of 3 biological replicates. There could be handling variation when the NPs were prepared by different people, leading to discrepancies in the results. As SRB are obligate anaerobes, every effort has been made to prevent the introduction of oxygen into the samples, the MIC plates were therefore not shaken during the experimental incubation period. LNP are likely to settle within the 48 h period and reduce the full potential of LNP antimicrobial activity, as LNP were less likely to be readily in contact with the bacteria in the culture. As the availability of iron can affect the antimicrobial potential of FUR TFD, the inhibition of iron metabolism may not be critical to SRB growth (Rodionov *et al.* 2004) if iron was not limiting in the anaerobic experimental setting, the addition of iron chelator may be needed to confirm this speculation.

SRB may be a more difficult target for TFD delivery

Combining the biological activity with the confocal microscopy data, results suggested that TFD delivery within SRB by 12-bis-THA was inefficient compared to *E. coli*. Longer LNP incubation was required for TFD internalisation in *E. coli* (as a positive control) and SRB, suggesting the batches of 12-bis-THA may be unstable or have lower delivery capacity, which could lead to less efficient TFD delivery. Although TFD fluorescence was observed in one bacterial cell in isolate 19, TFD fluorescence was presented as separate particle structures within the bacteria, which differs to the diffused TFDs signal observed within the *E. coli* cell (Chapter 4 Section 4.3.1).

Marin-Menendez *et al.* (2017) proposed the TFD delivery could be a 2-step process, 1) LNP interacts with bacterial membrane, indicated as green puncta amongst the red fluorescent-labelled cell wall on the confocal images; and 2) TFD are released within the cell cytoplasm. Interestingly, the green Alexa-488 fluorescent signal was observed to be diffused within the cytoplasm of *E. coli* and *C. difficile*. This diffused TFD phenomenon was not observed in SRB, on the contrary, the LNPs appeared as individual spherical structures following the entry of TFD within the cytoplasm, it may suggest that the TFD signal was internalised but yet to be diffused. As confocal microscopy only takes a snapshot of the bacterial sample, increased LNP dosage and extensive time course experiments may be required to determine the optimal transfection time for *D. pigr*.

On the whole, this may suggest that the cell wall structure of SRB may differ to those in *E. coli* and may be more difficult to gain entry within the cytoplasm. There may also be differences in the bacterial membrane structure of SRB compared to *E. coli* as we also saw reduced antimicrobial activity against *Pseudomonas aeruginosa* (Chapter 4 Section 4.3.3) which also have distinct cell wall structures compared to other Gram negative bacteria. Cardiolipin, a phospholipid on the bacterial membrane, was described to have a role in 12-bis-THA delivery (Marin-Menendez *et al.* 2017). The levels of cardiolipin were compared in *Desulfovibrio* spp. and *E. coli* and it was found that the levels of cardiolipin were comparable (5.8% (Makula and Finnerty 1974) and 5% (Garrett *et al.* 2012) by mass respectively) among all the phospholipids present on the bacterial membrane. Although the phospholipid composition of *D. pigr* is not yet described in the literature, cardiolipin synthase protein was present from *D. pigr* (NCBI 2017), suggesting that the lack of TFD delivery is unlikely due to absence of cardiolipin. To improve TFD delivery, TFD-conjugates can be utilised instead of LNP (Zhao *et al.* 2015), as they have smaller chemical structures compared to LNPs and may gain better entry to the bacterial membrane.

A prebiotic has shown specific modulation of gut microbiota by reducing *Desulfovibrio* spp., while reducing inflammation and increasing concentration of SCFA in the caecum in a mouse model (Sawin *et al.* 2015). Herbal saponins also demonstrated SRB reduction while enhancing beneficial bacteria and lessen the inflammatory phenotype as part of colorectal cancer prevention (Chen *et al.* 2016), indicating the potential benefit of SRB reduction. However, none have thus far specifically 'knocked out' SRB, thus the TFD approach remains a valuable tool for the direct study of disease association to further understand the role SRB perform in health and disease.

In conclusion, novel strains of human gut SRB were isolated and used for TFD testing. Although we could not identify the presence of *dsrB* gene in the presumptive *Veillonella* spp., they may have a different *dsrB* sequence that cannot be detected by our primer sets. We have found potential TFD targets that are predicted to be critical for SRB growth in stress conditions. However, antimicrobial activity was not demonstrated and this is likely due to low delivery efficiency by the delivery nanoparticles within the bacteria. TFD-conjugates may be a better system for future delivery of TFD targeting SRB.

General discussion

Chapter 7

Chapter 7: General discussion

The overall aim of the thesis was to determine whether nanoparticles loaded (LNPs) with transcription factor decoys (TFDs) are suitable for development as antimicrobials capable of altering the microbiome in a predictable manner. The work in this thesis established that LNPs have *in vitro* antimicrobial activity in pure cultures and also have effects on the gut microbiota community composition, diversity and metabonomic output when introduced in an *in vitro* batch fermentation model. These results formed the basis of an *in vivo* mouse model study which consolidated the findings from *in vitro* studies and further investigated the effects LNPs have on the host.

7.1. The use of TFD in LNP as target-specific antimicrobials

7.1.1 Can TFD specifically target organisms of interest?

In chapter 4, it was demonstrated via confocal scanning microscopy that TFDs can be incorporated within the cytoplasm of *E. coli*, indicating successful TFD delivery within *E. coli* cells. Chapter 3 established that the preferred hairpin TFD structure was stable against *in vitro* nuclease degradation for up to 6 h. The best LNP formulation against *E. coli* was identified by MIC assays, where TFD-specific activity was demonstrated in LNPs with 0.1% HPMC in the formulation, which decreased the MIC by ≥ 2 -fold compared to the empty nanoparticles (ENPs) and scrambled load nanoparticles (SLNPs). This LNP formulation was utilised for *E. coli*-related experiments thereafter. The optimal LNP dose was established by a dosing study in batch culture fermentations, which demonstrated TFD specificity in reducing *Enterobacteriaceae* viable bacterial communities from gut microbiota of multiple donors. The degree of antimicrobial activity against *Enterobacteriaceae* was found to be dependent on the starting *Enterobacteriaceae* levels upon the addition of treatment. No correlation was drawn with the starting total anaerobe community and TFD activity, thus indicating the TFD antimicrobial capacity is associated with levels of *Enterobacteriaceae* and not total anaerobes. *Enterobacteriaceae* reduction was also demonstrated by bacterial 16S rRNA gene community sequencing, indicating both culturable and non-culturable *Enterobacteriaceae* were targeted by TFD.

7.1.2 Does TFD targeting interrupt the commensal gut microbiota community *in vitro*?

LNP did not lead to major changes in the bacterial counts of the total anaerobes, *Bacteroides*, *Bifidobacterium*, *Clostridium*, and *Lactobacillus* in the *in vitro* batch culture fermentation experiments, while still demonstrating antimicrobial activity against *Enterobacteriaceae*. Non-specific antimicrobial activity from LNPs against anaerobes was only observed when a high dose was used (i.e. 30x higher than the usual 2% dose used in the batch culture fermentation), suggesting the LNP doses used in batch culture fermentation generally do not interrupt the commensal gut microbiota community.

16S rRNA gene community sequencing indicated that when *Enterobacteriaceae* was reduced with LNPs, bacterial diversity remained similar to the controls, suggesting LNPs did not interrupt other bacteria communities while reducing *Enterobacteriaceae*. From principal coordinates analysis, the gut microbiota structure in samples treated with LNPs more closely resembled the controls at previous time points, possibly indicating LNPs work by slowing down the dynamic changes in the gut microbiota to maintain stability. This was confirmed by metabonomic data showing LNP treatment delayed bacterial growth in the batch culture fermentation experiment with a declined usage of substrates for metabolic pathways. SLNPs induced shifts in the gut microbiota abundance at later time points, suggesting the delivery system could interfere with the gut microbiota composition regardless of the selectivity of TFD.

As other *Enterobacteria*-targeting antibiotics generally have side effects of decreased bacterial cell count, reduced abundance of anaerobes and declined bacterial diversity (Langdon *et al.* 2016), this suggests that TFD antimicrobials may be a better alternative to antibiotics as they reduced disruption to the gut microbiota and maintained microbiota diversity.

7.1.3 Can TFD antimicrobial activity be demonstrated *in vivo*?

After the *in vitro* antimicrobial assays of LNPs against *Enterobacteriaceae* were established (Chapter 4), we investigated whether the same effects can be observed in an *in vivo* setting. A wild type mouse model was utilised to evaluate the changes to the gut microbiota and the host upon LNP treatment, and LNP's TFD-specific activity against *Enterobacteriaceae* was again observed indicating the antimicrobial response was dose dependant (Chapter 5). The 16S rRNA

gene-based community analysis revealed the mouse gut microbiota consisted largely of unculturable organisms. The reduction in *Enterobacteriaceae* was observed despite this group making up only a tiny proportion of the total bacterial community. Non-TFD specific changes in LNP and SLNP include the reduction of the *S24-7* family in the Bacteroidales order, suggesting that the delivering NP may adversely affect this community. Decrease of *S24-7* has also been observed in a pathogen-selective treatment (Yao *et al.* 2016), indicating *S24-7* may be sensitive to other changes in the microbiota. The overall diversity remained constant despite TFD activity though changes in abundance were seen in some groups of bacteria.

7.1.4 Can LNP be used to target sulphate reducing bacteria?

Following the validation of TFD selective antimicrobial activity against *Enterobacteriaceae* using *in vitro* and *in vivo* systems, it was interesting to investigate whether TFDs can be designed to target SRB. After successful targeting of a well defined phylogenetic group we investigated whether TFD could be used to target SRB, a phylogenetically diverse group with similar metabolic capabilities.

Several transcription factors including *FUR*, *nrfR* and *RNAP σ 54* have been identified as crucial for SRB survival, and TFDs were designed according to the binding sites in a human gut *D. piger* strain UC15. Other novel strains of SRB were isolated from the human gut and were also used for antimicrobial testing, though no TFD-specific activity from LNP was observed compared to ENP and SLNP controls. The lack of TFD-specific antimicrobial activity was suspected to be due to reduced TFD delivery by the NP delivery system, as was evident in confocal scanning microscopy experiment. Batch to batch variation in 12-bis-THA occurred, leading to delayed delivery in *E. coli* positive control and this may have reduced the efficacy of delivery. Viable bacterial counts suggested LNP may not have reduced *Pseudomonas aeruginosa* in batch culture fermentation (Chapter 4), as they have different cell wall structure and this may affect LNP delivering TFD. Confocal scanning microscopy suggested SRB may also be a more difficult bacterial targets to deliver TFD using the current LNP system. A method of SRB quantification using qPCR were also established for future SRB detection in a complex human gut community. More method development needs to be performed to fully investigate LNP's therapeutic potential against SRB, including utilising a different formulation e.g. TFD-conjugates in the view to improve TFD delivery.

7.2 Future Research

7.2.1 Extensive LNP dosing range studies

In this thesis, it has been demonstrated both by viable culturing and non-culturing 16S rRNA gene community profiling that TFD can successfully and selectively reduce *Enterobacteriaceae* levels. However, ENP and/or SLNP had some antimicrobial capacity of their own, as was observed in MIC experiments (Chapter 3). Though not apparent from viable counts, non-target specific effects on the 16S rRNA gene community analysis were observed in the SLNP control in the *in vitro* (Chapter 4) and *in vivo* studies (Chapter 5), indicating the delivery system is not functionally inert and may induce shifts in the gut microbiota.

The effective antimicrobial dose of TFD was established in chapter 4, however, there is still a knowledge gap of the minimum LNPs needed to have specific activity without a broad spectrum effect on the gut microbiota. The dose dependent response needs to be fine-tuned for effective antimicrobial activity.

We expect the LNP effective dose to be affected by the total number of bacteria. However, it was interesting that there was instead a strong link between the LNP effective dose and the starting *Enterobacteriaceae* levels in both dosing range and batch culture fermentation experiments. This may suggest that the LNP efficiency is related only to the targeted bacterial group, regardless of the total bacterial community, making TFD a desirable tool for fine tuning the reduction of specific organisms for microbiome engineering without using excessive amounts of starting materials.

7.2.2 Alternative delivery system for TFD

It has been established that TFD can exert target-specific antimicrobial activity. However, the delivery nanoparticles themselves appeared to cause non-specific changes to the gut microbiota when the community structure was explored using 16S rRNA gene sequencing. Batch-to-batch NP variation led to difference in stability, along with NP handling difference between individuals, could lead to variation in nanoparticles' efficiency to deliver TFD. As there is a maximum amount of TFD that can be loaded, the current formulation of LNPs is limited to ensure proper complexation of LNPs; a large excess of 12-bis-THA was used compared to TFD which makes the TFD specific response less evident, as it was dampened by the 12-bis-THA side effects. TFD therapeutics in the form of LNPs therefore may not be the perfect system, factors that contribute

to LNP delivery can be further investigated to better exploit the mechanism to exert the full therapeutic potential of TFD antimicrobials.

To minimise the non-specific effects of 12-bis-THA, TFD-conjugates, which is a single compound connecting 12-bis-THA and TFD in 1:1 ratio, can be developed as an alternative system for TFD delivery (Zhao *et al.* 2015), they will allow increase amounts of TFD delivered per 12-bis-THA molecule, hence improving the therapeutic potential of TFD and minimising side effects related to 12-bis-THA.

7.2.3 Improving understanding of TFD mechanisms

As FNR activity is controlled by the repeated assembly and disassembly of iron-sulfur cluster (Khoroshilova *et al.* 1997), iron is required for the functionality of the gene regulation and survival of *Enterobacteriaceae*. The availability of iron may affect the impact of FNR reduction. It would also be interesting to explore how FNR repression affect cellular processes, it may be informative to perform batch culture fermentation experiments with and without iron or iron chelators to investigate how this affects antimicrobial activity.

7.2.4 Determining which bacteria LNP can transfect in the gut microbiota

Whether LNPs bind to all bacteria equally or have stronger affinity to certain bacteria remains to be tested. It would be interesting to determine which bacteria LNP can penetrate using FACS, to establish the range of bacterial interactions and identify other possible bacterial targets for the design of new TFDs. It would be useful to gain insight into the process of LNP interacting with bacterial cells before becoming internalised and reaching their TFD-specific target, and in turn expand our understanding and exploit the mechanisms to improve antimicrobial activity.

7.2.5 Incorporating qPCR for Enterobacteriaceae quantification

Metagenomic analysis showed that a large proportion of non-culturable bacteria were detected in mice gut microbiota in high abundance, while *Enterobacteriaceae* abundance was low. This meant it was difficult to confidently show TFD-specific antimicrobial activity by 16S rRNA gene community profiling. The incorporation of quantitative data using qPCR to detect *E. coli* and

anaerobes would be a valuable addition to confirm the decrease in *Enterobacteriaceae* or other communities.

7.2.6 Studying LNPs effect in a disease model

As a proof of principle, wild type mice were used to assess LNP antimicrobial activity, to establish the baseline effect LNPs have on a native gut microbiota and to elucidate possible side effects on the host. As the LNP antimicrobial response is quite rapid and exerted this effect within a few hours of gavage administration, the faecal samples were collected within short time intervals to assess the fast-acting antimicrobial activity, unlike other therapeutic studies which measure the effects at least a day after the drug administration (Rebello *et al.* 2015). It would be important to see if the system worked when higher quantities of *Enterobacteriaceae* were present e.g. in an infection scenario, as it was established that TFD may not diminish all *Enterobacteriaceae* at high abundances.

After establishing the baseline effects LNPs have on a wild type model using the improved TFD-conjugate delivery system, their effects can be studied on a model with predisposed microbiota alterations (Spees *et al.* 2013), enriched with *Enterobacteriaceae* (Savkovic *et al.* 2005, Winter *et al.* 2013) or a DSS-induced colitis (Huang *et al.* 2015). These studies would provide extra information on whether LNPs could help counteract the shifts in gut microbiota and improve prognosis of disease phenotypes. A study that monitors the gut microbiota in the mice pre- and post- diseased state could also be evaluated and ascertain whether alterations in the gut microbiota will recover after a period of time.

7.2.7 Improving understanding of host response upon LNP treatment

The gut microbiota composition and metabonomic profile between mice were variable within and between treatment groups at the start of the experiments, making it difficult to draw definitive conclusions on the effects of LNPs. Evaluation of the host response in the mouse model may have been enhanced by investigating the effects on the liver tissues to determine whether systemic toxicity is present. Also performing caspase staining on intestinal tissue for the detection of apoptosis (Kaushal *et al.* 2014) may have been useful to confirm any cellular damage in the epithelium.

7.2.8 Choice of TFD targets

It is important to choose a robust TFD target. It has to be specific to a selected organism or group without largely disrupting the commensal gut microbiota. Using metabolic genes (Matsui *et al.* 2013) as TFD targets allow us to target a larger range of organisms that may not necessarily be phylogenetically related (Korner *et al.* 2003) but perform similar functions e.g. sulphate reduction (Rabus *et al.* 2015).

After establishing the improved method of TFD delivery, it would be useful to confirm that SRB TFDs are good genomic targets for human gut SRBs. Whole genome analysis can be performed to confirm the TFD matching similarity to the transcription binding sites for genes of interest. Also, promoter reporter assays could be performed to confirm transcription factor inhibition by TFD. H₂S levels can be evaluated to quantify sulphite reducing functions in SRB after TFD treatment. These may help reinforce TFD's specificity in targeting human gut SRBs.

Other new TFD targets to move the technology forward would be to down-regulate virulence gene expression instead of killing the bacteria itself. Biological knowledge can be used to identify new TFD targets to decrease virulence in pathogens e.g. by preventing them from inducing attachment to the intestinal epithelial cell (Sule *et al.* 2017).

7.3 Conclusion

The TFD technology could be a good alternative to antibiotics in improving selectivity in bacterial targets and reducing disruption of the diversity of the commensal bacteria in complex microbial communities such as the gut microbiome, once side effects on host are understood. This technology establishes currently unmet needs, which demonstrates its potential in targeting any bespoke bacterial-associated condition that require a target-specific approach.

TFD reduced the levels of *Enterobacteriaceae* without major disturbance to the commensal bacterial diversity, and antimicrobial activity was also observed in an *in vivo* mouse model. Encountering variations in the degree of antimicrobial activity in different microbiotas highlighted the difficulty of targeting a specific organism in a diverse and complex microbiota. Also care has to be taken to ensure the dose is sufficient to provide the desired antimicrobial output. Some non-selective bacterial shifts in the 16S rRNA gene community were observed in SLNP treatment, along with its possible cytotoxic nature to eukaryotic cells, reduction in the 12-bis-THA: TFD ratio for TFD delivery would be the next step to move forward for future TFD-based antimicrobial research to improve the target selectivity and stability of the antimicrobial.

The designed TFDs for SRB can be the basis of new product development once TFD delivery is achieved. Further optimisation will be needed to transfect SRB to establish TFD's potential in targeting this phylogenetically diverse but functionally analogous bacteria.

References

References

- Agarwal, S. and R. S. Murthy (2015). "Effect of Different Polymer Concentration on Drug Release Rate and Physicochemical Properties of Mucoadhesive Gastroretentive Tablets." Indian J Pharm Sci **77**(6): 705-714.
- Altschul, S. F., T. L. Madden, A. A. Schaffer, J. Zhang, Z. Zhang, W. Miller and D. J. Lipman (1997). "Gapped BLAST and PSI-BLAST: a new generation of protein database search programs." Nucleic Acids Res **25**(17): 3389-3402.
- Amako, K., Y. Meno and A. Takade (1988). "Fine structures of the capsules of *Klebsiella pneumoniae* and *Escherichia coli* K1." J Bacteriol **170**(10): 4960-4962.
- Antunes, L. C. and B. B. Finlay (2011). "A comparative analysis of the effect of antibiotic treatment and enteric infection on intestinal homeostasis." Gut Microbes **2**(2): 105-108.
- Apprill, A., S. McNally, R. Parsons and L. Weber (2015). "Minor revision to V4 region SSU rRNA 806R gene primer greatly increases detection of SAR11 bacterioplankton." Aquatic Microbial Ecology **75**(2): 129-137.
- Arantes-Rodrigues, R., A. Henriques, R. Pinto-Leite, A. Faustino-Rocha, J. Pinho-Oliveira, C. Teixeira-Guedes, F. Seixas, A. Gama, B. Colaco, A. Colaco and P. A. Oliveira (2012). "The effects of repeated oral gavage on the health of male CD-1 mice." Lab Anim (NY) **41**(5): 129-134.
- Arias-Cartin, R., S. Grimaldi, P. Arnoux, B. Guigliarelli and A. Magalon (2012). "Cardiolipin binding in bacterial respiratory complexes: structural and functional implications." Biochim Biophys Acta **1817**(10): 1937-1949.
- Aron-Wisnewsky, J., J. Dore and K. Clement (2012). "The importance of the gut microbiota after bariatric surgery." Nat Rev Gastroenterol Hepatol **9**(10): 590-598.
- Arumugam, M., J. Raes, E. Pelletier, D. Le Paslier, T. Yamada, D. R. Mende, G. R. Fernandes, J. Tap, T. Bruls, J. M. Batto, M. Bertalan, N. Borruel, F. Casellas, L. Fernandez, L. Gautier, T. Hansen, M. Hattori, T. Hayashi, M. Kleerebezem, K. Kurokawa, M. Leclerc, F. Levenez, C. Manichanh, H. B. Nielsen, T. Nielsen, N. Pons, J. Poulain, J. Qin, T. Sicheritz-Ponten, S. Tims, D. Torrents, E. Ugarte, E. G. Zoetendal, J. Wang, F. Guarner, O. Pedersen, W. M. de Vos, S. Brunak, J. Dore, M. Antolin, F. Artiguenave, H. M. Blottiere, M. Almeida, C. Brechot, C. Cara, C. Chervaux, A. Cultrone, C. Delorme, G. Denariatz, R. Dervyn, K. U. Foerstner, C. Friss, M. van de Guchte, E. Guedon, F. Haimet, W. Huber, J. van Hylckama-Vlieg, A. Jamet, C. Juste, G. Kaci, J. Knol, O. Lakhdari, S. Layec, K. Le Roux, E. Maguin, A. Merieux, R. Melo Minardi, C. M'Rini, J. Muller, R. Oozeer, J. Parkhill, P. Renault, M. Rescigno, N. Sanchez, S. Sunagawa, A. Torrejon, K. Turner, G. Vandemeulebrouck, E. Varela, Y. Winogradsky, G. Zeller, J. Weissenbach, S. D. Ehrlich and P. Bork (2011). "Enterotypes of the human gut microbiome." Nature **473**(7346): 174-180.
- Attene-Ramos, M. S., G. M. Nava, M. G. Muellner, E. D. Wagner, M. J. Plewa and H. R. Gaskins (2010). "DNA damage and toxicogenomic analyses of hydrogen sulfide in human intestinal epithelial FHs 74 Int cells." Environ Mol Mutagen **51**(4): 304-314.
- Attene-Ramos, M. S., E. D. Wagner, H. R. Gaskins and M. J. Plewa (2007). "Hydrogen sulfide induces direct radical-associated DNA damage." Mol Cancer Res **5**(5): 455-459.
- Avendano-Perez, G., C. Nueno-Palop, A. Narbad, S. M. George, J. Baranyi and C. Pin (2015). "Interactions of *Salmonella* enterica subspecies enterica serovar Typhimurium with gut bacteria." Anaerobe **33**: 90-97.
- Backhed, F., H. Ding, T. Wang, L. V. Hooper, G. Y. Koh, A. Nagy, C. F. Semenkovich and J. I. Gordon (2004). "The gut microbiota as an environmental factor that regulates fat storage." Proc Natl Acad Sci U S A **101**(44): 15718-15723.

- Bae, H. S., M. E. Holmes, J. P. Chanton, K. R. Reddy and A. Ogram (2015). "Distribution, activities, and interactions of methanogens and sulfate-reducing prokaryotes in the Florida Everglades." Appl Environ Microbiol **81**(21): 7431-7442.
- Baker, G. C., J. J. Smith and D. A. Cowan (2003). "Review and re-analysis of domain-specific 16S primers." J Microbiol Methods **55**(3): 541-555.
- Bakker, G. J. and M. Nieuwdorp (2017). "Fecal Microbiota Transplantation: Therapeutic Potential for a Multitude of Diseases beyond *Clostridium difficile*." Microbiol Spectr **5**(4).
- Balletto, E. and M. Mikulska (2015). "Bacterial Infections in Hematopoietic Stem Cell Transplant Recipients." Mediterr J Hematol Infect Dis **7**(1): e2015045.
- Barbieri, N. L., B. Nicholson, A. Hussein, W. Cai, Y. M. Wannemuehler, G. Dell'Anna, C. M. Logue, F. Horn, L. K. Nolan and G. Li (2014). "FNR regulates expression of important virulence factors contributing to pathogenicity of uropathogenic *Escherichia coli*." Infect Immun **82**(12): 5086-5098.
- Barrangou, R. and J.-P. van Pijkeren (2016). "Exploiting CRISPR–Cas immune systems for genome editing in bacteria." Current Opinion in Biotechnology **37**(Supplement C): 61-68.
- Baskar, R., L. Li and P. K. Moore (2007). "Hydrogen sulfide-induces DNA damage and changes in apoptotic gene expression in human lung fibroblast cells." Faseb j **21**(1): 247-255.
- Basri, D. F., L. W. Xian, N. I. Abdul Shukor and J. Latip (2014). "Bacteriostatic antimicrobial combination: antagonistic interaction between epsilon-viniferin and vancomycin against methicillin-resistant *Staphylococcus aureus*." Biomed Res Int **2014**: 461756.
- Becattini, S., Y. Taur and E. G. Pamer (2016). "Antibiotic-Induced Changes in the Intestinal Microbiota and Disease." Trends in Molecular Medicine **22**(6): 458-478.
- Beinert, H. and P. J. Kiley (1999). "Fe-S proteins in sensing and regulatory functions." Curr Opin Chem Biol **3**(2): 152-157.
- Belkaid, Y. and T. W. Hand (2014). "Role of the microbiota in immunity and inflammation." Cell **157**(1): 121-141.
- Bender, K. O., M. Garland, J. A. Ferreyra, A. J. Hryckowian, M. A. Child, A. W. Puri, D. E. Solow-Cordero, S. K. Higginbottom, E. Segal, N. Banaei, A. Shen, J. L. Sonnenburg and M. Bogyo (2015). "A small-molecule antivirulence agent for treating *Clostridium difficile* infection." Sci Transl Med **7**(306): 306ra148.
- Bergin, I. L. and F. A. Witzmann (2013). "Nanoparticle toxicity by the gastrointestinal route: evidence and knowledge gaps." Int J Biomed Nanosci Nanotechnol **3**(1-2).
- Bernardez, L. A. and L. R. de Andrade Lima (2015). "Improved method for enumerating sulfate-reducing bacteria using optical density." MethodsX **2**: 249-255.
- Berry, J. D., M. J. Neeson, R. R. Dagastine, D. Y. Chan and R. F. Tabor (2015). "Measurement of surface and interfacial tension using pendant drop tensiometry." J Colloid Interface Sci **454**: 226-237.
- Beveridge, T. J. (2001). "Use of the gram stain in microbiology." Biotech Histochem **76**(3): 111-118.
- Bibbo, S., G. Ianiro, A. Gasbarrini and G. Cammarota (2017). "Fecal microbiota transplantation: past, present and future perspectives." Minerva Gastroenterol Dietol **63**(4): 420-430.
- Bikard, D., C. W. Euler, W. Jiang, P. M. Nussenzweig, G. W. Goldberg, X. Duportet, V. A. Fischetti and L. A. Marraffini (2014). "Exploiting CRISPR-Cas nucleases to produce sequence-specific antimicrobials." Nat Biotechnol **32**(11): 1146-1150.

Bikard, D., C. Loot, Z. Baharoglu and D. Mazel (2010). "Folded DNA in action: hairpin formation and biological functions in prokaryotes." Microbiol Mol Biol Rev **74**(4): 570-588.

Bode, C., G. Zhao, F. Steinhagen, T. Kinjo and D. M. Klinman (2011). "CpG DNA as a vaccine adjuvant." Expert Rev Vaccines **10**(4): 499-511.

Buffie, C. G., V. Bucci, R. R. Stein, P. T. McKenney, L. Ling, A. Gobourne, D. No, H. Liu, M. Kinnebrew, A. Viale, E. Littmann, M. R. M. van den Brink, R. R. Jenq, Y. Taur, C. Sander, J. R. Cross, N. C. Toussaint, J. B. Xavier and E. G. Pamer (2015). "Precision microbiome reconstitution restores bile acid mediated resistance to *Clostridium difficile*." Nature **517**(7533): 205-208.

Burlatsky, S. F., V. V. Atrazhev, D. V. Dmitriev, V. I. Sultanov, E. N. Timokhina, E. A. Ugolkova, S. Tulyani and A. Vincitore (2013). "Surface tension model for surfactant solutions at the critical micelle concentration." J Colloid Interface Sci **393**: 151-160.

Butlin, K. R., M. E. Adams and M. Thomas (1949). "The isolation and cultivation of sulphate-reducing bacteria." J Gen Microbiol **3**(1): 46-59.

Cammarota, G., L. Masucci, G. Ianaro, S. Bibbo, G. Dinoi, G. Costamagna, M. Sanguinetti and A. Gasbarrini (2015). "Randomised clinical trial: faecal microbiota transplantation by colonoscopy vs. vancomycin for the treatment of recurrent *Clostridium difficile* infection." Aliment Pharmacol Ther **41**(9): 835-843.

Campbell, E. A., N. Korzheva, A. Mustaev, K. Murakami, S. Nair, A. Goldfarb and S. A. Darst (2001). "Structural mechanism for rifampicin inhibition of bacterial rna polymerase." Cell **104**(6): 901-912.

Cani, P. D., J. Amar, M. A. Iglesias, M. Poggi, C. Knauf, D. Bastelica, A. M. Neyrinck, F. Fava, K. M. Tuohy, C. Chabo, A. Waget, E. Delmee, B. Cousin, T. Sulpice, B. Chamontin, J. Ferrieres, J. F. Tanti, G. R. Gibson, L. Casteilla, N. M. Delzenne, M. C. Alessi and R. Burcelin (2007a). "Metabolic endotoxemia initiates obesity and insulin resistance." Diabetes **56**(7): 1761-1772.

Cani, P. D. and N. M. Delzenne (2009). "The role of the gut microbiota in energy metabolism and metabolic disease." Curr Pharm Des **15**(13): 1546-1558.

Cani, P. D., A. M. Neyrinck, F. Fava, C. Knauf, R. G. Burcelin, K. M. Tuohy, G. R. Gibson and N. M. Delzenne (2007b). "Selective increases of bifidobacteria in gut microflora improve high-fat-diet-induced diabetes in mice through a mechanism associated with endotoxaemia." Diabetologia **50**(11): 2374-2383.

Cao, Q., L. Zhang, G. Yang, C. Xu and R. Wang (2010). "Butyrate-stimulated H₂S production in colon cancer cells." Antioxid Redox Signal **12**(9): 1101-1109.

Caporaso, J. G., C. L. Lauber, E. K. Costello, D. Berg-Lyons, A. Gonzalez, J. Stombaugh, D. Knights, P. Gajer, J. Ravel, N. Fierer, J. I. Gordon and R. Knight (2011a). "Moving pictures of the human microbiome." Genome Biol **12**(5): R50.

Caporaso, J. G., C. L. Lauber, W. A. Walters, D. Berg-Lyons, J. Huntley, N. Fierer, S. M. Owens, J. Betley, L. Fraser, M. Bauer, N. Gormley, J. A. Gilbert, G. Smith and R. Knight (2012). "Ultra-high-throughput microbial community analysis on the Illumina HiSeq and MiSeq platforms." ISME J **6**(8): 1621-1624.

Caporaso, J. G., C. L. Lauber, W. A. Walters, D. Berg-Lyons, C. A. Lozupone, P. J. Turnbaugh, N. Fierer and R. Knight (2011b). "Global patterns of 16S rRNA diversity at a depth of millions of sequences per sample." Proc Natl Acad Sci U S A **108** Suppl 1: 4516-4522.

Carabotti, M., A. Scirocco, M. A. Maselli and C. Severi (2015). "The gut-brain axis: interactions between enteric microbiota, central and enteric nervous systems." Annals of Gastroenterology : Quarterly Publication of the Hellenic Society of Gastroenterology **28**(2): 203-209.

Carbonero, F., A. C. Benefiel, A. H. Alizadeh-Ghamsari and H. R. Gaskins (2012). "Microbial pathways in colonic sulfur metabolism and links with health and disease." Front Physiol **3**: 448.

- Cardon, L. R., C. Burge, D. A. Clayton and S. Karlin (1994). "Pervasive CpG suppression in animal mitochondrial genomes." Proc Natl Acad Sci U S A **91**(9): 3799-3803.
- Caroff, M. and D. Karibian (2003). "Structure of bacterial lipopolysaccharides." Carbohydr Res **338**(23): 2431-2447.
- Carroll, I. M., T. Ringel-Kulka, J. P. Siddle and Y. Ringel (2012). "Alterations in composition and diversity of the intestinal microbiota in patients with diarrhea-predominant irritable bowel syndrome." Neurogastroenterol Motil **24**(6): 521-530, e248.
- Chakraborty, T., I. Chakraborty and S. Ghosh (2011). "The methods of determination of critical micellar concentrations of the amphiphilic systems in aqueous medium." Arabian Journal of Chemistry **4**(3): 265-270.
- Chassaing, B., G. Srinivasan, M. A. Delgado, A. N. Young, A. T. Gewirtz and M. Vijay-Kumar (2012). "Fecal lipocalin 2, a sensitive and broadly dynamic non-invasive biomarker for intestinal inflammation." PLoS One **7**(9): e44328.
- Chen, L., M. S. Brar, F. C. Leung and W. L. Hsiao (2016). "Triterpenoid herbal saponins enhance beneficial bacteria, decrease sulfate-reducing bacteria, modulate inflammatory intestinal microenvironment and exert cancer preventive effects in ApcMin/+ mice." Oncotarget **7**(21): 31226-31242.
- Citorik, R. J., M. Mimee and T. K. Lu (2014). "Sequence-specific antimicrobials using efficiently delivered RNA-guided nucleases." Nat Biotechnol **32**(11): 1141-1145.
- Claesson, M. J., I. B. Jeffery, S. Conde, S. E. Power, E. M. O'Connor, S. Cusack, H. M. Harris, M. Coakley, B. Lakshminarayanan, O. O'Sullivan, G. F. Fitzgerald, J. Deane, M. O'Connor, N. Harnedy, K. O'Connor, D. O'Mahony, D. van Sinderen, M. Wallace, L. Brennan, C. Stanton, J. R. Marchesi, A. P. Fitzgerald, F. Shanahan, C. Hill, R. P. Ross and P. W. O'Toole (2012). "Gut microbiota composition correlates with diet and health in the elderly." Nature **488**(7410): 178-184.
- Cole, J. R., Q. Wang, J. A. Fish, B. Chai, D. M. McGarrell, Y. Sun, C. T. Brown, A. Porras-Alfaro, C. R. Kuske and J. M. Tiedje (2014). "Ribosomal Database Project: data and tools for high throughput rRNA analysis." Nucleic Acids Res **42**(Database issue): D633-642.
- Conlon, M. A. and A. R. Bird (2015). "The Impact of Diet and Lifestyle on Gut Microbiota and Human Health." Nutrients **7**(1): 17-44.
- Constantinidou, C., J. L. Hobman, L. Griffiths, M. D. Patel, C. W. Penn, J. A. Cole and T. W. Overton (2006). "A reassessment of the FNR regulon and transcriptomic analysis of the effects of nitrate, nitrite, NarXL, and NarQP as *Escherichia coli* K12 adapts from aerobic to anaerobic growth." J Biol Chem **281**(8): 4802-4815.
- Crack, J., J. Green and A. J. Thomson (2004). "Mechanism of oxygen sensing by the bacterial transcription factor fumarate-nitrate reduction (FNR)." J Biol Chem **279**(10): 9278-9286.
- Crooke, S. T. (1998). "An overview of progress in antisense therapeutics." Antisense Nucleic Acid Drug Dev **8**(2): 115-122.
- Crooks, G. E., G. Hon, J. M. Chandonia and S. E. Brenner (2004). "WebLogo: a sequence logo generator." Genome Res **14**(6): 1188-1190.
- David, L. A., C. F. Maurice, R. N. Carmody, D. B. Gootenberg, J. E. Button, B. E. Wolfe, A. V. Ling, A. S. Devlin, Y. Varma, M. A. Fischbach, S. B. Biddinger, R. J. Dutton and P. J. Turnbaugh (2014). "Diet rapidly and reproducibly alters the human gut microbiome." Nature **505**(7484): 559-563.
- De Jong, W. H., W. I. Hagens, P. Krystek, M. C. Burger, A. J. Sips and R. E. Geertsma (2008). "Particle size-dependent organ distribution of gold nanoparticles after intravenous administration." Biomaterials **29**(12): 1912-1919.

- Desai, M. S., A. M. Seekatz, N. M. Koropatkin, N. Kamada, C. A. Hickey, M. Wolter, N. A. Pudlo, S. Kitamoto, N. Terrapon, A. Muller, V. B. Young, B. Henrissat, P. Wilmes, T. S. Stappenbeck, G. Nunez and E. C. Martens (2016). "A Dietary Fiber-Deprived Gut Microbiota Degrades the Colonic Mucus Barrier and Enhances Pathogen Susceptibility." *Cell* **167**(5): 1339-1353.e1321.
- Dethlefsen, L., S. Huse, M. L. Sogin and D. A. Relman (2008). "The pervasive effects of an antibiotic on the human gut microbiota, as revealed by deep 16S rRNA sequencing." *PLoS Biol* **6**(11): e280.
- Dethlefsen, L. and D. A. Relman (2011). "Incomplete recovery and individualized responses of the human distal gut microbiota to repeated antibiotic perturbation." *Proc Natl Acad Sci U S A* **108** **Suppl 1**: 4554-4561.
- Devkota, S., Y. Wang, M. W. Musch, V. Leone, H. Fehlner-Peach, A. Nadimpalli, D. A. Antonopoulos, B. Jabri and E. B. Chang (2012). "Dietary-fat-induced taurocholic acid promotes pathobiont expansion and colitis in Il10^{-/-} mice." *Nature* **487**(7405): 104-108.
- Di Stefano, M., P. Tana, C. Mengoli, E. Miceli, E. Pagani and G. R. Corazza (2011). "Colonic hypersensitivity is a major determinant of the efficacy of bloating treatment in constipation-predominant irritable bowel syndrome." *Intern Emerg Med* **6**(5): 403-411.
- Dias, N. and C. A. Stein (2002). "Antisense oligonucleotides: basic concepts and mechanisms." *Mol Cancer Ther* **1**(5): 347-355.
- Ding, T. and P. D. Schloss (2014). "Dynamics and associations of microbial community types across the human body." *Nature* **509**(7500): 357-360.
- Duenas, M., I. Munoz-Gonzalez, C. Cueva, A. Jimenez-Giron, F. Sanchez-Patan, C. Santos-Buelga, M. V. Moreno-Arribas and B. Bartolome (2015). "A survey of modulation of gut microbiota by dietary polyphenols." *Biomed Res Int* **2015**: 850902.
- Duffy, M., L. O'Mahony, J. C. Coffey, J. K. Collins, F. Shanahan, H. P. Redmond and W. O. Kirwan (2002). "Sulfate-reducing bacteria colonize pouches formed for ulcerative colitis but not for familial adenomatous polyposis." *Dis Colon Rectum* **45**(3): 384-388.
- Duncan, S. H., P. Louis and H. J. Flint (2007). "Cultivable bacterial diversity from the human colon." *Lett Appl Microbiol* **44**(4): 343-350.
- Eckburg, P. B., E. M. Bik, C. N. Bernstein, E. Purdom, L. Dethlefsen, M. Sargent, S. R. Gill, K. E. Nelson and D. A. Relman (2005). "Diversity of the human intestinal microbial flora." *Science* **308**(5728): 1635-1638.
- Eckstein, F. (2014). "Phosphorothioates, essential components of therapeutic oligonucleotides." *Nucleic Acid Ther* **24**(6): 374-387.
- Edgar, R. C. (2010). "Search and clustering orders of magnitude faster than BLAST." *Bioinformatics* **26**(19): 2460-2461.
- Ehrlich, S. D. (2011). MetaHIT: The European Union Project on Metagenomics of the Human Intestinal Tract. *Metagenomics of the Human Body*. K. E. Nelson, Springer New York: 307-316.
- Erben, U., C. Lodenkemper, K. Doerfel, S. Spieckermann, D. Haller, M. M. Heimesaat, M. Zeitz, B. Siegmund and A. A. Kuhl (2014). "A guide to histomorphological evaluation of intestinal inflammation in mouse models." *Int J Clin Exp Pathol* **7**(8): 4557-4576.
- Escaja, N., I. Gomez-Pinto, M. Rico, E. Pedrosa and C. Gonzalez (2003). "Structures and stabilities of small DNA dumbbells with Watson-Crick and Hoogsteen base pairs." *ChemBiochem* **4**(7): 623-632.
- Evans, C. C., K. J. LePard, J. W. Kwak, M. C. Stancukas, S. Laskowski, J. Dougherty, L. Moulton, A. Glawe, Y. Wang, V. Leone, D. A. Antonopoulos, D. Smith, E. B. Chang and M. J. Ciancio (2014).

"Exercise prevents weight gain and alters the gut microbiota in a mouse model of high fat diet-induced obesity." *PLoS One* **9**(3): e92193.

Everhardt Queen, A., M. Moerdyk-Schauwecker, L. M. McKee, L. J. Leamy and Y. M. Huet (2016). "Differential Expression of Inflammatory Cytokines and Stress Genes in Male and Female Mice in Response to a Lipopolysaccharide Challenge." *PLoS One* **11**(4): e0152289.

Falony, G., M. Joossens, S. Vieira-Silva, J. Wang, Y. Darzi, K. Faust, A. Kurilshikov, M. J. Bonder, M. Valles-Colomer, D. Vandeputte, R. Y. Tito, S. Chaffron, L. Rymenans, C. Verspecht, L. De Sutter, G. Lima-Mendez, K. D'Hoe, K. Jonckheere, D. Homola, R. Garcia, E. F. Tigchelaar, L. Eeckhaut, J. Fu, L. Henckaerts, A. Zhernakova, C. Wijmenga and J. Raes (2016). "Population-level analysis of gut microbiome variation." *Science* **352**(6285): 560-564.

Feng, Y., A. J. M. Stams, W. M. de Vos and I. Sanchez-Andrea (2017). "Enrichment of sulfidogenic bacteria from the human intestinal tract." *FEMS Microbiol Lett* **364**(4).

Fink, R. C., M. R. Evans, S. Porwollik, A. Vazquez-Torres, J. Jones-Carson, B. Troxell, S. J. Libby, M. McClelland and H. M. Hassan (2007). "FNR is a global regulator of virulence and anaerobic metabolism in *Salmonella enterica* serovar Typhimurium (ATCC 14028s)." *J Bacteriol* **189**(6): 2262-2273.

Finucane, M. M., T. J. Sharpton, T. J. Laurent and K. S. Pollard (2014). "A taxonomic signature of obesity in the microbiome? Getting to the guts of the matter." *PLoS One* **9**(1): e84689.

Fiorucci, S., E. Distrutti, G. Cirino and J. L. Wallace (2006). "The emerging roles of hydrogen sulfide in the gastrointestinal tract and liver." *Gastroenterology* **131**(1): 259-271.

Fishov, I. and C. L. Woldringh (1999). "Visualization of membrane domains in *Escherichia coli*." *Mol Microbiol* **32**(6): 1166-1172.

Flint, H. J., K. P. Scott, S. H. Duncan, P. Louis and E. Forano (2012). "Microbial degradation of complex carbohydrates in the gut." *Gut Microbes* **3**(4): 289-306.

Förster, A. H., J. Gescher (2014). "Metabolic engineering of *Escherichia coli* for production of mixed-acid fermentation end products." *Front Bioeng Biotechnol* **2**:16.

Fuhrhop, J. H. and T. Wang (2004). "Bolaamphiphiles." *Chem Rev* **104**(6): 2901-2937.

Fujimoto, J., K. Tanigawa, Y. Kudo, H. Makino and K. Watanabe (2011). "Identification and quantification of viable *Bifidobacterium breve* strain Yakult in human faeces by using strain-specific primers and propidium monoazide." *J Appl Microbiol* **110**(1): 209-217.

Fuller, Z., P. Louis, A. Mihajlovski, V. Rungapamestry, B. Ratcliffe and A. J. Duncan (2007). "Influence of cabbage processing methods and prebiotic manipulation of colonic microflora on glucosinolate breakdown in man." *Br J Nutr* **98**(2): 364-372.

Gallo, A., G. Passaro, A. Gasbarrini, R. Landolfi and M. Montalto (2016). "Modulation of microbiota as treatment for intestinal inflammatory disorders: An update." *World J Gastroenterol* **22**(32): 7186-7202.

Galtier, M., L. De Sordi, A. Sivignon, A. de Vallee, D. Maura, C. Neut, O. Rahmouni, K. Wannerberger, A. Darfeuille-Michaud, P. Desreumaux, N. Barnich and L. Debarbieux (2017). "Bacteriophages targeting adherent invasive *Escherichia coli* strains as a promising new treatment for Crohn's disease." *J Crohns Colitis*.

Gao, P., H. Tian, G. Li, H. Sun and T. Ma (2015). "Microbial diversity and abundance in the Xinjiang Luliang long-term water-flooding petroleum reservoir." *Microbiologyopen*.

Garrett, T. A., A. C. O'Neill and M. L. Hopson (2012). "Quantification of cardiolipin molecular species in *Escherichia coli* lipid extracts using liquid chromatography/electrospray ionization mass spectrometry." *Rapid Commun Mass Spectrom* **26**(19): 2267-2274.

- Garrett, W. S., C. A. Gallini, T. Yatsunenko, M. Michaud, A. DuBois, M. L. Delaney, S. Punit, M. Karlsson, L. Bry, J. N. Glickman, J. I. Gordon, A. B. Onderdonk and L. H. Glimcher (2010). "*Enterobacteriaceae* act in concert with the gut microbiota to induce spontaneous and maternally transmitted colitis." Cell Host Microbe **8**(3): 292-300.
- Geets, J., B. Borremans, L. Diels, D. Springael, J. Vangronsveld, D. van der Lelie and K. Vanbroekhoven (2006). "DsrB gene-based DGGE for community and diversity surveys of sulfate-reducing bacteria." J Microbiol Methods **66**(2): 194-205.
- Gevers, D., S. Kugathasan, L. A. Denson, Y. Vazquez-Baeza, W. Van Treuren, B. Ren, E. Schwager, D. Knights, S. J. Song, M. Yassour, X. C. Morgan, A. D. Kostic, C. Luo, A. Gonzalez, D. McDonald, Y. Haberman, T. Walters, S. Baker, J. Rosh, M. Stephens, M. Heyman, J. Markowitz, R. Baldassano, A. Griffiths, F. Sylvester, D. Mack, S. Kim, W. Crandall, J. Hyams, C. Huttenhower, R. Knight and R. J. Xavier (2014). "The treatment-naive microbiome in new-onset Crohn's disease." Cell Host Microbe **15**(3): 382-392.
- Ghosal, A. and P. E. Nielsen (2012). "Potent Antibacterial Antisense Peptide–Peptide Nucleic Acid Conjugates Against *Pseudomonas aeruginosa*." Nucleic Acid Therapeutics **22**(5): 323-334.
- Ghosh, I., D. Schenck, S. Bose, F. Liu and M. Motto (2013). "Identification of critical process parameters and its interplay with nanosuspension formulation prepared by top down media milling technology--a QbD perspective." Pharm Dev Technol **18**(3): 719-729.
- Giardina, G., S. Rinaldo, K. A. Johnson, A. Di Matteo, M. Brunori and F. Cutruzzola (2008). "NO sensing in *Pseudomonas aeruginosa*: structure of the transcriptional regulator DNR." J Mol Biol **378**(5): 1002-1015.
- Gibson, G. R., H. M. Probert, J. V. Loo, R. A. Rastall and M. B. Roberfroid (2004). "Dietary modulation of the human colonic microbiota: updating the concept of prebiotics." Nutr Res Rev **17**(2): 259-275.
- Gill, S. R., M. Pop, R. T. Deboy, P. B. Eckburg, P. J. Turnbaugh, B. S. Samuel, J. I. Gordon, D. A. Relman, C. M. Fraser-Liggett and K. E. Nelson (2006). "Metagenomic analysis of the human distal gut microbiome." Science **312**(5778): 1355-1359.
- Giloteaux, L., R. Duran, C. Casiot, O. Bruneel, F. Elbaz-Poulichet and M. Goni-Urriza (2013). "Three-year survey of sulfate-reducing bacteria community structure in Carnoules acid mine drainage (France), highly contaminated by arsenic." FEMS Microbiol Ecol **83**(3): 724-737.
- Gubern, M., M. Andriamihaja, T. Nubel, F. Blachier and F. Bouillaud (2007). "Sulfide, the first inorganic substrate for human cells." Faseb j **21**(8): 1699-1706.
- Grigg, J. B. and G. F. Sonnenberg (2017). "Host-Microbiota Interactions Shape Local and Systemic Inflammatory Diseases." J Immunol **198**(2): 564-571.
- Guan, J., B. L. Zhang, S. M. Mbadinga, J. F. Liu, J. D. Gu and B. Z. Mu (2014). "Functional genes (*dsr*) approach reveals similar sulphidogenic prokaryotes diversity but different structure in saline waters from corroding high temperature petroleum reservoirs." Appl Microbiol Biotechnol **98**(4): 1871-1882.
- Guinane, C. M. and P. D. Cotter (2013). "Role of the gut microbiota in health and chronic gastrointestinal disease: understanding a hidden metabolic organ." Therap Adv Gastroenterol **6**(4): 295-308.
- Guo, Y. and J. D. Gralla (1998). "Promoter opening via a DNA fork junction binding activity." Proc Natl Acad Sci U S A **95**(20): 11655-11660.
- Hacker, G., V. Redecke and H. Hacker (2002). "Activation of the immune system by bacterial CpG-DNA." Immunology **105**(3): 245-251.

Hill, C., F. Guarner, G. Reid, G. R. Gibson, D. J. Merenstein, B. Pot, L. Morelli, R. B. Canani, H. J. Flint, S. Salminen, P. C. Calder and M. E. Sanders (2014). "Expert consensus document. The International Scientific Association for Probiotics and Prebiotics consensus statement on the scope and appropriate use of the term probiotic." Nat Rev Gastroenterol Hepatol **11**(8): 506-514.

Holmes, E., J. V. Li, J. R. Marchesi and J. K. Nicholson (2012). "Gut microbiota composition and activity in relation to host metabolic phenotype and disease risk." Cell Metab **16**(5): 559-564.

Hooper, L. V. and J. I. Gordon (2001). "Commensal host-bacterial relationships in the gut." Science **292**(5519): 1115-1118.

Huang, K. C., R. Mukhopadhyay and N. S. Wingreen (2006). "A curvature-mediated mechanism for localization of lipids to bacterial poles." PLoS Comput Biol **2**(11): e151.

Huang, Y.-L., C. Chassard, M. Hausmann, M. von Itzstein and T. Hennet (2015). "Sialic acid catabolism drives intestinal inflammation and microbial dysbiosis in mice." Nature Communications **6**: 8141.

Hughes, D. and A. Karlen (2014). "Discovery and preclinical development of new antibiotics." Ups J Med Sci **119**(2): 162-169.

Huttenhower C, G. D., Knight R, Abubucker S, Badger JH, Chinwalla AT, Creasy HH, Earl AM, FitzGerald MG, Fulton RS, Giglio MG, Hallsworth-Pepin K, Lobos EA, Madupu R, Magrini V, Martin JC, Mitreva M, Muzny DM, Sodergren EJ, Versalovic J, Wollam AM, Worley KC, Wortman JR, Young SK, Zeng Q, Aagaard KM, Abolude OO, Allen-Vercoe E, Alm EJ, Alvarado L, Andersen GL, Anderson S, Appelbaum E, Arachchi HM, Armitage G, Arze CA, Ayvaz T, Baker CC, Begg L, Belachew T, Bhonagiri V, Bihan M, Blaser MJ, Bloom T, Bonazzi V, Brooks J, Buck GA, Buhay CJ, Busam DA, Campbell JL, Canon SR, Cantarel BL, Chain PS, Chen IM, Chen L, Chhibba S, Chu K, Ciulla DM, Clemente JC, Clifton SW, Conlan S, Crabtree J, Cutting MA, Davidovics NJ, Davis CC, DeSantis TZ, Deal C, Delehaunty KD, Dewhirst FE, Deych E, Ding Y, Dooling DJ, Dugan SP, Dunne WM, Durkin A, Edgar RC, Erlich RL, Farmer CN, Farrell RM, Faust K, Feldgarden M, Felix VM, Fisher S, Fodor AA, Forney LJ, Foster L, Di Francesco V, Friedman J, Friedrich DC, Fronick CC, Fulton LL, Gao H, Garcia N, Giannoukos G, Giblin C, Giovanni MY, Goldberg JM, Goll J, Gonzalez A, Griggs A, Gujja S, Haake SK, Haas BJ, Hamilton HA, Harris EL, Hepburn TA, Herter B, Hoffmann DE, Holder ME, Howarth C, Huang KH, Huse SM, Izard J, Jansson JK, Jiang H, Jordan C, Joshi V, Katancik JA, Keitel WA, Kelley ST, Kells C, King NB, Knights D, Kong HH, Koren O, Koren S, Kota KC, Kovar CL, Kyrpides NC, La Rosa PS, Lee SL, Lemon KP, Lennon N, Lewis CM, Lewis L, Ley RE, Li K, Liolios K, Liu B, Liu Y, Lo CC, Lozupone CA, Lunsford R, Madden T, Mahurkar AA, Mannon PJ, Mardis ER, Markowitz VM, Mavromatis K, McCorrison JM, McDonald D, McEwen J, McGuire AL, McInnes P, Mehta T, Mihindukulasuriya KA, Miller JR, Minx PJ, Newsham I, Nusbaum C, O'Laughlin M, Orvis J, Pagani I, Palaniappan K, Patel SM, Pearson M, Peterson J, Podar M, Pohl C, Pollard KS, Pop M, Priest ME, Proctor LM, Qin X, Raes J, Ravel J, Reid JG, Rho M, Rhodes R, Riehle KP, Rivera MC, Rodriguez-Mueller B, Rogers YH, Ross MC, Russ C, Sanka RK, Sankar P, Sathirapongsasuti J, Schloss JA, Schloss PD, Schmidt TM, Scholz M, Schriml L, Schubert AM, Segata N, Segre JA, Shannon WD, Sharp RR, Sharpton TJ, Shenoy N, Sheth NU, Simone GA, Singh I, Smillie CS, Sobel JD, Sommer DD, Spicer P, Sutton GG, Sykes SM, Tabbaa DG, Thiagarajan M, Tomlinson CM, Torralba M, Treangen TJ, Truty RM, Vishnivetskaya TA, Walker J, Wang L, Wang Z, Ward DV, Warren W, Watson MA, Wellington C, Wetterstrand KA, White JR, Wilczek-Boney K, Wu Y, Wylie KM, Wylie T, Yandava C, Ye L, Ye Y, Yooseph S, Youmans BP, Zhang L, Zhou Y, Zhu Y, Zoloth L, Zucker JD, Birren BW, Gibbs RA, Highlander SK, Methé BA, Nelson KE, Petrosino JF, Weinstock GM, Wilson RK, White O. (2012). "Structure, function and diversity of the healthy human microbiome." Nature **486**(7402): 207-214.

Ijssennagger, N., C. Belzer, G. J. Hooiveld, J. Dekker, S. W. van Mil, M. Muller, M. Kleerebezem and R. van der Meer (2015). "Gut microbiota facilitates dietary heme-induced epithelial hyperproliferation by opening the mucus barrier in colon." Proc Natl Acad Sci U S A **112**(32): 10038-10043.

- Ijssennagger, N., R. van der Meer and S. W. van Mil (2016). "Sulfide as a Mucus Barrier-Breaker in Inflammatory Bowel Disease?" Trends Mol Med **22**(3): 190-199.
- Jani, P., G. W. Halbert, J. Langridge and A. T. Florence (1990). "Nanoparticle uptake by the rat gastrointestinal mucosa: quantitation and particle size dependency." J Pharm Pharmacol **42**(12): 821-826.
- Järver, P., T. Coursindel, S. E. L. Andaloussi, C. Godfrey, M. J. A. Wood and M. J. Gait (2012). "Peptide-mediated Cell and *In vivo* Delivery of Antisense Oligonucleotides and siRNA." Molecular Therapy. Nucleic Acids **1**(6): e27.
- Jeffery, I. B., M. J. Claesson, P. W. O'Toole and F. Shanahan (2012). "Categorization of the gut microbiota: enterotypes or gradients?" Nat Rev Micro **10**(9): 591-592.
- Jia, W., R. N. Whitehead, L. Griffiths, C. Dawson, H. Bai, R. H. Waring, D. B. Ramsden, J. O. Hunter, M. Cauchi, C. Bessant, D. P. Fowler, C. Walton, C. Turner and J. A. Cole (2012). "Diversity and distribution of sulphate-reducing bacteria in human faeces from healthy subjects and patients with inflammatory bowel disease." FEMS Immunol Med Microbiol **65**(1): 55-68.
- Jonkman, J. and C. M. Brown (2015). "Any Way You Slice It-A Comparison of Confocal Microscopy Techniques." J Biomol Tech **26**(2): 54-65.
- Joshi, S. C. (2011). "Sol-Gel Behavior of Hydroxypropyl Methylcellulose (HPMC) in Ionic Media Including Drug Release." Materials **4**(10): 1861.
- Jovel, J., J. Patterson, W. Wang, N. Hotte, S. O'Keefe, T. Mitchel, T. Perry, D. Kao, A. L. Mason, K. L. Madsen and G. K. S. Wong (2016). "Characterization of the Gut Microbiome Using 16S or Shotgun Metagenomics." Frontiers in Microbiology **7**: 459.
- Ju, T., Y. Shoblak, Y. Gao, K. Yang, J. Fohse, B. B. Finlay, Y. W. So, P. Stothard and B. P. Willing (2017). "Initial gut microbial composition as a key factor driving host response to antibiotic treatment, as exemplified by the presence or absence of commensal *Escherichia coli*." Appl Environ Microbiol.
- Katouli, M. (2010). "Population structure of gut *Escherichia coli* and its role in development of extra-intestinal infections." Iran J Microbiol **2**(2): 59-72.
- Kaushal, V., C. Herzog, R. S. Haun and G. P. Kaushal (2014). "Caspase Protocols in Mice." Methods in molecular biology (Clifton, N.J.) **1133**: 141-154.
- Kawane, K., K. Motani and S. Nagata (2014). "DNA degradation and its defects." Cold Spring Harb Perspect Biol **6**(6).
- Kazmierczak, M. J., M. Wiedmann and K. J. Boor (2005). "Alternative sigma factors and their roles in bacterial virulence." Microbiol Mol Biol Rev **69**(4): 527-543.
- Kelly, C. R., A. Khoruts, C. Staley, M. J. Sadowsky, M. Abd, M. Alani, B. Bakow, P. Curran, J. McKenney, A. Tisch, S. E. Reinert, J. T. Machan and L. J. Brandt (2016). "Effect of Fecal Microbiota Transplantation on Recurrence in Multiply Recurrent *Clostridium difficile* Infection: A Randomized Trial." Ann Intern Med **165**(9): 609-616.
- Keum, J. W. and H. Bermudez (2009). "Enhanced resistance of DNA nanostructures to enzymatic digestion." Chem Commun (Camb)(45): 7036-7038.
- Khajah, M. A. (2017). "The potential role of fecal microbiota transplantation in the treatment of inflammatory Bowel disease." Scand J Gastroenterol: 1-13.
- Khoroshilova, N., C. Popescu, E. Münck, H. Beinert and P. J. Kiley (1997). "Iron-sulfur cluster disassembly in the FNR protein of *Escherichia coli* by O(2): [4Fe-4S] to [2Fe-2S] conversion with loss of biological activity." Proceedings of the National Academy of Sciences of the United States of America **94**(12): 6087-6092.

- Kibbe, W. A. (2007). "OligoCalc: an online oligonucleotide properties calculator." Nucleic Acids Res **35**(Web Server issue): W43-46.
- Kim, J. J., M. S. Shajib, M. M. Manocha and W. I. Khan (2012). "Investigating intestinal inflammation in DSS-induced model of IBD." J Vis Exp(60).
- Kim, J. S., D. H. Cho, M. Park, W. J. Chung, D. Shin, K. S. Ko and D. H. Kweon (2016). "CRISPR/Cas9-Mediated Re-Sensitization of Antibiotic-Resistant *Escherichia coli* Harboring Extended-Spectrum beta-Lactamases." J Microbiol Biotechnol **26**(2): 394-401.
- Kocincova, D. and J. S. Lam (2011). "Structural diversity of the core oligosaccharide domain of *Pseudomonas aeruginosa* lipopolysaccharide." Biochemistry (Mosc) **76**(7): 755-760.
- Koren, O., D. Knights, A. Gonzalez, L. Waldron, N. Segata, R. Knight, C. Huttenhower and R. E. Ley (2013). "A guide to enterotypes across the human body: meta-analysis of microbial community structures in human microbiome datasets." PLoS Comput Biol **9**(1): e1002863.
- Koressaar, T. and M. Remm (2007). "Enhancements and modifications of primer design program Primer3." Bioinformatics **23**(10): 1289-1291.
- Korner, H., H. J. Sofia and W. G. Zumft (2003). "Phylogeny of the bacterial superfamily of Crp-Fnr transcription regulators: exploiting the metabolic spectrum by controlling alternative gene programs." FEMS Microbiol Rev **27**(5): 559-592.
- Kostic, A. D., M. R. Howitt and W. S. Garrett (2013). "Exploring host-microbiota interactions in animal models and humans." Genes Dev **27**(7): 701-718.
- Kristensen, N. B., T. Bryrup, K. H. Allin, T. Nielsen, T. H. Hansen and O. Pedersen (2016). "Alterations in fecal microbiota composition by probiotic supplementation in healthy adults: a systematic review of randomized controlled trials." Genome Medicine **8**: 52.
- Kuczynski, J., J. Stombaugh, W. A. Walters, A. Gonzalez, J. G. Caporaso and R. Knight (2012). "Using QIIME to analyze 16S rRNA gene sequences from microbial communities." Curr Protoc Microbiol **Chapter 1**: Unit 1E.5.
- Kuruville, E., J. Joseph and D. Ramaiah (2005). "Novel Bifunctional Acridine–Acridinium Conjugates: Synthesis and Study of Their Chromophore-Selective Electron-Transfer and DNA-Binding Properties." The Journal of Physical Chemistry B **109**(46): 21997-22002.
- Lackraj, T., K. Johnson-Henry, P. M. Sherman, S. D. Goodman, A. M. Segall and D. Barnett Foster (2016). "Novel antimicrobial peptide prevents *C. rodentium* infection in C57BL/6 mice by enhancing acid-induced pathogen killing." Microbiology **162**(9): 1641-1650.
- Lai, C.-H., S.-R. Wu, J.-C. Pang, L. Ramireddy, Y.-C. Chiang, C.-K. Lin and H.-Y. Tsen (2016). "Designing primers and evaluation of the efficiency of propidium monoazide – Quantitative polymerase chain reaction for counting the viable cells of *Lactobacillus gasseri* and *Lactobacillus salivarius*." Journal of Food and Drug Analysis.
- Lam, V., J. Su, A. Hsu, G. J. Gross, N. H. Salzman and J. E. Baker (2016). "Intestinal Microbial Metabolites Are Linked to Severity of Myocardial Infarction in Rats." PLoS One **11**(8): e0160840.
- Langdon, A., N. Crook and G. Dantas (2016). "The effects of antibiotics on the microbiome throughout development and alternative approaches for therapeutic modulation." Genome Medicine **8**: 39.
- Lasch, J. and A. Hildebrand (2002). "Isothermic titration calorimetry to study CMCs of neutral surfactants and of the liposome-forming bolaamphiphile dequalinium." J Liposome Res **12**(1-2): 51-56.

- Laukens, D., B. M. Brinkman, J. Raes, M. De Vos and P. Vandenabeele (2016). "Heterogeneity of the gut microbiome in mice: guidelines for optimizing experimental design." *FEMS Microbiol Rev* **40**(1): 117-132.
- Lawley, T. D., S. Clare, A. W. Walker, M. D. Stares, T. R. Connor, C. Raisen, D. Goulding, R. Rad, F. Schreiber, C. Brandt, L. J. Deakin, D. J. Pickard, S. H. Duncan, H. J. Flint, T. G. Clark, J. Parkhill and G. Dougan (2012). "Targeted restoration of the intestinal microbiota with a simple, defined bacteriotherapy resolves relapsing *Clostridium difficile* disease in mice." *PLoS Pathog* **8**(10): e1002995.
- Le Chatelier, E., T. Nielsen, J. Qin, E. Prifti, F. Hildebrand, G. Falony, M. Almeida, M. Arumugam, J. M. Batto, S. Kennedy, P. Leonard, J. Li, K. Burgdorf, N. Grarup, T. Jorgensen, I. Brandslund, H. B. Nielsen, A. S. Juncker, M. Bertalan, F. Levenez, N. Pons, S. Rasmussen, S. Sunagawa, J. Tap, S. Tims, E. G. Zoetendal, S. Brunak, K. Clement, J. Dore, M. Kleerebezem, K. Kristiansen, P. Renault, T. Sicheritz-Ponten, W. M. de Vos, J. D. Zucker, J. Raes, T. Hansen, P. Bork, J. Wang, S. D. Ehrlich and O. Pedersen (2013). "Richness of human gut microbiome correlates with metabolic markers." *Nature* **500**(7464): 541-546.
- LeBlanc, J. G., C. Milani, G. S. de Giori, F. Sesma, D. van Sinderen and M. Ventura (2013). "Bacteria as vitamin suppliers to their host: a gut microbiota perspective." *Curr Opin Biotechnol* **24**(2): 160-168.
- Lee, G. C. and D. S. Burgess (2013). "Polymyxins and Doripenem Combination Against KPC-Producing *Klebsiella pneumoniae*." *J Clin Med Res* **5**(2): 97-100.
- Lee, K. A., B. Kim, J. Bhin, D. H. Kim, H. You, E. K. Kim, S. H. Kim, J. H. Ryu, D. Hwang and W. J. Lee (2015). "Bacterial uracil modulates *Drosophila* DUOX-dependent gut immunity via Hedgehog-induced signaling endosomes." *Cell Host Microbe* **17**(2): 191-204.
- Lee, K. A., S. H. Kim, E. K. Kim, E. M. Ha, H. You, B. Kim, M. J. Kim, Y. Kwon, J. H. Ryu and W. J. Lee (2013). "Bacterial-derived uracil as a modulator of mucosal immunity and gut-microbe homeostasis in *Drosophila*." *Cell* **153**(4): 797-811.
- Leloup, J., A. Loy, N. J. Knab, C. Borowski, M. Wagner and B. B. Jorgensen (2007). "Diversity and abundance of sulfate-reducing microorganisms in the sulfate and methane zones of a marine sediment, Black Sea." *Environ Microbiol* **9**(1): 131-142.
- Lewis, B. B., C. G. Buffie, R. A. Carter, I. Leiner, N. C. Toussaint, L. C. Miller, A. Gobourne, L. Ling and E. G. Pamer (2015). "Loss of Microbiota-Mediated Colonization Resistance to *Clostridium difficile* Infection With Oral Vancomycin Compared With Metronidazole." *J Infect Dis* **212**(10): 1656-1665.
- Lewis, R. N. and R. N. McElhaney (2009). "The physicochemical properties of cardiolipin bilayers and cardiolipin-containing lipid membranes." *Biochim Biophys Acta* **1788**(10): 2069-2079.
- Ley, R. E., D. A. Peterson and J. I. Gordon (2006). "Ecological and evolutionary forces shaping microbial diversity in the human intestine." *Cell* **124**(4): 837-848.
- Li, J., H. Jia, X. Cai, H. Zhong, Q. Feng, S. Sunagawa, M. Arumugam, J. R. Kultima, E. Prifti, T. Nielsen, A. S. Juncker, C. Manichanh, B. Chen, W. Zhang, F. Levenez, J. Wang, X. Xu, L. Xiao, S. Liang, D. Zhang, Z. Zhang, W. Chen, H. Zhao, J. Y. Al-Aama, S. Edris, H. Yang, J. Wang, T. Hansen, H. B. Nielsen, S. Brunak, K. Kristiansen, F. Guarner, O. Pedersen, J. Dore, S. D. Ehrlich, P. Bork and J. Wang (2014). "An integrated catalog of reference genes in the human gut microbiome." *Nat Biotechnol* **32**(8): 834-841.
- Li, S. S., A. Zhu, V. Benes, P. I. Costea, R. Hercog, F. Hildebrand, J. Huerta-Cepas, M. Nieuwdorp, J. Salojarvi, A. Y. Voigt, G. Zeller, S. Sunagawa, W. M. de Vos and P. Bork (2016). "Durable coexistence of donor and recipient strains after fecal microbiota transplantation." *Science* **352**(6285): 586-589.

- Loubinoux, J., J. P. Bronowicki, I. A. Pereira, J. L. Mougenel and A. E. Faou (2002). "Sulfate-reducing bacteria in human feces and their association with inflammatory bowel diseases." FEMS Microbiol Ecol **40**(2): 107-112.
- Luckey, T. D. (1972). "Introduction to intestinal microecology." Am J Clin Nutr **25**(12): 1292-1294.
- Lundberg, R., M. F. Toft, B. August, A. K. Hansen and C. H. Hansen (2016). "Antibiotic-treated versus germ-free rodents for microbiota transplantation studies." Gut Microbes **7**(1): 68-74.
- Lupp, C., M. L. Robertson, M. E. Wickham, I. Sekirov, O. L. Champion, E. C. Gaynor and B. B. Finlay (2007). "Host-mediated inflammation disrupts the intestinal microbiota and promotes the overgrowth of *Enterobacteriaceae*." Cell Host Microbe **2**(2): 119-129.
- Madan, J. C., S. F. Farzan, P. L. Hibberd and M. R. Karagas (2012). "Normal neonatal microbiome variation in relation to environmental factors, infection and allergy." Curr Opin Pediatr **24**(6): 753-759.
- Maderuelo, C., A. Zarzuelo and J. M. Lanao (2011). "Critical factors in the release of drugs from sustained release hydrophilic matrices." J Control Release **154**(1): 2-19.
- Makula, R. A. and W. R. Finnerty (1974). "Phospholipid Composition of *Desulfovibrio* Species." Journal of Bacteriology **120**(3): 1279-1283.
- Maleki, H., A. Rai, S. Pinto, M. Evangelista, R. M. Cardoso, C. Paulo, T. Carvalheiro, A. Paiva, M. Imani, A. Simchi, L. Duraes, A. Portugal and L. Ferreira (2016). "High Antimicrobial Activity and Low Human Cell Cytotoxicity of Core-Shell Magnetic Nanoparticles Functionalized with an Antimicrobial Peptide." ACS Appl Mater Interfaces **8**(18): 11366-11378.
- Mamusa, M., C. Resta, F. Barbero, D. Carta, D. Codoni, K. Hatzixanthis, M. McArthur and D. Berti (2016). "Interaction between a cationic bolaamphiphile and DNA: The route towards nanovectors for oligonucleotide antimicrobials." Colloids Surf B Biointerfaces **143**: 139-147.
- Mandalari, G., C. Nueno Palop, K. Tuohy, G. R. Gibson, R. N. Bennett, K. W. Waldron, G. Bisignano, A. Narbad and C. B. Faulds (2007). "*In vitro* evaluation of the prebiotic activity of a pectic oligosaccharide-rich extract enzymatically derived from bergamot peel." Appl Microbiol Biotechnol **73**(5): 1173-1179.
- Manichanh, C., L. Rigottier-Gois, E. Bonnaud, K. Gloux, E. Pelletier, L. Frangeul, R. Nalin, C. Jarrin, P. Chardon, P. Marteau, J. Roca and J. Dore (2006). "Reduced diversity of faecal microbiota in Crohn's disease revealed by a metagenomic approach." Gut **55**(2): 205-211.
- Mann, M. J. and V. J. Dzau (2000). "Therapeutic applications of transcription factor decoy oligonucleotides." J Clin Invest **106**(9): 1071-1075.
- Marchesi, J. R. (2011). "Human distal gut microbiome." Environ Microbiol **13**(12): 3088-3102.
- Marchesi, J. R., D. H. Adams, F. Fava, G. D. Hermes, G. M. Hirschfield, G. Hold, M. N. Quraishi, J. Kinross, H. Smidt, K. M. Tuohy, L. V. Thomas, E. G. Zoetendal and A. Hart (2016). "The gut microbiota and host health: a new clinical frontier." Gut **65**(2): 330-339.
- Marín-Menéndez, A., C. Montis, T. Díaz-Calvo, D. Carta, K. Hatzixanthis, C. J. Morris, M. McArthur and D. Berti (2017). "Antimicrobial Nanoplexes meet Model Bacterial Membranes: the key role of Cardiolipin." Scientific Reports **7**: 41242.
- Matsui, M., M. Tomita and A. Kanai (2013). "Comprehensive computational analysis of bacterial CRP/FNR superfamily and its target motifs reveals stepwise evolution of transcriptional networks." Genome Biol Evol **5**(2): 267-282.
- Maurice, C. F., H. J. Haiser and P. J. Turnbaugh (2013). "Xenobiotics shape the physiology and gene expression of the active human gut microbiome." Cell **152**(1-2): 39-50.
- McArthur, M. (2009a). TRANSCRIPTION FACTOR DECOYS

- McArthur, M. (2009b). Transcription factor decoys, compositions and methods, Google Patents.
- McArthur, M. (2014). Transcription factor decoys for the treatment and prevention of infections caused by bacteria including clostridium difficile, Google Patents.
- McArthur, M. (2015). Nucleic acid complexes, Google Patents.
- McArthur, M. (2017). Transcription factor decoys, compositions and methods, Google Patents.
- Medani, M., D. Collins, N. G. Docherty, A. W. Baird, P. R. O'Connell and D. C. Winter (2011). "Emerging role of hydrogen sulfide in colonic physiology and pathophysiology." Inflamm Bowel Dis **17**(7): 1620-1625.
- Membrez, M., F. Blancher, M. Jaquet, R. Bibiloni, P. D. Cani, R. G. Burcelin, I. Corthesy, K. Mace and C. J. Chou (2008). "Gut microbiota modulation with norfloxacin and ampicillin enhances glucose tolerance in mice." Faseb j **22**(7): 2416-2426.
- Menger, F. and S. Wrenn (1974). "Interfacial and Micellar Properties of Bolaform Electrolytes." The Journal of Physical Chemistry **78**(14): 1387-1390.
- Metris, A., S. M. George, F. Mulholland, A. T. Carter and J. Baranyi (2014). "Metabolic shift of *Escherichia coli* under salt stress in the presence of glycine betaine." Appl Environ Microbiol **80**(15): 4745-4756.
- Mileykovskaya, E. and W. Dowhan (2009). "Cardiolipin membrane domains in prokaryotes and eukaryotes." Biochim Biophys Acta **1788**(10): 2084-2091.
- Mirsepasi-Lauridsen, H. C., S. I. Halkjaer, E. M. Mortensen, M. C. Lydolph, I. Nordgaard-Lassen, K. A. Kroghelt and A. M. Petersen (2016). "Extraintestinal pathogenic *Escherichia coli* are associated with intestinal inflammation in patients with ulcerative colitis." Sci Rep **6**: 31152.
- Mishra, J., R. K. Verma, G. Alpini, F. Meng and N. Kumar (2013). "Role of Janus kinase 3 in mucosal differentiation and predisposition to colitis." J Biol Chem **288**(44): 31795-31806.
- Moayyedi, P., M. G. Surette, P. T. Kim, J. Libertucci, M. Wolfe, C. Onischi, D. Armstrong, J. K. Marshall, Z. Kassam, W. Reinisch and C. H. Lee (2015). "Fecal Microbiota Transplantation Induces Remission in Patients With Active Ulcerative Colitis in a Randomized Controlled Trial." Gastroenterology **149**(1): 102-109.e106.
- Moeller, A. H. and H. Ochman (2014). "Microbiomes are true to type." Proc Natl Acad Sci U S A **111**(26): 9372-9373.
- Mondhe, M., A. Chessher, S. Goh, L. Good and J. E. Stach (2014). "Species-selective killing of bacteria by antimicrobial peptide-PNAs." PLoS One **9**(2): e89082.
- Montis, C., S. Sostegni, S. Milani, P. Baglioni and D. Berti (2014). "Biocompatible cationic lipids for the formulation of liposomal DNA vectors." Soft Matter **10**(24): 4287-4297.
- Motta, J. P., K. L. Flannigan, T. A. Agbor, J. K. Beatty, R. W. Blackler, M. L. Workentine, G. J. Da Silva, R. Wang, A. G. Buret and J. L. Wallace (2015). "Hydrogen sulfide protects from colitis and restores intestinal microbiota biofilm and mucus production." Inflamm Bowel Dis **21**(5): 1006-1017.
- Muyzer, G. and A. J. Stams (2008). "The ecology and biotechnology of sulphate-reducing bacteria." Nat Rev Microbiol **6**(6): 441-454.
- Nakamura, N., H. C. Lin, C. S. McSweeney, R. I. Mackie and H. R. Gaskins (2010). "Mechanisms of microbial hydrogen disposal in the human colon and implications for health and disease." Annu Rev Food Sci Technol **1**: 363-395.
- Narula, N., Z. Kassam, Y. Yuan, J. F. Colombel, C. Ponsioen, W. Reinisch and P. Moayyedi (2017). "Systematic Review and Meta-analysis: Fecal Microbiota Transplantation for Treatment of Active Ulcerative Colitis." Inflamm Bowel Dis.

- Nava, G. M., F. Carbonero, J. A. Croix, E. Greenberg and H. R. Gaskins (2012). "Abundance and diversity of mucosa-associated hydrogenotrophic microbes in the healthy human colon." ISME J **6**(1): 57-70.
- NCBI, R. C. (2017). "Database Resources of the National Center for Biotechnology Information." Nucleic Acids Res **45**(D1): D12-d17.
- Nemeth, J., G. Oesch and S. P. Kuster (2015). "Bacteriostatic versus bactericidal antibiotics for patients with serious bacterial infections: systematic review and meta-analysis." J Antimicrob Chemother **70**(2): 382-395.
- Nguyen, T. L., S. Vieira-Silva, A. Liston and J. Raes (2015). "How informative is the mouse for human gut microbiota research?" Dis Model Mech **8**(1): 1-16.
- Nicholas, K. B., H. B. Nicholas and D. Deerfield (1997). "GeneDoc: analysis and visualization of genetic variation." Embnew. news **4**(1).
- Nicholson, J. K., E. Holmes and I. D. Wilson (2005). "Gut microorganisms, mammalian metabolism and personalized health care." Nat Rev Microbiol **3**(5): 431-438.
- Nieuwdorp, M., P. W. Gijljamse, N. Pai and L. M. Kaplan (2014). "Role of the Microbiome in Energy Regulation and Metabolism." Gastroenterology.
- Nokhodchi, A., S. Raja, P. Patel and K. Asare-Addo (2012). "The role of oral controlled release matrix tablets in drug delivery systems." Bioimpacts **2**(4): 175-187.
- Noti, M., N. Corazza, C. Mueller, B. Berger and T. Brunner (2010). "TNF suppresses acute intestinal inflammation by inducing local glucocorticoid synthesis." J Exp Med **207**(5): 1057-1066.
- Ohtani, N., S. Yoshimoto and E. Hara (2014). "Obesity and Cancer: A Gut Microbial Connection." Cancer Res.
- Okano, A., N. A. Isley and D. L. Boger (2017). "Peripheral modifications of [Psi[CH₂NH]Tpg₄]vancomycin with added synergistic mechanisms of action provide durable and potent antibiotics." Proc Natl Acad Sci U S A **114**(26): E5052-e5061.
- Ormerod, K. L., D. L. Wood, N. Lachner, S. L. Gellatly, J. N. Daly, J. D. Parsons, C. G. Dal'Molin, R. W. Palfreyman, L. K. Nielsen, M. A. Cooper, M. Morrison, P. M. Hansbro and P. Hugenholtz (2016). "Genomic characterization of the uncultured Bacteroidales family S24-7 inhabiting the guts of homeothermic animals." Microbiome **4**(1): 36.
- Osorio, F. A., P. Molina, S. Matiacevich, J. Enrione and O. Skurtys (2011). "Characteristics of hydroxy propyl methyl cellulose (HPMC) based edible film developed for blueberry coatings." Procedia Food Science **1**: 287-293.
- Padmanabhan, P., J. Grosse, A. B. Asad, G. K. Radda and X. Golay (2013). "Gastrointestinal transit measurements in mice with 99mTc-DTPA-labeled activated charcoal using NanoSPECT-CT." EJNMMI Res **3**(1): 60.
- Pankey, G. A. and L. D. Sabath (2004). "Clinical relevance of bacteriostatic versus bactericidal mechanisms of action in the treatment of Gram-positive bacterial infections." Clin Infect Dis **38**(6): 864-870.
- Parada, A. E., D. M. Needham and J. A. Fuhrman (2016). "Every base matters: assessing small subunit rRNA primers for marine microbiomes with mock communities, time series and global field samples." Environ Microbiol **18**(5): 1403-1414.
- Patil, S. D. and D. J. Burgess (2003). "DNA-based Biopharmaceuticals: therapeutics for the 21st Century." AAPS Newsmagazine. **6**(12): 27-27.
- Pelikan, C., C. W. Herbold, B. Hausmann, A. L. Muller, M. Pester and A. Loy (2015). "Diversity analysis of sulfite- and sulfate-reducing microorganisms by multiplex dsrA and dsrB amplicon

- sequencing using new primers and mock community-optimized bioinformatics." Environ Microbiol.
- Penchovsky, R. and M. Traykovska (2015). "Designing drugs that overcome antibacterial resistance: where do we stand and what should we do?" Expert Opin Drug Discov **10**(6): 631-650.
- Perez-Cobas, A. E., M. J. Gosalbes, A. Friedrichs, H. Knecht, A. Artacho, K. Eismann, W. Otto, D. Rojo, R. Bargiela, M. von Bergen, S. C. Neulinger, C. Daumer, F. A. Heinsen, A. Latorre, C. Barbas, J. Seifert, V. M. dos Santos, S. J. Ott, M. Ferrer and A. Moya (2013). "Gut microbiota disturbance during antibiotic therapy: a multi-omic approach." Gut **62**(11): 1591-1601.
- Petersen, A. M., E. M. Nielsen, E. Litrup, J. Brynskov, H. Mirsepasi and K. A. Krogh (2009). "A phylogenetic group of *Escherichia coli* associated with active left-sided inflammatory bowel disease." BMC Microbiol **9**: 171.
- Petersen, C. and J. L. Round (2014). "Defining dysbiosis and its influence on host immunity and disease." Cell Microbiol **16**(7): 1024-1033.
- Picknett, R. G. and R. Bexon (1977). "The evaporation of sessile or pendant drops in still air." Journal of Colloid and Interface Science **61**(2): 336-350.
- Pier, G. B. (2007). "Pseudomonas aeruginosa lipopolysaccharide: a major virulence factor, initiator of inflammation and target for effective immunity." Int J Med Microbiol **297**(5): 277-295.
- Pimentel, M., C. Chang, K. S. Chua, J. Mirocha, J. DiBaise, S. Rao and M. Amichai (2014). "Antibiotic treatment of constipation-predominant irritable bowel syndrome." Dig Dis Sci **59**(6): 1278-1285.
- Pimentel, M., A. Lembo, W. D. Chey, S. Zakko, Y. Ringel, J. Yu, S. M. Mareya, A. L. Shaw, E. Bortey and W. P. Forbes (2011). "Rifaximin therapy for patients with irritable bowel syndrome without constipation." N Engl J Med **364**(1): 22-32.
- Pimentel, M., S. Park, J. Mirocha, S. V. Kane and Y. Kong (2006). "The effect of a nonabsorbed oral antibiotic (rifaximin) on the symptoms of the irritable bowel syndrome: a randomized trial." Ann Intern Med **145**(8): 557-563.
- Pitcher, M. C., E. R. Beatty and J. H. Cummings (2000). "The contribution of sulphate reducing bacteria and 5-aminosalicylic acid to faecal sulphide in patients with ulcerative colitis." Gut **46**(1): 64-72.
- Platt, M. D., M. J. Schurr, K. Sauer, G. Vazquez, I. Kukavica-Ibrulj, E. Potvin, R. C. Levesque, A. Fedynak, F. S. Brinkman, J. Schurr, S. H. Hwang, G. W. Lau, P. A. Limbach, J. J. Rowe, M. A. Lieberman, N. Barraud, J. Webb, S. Kjelleberg, D. F. Hunt and D. J. Hassett (2008). "Proteomic, microarray, and signature-tagged mutagenesis analyses of anaerobic *Pseudomonas aeruginosa* at pH 6.5, likely representing chronic, late-stage cystic fibrosis airway conditions." J Bacteriol **190**(8): 2739-2758.
- Poole, K. and R. Srikumar (2001). "Multidrug efflux in *Pseudomonas aeruginosa*: components, mechanisms and clinical significance." Curr Top Med Chem **1**(1): 59-71.
- Pouokam, E. and M. Althaus (2016). "Epithelial Electrolyte Transport Physiology and the Gasotransmitter Hydrogen Sulfide." Oxid Med Cell Longev **2016**: 4723416.
- Prasad, V., D. Semwogerere and R. W. Eric (2007). "Confocal microscopy of colloids." Journal of Physics: Condensed Matter **19**(11): 113102.
- Price, M. N., A. M. Deutschbauer, J. V. Kuehl, H. Liu, H. E. Witkowska and A. P. Arkin (2011). "Evidence-based annotation of transcripts and proteins in the sulfate-reducing bacterium *Desulfovibrio vulgaris* Hildenborough." J Bacteriol **193**(20): 5716-5727.
- Prorok-Hamon, M., M. K. Friswell, A. Alswied, C. L. Roberts, F. Song, P. K. Flanagan, P. Knight, C. Codling, J. R. Marchesi, C. Winstanley, N. Hall, J. M. Rhodes and B. J. Campbell (2013). "Colonic

mucosa-associated diffusely adherent afaC+ *Escherichia coli* expressing lpfA and pks are increased in inflammatory bowel disease and colon cancer." Gut.

Qin, J., R. Li, J. Raes, M. Arumugam, K. S. Burgdorf, C. Manichanh, T. Nielsen, N. Pons, F. Levenez, T. Yamada, D. R. Mende, J. Li, J. Xu, S. Li, D. Li, J. Cao, B. Wang, H. Liang, H. Zheng, Y. Xie, J. Tap, P. Lepage, M. Bertalan, J. M. Batto, T. Hansen, D. Le Paslier, A. Linneberg, H. B. Nielsen, E. Pelletier, P. Renault, T. Sicheritz-Ponten, K. Turner, H. Zhu, C. Yu, S. Li, M. Jian, Y. Zhou, Y. Li, X. Zhang, S. Li, N. Qin, H. Yang, J. Wang, S. Brunak, J. Dore, F. Guarner, K. Kristiansen, O. Pedersen, J. Parkhill, J. Weissenbach, P. Bork, S. D. Ehrlich and J. Wang (2010). "A human gut microbial gene catalogue established by metagenomic sequencing." Nature **464**(7285): 59-65.

Rabus, R., S. S. Venceslau, L. Wohlbrand, G. Voordouw, J. D. Wall and I. A. Pereira (2015). "A Post-Genomic View of the Ecophysiology, Catabolism and Biotechnological Relevance of Sulphate-Reducing Prokaryotes." Adv Microb Physiol **66**: 55-321.

Rajeev, L., A. Chen, A. E. Kazakov, E. G. Luning, G. M. Zane, P. S. Novichkov, J. D. Wall and A. Mukhopadhyay (2015). "Regulation of Nitrite Stress Response in *Desulfovibrio vulgaris* Hildenborough, a Model Sulfate-Reducing Bacterium." J Bacteriol **197**(21): 3400-3408.

Rakoff-Nahoum, S., J. Paglino, F. Eslami-Varzaneh, S. Edberg and R. Medzhitov (2004). "Recognition of commensal microflora by toll-like receptors is required for intestinal homeostasis." Cell **118**(2): 229-241.

Reardon, S. (2017). "Modified viruses deliver death to antibiotic-resistant bacteria." Nature **546**(7660): 586-587.

Rebello, C. J., J. Burton, M. Heiman and F. L. Greenway (2015). "Gastrointestinal microbiome modulator improves glucose tolerance in overweight and obese subjects: A randomized controlled pilot trial." J Diabetes Complications **29**(8): 1272-1276.

Reeves, A. E., M. J. Koenigsnecht, I. L. Bergin and V. B. Young (2012). "Suppression of *Clostridium difficile* in the gastrointestinal tracts of germfree mice inoculated with a murine isolate from the family Lachnospiraceae." Infect Immun **80**(11): 3786-3794.

Reichardt, N., S. H. Duncan, P. Young, A. Belenguer, C. McWilliam Leitch, K. P. Scott, H. J. Flint and P. Louis (2014). "Phylogenetic distribution of three pathways for propionate production within the human gut microbiota." ISME J **8**(6): 1323-1335.

Reid, G., J. Howard and B. S. Gan (2001). "Can bacterial interference prevent infection?" Trends Microbiol **9**(9): 424-428.

Renner, L. D. and D. B. Weibel (2011). "Cardiolipin microdomains localize to negatively curved regions of *Escherichia coli* membranes." Proc Natl Acad Sci U S A **108**(15): 6264-6269.

Rey, F. E., M. D. Gonzalez, J. Cheng, M. Wu, P. P. Ahern and J. I. Gordon (2013). "Metabolic niche of a prominent sulfate-reducing human gut bacterium." Proc Natl Acad Sci U S A **110**(33): 13582-13587.

Rice, L. B. (2009). "The clinical consequences of antimicrobial resistance." Curr Opin Microbiol **12**(5): 476-481.

Rice, P., I. Longden and A. Bleasby (2000). "EMBOSS: the European Molecular Biology Open Software Suite." Trends Genet **16**(6): 276-277.

Rigottier-Gois, L. (2013). "Dysbiosis in inflammatory bowel diseases: the oxygen hypothesis." ISME J **7**(7):1256-1261

Riordan, J. T., J. A. Tietjen, C. W. Walsh, J. E. Gustafson and T. S. Whittam (2010). "Inactivation of alternative sigma factor 54 (RpoN) leads to increased acid resistance, and alters locus of enterocyte effacement (LEE) expression in *Escherichia coli* O157:H7." Microbiology **156**(Pt 3): 719-730.

- Rodionov, D. A., I. Dubchak, A. Arkin, E. Alm and M. S. Gelfand (2004). "Reconstruction of regulatory and metabolic pathways in metal-reducing delta-proteobacteria." Genome Biol **5**(11): R90.
- Roediger, W. E., A. Duncan, O. Kapaniris and S. Millard (1993a). "Reducing sulfur compounds of the colon impair colonocyte nutrition: implications for ulcerative colitis." Gastroenterology **104**(3): 802-809.
- Roediger, W. E., A. Duncan, O. Kapaniris and S. Millard (1993b). "Sulphide impairment of substrate oxidation in rat colonocytes: a biochemical basis for ulcerative colitis?" Clin Sci (Lond) **85**(5): 623-627.
- Roeselers, G., M. Ponomarenko, S. Lukovac and H. M. Wortelboer (2013). "Ex vivo systems to study host-microbiota interactions in the gastrointestinal tract." Best Pract Res Clin Gastroenterol **27**(1): 101-113.
- Romantsov, T., Z. Guan and J. M. Wood (2009). "Cardiolipin and the osmotic stress responses of bacteria." Biochim Biophys Acta **1788**(10): 2092-2100.
- Rooks, M. G., P. Veiga, L. H. Wardwell-Scott, T. Tickle, N. Segata, M. Michaud, C. A. Gallini, C. Beal, J. E. van Hylckama-Vlieg, S. A. Ballal, X. C. Morgan, J. N. Glickman, D. Gevers, C. Huttenhower and W. S. Garrett (2014). "Gut microbiome composition and function in experimental colitis during active disease and treatment-induced remission." ISME J **8**(7): 1403-1417.
- Round, J. L. and S. K. Mazmanian (2010). "Inducible Foxp3+ regulatory T-cell development by a commensal bacterium of the intestinal microbiota." Proc Natl Acad Sci U S A **107**(27): 12204-12209.
- Rowan, F. E., N. G. Docherty, J. C. Coffey and P. R. O'Connell (2009). "Sulphate-reducing bacteria and hydrogen sulphide in the aetiology of ulcerative colitis." Br J Surg **96**(2): 151-158.
- Salzman, N. H., H. de Jong, Y. Paterson, H. J. Harmsen, G. W. Welling and N. A. Bos (2002). "Analysis of 16S libraries of mouse gastrointestinal microflora reveals a large new group of mouse intestinal bacteria." Microbiology **148**(Pt 11): 3651-3660.
- Sambrook, J., E. F. Fritsch and T. Maniatis (1989). Molecular Cloning, A Laboratory Manual. N. Ford. United States of America, Cold Spring Harbour Laboratory Press. **1,2 and 3**.
- Samuel, B. S., A. Shaito, T. Motoike, F. E. Rey, F. Backhed, J. K. Manchester, R. E. Hammer, S. C. Williams, J. Crowley, M. Yanagisawa and J. I. Gordon (2008). "Effects of the gut microbiota on host adiposity are modulated by the short-chain fatty-acid binding G protein-coupled receptor, Gpr41." Proc Natl Acad Sci U S A **105**(43): 16767-16772.
- Sanders, M. E. (2016). "Probiotics and microbiota composition." BMC Medicine **14**(1): 82.
- Sarker, S. A., T. Ahmed and H. Brussow (2017). "Persistent diarrhea: A persistent infection with enteropathogens or a gut commensal dysbiosis?" Environ Microbiol.
- Savkovic, S. D., J. Villanueva, J. R. Turner, K. A. Matkowskyj and G. Hecht (2005). "Mouse model of enteropathogenic *Escherichia coli* infection." Infect Immun **73**(2): 1161-1170.
- Sawin, E. A., T. J. De Wolfe, B. Aktas, B. M. Stroup, S. G. Murali, J. L. Steele and D. M. Ney (2015). "Glycomacropptide is a prebiotic that reduces *Desulfovibrio* bacteria, increases cecal short-chain fatty acids, and is anti-inflammatory in mice." Am J Physiol Gastrointest Liver Physiol **309**(7): G590-601.
- Scanlan, P. D., F. Shanahan and J. R. Marchesi (2009). "Culture-independent analysis of desulfovibrios in the human distal colon of healthy, colorectal cancer and polypectomized individuals." FEMS Microbiol Ecol **69**(2): 213-221.

- Schmieder, R. and R. Edwards (2011). "Quality control and preprocessing of metagenomic datasets." Bioinformatics **27**(6): 863-864.
- Segal, G. M., T. D. Smith, M. C. Heinrich, F. S. Ey and G. C. Bagby, Jr. (1992). "Specific repression of granulocyte-macrophage and granulocyte colony-stimulating factor gene expression in interleukin-1-stimulated endothelial cells with antisense oligodeoxynucleotides." Blood **80**(3): 609-616.
- Sender, R., S. Fuchs and R. Milo (2016). "Are We Really Vastly Outnumbered? Revisiting the Ratio of Bacterial to Host Cells in Humans." Cell **164**(3): 337-340.
- Serino, M., E. Luche, S. Gres, A. Baylac, M. Berge, C. Cenac, A. Waget, P. Klopp, J. Iacovoni, C. Klopp, J. Mariette, O. Bouchez, J. Lluch, F. Ouarne, P. Monsan, P. Valet, C. Roques, J. Amar, A. Bouloumie, V. Theodorou and R. Burcelin (2012). "Metabolic adaptation to a high-fat diet is associated with a change in the gut microbiota." Gut **61**(4): 543-553.
- Shahinas, D., M. Silverman, T. Sittler, C. Chiu, P. Kim, E. Allen-Vercoe, S. Weese, A. Wong, D. E. Low and D. R. Pillai (2012). "Toward an understanding of changes in diversity associated with fecal microbiome transplantation based on 16S rRNA gene deep sequencing." MBio **3**(5).
- Shankar, V., M. J. Hamilton, A. Khoruts, A. Kilburn, T. Unno, O. Paliy and M. J. Sadowsky (2014). "Species and genus level resolution analysis of gut microbiota in *Clostridium difficile* patients following fecal microbiota transplantation." Microbiome **2**: 13.
- Siegmund, B., G. Fantuzzi, F. Rieder, F. Gamboni-Robertson, H. A. Lehr, G. Hartmann, C. A. Dinarello, S. Endres and A. Eigler (2001). "Neutralization of interleukin-18 reduces severity in murine colitis and intestinal IFN-gamma and TNF-alpha production." Am J Physiol Regul Integr Comp Physiol **281**(4): R1264-1273.
- Silhavy, T. J., D. Kahne and S. Walker (2010). "The Bacterial Cell Envelope." Cold Spring Harbor Perspectives in Biology **2**(5): a000414.
- Sleator, R. D. and C. Hill (2002). "Bacterial osmoadaptation: the role of osmolytes in bacterial stress and virulence." FEMS Microbiol Rev **26**(1): 49-71.
- Sohlenkamp, C. and O. Geiger (2016). "Bacterial membrane lipids: diversity in structures and pathways." FEMS Microbiol Rev **40**(1): 133-159.
- Sokol, H., B. Pigneur, L. Watterlot, O. Lakhdari, L. G. Bermudez-Humaran, J. J. Gratadoux, S. Blugeon, C. Bridonneau, J. P. Furet, G. Corthier, C. Grangette, N. Vasquez, P. Pochart, G. Trugnan, G. Thomas, H. M. Blottiere, J. Dore, P. Marteau, P. Seksik and P. Langella (2008). "Faecalibacterium prausnitzii is an anti-inflammatory commensal bacterium identified by gut microbiota analysis of Crohn disease patients." Proc Natl Acad Sci U S A **105**(43): 16731-16736.
- Solovyev, V. and A. Salamov (2011). Automatic Annotation of Microbial Genomes and Metagenomic Sequences. . In Metagenomics and its Applications in Agriculture, Biomedicine and Environmental Studies R. W. Li, Nova Science Publishers: 61-78.
- Spees, A. M., T. Wangdi, C. A. Lopez, D. D. Kingsbury, M. N. Xavier, S. E. Winter, R. M. Tsolis and A. J. Baumler (2013). "Streptomycin-induced inflammation enhances *Escherichia coli* gut colonization through nitrate respiration." MBio **4**(4).
- Spiro, S. (1994). "The FNR family of transcriptional regulators." Antonie Van Leeuwenhoek **66**(1-3): 23-36.
- Staley, C., T. Kaiser, L. K. Beura, M. J. Hamilton, A. R. Weingarden, A. Bobr, J. Kang, D. Masopust, M. J. Sadowsky and A. Khoruts (2017). "Stable engraftment of human microbiota into mice with a single oral gavage following antibiotic conditioning." Microbiome **5**(1): 87.

Steeenga, W. T., M. Mischke, C. Lute, M. V. Boekschoten, M. G. Pruis, A. Lendvai, H. J. Verkade, J. Boekhorst, H. M. Timmerman, T. Plosch and M. Muller (2014). "Sexually dimorphic characteristics of the small intestine and colon of prepubescent C57BL/6 mice." Biol Sex Differ **5**: 11.

Stull, R. A. and F. C. Szoka, Jr. (1995). "Antigene, ribozyme and aptamer nucleic acid drugs: progress and prospects." Pharm Res **12**(4): 465-483.

Sule, N., S. Pasupuleti, N. Kohli, R. Menon, L. J. Dangott, M. D. Manson and A. Jayaraman (2017). "The Norepinephrine Metabolite 3,4-Dihydroxymandelic Acid Is Produced by the Commensal Microbiota and Promotes Chemotaxis and Virulence Gene Expression in Enterohemorrhagic *Escherichia coli*." Infect Immun.

Sun, D., W. Zhang, N. Li, Z. Zhao, Z. Mou, E. Yang and W. Wang (2016). "Silver nanoparticles-quercetin conjugation to siRNA against drug-resistant *Bacillus subtilis* for effective gene silencing: *in vitro* and *in vivo*." Mater Sci Eng C Mater Biol Appl **63**: 522-534.

Tessler, M., J. S. Neumann, E. Afshinnekoo, M. Pineda, R. Hersch, L. F. M. Velho, B. T. Segovia, F. A. Lansac-Toha, M. Lemke, R. DeSalle, C. E. Mason and M. R. Brugler (2017). "Large-scale differences in microbial biodiversity discovery between 16S amplicon and shotgun sequencing." Sci Rep **7**(1): 6589.

Thornsberry, C., B. C. Hill, J. M. Swenson and L. K. McDougal (1983). "Rifampin: spectrum of antibacterial activity." Rev Infect Dis **5 Suppl 3**: S412-417.

Tian, H., P. Gao, Z. Chen, Y. Li, Y. Li, Y. Wang, J. Zhou, G. Li and T. Ma (2017). "Compositions and Abundances of Sulfate-Reducing and Sulfur-Oxidizing Microorganisms in Water-Flooded Petroleum Reservoirs with Different Temperatures in China." Front Microbiol **8**: 143.

Tremaroli, V. and F. Backhed (2012). "Functional interactions between the gut microbiota and host metabolism." Nature **489**(7415): 242-249.

Turnbaugh, P. J., M. Hamady, T. Yatsunenko, B. L. Cantarel, A. Duncan, R. E. Ley, M. L. Sogin, W. J. Jones, B. A. Roe, J. P. Affourtit, M. Egholm, B. Henrissat, A. C. Heath, R. Knight and J. I. Gordon (2009). "A core gut microbiome in obese and lean twins." Nature **457**(7228): 480-484.

Turnbaugh, P. J., R. E. Ley, M. Hamady, C. M. Fraser-Liggett, R. Knight and J. I. Gordon (2007). "The human microbiome project." Nature **449**(7164): 804-810.

Turnbaugh, P. J., R. E. Ley, M. A. Mahowald, V. Magrini, E. R. Mardis and J. I. Gordon (2006). "An obesity-associated gut microbiome with increased capacity for energy harvest." Nature **444**(7122): 1027-1031.

Turnbaugh, P. J., C. Quince, J. J. Faith, A. C. McHardy, T. Yatsunenko, F. Niazi, J. Affourtit, M. Egholm, B. Henrissat, R. Knight and J. I. Gordon (2010). "Organismal, genetic, and transcriptional variation in the deeply sequenced gut microbiomes of identical twins." Proc Natl Acad Sci U S A **107**(16): 7503-7508.

Ubeda, C., Y. Taur, R. R. Jenq, M. J. Equinda, T. Son, M. Samstein, A. Viale, N. D. Socci, M. R. van den Brink, M. Kamboj and E. G. Pamer (2010). "Vancomycin-resistant Enterococcus domination of intestinal microbiota is enabled by antibiotic treatment in mice and precedes bloodstream invasion in humans." J Clin Invest **120**(12): 4332-4341.

Unden, G. and J. Schirawski (1997). "The oxygen-responsive transcriptional regulator FNR of *Escherichia coli* : the search for signals and reactions." Molecular Microbiology **25**(2): 205-210.

Untergasser, A., I. Cutcutache, T. Koressaar, J. Ye, B. C. Faircloth, M. Remm and S. G. Rozen (2012). "Primer3--new capabilities and interfaces." Nucleic Acids Res **40**(15): e115.

van den Elsen, L. W., H. C. Poyntz, L. S. Weyrich, W. Young and E. E. Forbes-Blom (2017). "Embracing the gut microbiota: the new frontier for inflammatory and infectious diseases." Clin Transl Immunology **6**(1): e125.

Vandeputte, D., G. Falony, S. Vieira-Silva, R. Y. Tito, M. Joossens and J. Raes (2016). "Stool consistency is strongly associated with gut microbiota richness and composition, enterotypes and bacterial growth rates." Gut **65**(1): 57-62.

Vandeputte, D., G. Falony, S. Vieira-Silva, J. Wang, M. Sailer, S. Theis, K. Verbeke and J. Raes (2017). "Prebiotic inulin-type fructans induce specific changes in the human gut microbiota." Gut.

Vernocchi, P., F. Del Chierico and L. Putignani (2016). "Gut Microbiota Profiling: Metabolomics Based Approach to Unravel Compounds Affecting Human Health." Front Microbiol **7**: 1144.

von Kockritz-Blickwede, M., O. A. Chow and V. Nizet (2009). "Fetal calf serum contains heat-stable nucleases that degrade neutrophil extracellular traps." Blood **114**(25): 5245-5246.

Walker, A. W., S. H. Duncan, P. Louis and H. J. Flint (2014). "Phylogeny, culturing, and metagenomics of the human gut microbiota." Trends Microbiol.

Walker, M. K., J. R. Boberg, M. T. Walsh, V. Wolf, A. Trujillo, M. S. Duke, R. Palme and L. A. Felton (2012). "A less stressful alternative to oral gavage for pharmacological and toxicological studies in mice." Toxicol Appl Pharmacol **260**(1): 65-69.

Wallace, J. L., A. Ianaro and G. de Nucci (2017). "Gaseous Mediators in Gastrointestinal Mucosal Defense and Injury." Dig Dis Sci.

Wallace, J. L., L. Vong, W. McKnight, M. Dickey and G. R. Martin (2009). "Endogenous and exogenous hydrogen sulfide promotes resolution of colitis in rats." Gastroenterology **137**(2): 569-578, 578.e561.

Walters, W., E. R. Hyde, D. Berg-Lyons, G. Ackermann, G. Humphrey, A. Parada, J. A. Gilbert, J. K. Jansson, J. G. Caporaso, J. A. Fuhrman, A. Apprill and R. Knight (2016). "Improved Bacterial 16S rRNA Gene (V4 and V4-5) and Fungal Internal Transcribed Spacer Marker Gene Primers for Microbial Community Surveys." mSystems **1**(1).

Wang, J. Z., W. T. Du, Y. L. Xu, S. Z. Cheng and Z. J. Liu (2017). "Gut microbiome-based medical methodologies for early-stage disease prevention." Microb Pathog **105**: 122-130.

Wang, R. (2012). "Physiological implications of hydrogen sulfide: a whiff exploration that blossomed." Physiol Rev **92**(2): 791-896.

Wargo, M. J. (2013). "Homeostasis and catabolism of choline and glycine betaine: lessons from *Pseudomonas aeruginosa*." Appl Environ Microbiol **79**(7): 2112-2120.

Weatherbee, A., I. Popov and A. Vitkin (2017). "Accurate viscosity measurements of flowing aqueous glucose solutions with suspended scatterers using a dynamic light scattering approach with optical coherence tomography." J Biomed Opt **22**(8): 1-10.

Wegmann, U., C. Nueno Palop, M. J. Mayer, E. Crost and A. Narbad (2017). "Complete Genome Sequence of *Desulfovibrio piger* FI11049." Genome Announcements **5**(7): e01528-01516.

Weissig, V., C. Lizano, C. Ganellin and V. Torchilin (2001). "DNA binding cationic liposomes with delocalized charge center - A structure-activity relationship study." Stp Pharma Sciences **11**(1): 91-96.

Weissig, V., C. Lizano and V. P. Torchilin (2000). "Selective DNA release from DQAsome/DNA complexes at mitochondria-like membranes." Drug Deliv **7**(1): 1-5.

Wellen, K. E. and G. S. Hotamisligil (2005). "Inflammation, stress, and diabetes." J Clin Invest **115**(5): 1111-1119.

Wigneshweraraj, S., D. Bose, P. C. Burrows, N. Joly, J. Schumacher, M. Rappas, T. Pape, X. Zhang, P. Stockley, K. Severinov and M. Buck (2008). "Modus operandi of the bacterial RNA polymerase containing the sigma54 promoter-specificity factor." Mol Microbiol **68**(3): 538-546.

Winteler, H. V. and D. Haas (1996). "The homologous regulators ANR of *Pseudomonas aeruginosa* and FNR of *Escherichia coli* have overlapping but distinct specificities for anaerobically inducible promoters." Microbiology **142 (Pt 3)**: 685-693.

Winter, S. E., M. G. Winter, M. N. Xavier, P. Thiennimitr, V. Poon, A. M. Keestra, R. C. Laughlin, G. Gomez, J. Wu, S. D. Lawhon, I. E. Popova, S. J. Parikh, L. G. Adams, R. M. Tsolis, V. J. Stewart and A. J. Baumler (2013). "Host-derived nitrate boosts growth of *E. coli* in the inflamed gut." Science **339(6120)**: 708-711.

Wittig, B., C. Junghans and M. Schroff (2002). Method for making linear, covalently closed DNA constructs, Google Patents.

World Health Organisation (2017). GLOBAL PRIORITY LIST OF ANTIBIOTIC-RESISTANT BACTERIA TO GUIDE RESEARCH, DISCOVERY, AND DEVELOPMENT OF NEW ANTIBIOTICS.

Wu, G. D., J. Chen, C. Hoffmann, K. Bittinger, Y. Y. Chen, S. A. Keilbaugh, M. Bewtra, D. Knights, W. A. Walters, R. Knight, R. Sinha, E. Gilroy, K. Gupta, R. Baldassano, L. Nessel, H. Li, F. D. Bushman and J. D. Lewis (2011). "Linking long-term dietary patterns with gut microbial enterotypes." Science **334(6052)**: 105-108.

Yang, X., M. J. Luo, A. C. M. Yeung, P. J. Lewis, P. K. S. Chan, M. Ip and C. Ma (2017). "First-In-Class Inhibitor of Ribosomal RNA Synthesis with Antimicrobial Activity against *Staphylococcus Aureus*." Biochemistry.

Yao, J., R. A. Carter, G. Vuagniaux, M. Barbier, J. W. Rosch and C. O. Rock (2016). "A Pathogen-Selective Antibiotic Minimizes Disturbance to the Microbiome." Antimicrob Agents Chemother **60(7)**: 4264-4273.

Yatsunencko, T., F. E. Rey, M. J. Manary, I. Trehan, M. G. Dominguez-Bello, M. Contreras, M. Magris, G. Hidalgo, R. N. Baldassano, A. P. Anokhin, A. C. Heath, B. Warner, J. Reeder, J. Kuczynski, J. G. Caporaso, C. A. Lozupone, C. Lauber, J. C. Clemente, D. Knights, R. Knight and J. I. Gordon (2012). "Human gut microbiome viewed across age and geography." Nature **486(7402)**: 222-227.

Yiv, S., K. M. Kale, J. Lang and R. Zana (1976). "Chemical relaxation and equilibrium studies of association in aqueous solutions of bolaform detergents. 1. Dodecane-1,12-bis(trimethylammonium bromide)." The Journal of Physical Chemistry **80(24)**: 2651-2655.

Yoshikawa, K., C. Kurihara, H. Furuhashi, T. Takajo, K. Maruta, Y. Yasutake, H. Sato, K. Narimatsu, Y. Okada, M. Higashiyama, C. Watanabe, S. Komoto, K. Tomita, S. Nagao, S. Miura, H. Tajiri and R. Hokari (2016). "Psychological stress exacerbates NSAID-induced small bowel injury by inducing changes in intestinal microbiota and permeability via glucocorticoid receptor signaling." J Gastroenterol.

Youshia, J. and A. Lamprecht (2016). "Size-dependent nanoparticulate drug delivery in inflammatory bowel diseases." Expert Opin Drug Deliv **13(2)**: 281-294.

Zak-Golab, A., M. Olszanecka-Glinianowicz, P. Kocelak and J. Chudek (2014). "The role of gut microbiota in the pathogenesis of obesity." Postepy Hig Med Dosw (Online) **68(0)**: 84-90.

Zakostelska, Z., J. Malkova, K. Klimesova, P. Rossmann, M. Hornova, I. Novosadova, Z. Stehlikova, M. Kostovcik, T. Hudcovic, R. Stepankova, K. Juzlova, J. Hercogova, H. Tlaskalova-Hogenova and M. Kverka (2016). "Intestinal Microbiota Promotes Psoriasis-Like Skin Inflammation by Enhancing Th17 Response." PLoS One **11(7)**: e0159539.

Zgurskaya, H. I., C. A. Lopez and S. Gnanakaran (2015). "Permeability Barrier of Gram-Negative Cell Envelopes and Approaches To Bypass It." ACS Infect Dis **1(11)**: 512-522.

Zhao, X. L., B. C. Chen, J. C. Han, L. Wei and X. B. Pan (2015). "Delivery of cell-penetrating peptide-peptide nucleic acid conjugates by assembly on an oligonucleotide scaffold." Sci Rep **5**: 17640.

Zhernakova, A., A. Kurilshikov, M. J. Bonder, E. F. Tigchelaar, M. Schirmer, T. Vatanen, Z. Mujagic, A. V. Vila, G. Falony, S. Vieira-Silva, J. Wang, F. Imhann, E. Brandsma, S. A. Jankipersadsing, M. Joossens, M. C. Cenit, P. Deelen, M. A. Swertz, R. K. Weersma, E. J. Feskens, M. G. Netea, D. Gevers, D. Jonkers, L. Franke, Y. S. Aulchenko, C. Huttenhower, J. Raes, M. H. Hofker, R. J. Xavier, C. Wijmenga and J. Fu (2016). "Population-based metagenomics analysis reveals markers for gut microbiome composition and diversity." *Science* **352**(6285): 565-569.

Ziha-Zarifi, I., C. Llanes, T. Kohler, J. C. Pechere and P. Plesiat (1999). "*In vivo* emergence of multidrug-resistant mutants of *Pseudomonas aeruginosa* overexpressing the active efflux system MexA-MexB-OprM." *Antimicrob Agents Chemother* **43**(2): 287-291.

Zoetendal, E. G., J. Raes, B. van den Bogert, M. Arumugam, C. C. Booiijink, F. J. Troost, P. Bork, M. Wels, W. M. de Vos, M. Kleerebezem (2012). "The human small intestinal microbiota is driven by rapid uptake and conversion of simple carbohydrates." *ISME J* **6**(7):1415-1426.